Научном већу Института за физику у Београду

Београд, 19. 4. 2017.

Предмет: Молба за покретање поступка за избор у звање научни саветник

Молим Научно веће Института за физику у Београду да у складу са Правилником о поступку и начину вредновања и квантитативном исказивању научно-истраживачких резултата истраживача покрене поступак за мој избор у звање научни саветник.

У прилогу достављам:

1. Мишљење руководиоца пројекта са предлогом чланова комисије за избор у звање
2. Стручну биографију
3. Преглед научне активности
4. Елементе за квалитативну оцену научног доприноса
5. Елементе за квантитативну оцену научног доприноса
6. Списак објављених радова и њихове копије
7. Податке о цитираности радова
8. Фотокопију решења о избору у претходно звање
9. Додатке

Са поштовањем,

др Дарко Танасковић
виши научни сарадник
Институт за физику у Београду

Научном већу Института за физику у Београду

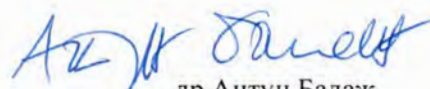Београд, 19. април 2017. године

Предмет: Мишљење руководиоца пројекта о избору др Дарка Танасковића у звање научни саветник

Др Дарко Танасковић је запослен у Лабораторији за примену рачунара у науци, у оквиру Националног центра изузетних вредности за изучавање комплексних система Института за физику у Београду и ангажован је на пројекту основних истраживања Министарства просвете, науке и технолошког развоја Републике Србије ОН171017, под називом "Моделирање и нумеричке симулације сложених вишечестичних физичких система", као и на пројекту ИИИ45018, под називом "Наноструктурни мултифункционални материјали и нанокомпозити". На поменутим пројектима ради на темама везаним за проучавање јако корелисаних електронских система. С обзиром да испуњава све предвиђене услове у складу са Правилником о поступку, начину вредновања и квантитативном исказивању научноистраживачких резултата истраживача МПНТР, сагласан сам са покретањем поступка за избор др Дарка Танасковића у звање научни саветник.

За састав комисије за избор др Дарка Танасковића у звање научни саветник предлажем:

(1) др Антун Балаж, научни саветник, Институт за физику у Београду
(2) академик Зоран В. Поповић, научни саветник, Институт за физику у Београду
(3) др Александар Белић, научни саветник, Институт за физику у Београду
(4) др Зоран С. Поповић, научни саветник, Институт за нуклеарне науке "Винча"

Руководилац пројекта ОН171017

др Антун Балаж
научни саветник

БИОГРАФСКИ ПОДАЦИ

Др Дарко Танасковић је рођен 1971. године у Београду где је завршио основну школу и Математичку гимназију. Дипломирао је на Физичком факултету у Београду 1996. године са просеком 9.79, где је и магистрирао 2000. године. У периоду од 1997. до 2000. године је био ангажован на Институту за физику у Београду као стипендиста Министарства просвете и науке. Потом одлази на докторске студије на Државном универзитету Флориде у Талахасију, САД. Докторски рад под насловом "Anomalous Metallic Behavior in Strongly Correlated Electron Systems with Disorder", урађен под менторством Проф. Владимира Добросављевића, одбранио је 2005. године. Након једне године постдокторског усавршавања на Државном универзитету Охаја, у Колумбусу, САД, враћа се на Институт за физику 2006. године где је ангажован у оквиру пројекта "Моделирање и нумеричке симулације комплексних физичких система" (ОИ 141035), односно касније на пројекту "Моделирање и нумеричке симулације сложених вишечестичних система" (ОН 171017). У периоду од 2007. до 2010. одлазио је на неколико студијских посета у САД у укупном трајању од шест месеци. У звање виши научни сарадник изабран је 30. октобра 2012. године. Руководио је Реинтеграционим пројектом „Electronic Structure Calculations of Complex Materials", у оквиру НАТО програма за науку и био руководилац два билатерална пројекта, "Квантни критични транспорт у близини Мотовог метал-изолатор прелаза" са истраживачима из Француске, односно "Јаке електронске корелације и суперпроводност" са колегама из Словеније.

Област научно-истраживачког рада др Дарка Танасковића је теоријска физика кондензоване материје. Главне теме рада су транспортне и термодинамичке особине јако корелисаних електронских система, физика Мотовог метал-изолатор прелаза и суперпроводност, као и прорачун фононских спектара. Др Танасковић је до сада објавио 25 радова, од чега 6 у часопису Physical Review Letters, као и једно поглавље у монографији. Према подацима са Web of Science на дан 3. 4. 2017. године, радови су цитирани укупно 255 пута (не укључујући самоцитате), уз h-index једнак 10. Рецензент је у часописима Physical Review Letters, Physical Review B и Journal of Physics Condensed Matter. Обављао је дужност секретара Друштва физичара Србије у периоду 2007-2010. До сада су под руководством др Танасковића урађене две докторске дисертације.

ПРЕГЛЕД НАУЧНЕ АКТИВНОСТИ

Научно-истраживачки рад др Дарка Танасковића одвијао се у области теоријске физике кондензованог стања материје. За време магистарских студија у Београду (1997-2000) кандидат је проучавао особине суперпроводника са d-симетријом спаривања Куперових парова у оквиру BCS теорије и магистрирао на теми "Утицај Паулијевог парамагнетизма на магнетне особине високотемпературних суперпроводника" урађеној под руководством Проф. Зорана Радовића, дописног члана САНУ. На докторским студијама на Државном универзитету Флориде у Талахасију, САД (2000-2005), др Танасковић је радио у области физике јако корелисаних електронских система и квантних фазних прелаза. Докторирао је на теми "Anomalous Metallic Behavior in Strongly Correlated Electron Systems with Disorder", урађеној под руководством Проф. Владимира Добросављевића. Једну годину је провео на постдокторском усавршавању на Државном универзитету Охаја у Колумбусу, САД. Проучавање система са јаким електронским корелацијама у близини Мотовог метал-изолатор прелаза остаје главна научно-истраживачка тема и након повратка на Институт за физику у Београду 2006. године. Други правац научно-истраживачког рада др Тансковића је прорачун и анализа фононског спектра суперпроводника на бази гвожђа и сродних једињења, као и различитих једињења са (анти)феромагнетним уређењем. Овај правац рада се одвија у непосредној сарадњи са Лабораторијом за Раманову спектроскопију Института за физику у Београду под руководством Академика Зорана Поповића.. Др Танасковић је до сада објавио 6 радова у најугледнијем часопису у области физике Physical Review Letters и 13 радова у најугледнијем часопису у области физике кондензоване материје Physical Review B. У наставку је приказан преглед главних научних резултата, уз нагласак на резултате остварене у периоду након претходног избора у звање.

Главни правац истраживања др Дарка Танасковића је **теорија јако корелисаних електронских система**, а посебно Мотов метал-изолатор прелаз, као једна од најважнијих последица јаких електронских интеракција и најактивнијих области истраживања у физици кондензоване материје. И експеримент и теорија јасно указују да је Мотов прелаз фазни прелаз првог реда и да испољава коегзистенцију металне и изолаторске фазе до неке критичне температуре T_c. На најнижим температурама обе фазе често развијају дугодометно уређење - антиферомагнетизам или суперпроводност. Мотов прелаз је квантни (T=0) фазни прелаз, али је квантна критична тачка замаскирана регионом коегзистенције и/или уређеном фазом. Транспортне особине материјала на температурама изнад критичне температуре T_c су једна од главних тема интересовања др Танасковића у претходних неколико година. Од претходног избора у звање др Танасковић је из ове тематике објавио следеће радове:

- J. Vučičević, **D. Tanasković**, M. J. Rozenberg and V. Dobrosavljević, *Bad-Metal Behavior Reveals Mott Quantum Criticality in Doped Hubbard Models*, Phys. Rev. Lett. **114,** 246402 (2015).
- H. Braganca, M. C. O. Aguiar, J. Vučičević, **D. Tanasković**, and V. Dobrosavljević, *Anderson Localization Effects Near the Mott Metal-insulator Transition*, Phys. Rev. B **92**, 125143(2015).
- J. Vučičević, H. Terletska, **D. Tanasković,** and V. Dobrosavljević, *Finite-temperature Crossover and the Quantum Widom Line Near the Mott Transition*, Phys. Rev. B **88**, 075143(2013).

Као и поглавље у монографији

- V. Dobrosavljević and **D. Tanasković**, *Wigner–Mott Quantum Criticality: From 2D-MIT to 3*He *and Mott Organics*, in *Strongly Correlated Electrons in Two Dimensions*, edited by Sergey Kravchenko, Chapter 1, pages 1-46, (Pan Stanford Publishing, 2017).

У овим радовима је проучаван транспорт наелектрисања у околини Мотовог прелаза на температурама изнад Тс из перспективе квантне критичности. Коришћена је теорија динамичког средњег поља (dynamical mean field theory, DMFT) која се користи за проучавање система у којима је присутна јака одбојна међуелектронска интеракција. У овим радовима је приказано до сада најдетаљније решење DMFT једначина за полупопуњени и допирани Хабардов модел у широком опсегу фазног дијаграма. Показано је да се особине Мотовог метал-изолатор прелаза у високо-температурном режиму између метала и изолатора поклапају са особинама које проистичу из претпоставке постојања квантне критичне тачке, упркос фазном прелазу првог реда и региону коегзистенције металне и изолаторске фазе којима је квантна критична тачка замаскирана. За полупопуњени Хабардов модел спроведена је детаљна анализа скалирања резултата за отпорност (како се то иначе чини у случају чисто квантних фазних прелаза) да би се утврдила функција скалирања, са температуром T у аргументу уместо удаљености од критичне тачке $|T- T_c|$. Утврђено је веома добро скалирање облика $\rho=\rho(U^*(T),T)\Phi[((U-U^*(T))/T^{-1/zv}]$, које је у међувремену нашло потврду и у експерименталном раду на Мотовим органским изолаторима који су колеге из Јапана објавиле у часопису Nature Physics у фебруару 2015. године (видети прилог за Научни ниво и значај резултата).

У случају допираног Хабардовог модела одређен је тродимензионални фазни дијаграм у (μ,U,T) простору. Показано је да се температура коегзистенције фаза T_c и регион коегзистенције драстично смањују са повећањем интеракције U и примењена је анализа скалирања на овај случај. У овом случају хемијски потенцијал μ улази уместо интеракције U у закон скалирања $\rho = \rho(\mu*(T),T)\Phi[((\mu-\mu*(T))/ T^{-1/zv}]$. Показано је да је Мотов прелаз повезан са универзалним високо-температурним транспортом, типичним за постојање квантне критичне тачке, што се у допираном случају поклапа са транспортним режимом лошег метала са линеарном отпорношћу у функцији температуре. Крећући од претпоставке о важењу скалирања, изведена је полуаналитичка формула која репродукује и линеарност и нагиб кривих отпорности у високо-температурном делу DMFT фазног дијаграма, уз добро квалитативно слагање са експериметима на познатом једињењу бакар-оксида $La_{2-x}Sr_xCuO_4$. Резултати за допирани Хабардов модел су такође послужили као непосредна мотивација за експериментални рад, Critical Behavior in Doping-Driven Metal–Insulator Transition on Single-Crystalline Organic Mott-FET, Sato et al., *Nano Lett.*, 2017, 17 (2), pp 708–714, у коме су експериментални резултати анализирани као што је предложено у теорији (видети прилог за Научни ниво и значај резултата).

Наведени резултати који се односу на квантну критичност у близини Мотовог метал-изолатор прелаза су блиско повезани са ранијим радовима (H. Terletska, J. Vučičević, **D. Tanasković**, and V. Dobrosavljević, *Quantum Critical Transport Near the Mott Transition*, Phys. Rev. Lett. **107**, 026401 (2011) и M. M. Radonjić, **D. Tanasković**, V. Dobrosavljević, G. Kotliar, and K. Haule, *Wigner-Mott Scaling of Transport Near the Two-dimensional Metal-insulator Transition*, Phys. Rev. B 85, 085133 (2012)) и представљали су основу за писање наведеног поглавља у монографији у коме је истакнут утицај јаких електронских корелација и

некохерентног расејања на траснпорт у разређеном дводимензионалном елекронском гасу у Si MOSFET-има (видети такође и прилог о монографији који се односи на Научни ниво и значај резултата).

Ефекат јаких електронских корелација је од пресудне важности и у физици квантних тачака. Основно стање квантне тачке спрегнуте са суперпроводником формира спински синглет или дублет у зависности од локалног енергијског новоа и јачине хибридизације. Кулонова интеракција тежи да формира спински дублет, док спински синглет настаје услед Кондо ефекта или суперпроводног спаривања. Позиција резонанци унутар суперпроводног процепа може да се одреди теоријски, односно нумерички, полазећи од модела Андерсонове нечистоће уроњене у суперпроводник. Овом темом је започета научна сарадња са колегама са Института "Јожеф Стефан" из Љубљане и недавно је објављен рад

- W. van Gerven Oei, **D. Tanasković,** and R. Žitko, *Magnetic Impurities in Spin-split Superconductors,* Phys. Rev. B **95,** 085115 (2017).

У овом раду је проучаван утицај Земановог магнетног поља на симетрију основног стања и положаје Шибиних резонанци унутар суперпроводног процепа. Користећи метод нумеричке ренормализационе групе показано је да је критично магнетно поље за синглет-дублет прелаз немонотона функција суперпроводног процепа: за мале вредности процепа фазни прелаз настаје услед затварања процепа магнетним пољем, а за веће вредности процепа прелаз настаје услед раздвајања Шибиних резонанци. Такође је показано како се Шибине резонанце шире у присуству додатне трансверзалне компоненте магнетног поља која настаје у присуству спин-орбитног спрезања.

Други правац научно-истраживачког рада др Дарка Танасковића везан је за **прорачун електронских и фононских спектара** различитих једињења, попут суперпровдника на бази гвожђа и њима сличних једињења, као и различитих једињења са (анти)феромагнетним уређењем. Прорачуни електронске структуре су извођени у оквиру теорије функционала густине (*Density functional theory - DFT*), док је динамика решетке проучавана помоћу пертурбативне теорије функционала густине (*Density functional perturbation theory - DFPT*). У непосредној сарадњи са колегама из Лабораторије за Раманову спектроскопију Института за физику у Београду објављено је до сада већ 7 заједничких радова, од чега је у овом приказу издвојено неколико радова.

- M. Опачић, N. Lazarević, M. M. Radonjić, M. Сћепановић, H. Ryu, A. Wang, **D. Tanasković**, C. Petrovic, and Z. V. Popović, *Raman Spectroscopy of $K_xCo_{2-y}Se_2$ Single Crystals Near the Ferromagnet–paramagnet Transition,* J. Phys. Cond. Matt. **28**, 485401 (2016).

Овај рад је изабран међу најбоље радове објављене у 2016. години у часопису Journal of Physics Condensed Matter (видети прилог за Научни ниво и значај резултата). Приказани резултати су указали на утицај спинских флуктуација на фононски спектар у близини феромагнетног прелаза.

У раду

- Z. V. Popović, M. Scepanović, N. Lazarević, M. M. Radonjić, **D. Tanasković**, H. Lei, and C. Petrovic, Phonon and *Magnetic Dimer Excitations in Fe-based S=2 Spin-ladder Compound BaFe2Se2O*, Phys. Rev. B **89**, 014301 (2014)

проучаван је S=2 "*spin-ladder*" систем BaFe2Se2O помоћу Раманове спектроскопије и фононских прорачуна. Анализом температурне зависности појединих модова уочено је дугодометно, антиферомагнетно уређење испод T=240K. Измерени спектри показују и постојање магнонског континума који нестаје на температури T=623K, што представља температуру на којој се нарушава краткодоментно магнетно уређење.

У раду

- N. Lazarević, M. M. Radonjić, **D. Tanasković**, R. Hu, C. Petrović and Z. V. Popović, *Lattice Dynamics of FeSb2*, J. Phys. Cond. Matt. **24**, 255402 (2012)

по први пут је измерен и израчунат фононски спектар једињења гвожђе диантимонида. Ово једињење је веома значајно због израђених термоелектричних особина, а утицај електронских корелација на својства овог материјала представља веома значајну тему истраживања у физици јако корелисаних електронских система.

ЕЛЕМЕНТИ ЗА КВАЛИТАТИВНУ ОЦЕНУ РАДА КАНДИДАТА

1. Квалитет научних резултата

1.1 Научни ниво и значај резултата, утицај научних радова

Др Дарко Танасковић је током научне каријере објавио укупно 25 радова у међународним часописима са ISI листе, од чега 6 категорије M21a, 13 категорије M21 и 3 категорије M22. Укупан импакт фактор радова је 108.5. Од одлуке Научног већа о предлогу за стицање претходног научног звања др Танасковић је објавио 1 M21a рад, 7 M21 радова, 2 M22 рада, као и 1 M21 рад између два избора у звање. Укупан импакт фактор ових радова је 35.388. Квалитет научног рада др Дарка Танасковића се може проценити, између осталог, из угледа часописа у којима су радови објављени: др Танасковић је до сада објавио 6 радова у најугледнијем часопису у области физике Physical Review Letters (ИФ=7.9) и 13 радова у најугледнијем часопису у области физике кондензоване материје Physical Review B (ИФ=3.7).

Најзначајнији радови др Танасковића у последњих неколико година су:

[1] J. Vučičević, **D. Tanasković**, M. J. Rozenberg and V. Dobrosavljević, *Bad-Metal Behavior Reveals Mott Quantum Criticality in Doped Hubbard Models*, Phys. Rev. Lett. **114,** 246402 (2015), ИФ=7.943, цитиран до сада 11 пута без аутоцитата.

[2] H. Terletska, J. Vučičević, **D. Tanasković**, and V. Dobrosavljević, *Quantum Critical Transport Near the Mott Transition*, Phys. Rev. Lett. **107**, 026401 (2011), ИФ=7.62, цитиран до сада 24 пута без аутоцитата.

[3] J. Vučičević, H. Terletska, **D. Tanasković** and V. Dobrosavljević, *Finite-temperature Crossover and the Quantum Widom Line Near the Mott Transition*, Phys. Rev. B **88**, 075143(2013), ИФ=3.767 цитиран до сада 7 пута без аутоцитата.

[4] M. M. Radonjić, **D. Tanasković**, V. Dobrosavljević, G. Kotliar, and K. Haule, *Wigner-Mott Scaling of Transport Near the Two-dimensional Metal-insulator Transition*, Phys. Rev. B 85, 085133 (2012), ИФ=3.774, цитиран до сада 9 пута без аутоцитата.

[5] M. Opačić, N. Lazarević, M. M. Radonjić, M. Sćepanović, H. Ryu, A. Wang, **D. Tanasković**, C. Petrovic, and Z. V. Popović, *Raman Spectroscopy of $K_xCo_{2-y}Se_2$ Single Crystals Near the Ferromagnet–paramagnet Transition*,J. Phys. Cond. Matt. **28**, 485401 (2016), selected for the journal Highlights of 2016, ИФ=2.546.

У радовима [1], [2] и [3] проучаван је транспорт наелектрисања у околини Мотовог прелаза на температурама изнад критичне температуре коегзистенције металне и изолаторске фазе из перспективе квантне критичности. Коришћена је теорија динамичког средњег поља (DMFT) која се користи за проучавање система у којима је присутна јака одбојна међу-електронска интеракција. У овим радовима је приказано до сада најдетаљније

решење DMFT једначина за полупопуњени и допирани Хабардов модел у широком опсегу парамератара на фазном дијаграму. Нумерички резултати су добијени у апроксимацији итеративне пертурбативне теорије и методом квантног Монте Карла у континуалном времену. Показано је да се особине Мотовог метал-изолатор прелаза у високо-температурном режиму између метала и изолатора поклапају са особинама које проистичу из претпоставке постојања квантне критичне тачке, упркос фазном прелазу првог реда и региону коегзистенције металне и изолаторске фазе којима је квантна критична тачка замаскирана. Значајно је истаћи да су теоријски резултати приказани у раду [1] за допирани Хабардов модел послужили као непосредна мотивација за експериментални рад Critical Behavior in Doping-Driven Metal–Insulator Transition on Single-Crystalline Organic Mott-FET, Sato et al., *Nano Lett.*, 2017, 17 (2), pp 708–714, у коме су експериментални резултати анализирани као што је предложено у раду [1] (изводи из рада Sato et al. су у прилогу). Теорија развијена у радовима [2] и [3] је такође послужила као основа за експеримент и верификована је у раду Quantum criticality of Mott transition in organic materials, Furukawa et al., Nature Physics 11, 221–224 (2105) (изводи из рада Furukawa et al. су у прилогу).

Рад [4] уз радове [1] и [2] представљао је основу за писање поглавља у монографији V. Dobrosavljević and D. Tanasković, *Wigner–Mott Quantum Criticality: From 2D-MIT to 3He and Mott Organics,* in *Strongly Correlated Electrons in Two Dimensions,* edited by Sergey Kravchenko, Chapter 1, pages 1-46, (Pan Stanford Publishing, 2017). Значај ове монографије и допринос др. Танасковића је засебно описан у прилогу о овој монографији.

Рад [5] је један од радова који су настали у сарадњи са Лабораторијом за Раманову спектроскпију на Институту за физику у Београду. Овај рад је изабран међу најбоље радове објављене у 2016. години у часопису Journal of Physics Condensed Matter (видети прилог).

Један од показатеља значаја научних радова је да су оба докторанта др Танасковића одмах након одбране дисертације одлазили на постдокторско усавршавање на веома угледне европске институте, Милош Радоњић на Institute of Physics, University of Augsburg, Germany, а Јакша Вучичевић на IPhT, CEA Saclay, France.

1.2 Позитивна цитираност научних радова кандидата

Према подацима са Web of Science на дан 3. 4. 2017. године, радови су цитирани укупно 255 пута (не укључујући самоцитате), уз h-index једнак 10 (видети прилог о цитираности). Посебно треба истаћи да је велики број цитата забележен у радовима који су објављени у часописима са високим импакт фактором (у прилогу су као илустрација приказани сви цитати за рад Phys. Rev. Lett. **107**, 026401 (2011)).

1.3 Параметри квалитета часописа

Др Танасковић је током научне каријере објавио укупно 25 радова у међународним часописима са ISI листе, од чега 6 категорије М21а, 13 категорије М21 и 3 категорије М22. Укупан импакт фактор радова је 108.5. Од одлуке Научног већа о предлогу за стицање претходног научног звања др Танасковић је објавио 1 М21а рад, 8 М21 радова, 2 М22 рада и једно поглавље у зборнику водећег међународног значаја М13. Укупан импакт фактор ових радова је 35.388.

Збирно приказано, др Танасковић је објавио:

6 радова у Physical Review Letters (средњи ИФ=7.7)
13 радова у Physical Review B (средњи ИФ=3.77)
3 рада у Journal of Physics Condensed Matter (средњи ИФ=2.5)
1 рад у Solid State Com*unications* (ИФ=1.897)
1 рад у Spectrochimica Acta Part A: Molecular and Biomolecular Spectroscopy (ИФ=2.353)
1 рад у Annalen der Physik (ИФ=1.58)

Након одлуке Научног већа о предлогу за стицање претходног научног звања др Танасковић је објавио:

1 рад у Physical Review Letters (ИФ=7.943)
6 радова у Physical Review B (ИФ=3.718 за 1 рад и 3.767 за 5 радова)
2 рада у Journal of Physics Condensed Matter (ИФ=2.346 и ИФ=2.546)
1 рад у Solid State Com*unications* (ИФ=1.897)
1 рад у Spectrochimica Acta Part A: Molecular and Biomolecular Spectroscopy (ИФ=2.353)

1.4 Степен самосталности и степен учешћа у реализацији радова у научним центрима у земљи и иностранству

Након повратка са докторских студија у САД, др Дарко Танасковић је покренуо два правца истраживања која се раније нису спроводила на Институту за физику и у Србији. Први правац рада је проучавање транспортних и термодинамичких особина материјала у близини Мотовог метал-изолатор прелаза. Ове теме су обрађиване блиско сарађујући са већим бројем истраживача из иностранства (САД, Француска, Словенија, Бразил,...) од којих посебно треба истаћи дугогодишњи заједнички рад са Проф. Владимиром Добросављевићем са Државног универзизтета Флориде. Др Танасковић је дао велики допринос у свим фазама рада у оквиру ове тематике: формулисању непосредних задатака, аналитичком и нумеричком раду, обучавању за рад доктораната, дискусијама резултата и писању радова. У радовима из ове тематике најчешће су првопотписани аутори били докторанти др Танасковића (М. Радоњић, Ј. Вучичевић, односно W.-V. van Gerven). Посебно треба истаћи да се рад састојао, поред осталог, и у свакодневним непосредним дискусијама са докторантима, као и дискусијама кроз бројне размењене поруке са сарадницима из иностранства.

Други покренути правац рада подразумева сарадњу са групом за Раманову спектроскопију на Институту за физику у Београду. По први пут су на Институту за физику, у оквиру ове теме, објављени експериментално-теоријски радови. Допринос др Танасковића у заједничким експериментално-теоријским радовима се огледа у нумеричким прорачунима фононских спектара, анализи и дискусији резултата, као и значајном учешћу у писању ових радова.

2. Ангажованост у развоју услова за научни рад, образовању и формирању научних кадрова

Под менторством др Дарка Танасковића су до сада урађене и одбрањене две докторске дисертације на Физичком факултету у Београду.

- Др Милош Радоњић је докторску тезу, под насловом „Influence of Disorder on Charge Transport in Strongly Correlated Materials Near the Metal-insulator transition" одбранио 2014. године (видети прилог), након чега је провео две године на постдокторском усавршавању у Немачкој.
- Др Јакша Вучичевић је докторску тезу, под називом „Signatures of Hidden Quantum Criticality in the High-temperature Charge Transport Near the Mott Transition" одбранио 2015. године (видети прилог), након чега је на постдокторском усавршавању у Француској. Он је за свој рад добио годишњу награду за најбољу докторску тезу урађену на Институту за физику у Београду.

Тренутно, др Танасковић руководи докторским радом Wilem-Victor van Gerven-а који је пријавио тему доктората „Magnetic impurities in superconductors: Subgap states in quantum dots and effects of periodic local moments" за одбрану пред Колегијумом на Физичком факултету (видети прилог).

Поред тога, под менторством др Танасковића су урађена 4 дипломска рада, израда једног мастер рада је у току, а пре пар месеци је започет рад још једног новог докторанта.

Др Дарко Танасковић је предавао физику у Математичкој гимназији у школској 1997/1998 години, а радио је и као асистент на предмету Општа физика на Државном универзитету Флориде 2000/2001. Изабран је 2015. године за предавача на предмету Електронски транспорт у јако корелисаним системима на докторским студијама на Физичком факултету у Београду (видети прилог).

3. Нормирање броја коауторских радова, патената и техничких решења

Теоријски радови др Танасковића објављени у периоду након одлуке Научног већа о предлогу за стицање претходног научног звања су базирани на аналитичким прорачунима и комплексним нумеричким симулацијама и имају пет или мање аутора, тако да улазе са пуном тежином у односу на број коаутора. Експериментално-теоријских радови подразумевају шире колаборације, а у теоријском делу рада су учествовали Д. Танасковић и М. Радоњић. Већина ових радова имају до седам аутора и такође улазе са пуном тежином у односу на број коаутора. Три рада имају 8 или 9 аутора и у тим случајевима је број М бодова нормиран по Правилнику. Укупан број М бодова након одлуке Научног већа о предлогу за стицање претходног научног звања је 95, односно након нормирања 89.54.

4 . Руковођење пројектима, потпројектима и пројектним задацима

Др Дарко Танасковић руководи потпројектом "Испитивање јако корелисаних квантних система" у оквиру пројекта основних истраживања ОН171017 "Моделирање и нумеричке симулације сложених вишечестичних система" Министарства просвете, науке и технолошког развоја Републике Србије.

Др Танасковић је руководилац билатералног пројекта „Јаке електронске симулације и суперпроводност" са колегама са Института „Јожеф Стефан" из Љубљане, Словенија, који је започет 2016. године са трајањем од две године. Пројекат финансирају Министарство просвете, науке и технолошког развоја Републике Србије и Javna agencija za raziskovalno dejavnost Republike Slovenije.

Др Танасковић је руководио пројектом "Квантни критични транспорт у близини Мотовог метал-изолатор прелаза" у оквиру билатералне сарадње са Француском, Универзитет Париз-југ, за период 2012-2013. година. Пројекат su финансирали Министарство просвете, науке и технолошког развоја Републике Србије и Centre national de la recherche scientifique, CNRS.

Др Танасковић је руководио пројектом *Electronic Structure Calculations of Complex Materials* у оквиру Reintegration Grant програма финансираног од Public Diplomacy Division, Collaborative Programme Section, NATO Science for Peace and Security Programme за период 2008-2010. година.

Руковођења овим пројектима, односно потпројектом, су документована у прилозима.

5. Активност у научним и научно-стручним друштвима

- Др Танасковић је обављао дужност Секретара Друштва физичара Србије у периоду од 2006. до 2010. године.
- У периоду 2012-2014 је био члан комисије за такмичења средњошколаца.
- Рецензент је за часописе Physical Review Letters, Physical Review B (издавач American Physics Society) и Journal of Physics Condensed Matter (издавач IOP Publishing). Рецензирао је пројекте у оквиру DECI иницијативе (Distributed European Computing Initiative) у оквиру PRACE (Partnership for Advanced Computing in Europe).
- Др Танасковић је био члан Орагизационог комитета конференције *XVII Symposium on Condensed Matter Physics*, Вршац, Serbia, 16-20 September 2007.

Све наведене активности су документоване у прилозима.

6. Утицајност научних резултата

Утицај научних резултата кандидата се огледа у броју цитата који су наведени у тачки 1. овог прилога као и у прилогу о цитираности. Значај резултата кандидата је такође описан у тачки 1.

7. Конкретан допринос кандидата у реализацији радова у научним центрима у земљи и иностранству

Др Танасковић је значајно допринео сваком раду у коме је учествовао. Покренуо је два правца рада која раније нису била заступљена на Институту за физику у Београду и у Србији. Први правац рада је теорија јако корелисаних електронских система и Мотовог метал-изолатор прелаза. Овај правац рада је резултовао са 4 објављена рада након претходног избора у звање. У три од ова четири рада водећи аутор је (тадашњи) докторант др Танасковића, а највећи део рада је урађен на Институту за физику у Београду, уз сарадњу са истраживачиа из САД, Француске и Словеније. Др Танасковић је био непосредно укључен у сваки сегмент израде ових радова: дефинисање теме рада, аналитиче и нумеричке прорачуне који су се одвијали уз свакодневне консултације са докторантима и колегама из иностранства и писање радова. Један од четири рада из ове тематике је укључивао и сарадњу са колегама из Бразила и допринос др Танасковића се огледао у дискусијама везаним за тему овог рада и примену нумеричких кодова и допринос у писању рада.

Други правац научно-истраживачког рада др Танасковића везан је за прорачун електронских и фононских спектара различитих кристалних једињења и такође није био раније заступљен на Институту за физику у Београду. Овај правац рада се одвија у непосредној сарадњи са колегама из Лабораторије за Раманову спектроскопију Института за физику у Београду, а објављено је 7 експериметално-теоријских радова у периоду након одлуке Научног већа о предлогу за стицање претходног научног звања. Теоријски, односно нумерички део рада су урадили др Танасковић и некадашњи његов докторант и сада већ дугогодишњи сарадник, др Милош Радоњић. Поред нумеричких прорачуна др Танасковић је дао значајан допринос и у анализи резулатата и писању ових радова.

8 . Уводна предавања на конференцијама и друга предавања

Након претходног избора у звање др Танасковић је одржао следећа предавања по позиву:

1. *Phonon spectra of K_xFe_{2-y-z}Co_zSe_2 single crystals*, Institute "Jožef Stefan", Ljubljana, Slovenia, 14.6.2016.
2. *Неконвенционални суперпроводници*, предавање у оквиру предмета Семинар савремене физике, Физички факултет, Београд, 25.4.2016.
3. *Mott quantum criticality and bad metal behavior*, Institute of Physics, University of Augsburg, Germany, 2.12.2015.
4. *Mott quantum criticality and bad metal behavior,* The 19th Symposium on Condensed Matter Physics, Belgrade, Serbia, 7–11 September 2015
5. *Bad metal behavior reveals quantum criticality in the doped Hubbard model*, Institute "Jožef Stefan", Ljubljana, Slovenia, 11.6.2014.
6. *Квантни критични транспорт у близини Моттовог метал-изолатор прелаза*, Дани физике кондензованог стања материје, Београд, 10-12 септембар 2013.
7. *Quantum critical transport in clean and disordered Mott systems*, at the workshop "Wigner meets Mott: charge ordering and related phenomena in Mott system", 16-17 December 2013, Grenoble, France.

8. *Електронски транспорт у јако корелисаним материјалима близу метал-изолатор прелаза*, предавање у оквиру предмета Семинар савремене физике, Физички факултет, Београд, 22.4.2013.

Пре претходног избора у звање др Танасковић је одржао следећа предавања по позиву:

1. *Spin Liquid Behavior in Electronic Griffiths Phases*, XVII Symposium on Condensed Matter Physics, Vršac, Serbia, 16-20 September 2007.

Прилог: позивна писма за ова предавања или програм конференције са веб сајта.

ЕЛЕМЕНТИ ЗА КВАНТИТАТИВНУ ОЦЕНУ НАУЧНОГ ДОПРИНОСА КАНДИДАТА

Др Дарко Танасковић је током научне каријере објавио укупно 25 радова у међународним часописима са ISI листе, од чега 6 категорије М21а, 13 категорије М21 и 3 категорије М22. Укупан импакт фактор радова је 108.5. Од одлуке Научног већа о предлогу за стицање претходног научног звања др Танасковић је објавио 1 М21а рад, 8 М21 радова, 2 М22 рада и једно поглавље у зборнику водећег међународног значаја М13. Укупан импакт фактор ових радова је 35.388. Према подацима са Web of Science на дан 3. 4. 2017. године, радови су цитирани укупно 255 пута (не укључујући самоцитате), уз h-index једнак 10.

Остварени резултати у периоду након одлуке Научног већа о предлогу за стицање претходног научног звања:

Категорија	М бодова по раду	Број радова	Укупно М бодова	Нормирани број М бодова
М13	7	1	**7**	**7**
М21а	10	1	**10**	**10**
М21	8	8	**64**	**60.38**
М22	5	2	**10**	**9.16**
М32	1.5	1	**1.5**	**1.5**
М34	0.5	3	**1.5**	**1.5**

Поређење са минималним квантитативним условима за избор у звање научни саветник:

Минималан број М бодова		Остварени резултти	Остварени нормирани резултати
Укупно	70	**94**	**89.54**
М10+М20+М31+М32+М33+М41+М42+М90	50	**92.5**	**88.05**
М11+М12+М21+М22+М23	35	**91**	**86.54**

СПИСАК РАДОВА ДР ДАРКА ТАНАСКОВИЋА

Монографска студија/поглавље у књизи (М13)

Радови објављени након претходног избора у звање
1. V. Dobrosavljević and **D. Tanasković**, *Wigner–Mott Quantum Criticality: From 2D-MIT to 3*He *and Mott Organics*, in *Strongly Correlated Electrons in Two Dimensions,* edited by Sergey Kravchenko, Chapter 1, pages 1-46, (Pan Stanford Publishing, 2017), DOI: 10.4032/9789814745383, ISBN 9789814745376.

Радови у међународним часописима изузетних вредности (М21а)

Радови објављени након претходног избора у звање
1. J. Vučičević, **D. Tanasković**, M. J. Rozenberg and V. Dobrosavljević, *Bad-Metal Behavior Reveals Mott Quantum Criticality in Doped Hubbard Models*, Phys. Rev. Lett. **114,** 246402 (2015), doi: 10.1103/PhysRevLett.114.246402, ISSN 1079-7114, IF=7.943

Радови објављени пре претходног избора у звање
1. H. Terletska, J. Vučičević, **D. Tanasković**, and V. Dobrosavljević, *Quantum Critical Transport Near the Mott Transition*, Phys. Rev. Lett. **107**, 026401 (2011), IF=7.62.
2. **D. Tanasković,** V. Dobrosavljević, and E. Miranda, *Spin Liquid Behavior in Electronic Griffiths Phases,* Phys. Rev. Lett. **95**, *167204 (2005),* IF=7.62.
3. S. Nakatsuji, V. Dobrosavljevicć, **D. Tanasković,** M. Minakata, H. Fukazawa, and Y. Maeno, *Mechanism of Hopping Transport in Disordered Mott Insulators ,* Phys. Rev. Lett. **93** , 146401 (2004), IF=7.62.
4. **D. Tanasković**, V. Dobrosavljević, E. Abrahams, and G. Kotliar, *Disorder Screening in Strongly Correlated Systems,* Phys. Rev. Lett. **91**, 066603 (2003), IF=7.62.
5. V. Dobrosavljević, **D. Tanasković,** and A. A. Pastor, *Glassy Behavior of Electrons Near Metal-Insulator Transitions*, Phys. Rev. Lett. 90, 016402 (2003), IF=7.62.

Радови у врхунским међународним часописима (М21)

Радови објављени након претходног избора у звање
1. W. van Gerven Oei, **D. Tanasković,** and R. Žitko, *Magnetic Impurities in Spin-split Superconductors*, Phys. Rev. B **95,** 085115 (2017), doi: 10.1103/PhysRevB.95.085115, ISSN 2469-9969, IF=3.718.
2. M. Opačić, N. Lazarević, M. M. Radonjić, M. Sćepanović, H. Ryu, A. Wang, **D. Tanasković**, C. Petrovic, and Z. V. Popović, *Raman Spectroscopy of $K_x Co_{2-y} Se_2$ Single Crystals Near the Ferromagnet–paramagnet Transition,*J. Phys. Cond. Matt. **28**, 485401 (2016), doi: 10.1088/0953-8984/28/48/485401, ISSN 1361-648X, IF=2.346.
3. H. Braganca, M. C. O. Aguiar, J. Vučičević, **D. Tanasković**, and V. Dobrosavljević, *Anderson Localization Effects Near the Mott Metal-insulator Transition*, Phys. Rev. B **92**, 125143(2015), doi: 10.1103/PhysRevB.92.125143, ISSN 2469-9969, IF=3.767.
4. Z. V. Popović, M. Scepanović, N. Lazarević, M. Opačić, M. M. Radonjić, **D. Tanasković**, H. Lei, and C. Petrovic, *Lattice Dynamics of $BaFe_2X_3(X=S,Se)$ Compounds*, Phys. Rev. B **91**, 064303(2015),doi: 10.1103/PhysRevB.91.064303, ISSN 2469-9969, IF=3.767.
5. Z. V. Popović, M. Scepanović, N. Lazarević, M. M. Radonjić, **D. Tanasković**, H. Lei, and C. Petrovic, Phonon and *Magnetic Dimer Excitations in Fe-based S=2 Spin-ladder Compound*

BaFe2Se2O, Phys. Rev. B **89**, 014301 (2014), doi: 10.1103/PhysRevB.89.014301, ISSN 2469-9969, IF=3.767.

6. J. Vučičević, H. Terletska, **D. Tanasković,** and V. Dobrosavljević, *Finite-temperature Crossover and the Quantum Widom Line Near the Mott Transition*, Phys. Rev. B **88**, 075143(2013), doi: 10.1103/PhysRevB.88.075143, ISSN 2469-9969, IF=3.767.

7. N. Lazarević, M. M. Radonjić, M. Scepanović, H. Lei, **D. Tanasković**, C. Petrovic and Z. V. Popović, *Lattice Dynamics of KNi2Se2*, Phys. Rev. B **87**, 144305 (2013), doi: 10.1103/PhysRevB.87.144305, ISSN 2469-9969, IF=3.767.

Радови објављени између два избора у звање
1. N. Lazarević, M. M. Radonjić, **D. Tanasković**, R. Hu, C. Petrović and Z. V. Popović, *Lattice Dynamics of FeSb2*, J. Phys. Cond. Matt. **24**, 255402 (2012), ISSN 1361-648X, IF=2.546.

Радови објављени пре претходног избора у звање
1. N. Lazarević, M. M. Radonjić, R. Hu, **D. Tanasković**, C. Petrovic, and Z. V. Popović, *Phonon Properties of CoSb2 Single Crystals*, J. Phys. Cond. Matt. **24,** 135402 (2012), IF=2.546.

2. M. M. Radonjić, **D. Tanasković**, V. Dobrosavljević, G. Kotliar, and K. Haule, *Wigner-Mott Scaling of Transport Near the Two-dimensional Metal-insulator Transition,* Phys. Rev. B 85, 085133 (2012) IF=3.774.

3. **D. Tanasković**, K. Haule, G. Kotliar, and V. Dobrosavljević, *Phase diagram, energy scales and nonlocal correlations in the Anderson lattice mode*l, Phys. Rev. B **84**, 115105 (2011), IF=3.774.

4. A. Amaricci, A. Camjayi, K. Haule, G. Kotliar, **D. Tanasković**, and V. Dobrosavljević, *Extended Hubbard model: Charge Ordering and Wigner-Mott transition*, Phys. Rev. B **82**, 155102 (2010), IF=3.774.

5. M. M. Radonjić, **D. Tanasković**, V. Dobrosavljević and K. Haule, *Influence of disorder on incoherent transport near the Mott transition*, Phys. Rev. B **81,** 075118 (2010), IF=3.774.

6. J. Sobota, **D. Tanasković**, and V. Dobrosavljević, *RKKY interactions in the regime of strong localization* , Phys. Rev. B **76** , 245106 (2007), IF=3.77.

7. **D. Tanasković**, E. Miranda, and V. Dobrosavljević, *Effective Model of the Electronic Griffiths Phase*, Phys. Rev. B. **70** , 205108 (2004), IF=3.77.

8. **D. Tanasković,** Radović, and L. Dobrosavljević-Grujić, *Spin paramagnetism in d-wave superconductors*, Phys. Rev. B **62**, 138 (2000), IF=3.77.

Радови у истакнутим међународним часописима (M22)

Радови објављени након претходног избора у звање
1. Z. V. Popović, N. Lazarević, S. Bogdanović, M. M. Radonjić, **D. Tanasković**, R. Hu, H. Lei and C. Petrovic, *Signatures of the Spin-phonon Coupling in Fe_{1+y}Te_{1-x}Se_x Alloys*, Solid State Comm. **193,** 51 (2014), doi: 10.1016/j.ssc.2014.05.025, ISSN 0038-1098, IF=1.897.

2. J. J. Lazarević, S. Uskoković-Marković, M. Jelkic-Stankov, M. M. Radonjić, **D. Tanasković**, N. Lazarević and Z. V. Popović, *Intermolecular and Low-frequency Intramolecular Raman Scattering Study of Racemic Ibuprofen*, Spectroc. Acta Pt. A-Molec. Biomolec. Spectr. **126,** 301 (2014), doi: 10.1016/j.saa.2014.01.135, ISSN 1386-1425, IF=2.353.

Радови објављени пре претходног избора у звање
1. M. Eckstein, M. Kollar, K. Byczuk, D. Vollhardt, N. Blumer, P. v. Dongen, M. H. Radke de Cuba, W. Metzner, **D. Tanasković**, V. Dobrosavljević, G. Kotliar, *Nearest- and next-nearest-neighbor hopping on the Bethe lattice* , Ann. Phys. (Leipzig) **14**, 642 (2005), IF=1.58.

Предавања по позиву са међународних скупова штампана у целини (М31)

Радови објављени пре претходног избора у звање
1. D. Tanaskovic, V. Dobrosavljevic, and E. Miranda, *Spin Liquid Behavior in Electronic Griffiths Phases*, XVII Symposium on Condensed Matter Physics, Vršac, Serbia, 16-20 September 2007.

Предавања по позиву са међународних скупова штампана у изводу (М32)

Радови објављени након претходног избора у звање
1. D. Tanaskovic, J. Vucicevic, and V. Dobrosavljevic, *Mott quantum criticality and bad metal behavior*, The 19th Symposium on Condensed Matter Physics, Belgrade, Serbia, 7–11 September 2015, p. 56).

Саопштења са међународних скупова штампана у изводу (М34)

Радови објављени након претходног избора у звање
1. Tsung-Han Lee, V. Dobrosavljevic, J. Vucicevic, D. Tanaskovic, E. Miranda, Unstable Domain-Wall Solution in the Metal-Mott Insulator Coexisting Regime, APS March Meeting 2015, San Antonio, Texas, USA.

Радови објављени између два избора у звање
1. J. Vučičević, M. Radonjić, D. Tanasković, *Iterative Perturbative Method for a Study of Disordered Strongly Correlated Systems*, HP-SEE User Forum 2012, Belgrade, Serbia.
2. Milos M. Radonjić, N. Lazarević, D.Tanasković, Z. Popović, *Electronic Structure and Lattice Dynamics Calculations of FeSb2 and CoSb2*, HP-SEE User Forum 2012, Belgrade, Serbia

Радови објављени пре претходног избора у звање
1. M. M. Radonjic, D. Tanaskovic, V. Dobrosavljevic, G. Kotliar, and K. Haule, *Wigner-Mott Scaling of Transport Near the Two-dimensional Metal-insulator Transition,* APS March Meeting 2012, Boston, Massachusetts , USA.
2. D. Tanaskovic, K. Haule, G. Kotliar, and V. Dobrosavljevic, *Phase diagram, energy scales and nonlocal correlations in the Anderson lattice mode*l, XVIII Symposium on Condensed Matter Physics – SFKM 2011, Belgrade, Serbia.
3. H. Terletska, J. Vucicevic, D. Tanaskovic, and V. Dobrosavljevic, *Quantum Critical Transport Near he Mott Transition*, XVIII Symposium on Condensed Matter Physics – SFKM 2011, Belgrade, Serbia.
4. M. M. Radonjic, D. Tanaskovic, V. Dobrosavljevic, G. Kotliar, and K. Haule, *Wigner-Mott Scaling of Transport Near the Two-dimensional Metal-insulator Transition*, XVIII Symposium on Condensed Matter Physics – SFKM 2011, Belgrade, Serbia.
5. N. Lazarević, Z. V. Popović, M. Radonjic, D. Tanaskovic, Rongwei Hu, C. Petrovic, Raman Scattering Study Of FeSb2 Single Crystals, XVIII Symposium on Condensed Matter Physics – SFKM 2011, Belgrade, Serbia.
6. D. Tanaskovic, V. Dobrosavljevic, and E. Miranda, *Spin Liquid Behavior in Electronic Griffiths Phases,*APS March Meeting 2004, Montreal, Canada.
7. D. Tanaskovic, E. Miranda, and V. Dobrosavljevic, *Effective Model of the Electronic Griffiths Phase*, APS March Meeting 2004, Montreal, Canada.

8. D. Tanaskovic, V. Dobrosavljevic, E. Abrahams, and G. Kotliar, *Disorder Screening in Strongly Correlated Systems*, APS March Meeting 2003, Austin, Texas , USA.

Одбрањена докторска дисертација (M71)

1. *Anomalous Metallic Behavior in Strongly Correlated Electron Systems with Disorder*, **D. Tanasković**, Florida State University, Tallahassee, Florida, USA (2005).

Одбрањена магистарски рад (M72)

1. *Утицај Паулијевог парамагнетизма на магнетне особине високотемпературних суперпроводника*, **Д. Танасковић**, Физички факултет Универзитета у Београду (2000).

ОБЈАВЉЕНИ РАДОВИ
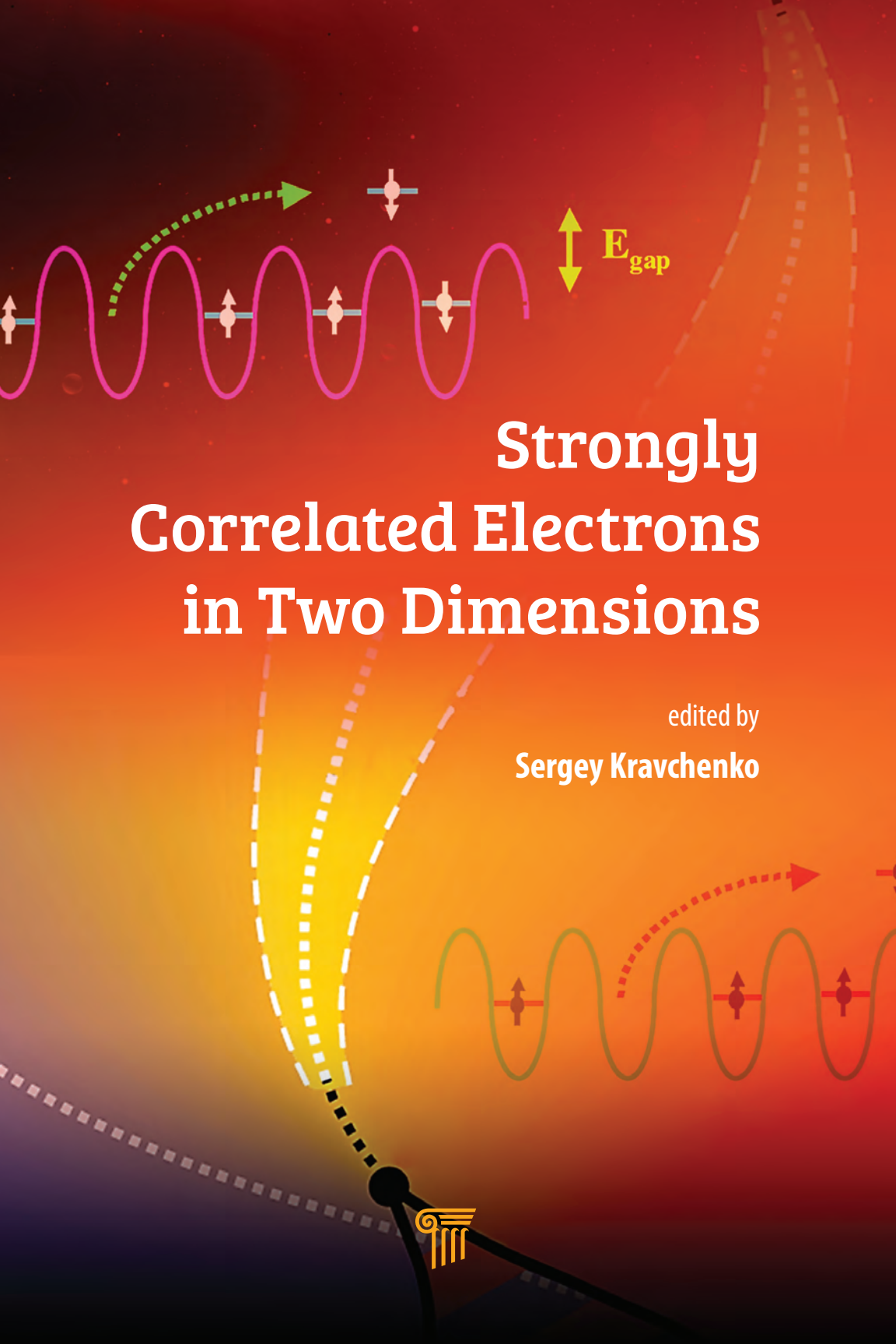
Strongly Correlated Electrons in Two Dimensions

E_{gap}

edited by

Sergey Kravchenko

**Strongly
Correlated Electrons
in Two Dimensions**

Strongly Correlated Electrons in Two Dimensions

edited by

Sergey Kravchenko

Strongly Correlated Electrons in Two Dimensions

Printed in the USA

Contents

Preface

Properties of strongly correlated electrons confined in two dimensions are a forefront area of modern condensed matter physics. Two-dimensional (2D) electron systems can be realized on semiconductor surfaces (metal-insulator-semiconductor structures, heterostructures, quantum wells); other examples include electrons on a surface of liquid helium or a single layer of carbon atoms (graphene). In some of these systems, Coulomb repulsion between electrons is small compared to the kinetic energy of electrons; such systems can be well described by Fermi liquid theory introduced by Landau in 1956. However, when the energy associated with the Coulomb interactions becomes larger (sometimes by orders of magnitude or even more) than the Fermi energy, perturbation theories fail and one may expect novel states of matter to form.

In a zero magnetic field, idealized (noninteracting) 2D electrons were predicted by the "Gang of Four" (Abrahams, Anderson, Licciardello, and Ramakrishnan, 1979) to become localized in the limit of zero temperature, no matter how weak the disorder in the system. Weak interactions between electrons are expected to contribute to the localization (Altshuler, Aronov, and Lee, 1980). Therefore, it came as a surprise when the metallic (delocalized) state and the metal–insulator transition were observed in a 2D electron system formed in low-disordered silicon transistors (Kravchenko et al., 1994). Since then, a tremendous effort has been made, in both theory and experiment, to produce an adequate understanding of the situation; however, a consensus has still not been reached.

In the limit of very strong interactions, electrons are supposed to crystalize into a lattice to minimize their repulsion energy (Wigner, 1934). A classical Wigner crystal has indeed been realized for electrons on the surface of liquid helium. Although indications

exist that Wigner crystallization also occurs in very dilute electron systems on semiconductor surfaces (where the crystal should be quantum), the "smoking-gun evidence" has never been obtained.

These are just two examples of many outstanding unsolved problems in the physics of strong correlations in two dimensions.

This book, intended for advanced graduate students and researches entering the field, contains six chapters. In Chapter 1, a review is given on the recent theoretical work exploring quantum criticality of Mott and Wigner–Mott transitions. The authors argue that the most puzzling features of the experiments find natural and physically transparent interpretations based on this perspective.

Chapter 2 is devoted to experiments on very clean and very dilute 2D electron systems. Experimental results on the metal–insulator transition and related phenomena in such systems are discussed. Special attention is given to recent results for the strongly enhanced spin susceptibility, effective mass, and thermopower in low-disordered silicon transistors.

In Chapter 3, the author shows how spin and isospin degrees of freedom affect low-temperature transport in strongly interacting disordered 2D electron systems and explains experimentally observed temperature and magnetic field dependencies of resistivity in silicon-based systems.

In Chapter 4, recent experimental studies on the Mott transitions of layered organic materials are reviewed with an emphasis on quantum-critical transport. The authors show that in the vicinity of the Mott transition, different kinds of phases emerge, such as antiferromagnetic Mott insulators, quantum spin liquids, Fermi liquids, and unconventional superconductors.

Chapter 5 is a review of experimental results obtained on 2D electron systems with different levels of disorder. In particular, the author shows that sufficiently strong disorder changes the nature of the metal–insulator transition. Comprehensive studies of the charge dynamics are also reviewed, describing evidence that the metal–insulator transition in a 2D electron system in silicon should be viewed as the melting of the Coulomb glass.

Finally, in Chapter 6, a microscopic theory of a strongly correlated 2D electron gas is presented. The authors suggest an explanation of the divergence of the effective electron mass experimentally

observed in silicon-based 2D structures. Possible condensation of fermions in 2D electron systems, closely related to the condensation of bosons in superconductors or in superfluids, is also discussed.

I hope that this book will stimulate further developments in the physics of strongly correlated electrons in two dimensions and lead to many discoveries of yet unforeseen new physics.

Sergey Kravchenko

Chapter 1

Wigner–Mott Quantum Criticality: From 2D-MIT to ³He and Mott Organics

V. Dobrosavljević[a] and D. Tanasković[b]

[a] *Department of Physics and National High Magnetic Field Laboratory, Florida State University, Tallahassee, Florida 32306, USA*
[b] *Scientific Computing Laboratory, Center for the Study of Complex Systems, Institute of Physics Belgrade, University of Belgrade, Pregrevica 118, 11080 Belgrade, Serbia*

vlad@magnet.fsu.edu, tanasko@ipb.ac.rs

Experiments performed over the last 20 years have revealed striking similarities between several two-dimensional (2D) fermion systems, including diluted two-dimensional electron liquids in semiconductors, ³He monolayers, and layered organic charge transfer salts. These experimental results, together with recent theoretical advances, provide compelling evidence that strong electronic correlations—Wigner–Mott physics—dominate the universal features of the corresponding metal–insulator transitions (MITs). Here we review the recent theoretical work exploring quantum criticality of Mott and Wigner–Mott transitions and argue that most puzzling features of the experiments find natural and physically transparent interpretation based on this perspective.

1.1 MIT in the Strong Correlation Era: The Mystery and the Mystique

The key physical difference between metals and insulators is obvious, even at first glance. Its origin, however, has puzzled curious minds since the dark ages of Newton's alchemy (Dobbs, 2002); centuries-long efforts have failed to unravel the mystery. Some basic understanding emerged in the early 1900s with the advent of quantum mechanics, based on the nature of electronic spectra in periodic (crystalline) solids. The corresponding band theory of solids (BTS) [Ashcroft and Mermin, 1976) provided a reasonable description of many features of good metals, such as silver or gold, but also of good insulators, such as germanium and silicon.

From the perspective of the BTS, metals and insulators represent very different phases of matter. On the other hand, the rise of electronic technology, which rapidly accelerated in the second half of the 20th century, demanded the fabrication of materials with properties that can be conveniently tuned from the limit of good metals all the way to poor conductors and even insulators. This requirement is typically satisfied by chemically or otherwise introducing a modest number of electrical carriers into an insulating parent compound, thus reaching an unfamiliar and often puzzling regime. The need to understand the properties of this intermediate metal–insulator transition (MIT) region (Mott, 1990) opened an important new Pandora's box, both from the technological and the basic science perspective.

The fundamental question thus arises: What is the physical nature of the MIT phase transition (Dobrosavljević et al., 2012), and what degrees of freedom play a dominant role in its vicinity? The answer is relatively simple in instances where the MIT is driven by an underlying thermodynamic phase transition to an ordered state. This happens, for example, with onset of antiferromagnetic (AFM) order or charge order (CO), which simply modifies the periodic potential experienced by the mobile electrons, and the BTS picture suffices (Slater, 1951). Here, the MIT can simply be regarded as an experimental manifestation of the emerging order, reflecting the static symmetry change of the given material.

The situation is much more interesting in instances where the MIT is not accompanied with some incipient order. Here, the physical reason for a sharp MIT must reside beyond the BTS description, involving either strong electron–electron interactions (Mott, 1949) or disorder (Anderson, 1958). The interplay of both effects proves difficult to theoretically analyze, although considerable effort has been invested, especially within Fermi liquid (FL) (weakly interacting) approaches at weak disorder (Lee and Ramakrishnan, 1985; Finkel'stein, 1983, 1984). More recent work found evidence that disorder may even more significantly modify the properties of strongly correlated metals, sometimes leading to "non-Fermi liquid" metallic behavior (Miranda and Dobrosavljevic, 2005). In any case, the MIT problem in presence of both strong electron–electron interactions and disorder is still far from being fully understood despite recent advances (Dobrosavljević et al., 2012).

On physical grounds, however, one may expect that in specific materials either the correlations or the disorder may dominate, so a simpler theory may suffice. In this chapter we shall not discuss many of the interesting experimental systems where the MIT problem has been investigated so far; a comprehensive overview is given in the chapter by D. Popović. Instead, we shall focus on three specific classes of low-disorder materials showing remarkable similarities in their phenomenology. Our story begins with a short overview of the key experimental features observed in ultraclean diluted two-dimensional electron gases (2DEGs) in semiconductors, displaying the so-called two-dimensional metal–insulator transition (2D-MIT) in a zero magnetic field. Next, we review experiments where very similar behavior is observed for ^{3}He monolayers and also in quasi-2D organic charge transfer salts of the κ-family, both of which are believed to represent model systems displaying the Mott (interaction-driven) MIT. Finally, we provide a direct comparison between these experimental findings and recent theoretical results for interaction-driven (Mott and Wigner–Mott) MITs in absence of disorder. Our message is that the Mott picture represents the dominant physical mechanism in all these systems and should be regarded as the proper starting point for the study of related materials with stronger disorder.

1.2 Phenomenology of 2D-MIT in the Ultraclean Limit

2DEG devices in semiconductors have been studied for almost 50 years since the pivotal 2DEG discovery in 1966 (Fowler et al., 1966). Because they served as basis for most modern electronics, 2DEG systems have been very carefully studied and characterized (Ando et al., 1982) from the materials point of view, allowing the fabrication of ultrahigh-mobility materials by the 1990s. However, their use as an ideal model system for the study of MIT has been recognized relatively late, with the pioneering work of Sergey Kravchenko and collaborators (Kravchenko et al., 1995). The reason was the long-held belief that all electronic states remain localized at $T = 0$, even in the presence of infinitesimally weak disorder, based on the influential scaling theory of localization (Abrahams et al., 1979). This result—the absence of a sharp MIT in two dimensions—was firmly established only for models of noninteracting electrons with disorder, and although even early results on interacting models (Finkel'stein, 1983, 1984) suggested otherwise, Kravchenko's initial work was initially met with extraordinary skepticism and disbelief (Altshuler et al., 2001).

Soon enough, however, clear evidence of a sharp 2D-MIT in high-mobility silicon was confirmed on IBM samples (the original material Kravchenko used came from Russia), with almost identical results (Popović et al., 1997). This marked the beginning of a new era; the late 1990s witnessed a veritable avalanche of experimental and theoretical work on the subject, giving rise to much controversy and debate. This article will not discuss all the interesting results obtained in different regimes, many of which are reviewed in the chapter by D. Popović in this volume. Our focus here will be on documenting evidence that strong electronic correlations—and not disorder—represent the main driving force for 2D-MIT in high-mobility samples. In the following sections, we follow the historical development of the field, with emphasis on those experimental signatures that emerge as robust and rather universal features of interaction-driven MITs in a variety of systems.
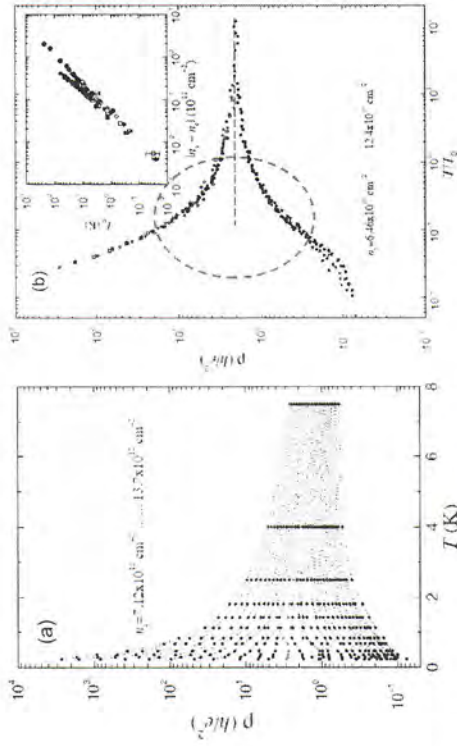
Figure 1.1 (a) Resistivity curves (left panel) for a high-mobility 2DEG in silicon (Kravchenko et al., 1995). (b) Scaling behavior is found over a comparable temperature range. The remarkable mirror symmetry (Simonian et al., 1997a; Dobrosavljević et al., 1997) of the scaling curves (indicated by the dashed oval) seems to hold over more than an order of magnitude for the resistivity ratio. Reprinted (figure) with permission from [Kravchenko, S. V., Mason, W. E., Bowker, G. E., Furneaux, J. E., Pudalov, V. M., and D'Iorio, M. (1995). *Phys. Rev. B* **51**, p. 7038.] Copyright (1995) by the American Physical Society.

1.2.1 Finite-Temperature Transport

2DEG devices provide a very convenient setup for the study of MITs because one can readily control the carrier density in a single device. Thus one easily obtains an entire family of resistivity curves, covering a broad interval of densities and temperatures. Typical results for a high-mobility 2DEG in silicon are shown in Fig. 1.1a, showing a dramatic metal–insulator crossover as the density is reduced below $n_c \approx 10^{11}$ cm^{-2}.

One can observe a rather weak temperature dependence of the resistivity around the critical density (shown as a dashed oval in Fig. 1.1a), with much stronger metallic (insulating) behavior at higher (lower) densities. Note that the system has "made up its mind" whether to be a metal or an insulator even at, relatively speaking, surprisingly high temperatures $T \approx T_F \approx 10$ K. This behavior

should be contrasted to that typical of good metals such as silver or gold, where at accessible temperatures $T \ll T_F \approx 10^4$ K. Physically, this means that for 2D-MIT the physical processes relevant for localization already kick in at relatively high temperatures. Here, the system can no longer be regarded as a degenerate electron liquid with dilute elementary excitations. In contrast, simple estimates show (Abrahams et al., 2001) that around the critical density, the characteristic Coulomb energy (temperature) $T_{Coul} \approx 10 \, T_F \approx$ 100 K. Clearly, the transition occurs in the regime where Coulomb interactions dominate over all other energy scales in the problem. We should also mention that in the Kelvin range, there essentially are no phonons in silicon (Ando et al., 1982).

We conclude that in the relevant temperature regime, transport should be dominated by inelastic electron–electron scattering, not the impurity-induced (Anderson) localization of quasiparticles, as described by disordered FL theories of Finkel'stein and followers (Finkel'stein, 1983, 1984; Punnoose and Finkel'stein, 2001). As illustrated schematically in Fig. 1.2, transport in this incoherent regime has a very different character than in the coherent "diffusive" regime found in good metals with disorder. Incoherent transport dominated by inelastic electron–electron scattering is typical of systems featuring strong electronic correlations, such as heavy-fermion compounds (Stewart, 1984) or transition metal oxides (TMOs) (Goodenough, 1963) close to the Mott (interaction-driven) MIT (Mott, 1990). Understanding this physical regime requires not only a different set theoretical tools but also an entirely different conceptual picture of electron dynamics. As we shall explain next, modern dynamical mean-field theory (DMFT) methods (Georges et al., 1996) make it possible to qualitatively and even quantitatively explain most universal features within this incoherent transport regime dominated by strong correlation effects.

1.2.2 Scaling Phenomenology and Its Interpretation

There is no doubt that dramatic changes of transport arise in a narrow density range around $n \approx n_c$, but this alone is not enough to mark the existence of a second-order (continuous) phase transition. In particular, all known classical (Goldenfeld, 1992)
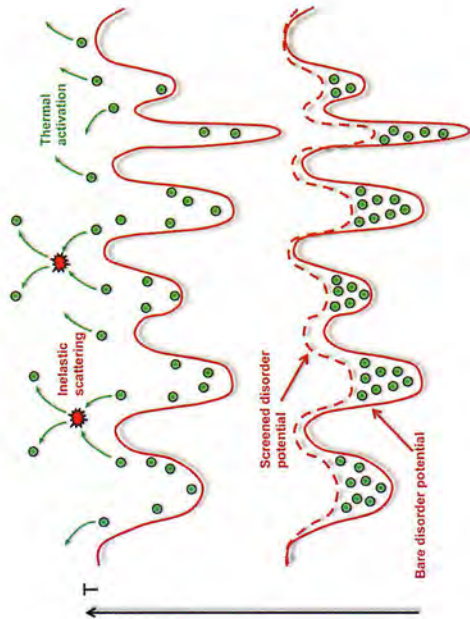
Figure 1.2 In the disordered Fermi liquid picture, the leading low-temperature dependence of transport reflects elastic scattering off a renormalized but temperature-dependent random potential (dashed line). At low temperatures (bottom), the potential wells "fill up" with electrons; in the presence of repulsive (Coulomb) interactions, the screened (renormalized) potential has reduced amplitude (dashed line), leading to effectively weaker disorder. As the temperature increases (top), electrons thermally activate (shown by arrows) out of the potential wells, reducing the screening effect. This physical mechanism, which operates both in the ballistic and in the diffusive regime (Zala et al., 2001), is at the origin of all "quantum corrections" found within the FL picture (Lee and Ramakrishnan, 1985). It is dominant, provided that inelastic electron–electron scattering can be ignored. While this approximation is well justified in good metals, inelastic scattering (star symbol) is considerably enhanced in the presence of strong correlation effects, often leading to disorder-driven non-Fermi liquid behavior (Miranda and Dobrosavljevic, 2005) and electronic Griffiths phases (Andrade et al., 2009).

and even quantum (Sachdev, 2011) critical points also display the characteristic scaling phenomenology. In the case of MITs, one expects (Dobrosavljević et al., 2012) that the resistivity assumes the following scaling form as a function of the reduced density $\delta_n = (n - n_c)/n_c$ and temperature

$$\rho^*(\delta_n, T) = \rho(\delta_n, T)/\rho(\delta_n = 0, T) = F(T/T_o(\delta_n)), \qquad (1.1)$$

where $\rho^*(T) = \rho(\delta_n, T)/\rho(\delta_n = 0, T)$ is the reduced resistivity and $T_o(\delta_n) \approx \delta_n^{\nu z}$ is the corresponding crossover temperature. While

similar families of resistivity curves were reported earlier; a big breakthrough for 2D-MIT occurred when Kravchenko demonstrated (Kravchenko et al., 1995) precisely such scaling behavior, providing strong evidence of quantum-critical (QC) behavior expected at a sharply defined $T = 0$ MIT point. It should be stressed, though, that such scaling behavior must arise at any quantum phase transition (QPT), but this alone does not provide direct insight into its physical content or mechanism.

On the other hand, soon after the discovery of 2D-MIT, another interesting feature was noticed (Simonian et al., 1997a), which is not necessarily expected to hold for any general QPT. By carefully examining the form of the relevant scaling function (see Fig. 1.1b), one observes a remarkable mirror symmetry of the two branches such that

$$\rho^*(\delta_n, T) \approx \sigma^*(-\delta_n, T) = [\rho^*(-\delta_n, T)]^{-1}, \qquad (1.2)$$

which was found to hold within the entire QC region, for example, at $T > T_o(\delta)$. In practical terms, this means that in the corresponding QC regime the resistivity assumes a stretched-exponential form

$$\rho(\delta_n, T) \approx \exp\{A\delta_n/T^x\}, \qquad (1.3)$$

where A is a constant and $x = 1/\nu z$. Such exponentially strong temperature dependence is not surprising on the insulating side, where it obtains from activated or hopping transport (Shklovskii and Efros, 1984). In contrast, such inverse activation behavior is highly unusual on the metallic side, where it reflects the dramatic drop of resistivity at low temperatures, at densities just above the transition.

A plausible physical interpretation was quickly proposed (Dobrosavljević et al., 1997) soon after the experimental discovery, based on general scaling considerations. It emphasized that such stretched-exponential form for the relevant scaling function should be interpreted as a signature of strong coupling behavior. Physically, it indicates that the critical region is more akin to the insulating than to the metallic phase. This observation, while having purely phenomenological character, emphasized the key question that one should focus on: the clue to the nature of 2D-MIT should be contained in understanding the physical nature of the insulating state. Is the insulating behavior essentially the result of impurities
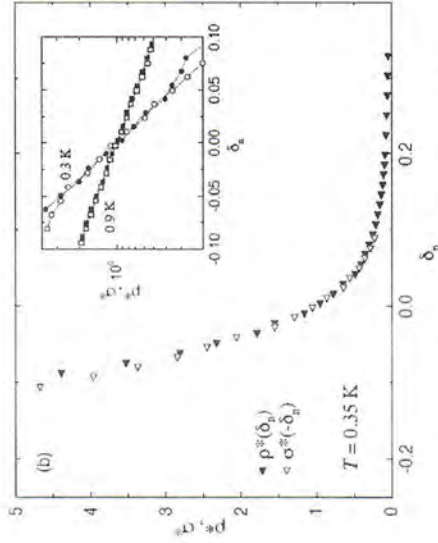
Figure 1.3 Experimental data (Simonian et al., 1997a) displaying mirror symmetry. The inset shows the same data on a semilogarithmic scale, emphasizing linear density dependence of ln ρ consistent with Eq. 1.3, that is, the stretched-exponential phenomenology (Dobrosavljević et al., 1997). Reprinted (figure) with permission from [Simonian, D., Kravchenko, S. V., and Sarachik, M. P. (1997a). *Phys. Rev. B* **55**, p. R13421.] Copyright (1997a) by the American Physical Society.

trapping the mobile electrons, or is the electron–electron repulsion preventing them to move around? If the correlation effects—and not disorder—represent the dominant physical mechanism for localization in other systems, then all the scaling features observed in the 2DEG should again be found. Remarkably, this is exactly what is observed (see later) in very recent experiments on organic Mott systems (Furukawa et al., 2015).

1.2.3 Resistivity Maxima in the Metallic Phase

The QC resistivity scaling has been observed close to the critical density, but other interesting features are also found further out on the metallic side. Here, especially in the cleanest samples, one observes increasingly pronounced resistivity maxima at temperatures $T = T_{\max}(\delta)$, which decrease as the transition is approached. Remarkably, the family of curves displaying such maxima persists even relatively deep inside the metallic phase, far outside the critical
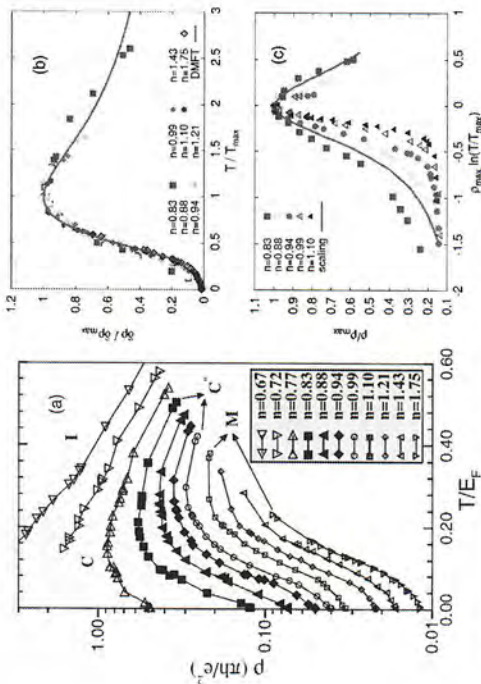
Figure 1.4 (a) Resistivity as a function of temperature from the experiments on a 2DEG in silicon (Pudalov et al., 1998). Only data points indicated by full black symbols have been estimated to lie in the diffusive (coherent) regime, while all metallic curves have an almost identical shape. (b) Same data scaled according to the procedure based on the Wigner–Mott (disorder-free) picture (Radonjić et al., 2010). (c) The scaling procedure based on the disorder-screening scenario (Punnoose and Finkel'stein, 2001) does not produce a convincing collapse. In both scaling plots, the full line is the result of the respective theoretical calculations. Reprinted (figures) with permission from [Radonjić, M. M., Tanasković, D., Dobrosavljević, V., Haule, K., and Kotliar, G. (2012). *Phys. Rev. B* **85**, p. 085133.] Copyright (2012) by the American Physical Society.

region. However, even a quick glance at the experimental data (Fig. 1.4) reveals that all such curves have essentially the same qualitative shape and only differ by the density-dependent values of T_{max} and $\rho_{max} = \rho(T_{max})$.

While this phenomenology is clearly seen, its origin is all but obvious, since resistivity maxima can arise in many unrelated situations. One possibility is the competition of two different disorder-screening mechanisms, as envisioned within the Finkel'stein picture of a disordered FL (Punnoose and Finkel'stein, 2001). However, this mechanism applies (as the authors themselves pointed out) only within the disorder-dominated diffusive regime, which is confined to low temperatures and sufficiently strong impurity scattering. According to reasonable estimates (Punnoose and Finkel'stein,

2001) for the experiment of Fig. 1.4, this picture should only apply to the three curves (full black symbols) close to the critical density, and completely different physics should kick in deeper in the metallic regime (open symbols). This seems unreasonable, since the experimental curves show very similar form at all metallic densities. The key test of these ideas, therefore, should be to examine different materials with strong correlations and weaker disorder; where most of the relevant temperature range is well outside the diffusive regime. If the resistivity maxima, with similar features, persist in such systems, their origin must be of a completely different nature than the disorder-screening mechanism described by the disordered FL picture.

A related issue is the origin of the pronounced resistivity drop at $T < T_{max}$, which can be as large as 1 order of magnitude. Here again very different theoretical interpretations have been proposed, which may or may not apply in a broad class of systems. One issue is the role of impurities (Punnoose and Finkel'stein, 2001), which may be addressed by experimentally examining materials with weak or negligible amounts of disorder. Another curious viewpoint is that of Kivelson and Spivak (Jamei et al., 2005), who proposed that the microscopic phase coexistence (bubble and/or stripe phases) between the Wigner crystal and an FL may explain this behavior, even in the absence of disorder. This possibility may be relevant in some regimes, but certainly not in lattice systems such as heavy-fermion compounds, or systems displaying the (interaction-induced) Mott transition in the absence of any significant disorder:

1.2.4 Effect of Parallel Magnetic Fields

One of the most important clues about 2D-MIT has been obtained soon following its discovery, from studies of magnetotransport. While much of the traditional work on 2DEG systems focuses on the role of perpendicular magnetic fields and the associated quantum Hall regime, for 2D-MIT the application of magnetic fields parallel to the 2D layer sheds important new light. It was found (Simonian et al., 1997b) that the application of parallel magnetic fields can dramatically suppress (Fig. 1.5) the resistivity maxima and the pronounced low-temperature resistivity drop on the metallic side of the transition. This finding is significant because parallel fields
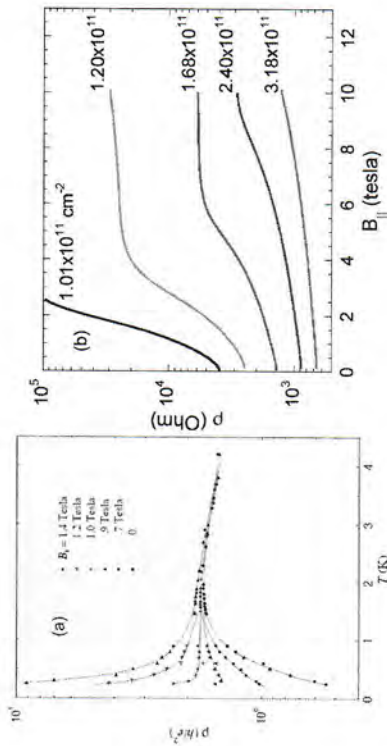
Figure 1.5 (a) Resistivity versus temperature for five different fixed magnetic fields applied parallel to the plane of a low-disordered silicon MOSFET. Here $n = 8.83 \times 10^{10}$ cm^{-2}. Reprinted (figure) with permission from [Simonian, D., Kravchenko, S. V., Sarachik, M. P., and Pudalov, V. M. (1997b). *Phys. Rev. Lett.* **79**, p. 2304.] Copyright (1997b) by the American Physical Society. (b) Low-temperature magnetoresistance as a function of parallel magnetic field at different electron densities above n_c. Reprinted (figure) with permission from [Shashkin, A. A., Kravchenko, S. V., Dolgopolov, V. T., and Klapwijk, T. M. (2001). *Phys. Rev. Lett.* **87**, p. 086801.] Copyright (2001) by the American Physical Society.

couple only to the electron spin (Zeeman splitting), not to the orbital motion of the electron. It points to the important role of spin degrees of freedom in stabilizing the metallic phase.

An interesting fundamental issue relates to the precise role of Zeeman splitting on the ground state of a 2DEG. Is an infinitesimally small value of the parallel field sufficient to suppress the true metal at $T = 0$, or is there a field-driven MIT at some finite value of the parallel field? This important question was initially a subject of much controversy, but careful experimental investigation at ultralow temperatures has established (Shashkin et al., 2001; Eng et al., 2002) the existence of a field-driven MIT (Fig. 1.6) at a finite parallel field but only within a density range close to the $B = 0$ MIT. Interestingly, this field-driven transition appears to belong to a different universality class (Eng et al., 2002) than the zero-field transition (see also the chapter by D. Popović), somewhat similar to what happens in bulk doped semiconductors (Sarachik, 1995).
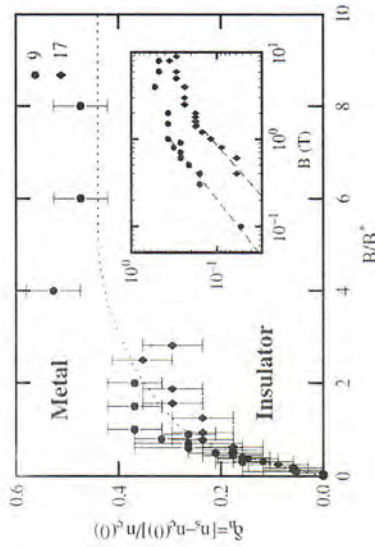
Figure 1.6 Phase diagram for a high-mobility 2DEG in silicon (Eng et al., 2002) as a function of electron density and the parallel magnetic field. The field-driven MIT is found only in the narrow density range $0 < \delta_n < 0.4$, close to the $B = 0$ critical density. Reprinted (figure) with permission from [Eng, K., Feng, X. G., Popović, D., and Washburn, S. (2002). *Phys. Rev. Lett.* **88**, p. 136402.] Copyright (2002) by the American Physical Society.

1.2.5 Thermodynamic Response

The early evidence for the existence of 2D-MIT relied on scaling features of transport in a zero magnetic field (Abrahams et al., 2001), but despite the obvious beauty and elegance of the data, some people (Altshuler et al., 2001) remained skeptical and unconvinced. Complementary insight was therefore of crucial importance, and in the last 15 years this sparked a flurry of experimental work focusing on a thermodynamic response. A detailed account of this large and impressive body of work has been given elsewhere (Kravchenko and Sarachik, 2004); it is also covered in the chapter by Shashkin and Kravchenko. Several outstanding features have been established by these experiments, as follows.

(1) The spin susceptibility is strongly enhanced at low temperatures, and it seems to evolve (Prus et al., 2003) from a Pauli-like form at higher densities (typical for metals) to a Curie-like form (expected for localized magnetic moments) as the transition is approached. This result indicates that most electrons convert into spin-1/2 localized magnetic moments within the insulating state.
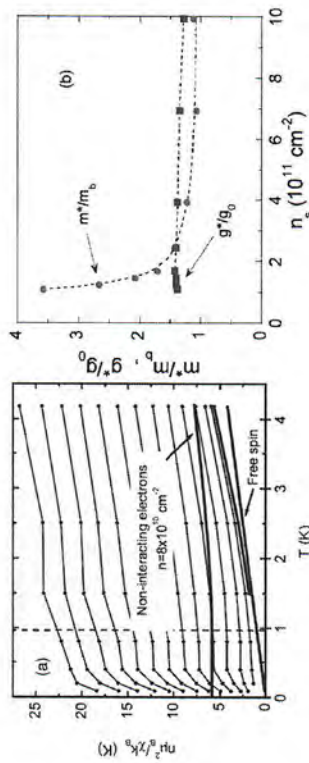
Figure 1.7 (a) Inverse spin susceptibility normalized per carrier, as obtained from magnetocapacitance experiments (Prus et al., 2003). Experimental curves from bottom to top correspond to densities $0.8 - 6 \times 10^{11}$ cm^{-2} in 4×10^{10} cm^{-2} steps. The thick straight line marks the Curie law (slope given by the Bohr magneton), and the dashed line marks $T = (g_B/k_B)0.7T$. Reprinted (figure) with permission from [Prus, O., Yaish, Y., Reznikov, M., Sivan, U., and Pudalov, V. (2003). *Phys. Rev. B* **67**, p. 205407.] Copyright (2003) by the American Physical Society. (b) Renormalization of the effective mass (dots) and the g-factor (squares), as a function of electron density. Reprinted (figure) with permission from [Shashkin, A. A., Kravchenko, S. V., Dolgopolov, V. T., and Klapwijk, T. M. (2002). *Phys. Rev. B* **66**, p. 073303.] Copyright (2002) by the American Physical Society.

(2) Various complementary experimental methods have firmly established (Kravchenko and Sarachik, 2004) pronounced interaction-induced enhancement of the (quasiparticle) effective mass m^*, which appears to linearly diverge at $n = n_c$. In contrast, the corresponding g-factor does not display any significant renormalization. This important observation rules out incipient ferromagnetism as a possible origin of enhanced spin susceptibility. Instead, it points to local magnetic moment formation within the insulating regime. These earlier findings were recently confirmed by spectacular thermopower measurements, where values of m^*/m as large as 25 were reported [Mokashi et al., 2012].

(3) The vast majority of the relevant experiments in this category have been performed within the ballistic regime. This is significant because the predictions of the disordered FL picture of Finkel'stein (Punnoose and Finkel'stein, 2001) apply only

Figure 1.8 In a Mott insulator, each electron resides in a bound electronic state, forming a spin-1/2 local magnetic moment. The lowest energy charge excitation costs an energy comparable to the on-site Coulomb repulsion U.
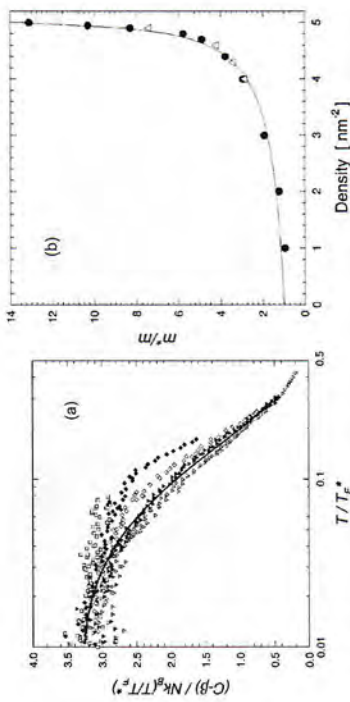
within the diffusive regime and thus cannot provide any insight into the origin of these thermodynamic anomalies.

(4) All these thermodynamic signatures are best seen in the cleanest samples, and they display surprisingly weak dependence on the sample mobility (level of disorder). This again points to strong correlations as the dominant mechanism in this regime.

1.3 Comparison to Conventional Mott Systems

Experiments on 2DEG systems have firmly suggested that 2D-MIT should best be viewed as an interaction-driven MIT, where the insulator consists of localized magnetic moments. To put these ideas in perspective, it is useful to compare these findings to the properties of other 2D systems known to display the Mott (interaction-driven) MIT (Mott, 1949, 1990).

Mott insulators often display some form of magnetic order at low temperatures, but in contrast to the band picture (Slater, 1934), their insulating nature is not tied down to magnetic order. Indeed, a substantial gap in charge transport is typically seen even at temperatures much higher than the magnetic ordering temperature. Such a QPT (Dobrosavljević et al., 2012) between a paramagnetic FL metal and a paramagnetic Mott insulator—the "pure" Mott transition—is our main focus here. In particular, we shall focus on two specific examples of the broad family of Mott materials, where

The associated solidification transition has long been viewed as a realization of the Mott MIT. Many of its low-temperature properties, on the fluid side, can be described (Vollhardt, 1984) by the variational solution of the Hubbard model based on the Gutzwiller approximation (Brinkman and Rice, 1970), predicting the divergence of the effective mass as

$$m^*/m \approx (P_c - P)^{-1}. \qquad (1.4)$$

However, similarly as in most other freezing transitions, bulk ^{3}He displays a rather robust first-order solidification phase transition associated with the emergence of ferromagnetic (FM) order within the crystalline phase. Consequently, one is able to observe only a restricted range of m^* values, making it difficult to compare to theory. Despite these limitations, many qualitative and even quantitative features can be understood from this perspective, including the findings that application of strong magnetic fields may trigger the destruction of the FL state (Vollhardt, 1984) and the associated field-induced solidification of ^{3}He.

More recent work by Saunders and collaborators (Casey et al., 2003) has focused on ^{3}He fluid monolayers placed on graphite, where again one can study the approach to the Mott transition by controlling hydrostatic pressure. Most remarkably, the first-order jump at solidification is then suppressed, presumably because the solid ^{3}He monolayer on graphite displays no magnetic order down to $T = 0$. Instead, nonmagnetic spin liquid behavior is found within the solid phase, due to important ring exchange processes in this 2D triangular lattice (Misguich et al., 1998). The corresponding Mott transition is found to be of second order, with rather spectacular agreement with the Brinkmann–Rice (BR) theory for the m^* divergence. According to FL theory (Pines and Nozières, 1965), the Sommerfeld coefficient $\gamma = C/T \approx m^*$ depends only on the effective mass, while the spin susceptibility $\chi \approx m^*/(1 + F_0^a) = m^* g^*$ also involves the (renormalized) g-factor. This is significant because the behavior of the g-factor distinguishes the BR (Mott) transition from an FM instability, although χ diverges in both instances. Namely, g^* is expected to diverge at the FM transition (Pines and Nozières, 1965), while it should remain constant at the BR point (Vollhardt, 1984).

Figure 1.9 Approaching the Mott transition in ^{3}He monolayers on graphite. (a) Reduced fluid heat capacity as a function of reduced temperature, showing emergence of a Fermi liquid at low temperatures. Here $T_F^* = T_F(m^*/m)$ is the quasiparticle Fermi temperature. (b) Effective mass ratio as a function of ^{3}He fluid density inferred from heat capacity (full circle) and magnetization (open triangles), showing apparent divergence. The fact that both quantities display the same critical behavior indicates that $g^* \approx$ const. Reprinted (figure) with permission from [Casey, A., Patel, H., Nyˊeki, J., Cowan, B. P., and Saunders, J. (2003). *Phys. Rev. Lett.* **90**, p. 115301.] Copyright (2003) by the American Physical Society.

it proved possible to experimentally study several features with striking similarity to the behavior found in a 2DEG displaying 2D-MIT.

1.3.1 Mott Transition in ^{3}He Monolayers on Graphite

The ^{3}He liquid consists of charge-neutral spin-1/2 atoms with Fermi statistics; its normal phase at ambient pressure is often regarded as a model system for a strongly correlated FL (Vollhardt, 1984). This includes significant enhancements of the specific heat and the spin susceptibility, reflecting the emergence of heavy quasiparticles (Pines and Nozières, 1965), as first predicted by Landau (Landau, 1957). ^{3}He will solidify under increasing hydrostatic pressure, due to strong interatomic repulsion at short distances. Each spin-1/2 He^3 atom then sits on a different lattice site, thus forming a Mott insulator:

To address this important issue, it suffices to determine both m^* and g^* or, equivalently, to measure both γ and χ. Precisely such an analysis was carried out for ^{3}He monolayers (Casey et al., 2003), where an m^* enhancement as large as 15 was reported, while g^* was found to remain constant in the critical region and assume a value close to the BR prediction. This finding is strikingly similar to what is observed in analogous studies (Kravchenko and Sarachik, 2004) for ultraclean 2DEG systems close to 2D-MIT; it suggests that both phenomena may have a common physical origin: the behavior of a strongly correlated FL in the proximity of the Mott insulating phase.

Transport properties are more difficult to probe in ^{3}He, because its charge neutrality precludes direct coupling of electric fields to density currents. One cannot, therefore, easily compare its transport properties to that of 2DEG systems in order to further test the Mott picture. To do this, we next turn to other classes of canonical Mott systems where recent work has provided important insights. Over the last 30 years, many studies of the Mott transition have focused on various TMOs (Goodenough, 1963), especially after the discovery of high-temperature superconductivity in the late 1980s. These materials, however, are notorious for displaying all kinds of problems in material preparation and sample growth and often contain substantial amounts of impurities and defects. Another class of systems where better sample quality is somewhat easier to obtain is the so-called organic Mott systems, which we discuss next.

1.3.2 Mott Organics

The organic Mott systems have emerged, over 30 years, as a very popular set of materials for the study of the Mott MIT: These are organic charge transfer salts consisting of a quasi-2D lattice of rather large organic molecules, with typically a single molecular orbital close to the Fermi energy. Since the intermolecular overlap of such orbitals is typically modest, these crystals usually have very narrow electronic bands with substantial intraorbital (on-site) Coulomb repulsion and hence are well described by 2D single-band Hubbard-type models (Powell and McKenzie, 2011).

There exist two general families of organic Mott crystals, the κ-family, corresponding to a half-filled Hubbard model, and the
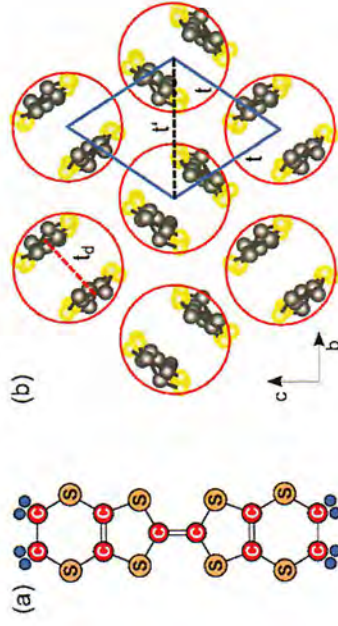
Figure 1.10 Sketch of the BEDT-TTF molecule (Elsässer et al., 2012). For κ-(BEDT-TTF)$_2$X, the molecules are arranged in dimers, which constitute an anisotropic triangular lattice within the conduction layer. Reprinted (figure) with permission from [Elsässer, S., Wu, D., Dressel, M., and Schlueter, J. A. (2012). *Phys. Rev. B* **86**, p. 155150.] Copyright (2012) by the American Physical Society.

θ-family, corresponding to quarter filling. The former class is particularly useful for the study of the bandwidth-driven Mott transition at half filling, since the electronic bandwidth can be conveniently tuned via hydrostatic pressure. A notable feature of these materials is a substantial amount of magnetic frustration, due to nearly isotropic triangular lattices formed by the organic molecules within each 2D layer. As a result, several members of this family (such as κ-(BEDT-TTF)$_2$Cu$_2$(CN)$_3$) display no magnetic order down to the lowest accessible temperatures, while others (such as κ-(BEDT-TTF)$_2$Cu[N(CN)$_2$]Cl) feature an AFM order in the insulating phase. Another important property of these materials is the excellent quality of crystals, with very little disorder, making the dominance of strong correlation effects obvious in all phenomena observed.

On the metallic side, in all these materials display well characterized FL behavior, with substantial effective mass enhancements, similarly to other Mott systems. In contrast to the conventional QC scenario, however, here the phase diagram features a first-order MIT and the associated coexistence region, terminating at the critical end point $T = T_c$. Still, as emphasized in recent theoretical (Terletska et al., 2011) and experimental (Furukawa et al., 2015) work, the
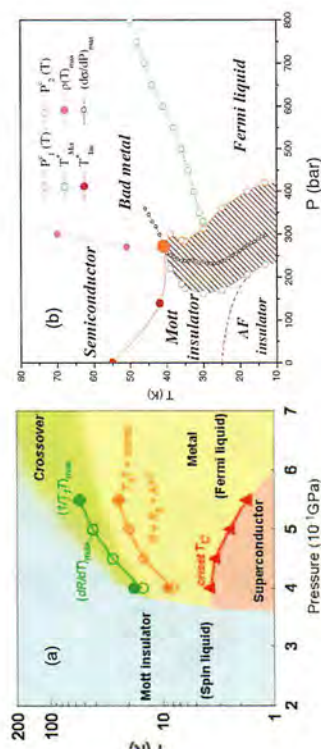
Figure 1.11 Phase diagrams of (a) κ-(BEDT-TTF)$_2$Cu$_2$(CN)$_3$ displaying no magnetic order. Reprinted (figure) with permission from [Kurosaki, Y., Shimizu, Y., Miyagawa, K., Kanoda, K., and Saito, G. (2005). *Phys. Rev. Lett.* **95**, p. 177001.] Copyright (2005) by the American Physical Society. and (b) κ-(BEDT-TTF)$_2$Cu[N(CN)$_2$]Cl featuring an AFM order (Limelette et al., 2003) on the insulating side. Reprinted (figure) with permission from [Limelette, P., Wzietek, P., Florens, S., Georges, A., Costi, T. A., Pasquier, C., Jerome, D., Meziere, C., and Batail, P. (2003). *Phys. Rev. Lett.* **91**, p. 016401.] Copyright (2003) by the American Physical Society.

temperature range associated with this Mott coexistence region is typically very small ($T_c \approx 20$–40 K) in comparison to the Coulomb interaction or the (bare) Fermi temperature ($T_F \approx 2000$ K). Note that the comparable temperature range in 2DEG systems would be extremely small, viz., $T < 10^{-2} T_F \approx 0.1$ K, while most experimental results (especially those obtained in the ballistic regime) correspond to much higher temperatures.

We should emphasize that different materials in this class display various magnetic or even superconducting orders within the low-temperature regime $T < T_c$ (Fig. 1.11), which strongly depend on material details, such as the precise amount of magnetic frustration. In contrast, the behavior above the coexistence dome is found to be remarkably universal, featuring very similar behavior in all compounds. Here, one finds a smooth crossover between an FL metal and a Mott insulator, displaying a family of resistivity curves with a general form very similar to those found in 2DEG systems close to 2D-MIT, in a temperature range comparable to a fraction of T_F. In addition to a fan-like shape at high temperatures, we note the existence of resistivity maxima on the metallic side, which become
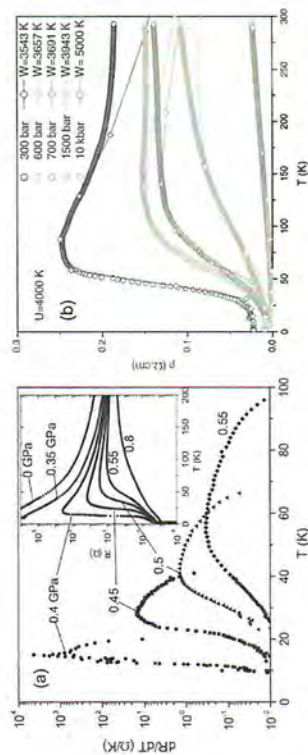
Figure 1.12 Transport in Mott organic materials. (a) κ-(BEDT-TTF)$_2$Cu$_2$(CN)$_3$. Reprinted (figure) with permission from [Kurosaki, Y., Shimizu, Y., Miyagawa, K., Kanoda, K., and Saito, G. (2005). *Phys. Rev. Lett.* **95**, p. 177001.] Copyright (2005) by the American Physical Society. (b) κ-(BEDT-TTF)$_2$Cu[N(CN)$_2$]Cl. The lines are obtained from DMFT. Reprinted (figure) with permission from [Limelette, P., Wzietek, P., Florens, S., Georges, A., Costi, T. A., Pasquier, C., Jerome, D., Meziere, C., and Batail, P. (2003). *Phys. Rev. Lett.* **91**, p. 016401.] Copyright (2003) by the American Physical Society.

more pronounced closer to the transition, precisely as in many 2DEG examples.

In addition, very recent experimental work (Furukawa et al., 2015) performed a careful scaling analysis of the resistivity data in the high-temperature region ($T > T_c$), providing clear and convincing evidence of QC behavior associated with the Mott point. The analysis was performed on three different materials (including two compounds discussed above), featuring very different magnet ground states (AFM order *vs.* spin liquid behavior) on the insulating side. Nevertheless, the scaling analysis succeeded in extracting the universal aspects of transport in this QC regime, finding impressive universality (Fig. 1.13) both in the form of the corresponding scaling function and in the values of the critical exponents, with excellent agreement with earlier DMFT predictions (Terletska et al., 2011).

Most remarkably, the experimentally determined scaling functions display precisely the same mirror symmetry as earlier found on 2DEG systems (Simonian et al., 1997a), with exactly the stretched-exponential form proposed by phenomenological scaling theory (Dobrosavljević et al., 1997). Given the fact that 2DEG systems and these organic Mott crystals have completely different
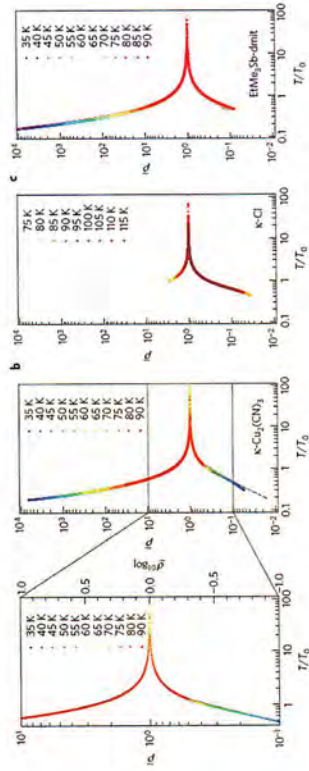
Figure 1.13 Quantum-critical scaling of the resistivity curves for three different organic Mott materials, demonstrating (Furukawa et al., 2015) universal behavior insensitive to a low-temperature magnetic order. Reprinted by permission from Macmillan Publishers Ltd: [*Nature Physics*] (Furukawa, T., Miyagawa, K., Taniguchi, H., Kato, R., and Kanoda, K. (2015). *Nat. Phys.* **11**, pp. 221–224), copyright (2015).

microscopic character; these experimental findings provide direct and clear evidence of a surprisingly robust universality of the QC behavior in interaction-driven MITs. If one and the same basic physical processes—Mott localization—indeed dominate all these phenomena, then one can hope that even a theory based on simple models may account for the main trends.

1.4 Theory of Interaction-Driven MITs

Interaction-driven MITs in the absence of static symmetry breaking—the Mott transition—have first proposed (Mott, 1949) as a possible mechanism in doped semiconductors. Soon enough, it became apparent that they are the right physical picture for many systems at the brink of magnetism, for example, various TMOs (Mott, 1990; Goodenough, 1963). Such systems are typically characterized by a narrow valence band close to half filling, with a substantial on-site (intra-orbital) Coulomb interaction U. The simplest generic model describing this situation is the single-band Hubbard model given by the Hamiltonian

$$H = -t \sum_{\langle ij \rangle \sigma} c_{i\sigma}^\dagger c_{j\sigma} + U \sum_i n_{i\uparrow} n_{i\downarrow}. \tag{1.5}$$

Here, t is the hopping amplitude, $c_{i\sigma}^\dagger$ ($c_{j\sigma}$) are the creation (annihilation) operators, $n_i = n_{i\uparrow} + n_{i\downarrow}$ is the occupation number operator on site i, and U is the on-site Coulomb interaction.

Theoretical investigations of the Hubbard model go back to the pioneering investigations in the early 1960s (Hubbard, 1963) when it already became clear that, even in the absence of any magnetic order, a Hubbard–Mott gap will open for a sufficiently large U/t. Approaching the transition from the metallic side was predicted (Brinkman and Rice, 1970) to result in substantial effective mass enhancement as a precursor of the Mott transition, as confirmed in numerous TMOs and other materials. A reliable description of the transition region, however, remained elusive for many years. Still, the existence a broad class of Mott insulators, containing localized magnetic moments, has long been regarded as being well established (Goodenough, 1963).

1.4.1 The DMFT Approach

Modern theories of Mott systems were sparked by the discovery of high-temperature superconductors in the late 1980s, which triggered considerable renewed interest in the physics of TMOs and related materials. A veritable zoo of physical ideas and theoretical approaches was put forward, but few survived the test of time. Among those, DMFT (Georges et al., 1996) proved to be the most useful, reliable, and flexible tool, applicable both in modeling
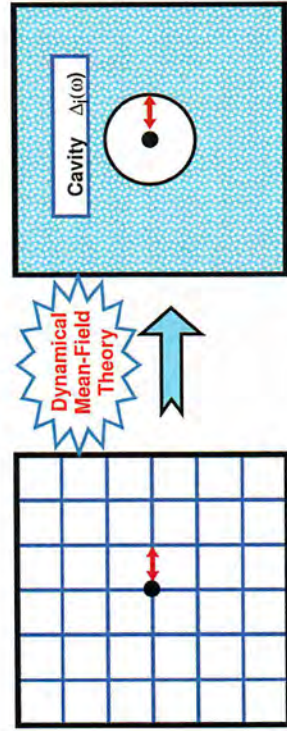
Figure 1.14 In dynamical mean-field theory, the environment of a given site is represented by an effective medium represented by its cavity spectral function $\Delta_i(\omega)$.

Hamiltonians but also in first-principles theories (Kotliar et al., 2006) of correlated matter.

In its simplest (single-site) implementation, DMFT provides a local approximation for many-body corrections in strongly interacting systems. The central quantity it self-consistently calculates is the single-particle self-energy $\Sigma_i(\omega, T)$, which is obtained within a local approximation. Its real part describes the interaction (or temperature) dependence of the electronic spectra, allowing substantial narrowing of the quantum phase (QP) bandwidth (i.e., the effective mass m^* enhancement) and the eventual opening of the Mott gap. Its imaginary part, on the other hand, describes electron–electron (inelastic) scattering processes, leading to the ultimate destruction of the coherent QPs at sufficiently large T or U.

Most importantly, DMFT does not suffer from limitations of standard FL approaches, which are largely restricted to situations with dilute QPs (i.e., the lowest temperatures). In fact, DMFT is most reliable at high temperatures, within the incoherent regime (with large inelastic scattering), where its local approximation becomes essentially exact. Indeed, systematic (nonlocal) corrections to single-site DMFT have established (Tanasković et al., 2011) that there exists, in general, a well-defined crossover temperature scale $T^*(U)$, above which the nonlocal corrections are negligibly small. This scale is typically much smaller than the basic energy scale of the problem (e.g., the bandwidth or the interaction U), so DMFT often proves surprisingly accurate over much of the experimentally relevant temperature range.

Another important aspect of the DMFT approach deserves special emphasis. In contrast to conventional (Slater-like) theories focusing on effects of various incipient orders, DMFT focuses on dynamical correlation effects unrelated to orders. From the technical perspective, its local character suppresses the spatial correlations associated with magnetic, charge, or structural correlations. Physically, such an approximation becomes accurate in presence of sufficiently strong frustration effects due to competing interactions or competing orders, a situation that is typical for most correlated electronic systems. Frustration effects generally lead to a dramatic proliferation of low-lying excited states, which further invalidates the conventional FL picture of dilute elementary excitations; this

situation demands an accurate description of incoherent transport regimes—precisely what is provided by DMFT.

Historically, since its discovery more than 20 years ago, DMFT has been applied to many models and various physical systems. Recent developments have also included the application to inhomogeneous electronic systems in the presence of disorder and were able to incorporate the relevant physical processes such as Anderson localization and even the glassy freezing of electrons (the description of quantum Coulomb glasses). These interesting developments have been reviewed elsewhere (Dobrosavljević et al., 2012; Miranda and Dobrosavljević, 2005) but will not be discussed here. In the following, we briefly review the key physical results of DMFT when applied to the simplest model of a Mott transition at half filling and the associated Wigner–Mott transition away from half filling.

1.4.2 The Mott Transition

Many insulating materials have an odd number of electrons per unit cell; thus band theory would predict them to be metals—in contrast to experiments. Such compounds (e.g., TMOs) often have AFM ground states, leading Slater to propose that spin density wave formation (Slater, 1951) is likely at the origin of the insulating behavior. This mechanism does not require any substantial modification of the band theory picture, since the insulating state is viewed as a consequence of a band gap opening at the Fermi surface.

According to Slater (Slater, 1951), such insulating behavior should disappear above the Neel temperature, which is typically in the 10^2 K range. Most remarkably, in most AFM oxides, clear signatures of insulating behavior persist at temperatures well above any magnetic ordering, essentially ruling out Slater's weak coupling picture.

What goes on in such cases was first clarified in early works by Mott (Mott, 1949) and Hubbard (Hubbard, 1963), tracing the insulating behavior to strong Coulomb repulsion between electrons occupying the same orbital. When the lattice has integer filling per unit cell, then electrons can be mobile only if they have enough
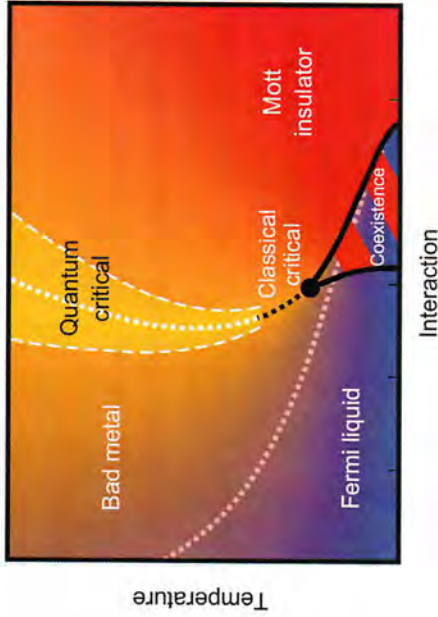
Figure 1.15 Phase diagram of the half-filled Hubbard model calculated from DMFT. At very low temperatures $T < T_c \lesssim 0.03T_F$ the Fermi liquid and the Mott insulating phases are separated by a first-order transition line and the associated coexistence region. Very recent work (Terletska et al., 2011; Vučičević et al., 2013, 2015) has established that in a very broad intermediate-temperature region $T_c < T < T_F$, one finds characteristic metal–insulator crossover behavior showing all features expected of quantum criticality. Reprinted (figure) with permission from [Vučičević, J., Terletska, H., Tanasković, D., and Dobrosavljević, V. (2013). *Phys. Rev. B* **88**, p. 075143.] Copyright (2013) by the American Physical Society.

kinetic energy ($E_K \approx t$) to overcome the Coulomb energy U. In the narrow band limit of $t \ll U$, the electrons do not have enough kinetic energy, and a gap opens in the single-particle excitation spectrum, leading to Mott insulating behavior. This gap $E_g \approx U - B$ (here $B \approx 2zt$ is the electronic bandwidth; z being the lattice coordination number) is the energy an electron has to pay to overcome the Coulomb repulsion and leave the lattice site.

In the ground state, each lattice site is singly occupied, and the electron occupying it behaves as a spin-1/2 local magnetic moment. These local moments typically interact through magnetic superexchange interactions (Anderson, 1959) of the order $J \approx t^2/U$, leading to magnetic ordering at temperatures of the order T. The insulating behavior, however, is not caused by magnetic ordering and typically persists all the way to temperatures $T \approx E_g \gg T_J$.

In oxides, $E_g \approx 10^3$–10^4 K is typically on the atomic (eV) scale, while magnetic ordering emerges at temperatures roughly an order of magnitude lower $T_J \approx 100$–300 K.

1.4.3 Correlated Metallic State

An important step in elucidating the approach to the Mott transition from the metallic side was provided by the pioneering work of Brinkmann and Rice (Brinkman and Rice, 1970). This work, which was motivated by experiments on the normal phase of ^{3}He (Vollhardt, 1984), predicted a strong effective mass enhancement close to the Mott transition. In the original formulation, as well as in its subsequent elaborations (slave boson mean-field theory (Kotliar and Ruckenstein, 1986), DMFT (Georges et al., 1996), the effective mass is predicted to continuously diverge as the Mott transition is approached from the metallic side

$$\frac{m^*}{m} \approx (U_c - U)^{-1}. \tag{1.6}$$

A corresponding coherence (effective Fermi) temperature

$$T^* \approx T_F/m^* \tag{1.7}$$

is predicted above which the quasiparticles are destroyed by thermal fluctuations. As a result, one predicts (e.g., within DMFT) a large resistivity increase around the coherence temperature and a crossover to insulating (activated) behavior at higher temperatures. Because the low-temperature FL is a spin singlet state, a modest magnetic field of the order

$$B^* \approx T^* \approx (m^*)^{-1} \tag{1.8}$$

is expected to also destabilize such a correlated metal and lead to a large and positive magnetoresistance. Note that both T^* and B^* are predicted to continuously vanish as the Mott transition is approached from the metallic side, due to the corresponding m^* divergence. Precisely such behavior is found in all the three classes of physical systems we discussed above.

1.4.4 Effective Mass Enhancement

How should we physically interpret the large effective mass enhancement which is seen in all these systems? What determines its magnitude if it does not actually diverge at the transition? An answer to this important question can be given using a simple thermodynamic argument which does not rely on any particular microscopic theory or a specific model. In the following section, we present this simple argument for the case of a clean FL, although its physical context is, of course, much more general.

In any clean FL (Pines and Nozières, 1965) the low-temperature specific heat assumes the leading form

$$C(T) = \gamma T + \cdots, \tag{1.9}$$

where the Sommerfeld coefficient

$$\gamma \approx m^*. \tag{1.10}$$

In the strongly correlated limit ($m^*/m \gg 1$) this behavior is expected only at $T \lesssim T^* \approx (m^*)^{-1}$, while the specific heat should drop to much smaller values at higher temperatures where the quasiparticles are destroyed. Such behavior is indeed observed in many systems showing appreciable mass enhancements.

On the other hand, from general thermodynamic principles, we can express the entropy as

$$S(T) = \int_0^T dT \frac{C(T)}{T}. \tag{1.11}$$

Using the above expressions for the specific heat, we can estimate the entropy around the coherence temperature

$$S(T^*) \approx \gamma T^* \approx O(1). \tag{1.12}$$

The leading effective mass dependence of the Sommerfeld coefficient γ and that of the coherence temperature T^* cancel out!

Let us now explore the consequences of the assumed (or approximate) effective mass divergence at the Mott transition. As $m^* \to \infty$, the coherence temperature $T^* \to 0+$, resulting in large residual entropy

$$S(T \to 0+) \approx O(1). \tag{1.13}$$

We conclude that the effective mass divergence indicates the approach to a phase with finite residual entropy!

Does not this result violate the third law of thermodynamics? And how can it be related to the physical picture of the Mott transition? The answer is, in fact, very simple. Within the Mott insulating phase the Coulomb repulsion confines the electrons to individual lattice sites, turning them into spin-1/2 localized magnetic moments. To the extend that we can ignore the exchange interactions between these spins, the Mott insulator can be viewed as a collection of free spins with large residual entropy $S(0+) = R \ln 2$. This is precisely what happens within the BR picture; similar results are obtained from DMFT, a result that proves exact in the limit of large lattice coordination (Georges et al., 1996).

In reality, the exchange interactions between localized spins always exist, and they generally lift the ground-state degeneracy, restoring the third Law. This happens below a low-temperature scale T_J, which measures the effective dispersion of intersite magnetic correlations (Moeller et al., 1999; Park et al., 2008) emerging from such exchange interactions. In practice, this magnetic correlation temperature T_J can be very low, either due to effects of geometric frustration or due to additional ring exchange processes which lead to competing magnetic interactions. Such a situation is found both in organic Mott systems, and for 2D Wigner crystals, where the insulating state corresponds to a geometrically frustrated triangular lattice. In addition, numerical calculations by Ceperley and others (Cândido et al., 2004) have established that for 2D Wigner crystals significant ring exchange processes indeed provide additional strong frustration effects, further weakening the intersite spin correlation effects.

We conclude that the effective mass enhancement, whenever observed in experiment, indicates the approach to a phase where large amounts of entropy persist down to very low temperatures. Such situations very naturally occur in the vicinity of the Mott transition, since the formation of local magnetic moments on the insulating side gives rise to large amounts of spin entropy being released at very modest temperatures. A similar situation is routinely found (Stewart, 1984; Flouquet, 2005; Hewson, 1993) in the so-called heavy-fermion compounds (e.g., rare-earth intermetallics)
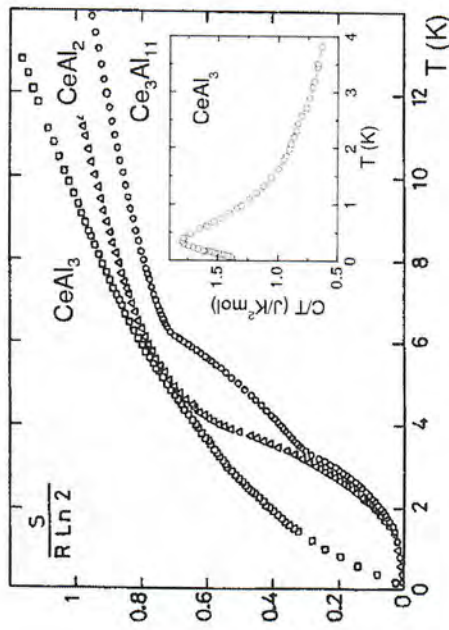
Figure 1.16 Temperature dependence of entropy extracted from specific heat (inset) experiments (Flouquet, 2005) on several heavy-fermion materials. Essentially the entire doublet entropy $S = R \ln 2$ is recovered by the time the temperature has reached $T^* \approx 10$ K, consistent with a large mass enhancement $m^* \approx 1/T^*$. Reprinted from Flouquet, J., Lasjaunias, J. C., Peyrard, J., and Ribault, M. (1982). *J. Appl. Phys.* **53**, pp. 2127–2130. With the permission from AIP Publishing.

featuring huge effective mass enhancements. Here, local magnetic moments coexist with conduction electrons giving rise to the Kondo effect, which sets the scale for the FL coherence temperature $T^* \approx 1/m^*$, above which the entire free spin entropy $S(T^*) \approx R \ln 2$ is recovered (Fig. 1.16). This entropic argument is, in turn, often used to experimentally prove the very existence of localized magnetic moments within a metallic host.

We should mention that other mechanisms of effective mass enhancement have also been considered. General arguments (Millis, 1993) indicate that m^* can diverge when approaching a quantum-critical point (QCP) corresponding to some (magnetically or charge) long-range ordered state. This effect is, however, expected only below an appropriate upper critical dimension (Sachdev, 2011), reflecting an anomalous dimension of the incipient ordered state. In addition, this is a mechanism dominated by long-wavelength order-parameter fluctuations and is thus expected to contribute only a

small amount of entropy per degree of freedom in contrast to local moment formation.

It is interesting to mention that weak coupling approaches, such as the popular on-shell interpretation of the random phase approximation (RPA) (Ting et al., 1975), often result in inaccurate or even misleading predictions (Zhang and Das Sarma, 2005) for the effective mass enhancement behavior. Indeed, more accurate modern theories such as DMFT can be used (Dobrosavljević et al., 2012) to benchmark these and other weak coupling theories and to reveal the origin of the pathologies resulting from their inappropriate applications to strong coupling situations.

1.4.5 Resistivity Maxima

Within the strongly correlated regime close to the Mott transition, transport is carried by heavy quasiparticles. As temperature increases, inelastic electron–electron scattering kicks in, leading to a rapid increase of resistivity with temperature. Within FL theory, this gives rise to the temperature dependence of the form $\rho(T) \approx AT^2$, with $A \approx (m^*)^2$ according to the Kadowaki–Woods law (Hewson, 1993). Such behavior is indeed observed in most known correlated system, in agreement with DMFT predictions (Jacko et al., 2009). This argument makes it clear that increasingly strong temperature dependence emerges in the correlated regime, but it does not tell us what happens above the corresponding QP coherence temperature $T^* \approx 1/m^*$.

In this regime inaccessible to conventional FL theories, DMFT provided an illuminating answer (Radonjić et al., 2012). It described the thermal destruction of QPs, and the consequent opening of a Mott pseudogap at $T > T^*$, leading to resistivity maxima. While much of the earlier DMFT work focussed on the low-T regime, more recent advances (Gull et al., 2011) in quantum Monte Carlo methods (needed to solve the DMFT equations) allowed a careful and precise characterization of this transport regime. One finds a family of curves displaying pronounced resistivity maxima with increasing height at temperatures that decrease close to the transition.

These curves all assume essentially the same functional form (Fig. 1.17) and therefore can all be collapsed on a single scaling
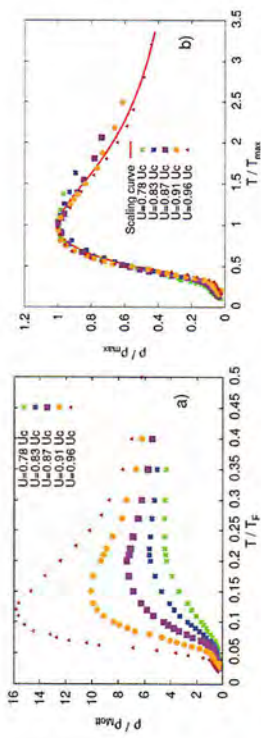
Figure 1.17 (a) Resistivity maxima in the strongly correlated metallic regime of a half-filled Hubbard model within DMFT (Radonjić et al., 2012). (b) Scaling collapse of the resistivity maxima. Reprinted (figure) with permission from [Radonjić, M. M., Tanasković, D., Dobrosavljević, V., Haule, K., and Kotliar, G. (2012). *Phys. Rev. B* **85**, p. 085133.] Copyright (2012) by the American Physical Society.

function by rescaling the temperature with that of the resistivity maximum T_{max} and the resistivity with its maximum value ρ_{max}. From these numerical results one can extract a universal scaling function describing the entire family of curves (as shown by the thick red line in Fig. 1.17). A direct comparison can now be made with data obtained from experiments on a 2DEG in silicon close to 2D-MIT; one finds surprisingly good agreement between theory and experiment, with no adjustable parameters (see Fig. 1.4). Similar data are found also from experiments on Mott organics and other conventional Mott systems, where successful comparison with DMFT has already been established (Radonjić et al., 2010; Limelette et al., 2003).

Further comparison between experiment and theory is obtained by plotting T_{max} vs. m^*, where both quantities can be independently obtained both from DMFT and from 2DEG experiments. Here we express T_{max} in units of the Fermi temperature and m^* in the units of the known band mass in order to perform a comparison with no adjustable parameters. Again, one finds excellent agreement between DMFT and experiments, giving

$$T_{max}/T_F \approx 0.7(m/m^*), \tag{1.14}$$

where even the numerical prefactor close to 0.7 is obtained in both cases.

A clear physical understanding of the Mott transition within DMFT, together with spectacular agreement between DMFT and
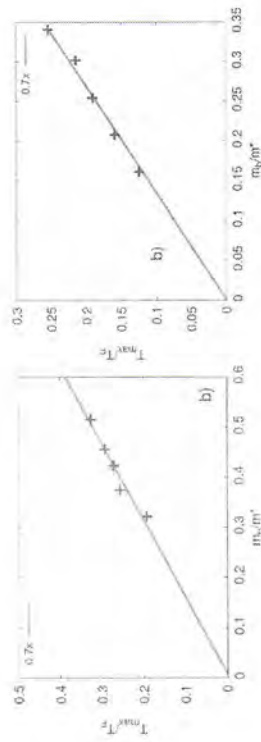
Figure 1.18 Dependence of T_{max} on m^* from (a) DMFT and (b) experiments on a 2DEG close to 2D-MIT. Reprinted (figure) with permission from [Radonjić, M. M., Tanasković, D., Dobrosavljević, V., Haule, K., and Kotliar, G. (2012). *Phys. Rev. B* **85**, p. 085133.] Copyright (2012) by the American Physical Society.

2DEG experiments, paints a convincing and transparent picture of the mechanism for the resistivity maxima, as follows:

- Heavy quasiparticles that exist near the Mott transition are characterized by a small coherence temperature $T^* \approx 1/m^*$.
- Given that both theory and experiments find $T_{max} \approx 1/m^*$, we can directly identify the resistivity maxima with the thermal destruction of heavy quasiparticles.
- The above physical picture is not only well established within DMFT but is also well documented in all strongly correlated electronic systems such as various TMO materials, organic Mott systems, and even heavy-fermion compounds.
- The complete thermal destruction of quasiparticles around $T \approx T_{max}$ is a physical picture completely different than the situation described by the disordered FL scenario (Punnoose and Finkel'stein, 2001), which does not even provide a good data collapse. In this scenario, the relevant quasiparticle regime extends both below and above T_{max}, and the maxima result from the competition of two different elastic (but temperature-dependent) scattering mechanisms (Zala et al., 2001).
- We have seen that, both in DMFT and in all known Mott systems, the metal–insulator coexistence region does exist close to the MIT, but it remains confined to very low

temperatures, typically 2 orders of magnitude smaller than the Fermi energy or the Coulomb repulsion U.

- The resistivity maxima, in contrast, are found at much higher temperatures, typically as high as a 10%–20% of the Fermi temperature. This feature is clearly found both in DMFT, in all conventional Mott systems, but also in 2DEG materials close to 2D-MIT.

- In contrast to DMFT and the known behavior of many conventional Mott systems, the phase separation scenario proposed by Kivelson and Spivak (Jamei et al., 2005) can hold only within the metal–insulator coexistence region. It therefore appears very unconvincing as a possible mechanism behind the resistivity maxima found in 2DEG systems.

1.4.6 Quantum Criticality and Scaling

What is the physical nature of the Mott transition? The physical picture of Brinkmann and Rice (Brinkman and Rice, 1970) makes it plausible that the Mott transition should be viewed as a QCP, since the characteristic energy scale of the correlated FL $T^* \approx T_F/m^*$ continuously decreases as the transition is approached. On the other hand, the Mott transition discussed here describes the opening of a correlation-induced spectral gap in the absence of magnetic ordering, that is, within the paramagnetic phase. Such a phase transition is not associated with spontaneous symmetry breaking associated with any static order parameter. Why should the phase transition then have any second-order (continuous) character at all?

More insight into this fundamental question followed the development of DMFT methods (Georges et al., 1996), which extended the BR theory to include incoherent (inelastic) processes at finite temperature. According to this formulation, the Mott transition does assume first-order character with the associated metal–insulator coexistence dome. However, this is found only below the very low critical end-point temperature $T_c \approx 0.02 T_F$, and a smooth crossover behavior arises in the very broad intermediate-temperature interval $T_c < T < T_F$. Precisely the same features for the Mott transition
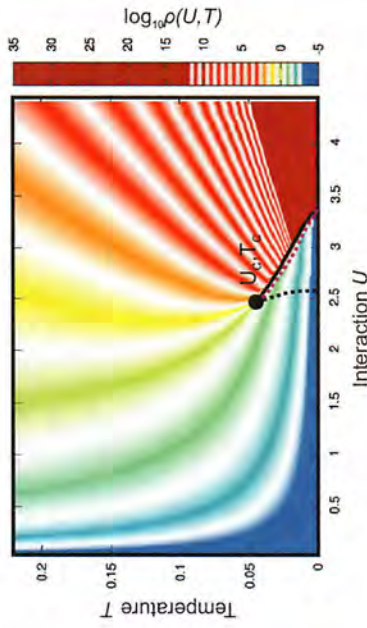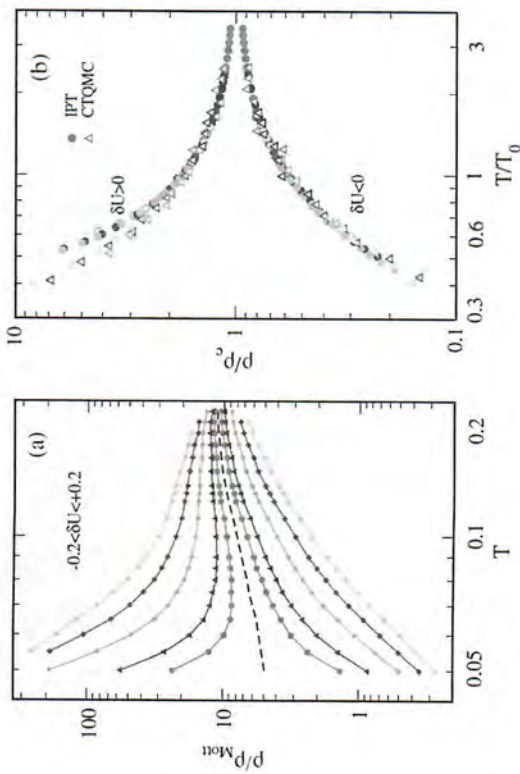
Figure 1.19 Color-coded plot of resistivity across the DMFT phase diagram of a half-filled Hubbard model. Reprinted (figure) with permission from [Vučičević, J., Terletska, H., Tanasković, D., and Dobrosavljević, V. (2013). *Phys. Rev. B* **88**, p. 075143.] Copyright (2013) by the American Physical Society.

phase diagram are found, not only in many TMO materials, but also in Mott organics we discussed above.

A visually striking illustration of what happens in the intermediate-temperature range is seen by color-coding the resistivity across the DMFT phase diagram (Vučičević et al., 2013), where each white band indicates another order of magnitude in resistivity. If one ignores the low-temperature coexistence region, one immediately notices a fan-like shape of the constant resistivity lines, characteristic of what is generally expected (Sachdev, 2011) for quantum criticality. Given the fact that the coexistence dome is a very small energy feature, one should consider the Mott transition as having weakly first-order (WFO) character. At WFO points, which are well known in standard critical phenomena (Goldenfeld, 1992), the transition assumes a first-order character only very close to the critical point; further away, the behavior is precisely that of a conventional second-order phase transition, including all aspects of the scaling phenomenology.

In the case of MITs, the QCP is expected (Dobrosavljević et al., 2012) to occur at $T = 0$. Therefore, if a QPT assumes WFO character, as we find here, we still expect to observe all features of quantum criticality in a broad intermediate-temperature region above the

transition was first carried out a few years ago (Terletska et al., 2011), revealing compelling evidence of QC behavior. Follow-up work further established that such QC behavior is a robust feature of the Mott point both at half filling (Vučičević et al., 2013) and for doping-driven Mott transitions (Vučičević et al., 2015). The latter result also provided important new insight into the origin of the so-called "bad metal" (linear resistivity) behavior in a doped Mott insulator, a long-time puzzle (Emery and Kivelson, 1995) in the field of correlated electrons.

The discovery of the Mott QC regime within DMFT (Terletska et al., 2011) was directly motivated by the pioneering works on 2D-MIT (Kravchenko et al., 1995; Popović et al., 1997), which first revealed intriguing features of QC scaling near the MIT. The results obtained from DMFT presented surprising similarity to the experiment, both in identifying previously overlooked scaling behavior in interaction-driven MITs without disorder and in producing microscopic underpinning for early scaling phenomenology (Dobrosavljević et al., 1997) for the mirror symmetry. Still, this model calculation, based on the single-band Hubbard model at half filling, should really not be viewed as an accurate description of dilute 2DEG systems, where the experiments have been performed.

In contrast, organic Mott systems of the κ-family should be considered (Powell and McKenzie, 2011) as a much more faithful realization of the half-filled Hubbard model. This notion stimulated further experimental investigation, following the 2011 theoretical discovery, focusing on the previously overlooked intermediate-temperature region $T_c < T < T_F$. The experiments took several years of very careful work on several different materials in this family, but the results published by 2015 provided (Furukawa et al., 2015) spectacular confirmation of the DMFT theoretical predictions.

1.4.6.1 Is Wigner crystallization a Mott transition in disguise?

The original ideas of Mott (Mott, 1949), who thought about doped semiconductors, envisioned electrons hopping between well-localized atomic orbitals corresponding to donor ions. In other Mott systems, such as TMOs, the electrons travel between the atomic

Figure 1.20 Scaling behavior of the resistivity curves in the quantum-critical region of the Mott transition at half filling, as obtained from DMFT (Terletska et al., 2011). Note the remarkable mirror symmetry of the corresponding scaling function, as experimentally found both in 2DEG systems near 2D-MIT (Simonian et al., 1997a) and also in very recent experiments in Mott organics (Furukawa et al., 2015). Reprinted (figure) with permission from [Terletska, H., Vučičević, J., Tanasković, D., and Dobrosavljević, V. (2011). Phys. Rev. Lett. **107**, p. 026401.] Copyright (2011) by the American Physical Society.

coexistence dome. Similar situations are not uncommon in general QC phenomena (Sachdev, 2011), since the immediate vicinity of many QCPs is often masked by the dome of an appropriate ordered state induced by critical fluctuations.

If these ideas are correct, then an appropriate scaling analysis should be able to reveal the expected QC scaling of the resistivity curves in a broad intermediate-temperature range $T_c < T < T_F$. To perform such an analysis, one needs to follow a judiciously chosen trajectory across the phase diagram, corresponding to the center of the QC region. Such a trajectory—the so-called Widom line—was identified a long time ago (Widom, 1965) in the context of conventional (thermal) critical phenomena. Directly applying these standard scaling procedures to the DMFT description of the Mott

orbitals of the appropriate transition metal ions. In all these cases, the Coulomb repulsion restricts the occupation of such localized orbitals, leading to the Mott insulating state, but it does not provide the essential mechanism for the formation of such tightly bound electronic states. The atomic orbitals in all these examples result from the (partially screened) ionic potential within the crystal lattice.

The situation is more interesting if one considers an idealized situation describing an interacting electron gas in the absence of any periodic (or random) lattice potential due to ions. Such a physical situation is achieved, for example, when dilute carriers are injected in a semiconductor quantum well (Ando et al., 1982), where all the effects of the crystal lattice can be treated within the effective mass approximation (Ashcroft and Mermin, 1976). This picture is valid if the Fermi wavelength of the electron is much longer then the lattice spacing and the quantum mechanical dynamics of the Bloch electron can be reduced to that of a free itinerant particle with a band mass m_b. In such situations, the only potential energy in the problem corresponds to the Coulomb repulsion E_C between the electrons, which is the dominant energy scale in low-carrier-density systems. At the lowest densities, $E_C \gg E_F$, and the electrons form a Wigner crystal lattice (Wigner, 1934) to minimize the Coulomb repulsion.

Here, each electron is confined not by an ionic potential but by the formation of a deep potential well produced by repulsion from other electrons. The same mechanism prevents double occupation of such localized orbitals, and each electron in the Wigner lattice reduces to a localized $S = 1/2$ localized magnetic moment. A Wigner crystal is therefore nothing but a magnetic insulator: a Mott insulator in disguise. At higher densities, the Fermi energy becomes sufficiently large to overcome the Coulomb repulsion, and the Wigner lattice melts (Tanatar and Ceperley, 1989). The electrons then form an FL. The quantum melting of a Wigner crystal is therefore a metal–insulator transition, perhaps in many ways similar to a conventional Mott transition. What kind of phase transition is this? Despite years of effort, this important question is still not fully resolved.

What degrees of freedom play the leading role in destabilizing the Wigner crystal as it melts? Even in absence of an accepted and detailed theoretical picture describing this transition, we may immediately identify two possible classes of elementary excitations which potentially contribute to melting, as follows:

(1) *Collective charge excitations* (elastic deformations) of the Wigner crystal. In the quantum limit, these excitations have a bosonic character, but they persist and play an important role even in the semiclassical ($k_B T \gg E_F$) limit, where they contribute to the thermal melting of the Wigner lattice (Thouless, 1978). They clearly dominate in the quantum Hall regime (Chen et al., 2006), where both the spin degrees of freedom and the kinetic energy are suppressed due to Landau quantization. But for 2D-MIT in a zero magnetic field, these degrees of freedom may not be so important.

(2) *Single-particle excitations* leading to vacancy interstitial pair formation (Fig. 1.21). These excitations have a fermionic character, where the spin degrees of freedom play an important role. Recent quantum Monte Carlo simulations indicate (Cândido et al., 2001) that the effective gap for vacancy interstitial pair formation seems to collapse precisely around the quantum melting of the Wigner crystal. If these excitation dominate, then quantum melting of the Wigner crystal is a process very similar to the Mott MIT and may be expected to produce a strongly correlated FL on the metallic side. This physical picture is the central idea of this article.
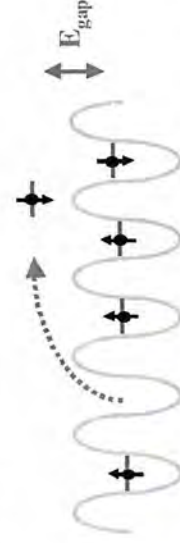
Figure 1.21 In a Wigner crystal, each electron is confined to a potential well produced by Coulomb repulsion from neighboring electrons, forming a spin-1/2 local moment. The lowest-energy particle hole excitation creates a vacancy interstitial pair (Cândido et al., 2001), which costs an energy E_{gap} comparable to the Coulomb repulsion.

We should mention, however, that the Wigner crystal melting in a zero magnetic field is believed (Tanatar and Ceperley, 1989) to be a WFO phase transition. Conventional (e.g., liquid-gas or liquid-crystal) first-order transitions are normally associated with a density discontinuity and global phase separation within the coexistence dome. For charged systems, however, global phase separation is precluded by charge neutrality (Gor'kov and Sokol, 1987). In this case, one may expect the emergence of various modulated intermediate phases, leading to bubble or stripe (Jamei et al., 2005) or possibly even stripe glass (Schmalian and Wolynes, 2000; Mahmoudian et al., 2015) order. While convincing evidence for the relevance of such nanoscale phase separation has been identified (Terletska and Dobrosavljević, 2011) in certain systems (Jaroszyński et al., 2007), recent work seems to indicate (Waintal, 2006; Clark et al., 2009) that such effects may be negligibly small for Wigner crystal melting.

A complementary line of work, where the Mott character of the transition is the focus (Pankov and Dobrosavljevic, 2008), has been the subject of recent model calculations based on DMFT approaches. These works considered a toy lattice model for the Wigner–Mott transition by examining an extended Hubbard model at quarter

filling (Camjayi et al., 2008; Amaricci et al., 2010), which has also been discussed (Fratini and Merino, 2009; Merino et al., 2013) in the context of the θ-family of Mott organics. In general, a spatially uniform phase cannot become a Mott insulator away from half filling, even for arbitrarily large values of the on-site repulsion U. However, when the intersite interaction V is sufficiently large (as compared to the bandwidth W), the electronic system undergoes charge ordering, where one sublattice becomes close to half filling, while the other one become nearly empty. Such charge ordering, which is the lattice analogue of Wigner crystallization, results in a Mott insulating state, having localized spin-1/2 magnetic moments on each site of the carrier-rich sublattice.

The corresponding MIT has a character very similar to the conventional Mott transition, and the approach from the metallic side resembles the familiar BR scenario (Brinkman and Rice, 1970). One finds strong enhancement in both the spin susceptibility and the QP effective mass m^* in agreement with experiments. A new feature, which differs from the standard Mott transition at half filling, is the response to (parallel) magnetic fields (Zeeman coupling). This calculation finds (Camjayi et al., 2008), in agreement with experiment on 2DEG systems (Shashkin et al., 2001; Eng et al., 2002), that a field-driven MIT arises only sufficiently close to the $B = 0$ MIT, while deeper in the metallic phase even full spin polarization cannot completely destroy the metal.

1.5 Conclusions

In this chapter we presented evidence suggesting that 2D-MIT found in ultraclean 2DEG devices should be viewed as an interaction-driven MIT with many features in common with conventional Mott systems. Striking similarities were established between thermodynamic and transport properties of the respective experiments but also with the predictions of generic theoretical models describing Mott and Wigner–Mott transitions. The resulting DMFT physical picture seems to offer, for quantum fluids, a perspective comparable to what the very successful van der Waals theory provided for the classical liquid–gas critical point. It should give the proper starting
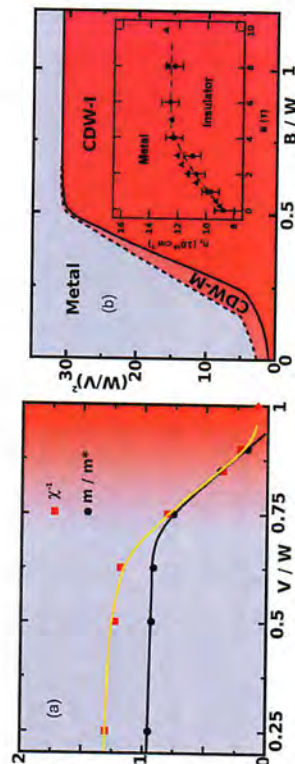
Figure 1.22 Toy model for Wigner crystallization. Results from the DMFT solution of a Hubbard model at quarter filling (Camjayi et al., 2008) show that (a) both the spin susceptibility χ and the effective mass m^* are strongly enhanced as the transition is approached. (b) Phase diagram in the presence of (parallel) magnetic field. A field-driven transition is found only sufficiently close to the insulating state in agreement with experiments. The inset shows the experimental phase diagram (Shashkin et al., 2001; Eng et al., 2002).

point for future theoretical studies of more complicated experiments containing nontrivial interplay between strong correlations and disorder, as described in the chapter by D. Popovic. This fascinating research direction remains a challenge for upcoming theoretical work.

Acknowledgments

References

Abrahams, E., Anderson, P. W., Licciardello, D. C., and Ramakrishnan, T. V. (1979). *Phys. Rev. Lett.* **42**, p. 673.

Abrahams, E., Kravchenko, S. V., and Sarachik, M. P. (2001). *Rev. Mod. Phys.* **73**, p. 251.

Amaricci, A., Camjayi, A., Haule, K., Kotliar, G., Tanasković, D., and Dobrosavljević, V. (2010). *Phys. Rev. B* **82**, p. 155102.

Altshuler, B. L., Maslov, D. L., and Pudalov, V. M. (2001). *Physica (Amsterdam)* **9E**, p. 209.

Anderson, P. (1958). *Phys. Rev.* **109**, p. 1492.

Anderson, P. W. (1959). *Phys. Rev.* **115**, p. 2.

Ando, T., Fowler, A. B., and Stern, F. (1982). *Rev. Mod. Phys.* **54**, p. 437.

Andrade, E. C., Miranda, E., and Dobrosavljević, V. (2009). *Phys. Rev. Lett.* **102**, p. 206403.

Ashcroft, N. W., and Mermin, D. (1976). *Solid State Physics* (Saunders College, Philadelphia).

Brinkman, W. F., and Rice, T. (1970). *Phys. Rev. B* **2**, p. 4302.

Camjayi, A., Haule, K., Dobrosavljević, V., and Kotliar, G. (2008). *Nat. Phys.* **4**, p. 932.

Cândido, L., Bernu, B., and Ceperley, D. M. (2004). *Phys. Rev. B* **70**, p. 094413.

Cândido, L., Phillips, P., and Ceperley, D. M. (2001). *Phys. Rev. Lett.* **86**, p. 492.

Casey, A., Patel, H., Nyéki, J., Cowan, B. P., and Saunders, J. (2003). *Phys. Rev. Lett.* **90**, p. 115301.

Chen, Y. P., Sambandamurthy, G., Wang, Z. H., Lewis, R. M., Engel, L. W., Tsui, D. C., Ye, P. D., Pfeiffer, L. N., and West, K. W. (2006). *Nat. Phys.* **2**, p. 452.

Dobbs, B. J. T. (2002). *The Janus Faces of Genius: The Role of Alchemy in Newtons Thought* (Cambridge University Press, UK).

Clark, B. K., Casula, M., and Ceperley, D. M. (2009). *Phys. Rev. Lett.* **103**, p. 055701.

Dobrosavljević, V., Abrahams, E., Miranda, E., and Chakravarty, S. (1997). *Phys. Rev. Lett.* **79**, p. 455.

Dobrosavljević, V., Trivedi, N., and Valles Jr., J. M. (2012). *Conductor Insulator Quantum Phase Transitions* (Oxford University Press, UK).

Emery, V. J., and Kivelson, S. A. (1995). *Phys. Rev. Lett.* **74**, p. 3253.

Elsässer, S., Wu, D., Dressel, M., and Schlueter, J. A. (2012). *Phys. Rev. B* **86**, p. 155150.

Eng, K., Feng, X. G., Popović, D., and Washburn, S. (2002). *Phys. Rev. Lett.* **88**, p. 136402.

Finkel'stein, A. M. *Zh. Eksp. Teor. Fiz.* **84**, p. 168; (1983) *Sov. Phys. JETP* **57**, p. 97.

Finkel'stein, A. M. (1984). *Zh. Eksp. Teor. Fiz.* **86**, p. 367; (1983) *Sov. Phys. JETP* **59**, p. 212.

Flouquet, J., Lasjaunias, J. C., Peyrard, J., and Ribault, M. (1982). *J. Appl. Phys.* **53**, pp. 2127–2130.

Flouquet, J. (2005). *Progress in Low Temperature Physics*, Vol. 15 (Elsevier, Amsterdam) pp. 139–281.

Fowler, A. B., Fang, F. F., Howard, W. E., and Stiles, P. J. (1966). *Phys. Rev. Lett.* **16**, p. 901.

Fratini, S., and Merino, J. (2009). *Phys. Rev. B* **80**, p. 165110.

Furukawa, T., Miyagawa, K., Taniguchi, H., Kato, R., and Kanoda, K. (2015). *Nat. Phys.* **11**, pp. 221–224.

Georges, A., Kotliar, G., Krauth, W., and Rozenberg, M. J. (1996). *Rev. Mod. Phys.* **68**, p. 13.

Goldenfeld, N. (1992). *Lectures on Phase Transitions and the Renormalization Group* (Addison-Wesley, Reading).

Goodenough, J. B. (1963). *Magnetism and the Chemical Bond* (John Wiley & Sons, New York- London).

Gor'kov, L. P., and Sokol, A. V. (1987) *JETP Lett.* **46**, p. 420.

Gull, E., Millis, A. J., Lichtenstein, A. I., Rubtsov, A. N., Troyer, M., and Werner, P. (2011). *Rev. Mod. Phys.* **83**, p. 349.

Hewson, A. C. (1993). *The Kondo Problem to Heavy Fermions* (Cambrige University Press, Cambridge).

Hubbard, J. (1963). *Proc. R. Soc. (London) A* **276**, p. 238.

Jacko, A. C., Fjaerestad, J. O., and Powell, B. J. (2009). *Nat. Phys.* **5**, pp. 422–425.

Jamei, R., Kivelson, S., and Spivak, B. (2005). *Phys. Rev. Lett.* **94**, p. 056805.

Jaroszyński, J., Andrearczyk, T., Karczewski, G., Wr?bel, J., Wojtowicz, T., Popović, D., and Dietl, T. (2007). *Phys. Rev. B* **76**, p. 045322.

Kotliar, G., and Ruckenstein, A. E. (1986). *Phys. Rev. Lett.* **57**, p. 1362.

Kotliar, G., Savrasov, S. Y., Haule, K., Oudovenko, V. S., Parcollet, O., and Marianetti, C. A. (2006). *Rev. Mod. Phys.* **78**, p. 865.

Kravchenko, S. V., and Sarachik, M. P. (2004). *Rep. Prog. Phys.* **67**, p. 1.

Kravchenko, S. V., Mason, W. E., Bowker, G. E., Furneaux, J. E., Pudalov, V. M., and D'Iorio, M. (1995). *Phys. Rev. B* **51**, p. 7038.

Kurosaki, Y., Shimizu, Y., Miyagawa, K., Kanoda, K., and Saito, G. (2005). *Phys. Rev. Lett.* **95**, p. 177001.

Landau, L. D. (1957). *Sov. Phys. JETP* **3**, p. 920.

Lee, P. A., and Ramakrishnan, T. V. (1985). *Rev. Mod. Phys.* **57**, p. 287.

Limelette, P., Wzietek, P., Florens, S., Georges, A., Costi, T. A., Pasquier, C., Jerome, D., Meziere, C., and Batail, P. (2003). *Phys. Rev. Lett.* **91**, p. 016401.

Mahmoudian, S., Rademaker, L., Ralko, A., Fratini, S., and Dobrosavljević, V. (2015). *Phys. Rev. Lett.* **115**, p. 025701.

Merino, J., Ralko, A., and Fratini, S. (2013). *Phys. Rev. Lett.* **111**, p. 126403.

Millis, A. J. (1993). *Phys. Rev. B* **48**, p. 7183.

Misguich, G., Bernu, B., Lhuillier, C., and Waldtmann, C. (1998). *Phys. Rev. Lett.* **81**, p. 1098.

Miranda, E., and Dobrosavljević, V. (2005). *Rep. Prog. Phys.* **68**, p. 2337.

Moeller, G., Dobrosavljević, V., and Ruckenstein, A. E. (1999). *Phys. Rev. B* **59**, p. 6846.

Mokashi, A., Li, S., Wen, B., Kravchenko, S. V., Shashkin, A. A., Dolgopolov, V. T., and Sarachik, M. P. (2012). *Phys. Rev. Lett.* **109**, p. 096405.

Mott, N. F. (1949). *Proc. Phys. Soc. (London) A* **62**, p. 416.

Mott, N. F. (1990). *Metal-Insulator Transition* (Taylor & Francis, London).

Pankov, S., and Dobrosavljević, V. (2008). *Physica B* **403**, p. 1440.

Park, H., Haule, K., and Kotliar, G. (2008). *Phys. Rev. Lett.* **101**, p. 186403.

Pfeiffer, L. N., and West, K. W. (2006). *Nat. Phys.* **2**, p. 452.

Pines, D., and Nozières, P. (1965). *The Theory of Quantum Liquids* (Benjamin, New York).

Popović, D., Fowler, A. B., and Washburn, S. (1997). *Phys. Rev. Lett.* **79**, p. 1543.

Powell, B. J. and McKenzie, R. H. (2011). *Rep. Prog. Phys.* **74**, p. 056501.

Prus, O., Yaish, Y., Reznikov, M., Sivan, U., and Pudalov, V. (2003). *Phys. Rev. B* **67**, p. 205407.

Pudalov, V., Brunthaler, G., Prinz, A., and Bauer, G. (1998). *Physica E* **3**, pp. 79–88.

Punnoose, A., and Finkel'stein, A. M. (2001). *Phys. Rev. Lett.* **88**, p. 016802.

Radonjić, M. M., Tanasković, D., Dobrosavljević, V., and Haule, K. (2010). *Phys. Rev. B* **81**, p. 075118.

Radonjić, M. M., Tanasković, D., Dobrosavljević, V., Haule, K., and Kotliar, G. (2012). *Phys. Rev. B* **85**, p. 085133.

Sachdev, S. (2011). *Quantum Phase Transitions*, 2nd Edition (Cambridge University Press, UK)

Sarachik, M. P. (1995). In *Metal-Insulator Transitions Revisited*, eds. Edwards, P., and Rao, C. N. R. (Taylor and Francis, London).

Schmalian, J., and Wolynes, P. G. (2000). *Phys. Rev. Lett.* **85**, p. 836.

Shashkin, A. A., Kravchenko, S. V., Dolgopolov, V. T., and Klapwijk, T. M. (2001). *Phys. Rev. Lett.* **87**, p. 086801.

Shashkin, A. A., Kravchenko, S. V., Dolgopolov, V. T., and Klapwijk, T. M. (2002). *Phys. Rev. B* **66**, p. 073303.

Simonian, D., Kravchenko, S. V., and Sarachik, M. P. (1997a). *Phys. Rev. B* **55**, p. R13421.

Simonian, D., Kravchenko, S. V., Sarachik, M. P., and Pudalov, V. M. (1997b). *Phys. Rev. Lett.* **79**, p. 2304.

Shklovskii, B. I., and Efros, A. L. (1984). *Electronic Properties of Doped Semiconductors* (Springer-Verlag, Berlin, Heidelberg).

Slater, J. C. (1934). *Rev. Mod. Phys.* **6**, p. 209.

Slater, J. C. (1951). *Phys. Rev.* **82**, p. 538.

Stewart, G. R. (1984). *Rev. Mod. Phys.* **56**, p. 755.

Tanasković, D., Haule, K., Kotliar, G., and Dobrosavljević, V. (2011). *Phys. Rev. B* **84**, p. 115105.

Tanatar, B., and Ceperley, D. M. (1989). *Phys. Rev. B* **39**, p. 5005.

Terletska, H., and Dobrosavljević, V. (2011). *Phys. Rev. Lett.* **106**, p. 186402.

Terletska, H., Vučičević, J., Tanasković, D., and Dobrosavljević, V. (2011). *Phys. Rev. Lett.* **107**, p. 026401.

Thouless, D. J. (1978). *J. Phys. C: Solid State Phys.* **11**, p. L189.

Ting, C. S., Lee, T. K., and Quinn, J. J. (1975). *Phys. Rev. Lett.* **34**, p. 870.

Vollhardt, D. (1984). *Rev. Mod. Phys.* **56**, p. 99.

Vučičević, J., Terletska, H., Tanasković, D., and Dobrosavljević, V. (2013). *Phys. Rev. B* **88**, p. 075143.

Vučičević, J., Tanasković, D., Rozenberg, M. J., and Dobrosavljević, V. (2015). *Phys. Rev. Lett.* **114**, p. 246402.

Waintal, X. (2006). *Phys. Rev. B* **73**, p. 075417.

Widom, B. (1965). *J. Chem. Phys.* **43**, p. 3898.

Wigner, E. (1934). *Phys. Rev.* **46**, p. 1002.

Zala, G., Narozhny, B. N., and Aleiner, I. L. (2001). *Phys. Rev. B* **64**, p. 214204.

Zhang, Y., and Das Sarma, S. (2005). *Phys. Rev. B* **71**, p. 045322.

Chapter 2

Metal–Insulator Transition in a Strongly Correlated Two-Dimensional Electron System

A. A. Shashkin[a] and S. V. Kravchenko[b]

[a]*Institute of Solid State Physics, Chernogolovka, Moscow District 142432, Russia*
[b]*Physics Department, Northeastern University, Boston, Massachusetts 02115, USA*
shashkin@issp.ac.ru, s.kravchenko@northeastern.edu

Experimental results on the metal–insulator transition and related phenomena in strongly interacting two-dimensional electron systems are discussed. Special attention is given to recent results for the strongly enhanced spin susceptibility, effective mass, and thermopower in low-disordered silicon MOSFETs.

2.1 Strongly and Weakly Interacting 2D Electron Systems

In two-dimensional (2D) electron systems, the electrons are confined in a 1D potential well and are free to move in a plane. The strongly interacting limit is reached in such systems at low

Bad-Metal Behavior Reveals Mott Quantum Criticality in Doped Hubbard Models

J. Vučičević,[1] D. Tanasković,[1] M. J. Rozenberg,[2] and V. Dobrosavljević[3]

[1]*Scientific Computing Laboratory, Institute of Physics Belgrade, University of Belgrade, Pregrevica 118, 11080 Belgrade, Serbia*
[2]*Laboratoire de Physique des Solides, CNRS-UMR8502, Université de Paris-Sud, Orsay 91405, France and Departamento de Física,*
FCEN, Universidad de Buenos Aires, Ciudad Universitaria Pabellón I, (1428) Buenos Aires, Argentina
[3]*Department of Physics and National High Magnetic Field Laboratory, Florida State University, Tallahassee, Florida 32306, USA*

Bad-metal (BM) behavior featuring linear temperature dependence of the resistivity extending to well above the Mott-Ioffe-Regel (MIR) limit is often viewed as one of the key unresolved signatures of strong correlation. Here we associate the BM behavior with the Mott quantum criticality by examining a fully frustrated Hubbard model where all long-range magnetic orders are suppressed, and the Mott problem can be rigorously solved through dynamical mean-field theory. We show that for the doped Mott insulator regime, the coexistence dome and the associated first-order Mott metal-insulator transition are confined to extremely low temperatures, while clear signatures of Mott quantum criticality emerge across much of the phase diagram. Remarkable scaling behavior is identified for the entire family of resistivity curves, with a quantum critical region covering the entire BM regime, providing not only insight, but also quantitative understanding around the MIR limit, in agreement with the available experiments.

Metallic transport inconsistent with Fermi liquid theory has been observed in many different systems; it is often linked to quantum criticality around some ordering phase transition [1,2]. Such behavior is notable near quantum critical points in good conductors, for example in heavy fermion compounds [3,4]. In several other classes of materials, however, much more dramatic departures from conventional metallic behavior are clearly observed, where resistivity still rises linearly with temperature, but it reaches paradoxically large values, well past the Mott-Ioffe-Regel (MIR) limit [5,6]. This bad-metal (BM) behavior [7] was first identified in the heyday of high-temperature superconductivity, in materials such as $La_{2-x}Sr_xCuO_4$ [8]. While the specific copper-oxide family and related high-T_c materials remain ill-understood and marred with controversy, it soon became clear that BM behavior is a much more general feature [6] of materials close to the Mott metal-insulator transition (MIT) [9]. Indeed, it has been clearly identified also in various oxides [10,11], organic Mott systems [12–14], as well as more recently discovered families of iron pnictides [15]. Despite years of speculation and debate, so far its clear physical interpretation has not been established.

To gain reliable insight into the origin of BM behavior, it is useful to examine an exactly solvable model system, where one can suppress all possible effects associated with the approach to some broken symmetry phase, or those specific to low dimensions and a given lattice structure. This can be achieved by focusing on the maximally frustrated Hubbard model, where an exact solution can be obtained by solving dynamical mean-field theory (DMFT) equations [16] in the paramagnetic phase. Although various aspects of the DMFT equation have been studied for more than twenty years, only very recent work [17,18] established how to identify the quantum critical (QC) behavior

associated with the interaction-driven Mott transition at half-filling.

Here we present a large-scale computational study across the entire phase diagram, showing that qualitatively different transport behavior is found in doped Mott insulators. Our study reveals a clear and quantitative connection between BM phenomenology and the signatures of Mott quantum criticality, including the characteristic mirror symmetry [19] of the relevant scaling function. We demonstrate that the associated QC region, featuring linear temperature dependence of resistivity around the MIR limit, corresponds to a fully incoherent transport regime. In contrast, the coherent Fermi liquid (FL) regime and even the resilient-quasiparticle regime [20,21] do emerge at lower temperature, but here the resistivity remains well below the MIR limit. Our results provide strong evidence that bad-metallic behavior represents a universal feature of high-temperature transport close to the Mott transition, presenting intriguing parallels with recent ideas based on holographic duality [22,23].

Phase diagram.—We consider a single-band Hubbard model defined by the Hamiltonian

$$H = -t \sum_{\langle i,j \rangle, \sigma} (c_{i\sigma}^{\dagger} c_{j\sigma} + \text{H.c.}) + U \sum_i n_{i\uparrow} n_{i\downarrow} - \mu \sum_{i,\sigma} c_{i\sigma}^{\dagger} c_{i\sigma},$$

where t stands for the nearest-neighbor hopping amplitude, U is the on-site interaction, and μ denotes the chemical potential. The creation and annihilation operators for spin orientation σ are denoted by $c_{\sigma}^{\dagger}$ and c_{σ}, and $n_{i\sigma} = c_{i\sigma}^{\dagger} c_{i\sigma}$. We solve the DMFT equations using the continuous-time quantum Monte Carlo (CTQMC) algorithm for the impurity solver [24–26]. We focus on the paramagnetic solution which is a physically justified assumption for frustrated lattices. We

use the semielliptic bare density of states and set the half-bandwidth $D = 1$ as the unit of energy. This corresponds to the infinitely dimensional Bethe lattice, as well as the fully connected lattice with random hopping amplitudes [16].

At half-filling, strong enough on-site interaction U opens a spectral gap at the Fermi level and produces the Mott insulating state [16]. The Mott insulator can also be destroyed by adding electrons to the system, i.e., raising the chemical potential μ. When μ reaches the upper Hubbard band, the system is once again conducting [20]. In both cases, at low temperature the transition is of the first order, and features a pronounced jump in the value of resistivity and other quantities [27]. Around the first-order transition line, a small coexistence region is present, where both metallic and insulating phases are locally stable. Our calculations show (see the Supplemental Material, Secs. I and II [28]) that the critical end-point temperature $T_c(U)$ for the doping-driven transition rapidly drops with increasing interaction, and at $U = 4$ it already is less than 10% of that at half-filling. This is illustrated in Fig. 1(a). At the critical end-point (red dots), the two solutions merge, and above it no true distinction between the phases exists; only a rapid

crossover is observed upon variation of U or μ. Previous work [17,18] examined the vicinity of the interaction-driven MIT at half-filling; here we analyze the broad finite temperature crossover region between the half-filled Mott insulator and the doped Fermi liquid state [27,34–36]. This bad-metal regime, displaying very different transport behavior than that found at half-filling, is the main focus of this work.

In Fig. 1(b), we color-code the resistivity in the (μ, T) plane, calculated for $U = 4$. The resistivity is given in units of the Mott-Ioffe-Regel limit ρ_{MIR} which is defined as the highest possible resistivity in a Boltzmann semiclassical metal, corresponding to the scattering length of one lattice spacing. Numerical value for ρ_{MIR} is taken consistently with Ref. [21]. At $\mu = U/2$, the system is half-filled. At approximately $\mu = U - D = 3$, the Fermi level enters the upper Hubbard band, and a first-order doping-driven MIT is observed at temperatures below $T_c = 0.003D$. While the chemical potential is within the gap, a clear activation behavior, $\rho \sim e^{E_g/T}$, is found at low temperatures. On the metallic side of the MIT, due to the strong electron-electron scattering, the resistivity grows rapidly with temperature, and typical Fermi-liquid behavior is observed only below rather low coherence temperature T_{FL} (denoted with the gray dashed line).

Quantum critical scaling.—In the standard scenario for quantum criticality [1,9], the system undergoes a zero-temperature phase transition at a critical value of some control parameter $g = g_c$, and within a V-shaped finite temperature region, physical quantities display scaling behavior of the form $A(g, T) = A_c(T)F[T/(g - g_c)^{z\nu}]$. Mott MIT is a first-order phase transition [37], but the corresponding coexistence region is confined to extremely low temperatures, and at temperatures sufficiently above the critical end-point T_c, the quantum effects are expected to set in [1], and restore the QC behavior.

To test the QC scaling hypothesis in the case of a Mott transition, one must first identify the appropriate $g_c(T)$ instability trajectory [17,18] which enters the argument of the scaling function (for illustration, see the Supplemental Material, Fig. 2 [28]). $g_c(T)$ marks, on the phase diagram, a trajectory where the system is least stable (i.e., is found in equal proximity to both the metal and the insulator), and is therefore most prone to fluctuations. The relevant thermodynamic stability is most easily determined from the curvature λ of the free energy functional $\mathcal{F}[G(i\omega_n)]$ near its global minimum; this can be numerically determined by monitoring the convergence rate in the DMFT self-consistency loop [17]. Having in mind the analogy of this definition with the standard Widom crossover line for classical liquid-gas transitions [38], we refer to the insta-bility line as the "quantum Widom line" (QWL) [18].

We carried out a careful λ analysis for the doped Mott insulator (see the Supplemental Material, Sec. III [28]), and we display the resulting QWL trajectory $\mu^*(T)$ as an orange line in all plots [throughout this Letter, an asterisk in the superscript indicates physical quantities evaluated along the
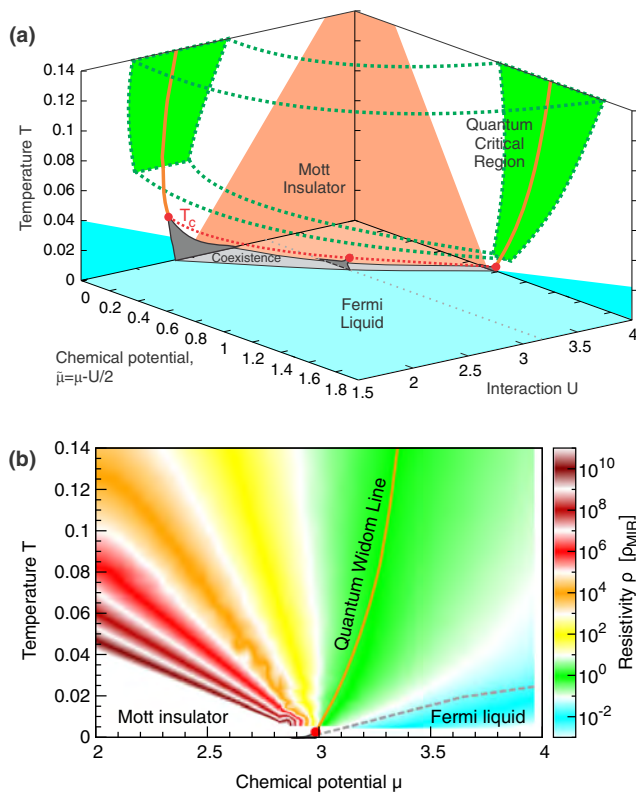

FIG. 1 (color online). (a) Phase diagram of the maximally frustrated Hubbard model. The quantum critical scaling is observed in the green region which extends to lower temperatures as T_c (red dots) is reduced. (b) Color plot of the resistivity in the (μ, T) plane for $U = 4$. The quantum Widom line (see text) passes through the crossover region where the resistivity is around the MIR limit. The coexistence region (gray) is barely visible on the scale of this plot.

QWL; e.g., $\rho^*(T)$ is resistivity calculated at temperature T at $\mu = \mu^*(T)$]. The QC region (green) spreads above the critical end point (red points and dotted line) and quickly extends to much lower temperatures as T_c is reduced [Fig. 1(a)]. The QWL, separating the metalliclike and the insulatinglike behavior, marks the center of the corresponding QC region, where the resistivity curves are expected to display the scaling behavior of the form

$$\rho(\mu, T) = \rho^*(T)F[T/T_0(d\mu)]. \tag{1}$$

Here the parameter T_0 should assume power-law dependence on the deviation from the QWL: $T_0(d\mu) \sim d\mu^{z\nu}$, with $d\mu = \mu - \mu^*(T)$.

To check validity of the scaling hypothesis, Eq. (1), we calculate the resistivity along the lines parallel to the QWL, as shown in Fig. 2(a). We find that, for the doped Mott insulator, the resistivity shows very weak temperature dependence along the QWL. In particular, above $T = 0.08$, it follows the line of constant resistivity *which coincides* with the MIR limit, $\rho^*(T > 0.08) = \rho_{MIR}$ (in contrast to the behavior previously established at half-filling [17,18], where $\rho \gg \rho_{MIR}$ along the QWL). In fact, all curves converge *precisely* to the MIR limit at high temperatures, suggesting its fundamental role in characterizing the metal-insulator crossover for doped Mott insulators. The curves also display the characteristic bifurcation upon reducing temperature, and a clear change in trend upon crossing the QWL. The scaling analysis confirms that all the curves indeed display fundamentally the same functional dependence on temperature, and that they all can be collapsed onto two distinct branches of the corresponding scaling function [Fig. 2(b)]. The scaling exponent has been estimated to be $z\nu \approx 1.35 \pm 0.1$ for both branches of the

scaling function, which display mirror symmetry [17,19] over almost two decades in T/T_0, and the scaling covers more than 3 orders of magnitude in resistivity.

Bad-metal behavior.—We demonstrated the emergence of clearly defined quantum critical behavior through an analysis of the (μ, T) phase diagram, with $d\mu = \mu - \mu^*$ as the scaling parameter. From the experimental point of view, it is, however, crucial to identify the corresponding QC region in the (δ, T) plane and understand its implications for the form of the resistivity curves for fixed level of doping $\rho(T)|_\delta$. By performing a careful calculation of the $\delta(\mu, T)$ dependence (see the Supplemental Material, Fig. 4 [28]), it is straightforward to replot our phase diagram and resistivity curves in the (δ, T) plane. Remarkably, we find that the quantum critical scaling region covers a broad range of temperatures and dopings, and almost perfectly matches the region of the well-known bad-metal transport [21,39], characterized by the absence of long-lived quasiparticles and linear $\rho(T)|_\delta$ curves. We first analyze the (δ, T) phase diagram in detail, and then establish a connection between the slope of $\rho(T)|_\delta$ curves in the bad-metal regime and the QC scaling exponent νz.

In Fig. 3(a), we show the phase diagram of the doped Mott insulator. At $T = 0$, the Mott insulator phase is found exclusively at zero doping. At low enough temperature and finite doping, characteristic Fermi liquid behavior is always observed. Here, the resistivity is quadratic in temperature, while a clear Drude peak is observed at low frequencies in optical conductivity and density of states (see the Supplemental Material, Fig. 5 [28]). The coherence temperature T_{FL} is found to be proportional to the amount of doping δ, however, with a small prefactor of about 0.1, in agreement with Refs. [20,21]. In a certain temperature range above T_{FL}, a Drude peak is still present as well as the quasiparticle resonance in the single-particle density of states, but the resistivity no longer follows the FL T^2 dependence. This corresponds to the resilient-quasiparticle (RQP) transport regime, which was carefully examined in Ref. [21]. At even higher temperatures, the temperature-dependent resistivity at fixed doping $\rho(T)|_\delta$ enters a prolonged linear regime [see Fig. 3(b)] [40], which is accompanied by the eventual disappearance of the Drude peak around the MIR limit. This behavior is usually referred to as the bad-metal regime [21]. The resistivity is comparable to the MIR limit throughout the BM region, and the QWL (as determined from our thermodynamic analysis) passes through its middle.

The region of linear $\rho(T)|_\delta$ dependence is found to be completely encompassed by the QC scaling region between the dashed lines on Fig. 3(a) (see the Supplemental Material, Sec. VI [28]). We therefore expect that the emergence of the linear T dependence of the resistivity, as well as the doping dependence of its slope, should be directly related to the precise form of the corresponding scaling function. Indeed, at high temperature and close
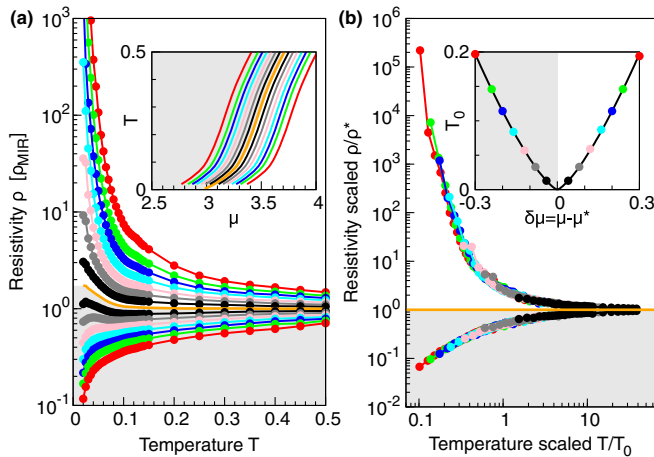

FIG. 2 (color online).   (a) Family of resistivity curves calculated along lines parallel to the QWL (orange). (b) Upon rescaling the temperature with adequately chosen parameter T_0, the resistivity curves collapse and reveal mirror symmetry of metalliclike and insulatinglike behavior around the QWL. T_0 depends on the distance from the QWL as $T_0(d\mu) \sim d\mu^{z\nu}$, with $z\nu \approx 1.35$.
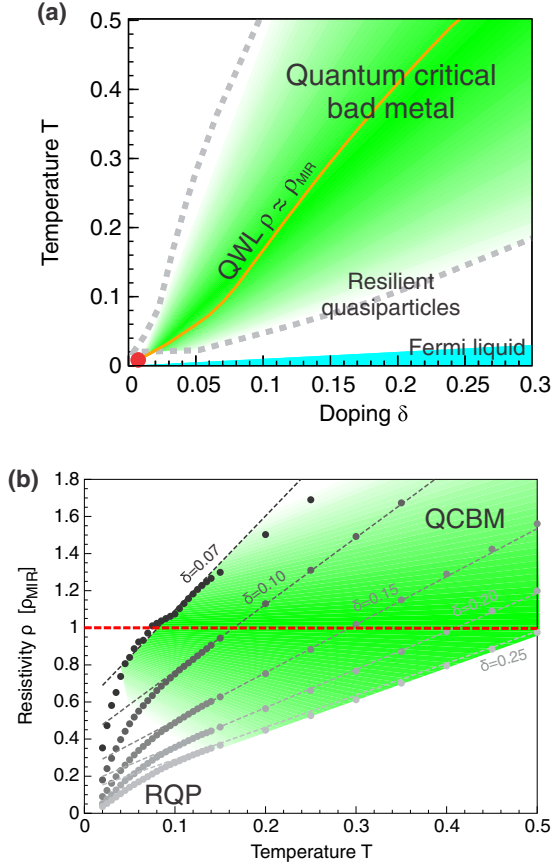
(a)

(b)

FIG. 3 (color online). (a) DMFT phase diagram of the doped Mott insulator on a frustrated lattice. The bad-metal (green) region matches perfectly the region of quantum critical scaling. (b) The bad-metal regime features linear temperature dependence of resistivity with the slope roughly proportional to an inverse power law of doping which we find to be a consequence of underlying quantum criticality.

to the QWL, the argument of the scaling function $x = d\mu/T^{1/z\nu}$ is always small, and the scaling function can be linearized, viz., $\tilde{F}(x) \approx 1 + Ax + \cdots$. We find that the coefficient A has the numerical value $A \approx -0.74$. The functional form for $\rho(T)|_\delta$ close to the QWL is then directly determined by the behavior of the scaling parameter $x(T)|_\delta$. We find that $x(T)|_\delta$ is a linear function in a wide range of temperatures around $T^*(\delta)$. Then, close to the QWL, the resistivity is well approximated by a linear function of the form

$$\rho(T)|_\delta \approx \rho^*(\delta)\left\{1 + A\left.\frac{\partial x}{\partial T}\right|_{\delta,T=T^*(\delta)}[T - T^*(\delta)]\right\}. \quad (2)$$

Furthermore, the slope of the scaling argument at the QWL can be expressed as $(\partial x/\partial T)|_{\delta,T=T^*(\delta)} = \{\chi^*(\delta)(dT^*/d\delta)\times [T^*(\delta)]^{1/z\nu}\}^{-1}$, where $\chi^*(\delta) = (\partial\delta/\partial\mu)|_{T=T^*(\delta)}$. Here, we observe that the charge compressibility is nearly constant along the QWL, $\chi^*(\delta) \approx \chi^* = 0.33$ (see the Supplemental Material, Fig. 6 [28]), which may be interpreted as
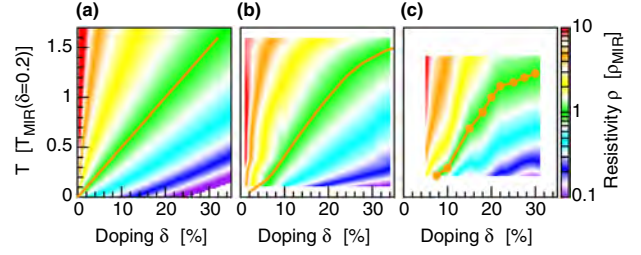

FIG. 4 (color online). Resistivity given by (a) the semianalytical formula obtained from the scaling hypothesis, (b) DMFT result, and (c) the experimental result on cuprate $La_{2-x}Sr_xCuO_4$ samples from Ref. [8].

another manifestation of the quantum critical behavior we identified. $T^*(\delta)$ is approximately a linear function $T^*(\delta) \approx K_0 + K\delta$, where $K \approx 2$ and K_0 is small. In Fig. 3(b), we compare the approximation stated in Eq. (2) with the DMFT result and find excellent agreement.

Finally, noting that for $\delta > 5\%$, $\rho^*(\delta) = \rho_{MIR}$, we arrive at the central result of this Letter,

$$\rho_{QCBM}(T)|_\delta \approx \rho_{MIR}[1 + C\delta^{-1/z\nu}(T - K\delta)]. \quad (3)$$

In the quantum critical bad-metal regime, the resistivity has a linear temperature dependence with the slope decreasing as a power $-1/z\nu$ of doping. This demonstrates a direct connection of the universal high-temperature behavior in the bad-metal regime with the (zero-temperature) quantum phase transition. The MIR limit of the resistivity is reached at temperature roughly proportional to the amount of doping, $T^*(\delta) \propto \delta$, since the doping level sets the main energy scale in the problem. The result of this simplified scaling formula is color-plotted in Fig. 4(a) (with $C = 0.69$, $K = 1.97$, and $z\nu = 1.35$) and shown to capture the features of the full DMFT solution at high temperatures.

Discussion.—Sufficiently systematic experimental studies of doped Mott insulators, covering an appreciable range of doping and temperature, remain relatively scarce. Still, approximately linear temperature dependence of the resistivity at high temperatures with a slope that decreases with doping has been observed, most notably in the seminal work of Takagi *et al.* [8] on $La_{2-x}Sr_xCuO_4$. To make a qualitative comparison with our theory and to highlight a universal link of bad-metal behavior and quantum criticality associated with the Mott metal-insulator transition, in Fig. 4 we color code the reported experimental data; here the temperature is shown in units of T_{MIR} at 20% doping and the resistivity is given in units of ρ_{MIR}, which in this material is estimated as 1.7 mΩ cm. The experimental results presented in Fig. 4(c) cover the temperature range of 150–1000 K at 5% to 30% doping. Here one observes a striking similarity between DMFT theory and the experiment, as already noted in early studies [39–41]. We established this result by focusing on an exactly solvable model, where all ordering tendencies are suppressed, and single-site DMFT becomes exact. Real materials, of course,

exist in finite (low) dimensions where systematic corrections to DMFT need to be included [42–45]. In many cases [46–48], these nonlocal corrections prove significant only at sufficiently low temperatures. Then our findings should be even quantitatively accurate in the high-temperature incoherent regime, as in the very recent experiments on organic materials [49] for the case of half-filling.

[1] S. Sachdev, *Quantum Phase Transitions* (Cambridge University Press, Cambridge, England, 1999).

[2] H. v. Löhneysen, A. Rosch, M. Vojta, and P. Wölfle, Rev. Mod. Phys. **79**, 1015 (2007).

[3] G. R. Stewart, Rev. Mod. Phys. **56**, 755 (1984).

[4] G. R. Stewart, Rev. Mod. Phys. **73**, 797 (2001).

[5] O. Gunnarsson, M. Calandra, and J. E. Han, Rev. Mod. Phys. **75**, 1085 (2003).

[6] N. E. Hussey, K. Takenaka, and H. Takagi, Philos. Mag. **84**, 2847 (2004).

[7] V. J. Emery and S. A. Kivelson, Phys. Rev. Lett. **74**, 3253 (1995).

[8] H. Takagi, B. Batlogg, H. L. Kao, J. Kwo, R. J. Cava, J. J. Krajewski, and W. F. Peck, Phys. Rev. Lett. **69**, 2975 (1992).

[9] V. Dobrosavljević, N. Trivedi, and J. M. Valles, Jr., *Conductor-Insulator Quantum Phase Transitions* (Oxford University Press, New York, 2012).

[10] M. M. Qazilbash, K. S. Burch, D. Whisler, D. Shrekenhamer, B. G. Chae, H. T. Kim, and D. N. Basov, Phys. Rev. B **74**, 205118 (2006).

[11] A. W. Tyler, A. P. Mackenzie, S. NishiZaki, and Y. Maeno, Phys. Rev. B **58**, R10107 (1998).

[12] P. Limelette, P. Wzietek, S. Florens, A. Georges, T. A. Costi, C. Pasquier, D. Jérome, C. Mézière, and P. Batail, Phys. Rev. Lett. **91**, 016401 (2003).

[13] F. Kagawa, K. Miyagawa, and K. Kanoda, Nature (London) **436**, 534 (2005).

[14] J. Merino, M. Dumm, N. Drichko, M. Dressel, and R. H. McKenzie, Phys. Rev. Lett. **100**, 086404 (2008).

[15] M. M. Qazilbash, J. J. Hamlin, R. E. Baumbach, L. Zhang, D. J. Singh, M. B. Maple, and D. N. Basov, Nat. Phys. **5**, 647 (2009).

[16] A. Georges, G. Kotliar, W. Krauth, and M. J. Rozenberg, Rev. Mod. Phys. **68**, 13 (1996).

[17] H. Terletska, J. Vučičević, D. Tanasković, and V. Dobrosavljević, Phys. Rev. Lett. **107**, 026401 (2011).

[18] J. Vučičević, H. Terletska, D. Tanasković, and V. Dobrosavljević, Phys. Rev. B **88**, 075143 (2013).

[19] V. Dobrosavljević, E. Abrahams, E. Miranda, and S. Chakravarty, Phys. Rev. Lett. **79**, 455 (1997).

[20] A. Camjayi, R. Chitra, and M. J. Rozenberg, Phys. Rev. B **73**, 041103 (2006).

[21] X. Deng, J. Mravlje, R. Žitko, M. Ferrero, G. Kotliar, and A. Georges, Phys. Rev. Lett. **110**, 086401 (2013).

[22] A. Donos and S. A. Hartnoll, Nat. Phys. **9**, 649 (2013).

[23] S. Hartnol, arXiv:1405.3651.

[24] P. Werner, A. Comanac, L. de Medici, M. Troyer, and A. J. Millis, Phys. Rev. Lett. **97**, 076405 (2006).

[25] K. Haule, Phys. Rev. B **75**, 155113 (2007).

[26] E. Gull, A. J. Millis, A. I. Lichtenstein, A. N. Rubtsov, M. Troyer, and P. Werner, Rev. Mod. Phys. **83**, 349 (2011).

[27] G. Kotliar, S. Murthy, and M. J. Rozenberg, Phys. Rev. Lett. **89**, 046401 (2002).

[28] See Supplemental Material at http://link.aps.org/supplemental/10.1103/PhysRevLett.114.246402, which includes Refs. [29–33], for numerical details, determination of T_c and quantum Widom line, and scaling analysis.

[29] D. S. Fisher, G. Kotliar, and G. Moeller, Phys. Rev. B **52**, 17112 (1995).

[30] M. J. Rozenberg, R. Chitra, and G. Kotliar, Phys. Rev. Lett. **83**, 3498 (1999).

[31] M. J. Case and V. Dobrosavljević, Phys. Rev. Lett. **99**, 147204 (2007).

[32] M. Jarrell and J. E. Gubernatis, Phys. Rep. **269**, 133 (1996).

[33] A. W. Sandvik, Phys. Rev. B **57**, 10287 (1998).

[34] R. Žitko, D. Hansen, E. Perepelitsky, J. Mravlje, A. Georges, and B. S. Shastry, Phys. Rev. B **88**, 235132 (2013).

[35] P. Werner and A. J. Millis, Phys. Rev. B **75**, 085108 (2007).

[36] A. Amaricci, G. Sordi, and M. J. Rozenberg, Phys. Rev. Lett. **101**, 146403 (2008).

[37] P. Nozières, Eur. Phys. J. B **6**, 447 (1998).

[38] G. G. Simeoni, T. Bryk, F. A. Gorelli, M. Krisch, G. Ruocco, M. Santoro, and T. Scopigno, Nat. Phys. **6**, 503 (2010).

[39] T. Pruschke, D. L. Cox, and M. Jarrell, Phys. Rev. B **47**, 3553 (1993).

[40] M. Jarrell and T. Pruschke, Phys. Rev. B **49**, 1458 (1994).

[41] The high-temperature slope of the resistivity curves is estimated to be proportional to δ^{-1} in Ref. [40]. However, only four doping levels were considered and having in mind the uncertainty of the analytical continuation, it is difficult to distinguish this value from our slope $\delta^{-1/z\nu} = \delta^{-1/1.35}$. Our numerical data are in agreement with high precision CTQMC data from Ref. [21].

[42] T. Maier, M. Jarrell, T. Pruschke, and M. H. Hettler, Rev. Mod. Phys. **77**, 1027 (2005).

[43] G. Kotliar, S. Y. Savrasov, K. Haule, V. S. Oudovenko, O. Parcollet, and C. A. Marianetti, Rev. Mod. Phys. **78**, 865 (2006).

[44] G. Sordi, P. Sémon, K. Haule, and A.-M. S. Tremblay, Phys. Rev. B **87**, 041101 (2013).

[45] E. Gull, O. Parcollet, and A. J. Millis, Phys. Rev. Lett. **110**, 216405 (2013).

[46] A. Georges, Ann. Phys. (Berlin) **523**, 672 (2011).

[47] D. Tanasković, K. Haule, G. Kotliar, and V. Dobrosavljević, Phys. Rev. B **84**, 115105 (2011).

[48] J. Kokalj and R. H. McKenzie, Phys. Rev. Lett. **110**, 206402 (2013).

[49] T. Furukawa, K. Miyagawa, H. Taniguchi, R. Kato, and K. Kanoda, Nat. Phys. **11**, 221 (2015).

Supplementary Information: Bad-metal behavior reveals Mott quantum criticality in doped Hubbard models

J. Vučičević,[1] D. Tanasković,[1] M. J. Rozenberg,[2] and V. Dobrosavljević[3]

[1] *Scientific Computing Laboratory, Institute of Physics Belgrade,*
University of Belgrade, Pregrevica 118, 11080 Belgrade, Serbia.
[2] *Laboratoire de Physique des Solides, CNRS-UMR8502, Université de Paris-Sud, Orsay 91405, France.*
[3] *Department of Physics and National High Magnetic Field Laboratory,*
Florida State University, Tallahassee, Florida 32306, USA.

I. NUMERICAL DETAILS: THE DMFT LOOP AND THE IMPURITY SOLVER

We have used the CTQMC impurity solver as implemented by K. Haule in Ref. 1. We have used $4-6 \times 10^9$ Monte Carlo steps. When $T > 0.14$, the high frequency tail was calculated from the atomic limit and Hubbard-I approximation was used otherwise. At high temperatures, 10-15 DMFT iterations were usually sufficient to reach the self-consistent solution with the accuracy $|G^i(i\omega_0) - G^{i-1}(i\omega_0)| \approx 10^{-4}$, where $\omega_0 = \frac{1}{2}\pi T$. In the coexistence region, we used a larger number of DMFT iterations (up to 30) to test the stability of the obtained solution.

II. DETERMINATION OF T_c

T_c from the position of the spinodals

The first order phase transition is most easily observed by looking at the occupation number. At very low temperature, while the chemical potential is within the spectral gap, filling is roughly a constant, i.e. $n(\mu) \approx 0.5$. When the chemical potential reaches the upper Hubbard band, a quasi particle peak forms abruptly at its lower edge causing an immediate transfer of spectral weight from the lower Hubbard band to the vicinity of the Fermi level [2, 3]. This is observed as a jump in the occupancy from nearly half-filling to around 2-3% doping. An insulating solution is not possible when μ is in the upper Hubbard band, hence its bottom edge determines the insulating (right) spinodal. However, a metallic solution is possible even when μ is in the gap. This type of state features an in-gap quasi-particle peak [4] and is observed in the coexistence region. The lowest value of the chemical potential at which the quasi particle peak can survive constitutes the metallic (left) spinodal. The disappearance of the QP peak at the metallic spinodal is also abrupt, and occurs at finite doping. Therefore, there is a range of doping that is not achievable locally at any value of the chemical potential, but only globally through phase separation. With increasing temperature, the forbidden doping range shrinks and disappear together with the hysteresis loop, precisely at T_c [5, 6]. Note also, that

the range of forbidden doping vanishes at $T = 0$ as well, where a metallic solution is possible even at infinitesimal doping [2], although in this case particle-hole symmetry is broken and $\mu \neq U/2$. In Supplementary Figure 1a,b we show the hysteresis curves of the occupancy for two values of interaction U. The position of spinodals and the width of the coexistence region are easily determined from the jumps in $n(\mu)$. We considered the lowest temperature at which no coexistence is observed to be the critical temperature. Note also that due to the numerical error of the CTQMC, some unphysical doping is observed in the insulating state at the lowest temperatures. We were not able to obtain physically meaningful results below $T \approx 0.0015$ and this is the lowest temperature at which we have found the method to be reliable. The numerical error from the CTQMC becomes significant at low temperature and a precise assessment of T_c's lower than ≈ 0.002 proves very difficult. The coexistence regions at the two values of U are shown in Supplementary Figure 1c and d. The $T = 0$ position of the left spinodal is taken from the ED calculation found in [4] and seems to fit well our finite temperature results.

T_c from the charge compressibility

The alternative way of determining T_c is by looking at the uniform charge susceptibility $\chi = \frac{\partial n}{\partial \mu}$. Precisely at the critical point, χ is divergent and above T_c, there is a line of maxima in $\chi(\mu)|_T$. Furthermore, it can be shown [7] that close to the critical point $\chi^{-1} \sim \frac{T-T_c}{a+b(T-T_c)}$. This is useful as one can extrapolate the values of $\chi_{\max}^{-1}(T)$ to lower temperatures and see where it goes to zero. However, such method is of inferior accuracy compared to the direct observation of the coexistence, and we use it only for cross-checking of our results. In Fig. 1e we show such calculation in the case of $U = 3.2$.

T_c from the λ analysis

In Supplementary Figure 1f we plot the values of λ along the instability line (see the next Section). Close to the the critical point, it is very difficult to make a precise estimate of the DMFT convergence rate, as high con-
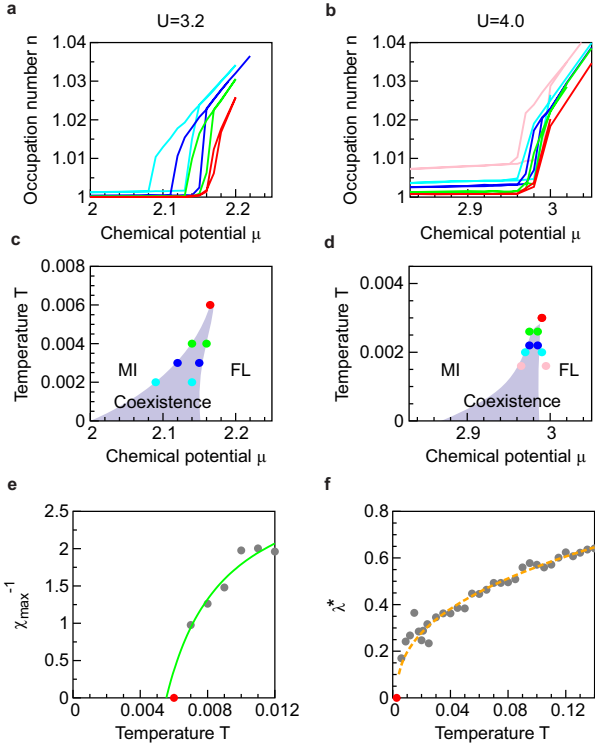
Figure 1: **Coexistence region of the first-order doping-driven Mott metal-insulator transition can be determined in different ways.** (a),(b),(c),(d) The position of spinodals can be determined from the jumps in the occupation number. In the coexistence region, two types of solution are possible, depending on the initial guess in the DMFT procedure. This is observed as a hysteresis loop in the occupation number and other quantities. (e),(f) Precisely at the critical point, physical quantities often have extremal values (zero or infinity). By extrapolating such quantities from higher temperatures, one can estimate the critical temperature. (e) The maxima of the inverse charge compressibility with respect to the chemical potential can be extrapolated to obtain a good estimate for T_c. (f) The values of λ along the instability line $\mu^*(T)$ become scattered and overestimated close to the critical point, due to numerical error from the CTQMC. This makes it unpractical to to use extrapolation of λ^* for estimation of T_c.

vergence is not achievable at all. The low temperature values are therefore much more scattered and systematically overestimated. Although in principle one could estimate T_c from higher temperatures by extrapolating $\lambda^*(T) \equiv \lambda(\mu^*(T), T)$, the numerical noise makes such a method very impractical. Further difficulty lies in the possibility of $\lambda^*(T)$ changing trend before going to zero, which introduces additional systematic error to the estimate of T_c.

III. QUANTUM WIDOM LINE AND THE λ ANALYSIS

In our previous work [8], we have discussed a possible generalization of the Widom line (originally defined in the context of classical liquid-gas transitions [9]), to strictly zero-temperature (quantum) phase transitions (see Supplementary Fig. 2). The most natural way of defining such a quantum Widom line is by looking at the free-energy landscape around the ground state of the system, as it is well defined in all physical models. Regardless of the specifics of the phase transition, precisely at the critical point, the free energy minimum is flat, i.e. its curvature λ is zero. At higher temperatures, this leads to a line of minima in λ with respect to the parameter that is driving the transition (at half-filling we had $\frac{\partial \lambda}{\partial U}\big|_T = 0$). It is at those minima that the fluctuations are most pronounced - the system is "equally close" to the two competing phases and thus the least stable. Now we utilize this concept in the case of doping-driven Mott transition, and at each temperature search for the minimum value of λ with respect to the chemical potential.

In practice, we calculate λ by monitoring the convergence rate of the iterative DMFT procedure [10]. Given the model parameters, the free energy functional $\mathcal{F}_{U,T,\mu}[G(i\omega_n)]$ yields a smooth manifold in the Hilbert space of the Green's functions. Being Taylor expandable, the local environment of any free-energy minimum has to be parabolic. Thus, in the advanced stage of the DMFT procedure, i.e. close to the self-consistent solution, a steady, exponential convergence should be observed. The curvature λ is then directly related to the exponent of
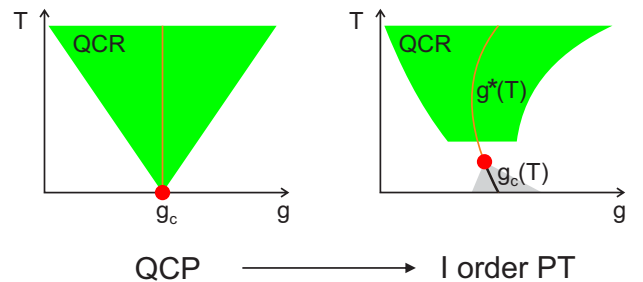

Figure 2: **Standard QCP scenario is modified in the case of the Mott MIT.** At low temperature, the Mott MIT is of (weakly) first order character, and features a coexistence region (gray) where both phases are locally stable. However, at temperatures sufficiently above the (very low) critical temperature T_c, the QC scaling holds (green). The critical transition-driving parameter g_c is replaced by a more general, temperature dependent quantity. Below T_c this is the line of first order transition $g_c(T)$ where the two states are equally favorable. Above T_c it is the line of "maximal instability" of the ground state (see text), or the quantum Widom line $g^*(T)$.

the functional dependence of the difference between the consecutive solutions versus the iteration index. When determining the convergence rate, however, it is not always sufficient to look at the Green's function in only the lowest Matsubara frequency, and one must use the generalized Raileigh-Ritz (RR) formula [11]

$$\lambda_i = 1 - \sum_n \frac{|G_n^{i+1} - G_n^i||G_n^i - G_n^{i-1}|}{|G_n^{i+1} - G_n^i|^2}, \qquad (1)$$

where i stands for the iteration index, and ideally, $\lambda = \lim_{i \to \infty} \lambda_i$. However, the highest achievable level of convergence is determined by the amount of statistical noise in the CTQMC result, and when it is reached, $G(i\omega_n)$ just fluctuates around the self-consistent solution, and no further convergence is observed. Especially near the critical point, CTQMC error becomes substantial and a high convergence can not be reached at all. Here, typically only a few iterations are available for the estimation of λ as most of the parabolic region is below the level of numerical noise, and one must look carefully for the range of iterations in which a steady exponential convergence is observed.

The result presented with gray dots in Fig. 3a is obtained by employing the RR formula from equation (1) at each iteration i, and then taking the average over the set of 5 consecutive iterations that shows the least variance, i.e. the one corresponding to the period of the steadiest exponential convergence.

Away from half-filling, however, there are additional difficulties. Namely, $G(i\omega_n)$ is complex, which means that it has additional degrees of freedom as compared to its purely imaginary analogue at particle-hole symmetry. Thus, the fluctuations encountered in the convergence rate of $G(i\omega_n)$ are more severe, and the λ-analysis is harder to perform compared to the half-filled case. This is why the data points presented with gray dots in Fig. 3 exhibit considerable scattering, but the overall trend is still rather obvious. In all of the calculations regarding the quantum critical (QC) scaling analysis, we use the smooth fit (orange dashed line) as the instability line and denote it with $\mu^*(T)$. Note that no other smoothing has been performed on the data, and all the minima are estimated automatically from the raw λ results. Although there are considerable error bars on each $\mu^*(T)$ value, the high resolution in temperature increases the certainty of the result.

It is interesting that $\mu^*(T)$ is very close to the line of maxima of the second derivative of the occupation number versus the chemical potential, $\left.\frac{\partial^2 n}{\partial \mu^2}\right|_T = \max$. This is the place where $n(\mu)$ changes trend, and as expected, the instability line separates the metallic-like and insulating-like behavior on the phase diagram. Also note that $\mu^*(T)$ roughly follows an iso-resistive curve and so the resistivity does not change considerably along the instability line. At $T > 0.08$ ρ^* is found to be constant and equal
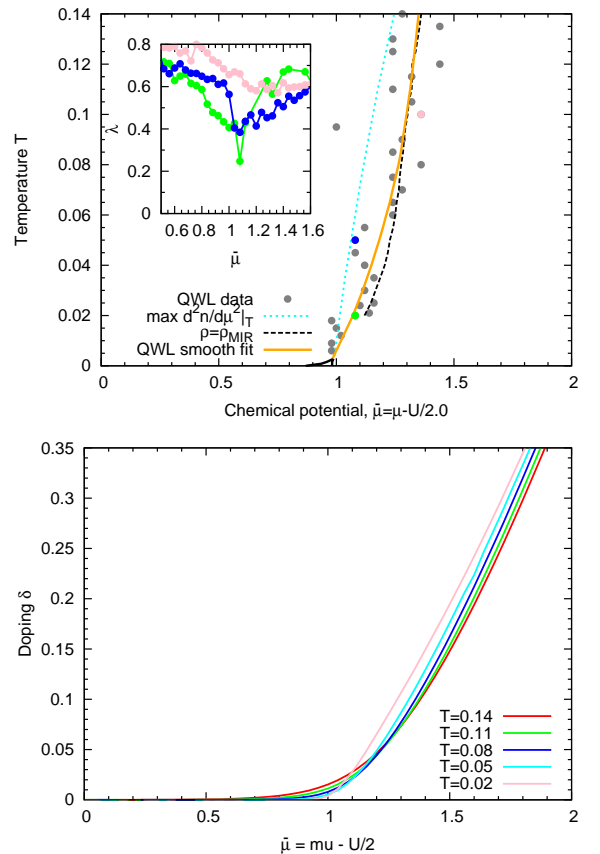

Figure 3: **The instability line $\mu^*(T)$ (orange dashed) corresponds to the minima in $\lambda(\mu)|_T$, which is related to the convergence rate of the DMFT loop.** (a) The precision of λ results is limited by the statistical noise in CTQMC. However, the minima in $\lambda(\mu)|_T$ are still clearly present, and $\mu^*(T)$ can be determined with satisfactory accuracy. At high temperature, QWL is found to coincide with the iso-resistive curve of the MIR limit (black dashed), which is then used to extrapolate the QWL to temperatures above $T = 0.14$, where λ-analysis is no longer reliable. (b) The QWL is also very close to the point where occupancy $n(\mu)|_T$ changes trend, i.e. has a maximum of the second derivative. The line of maxima in $d^2n/d\mu^2|_T$ can also be considered a crossover line between metallic and insulating behavior (light blue dotted line on panel (a)).

to the Mott-Ioffe-Regel (MIR) limit. Above $T = 0.14$, λ-analysis can not give reliable results as the minimum in $\lambda(\mu)|_T$ becomes very shallow, i.e. of depth comparable to the level of numerical noise. Throughout the paper we extrapolate the instability line to high temperatures $T > 0.14$ by imposing the criterion $\rho^* = \rho_{MIR}$. Also note that at very low temperature, the actual form of $\rho(\mu^*(T), T)$ depends strongly on the precise values of $\mu^*(T)$ because, in this region, the resistivity changes rapidly with the chemical potential.

IV. ANALYTICAL CONTINUATION AND CALCULATION OF RESISTIVITY

The straightforward application of the maximum entropy method (MEM) [12, 13] for analytical continuation of the Green's function can in some cases lead to unphysical results. In the metallic phase, this method tends to overestimate the height of the quasi-particle (QP) peak in the single-particle energy spectrum given by $-\frac{1}{\pi}\mathrm{Im}G(\omega+i0^+)$. Sometimes in those cases, the imaginary part of the self-energy falsely goes to zero at several frequencies (usually two or four), yielding an unphysical vanishing DC resistivity. Given the analytically continued Green's function on the real axis, the self-energy is obtained from the DMFT self-consistency condition

$$\Sigma(\omega) = \omega + \mu - G^{-1}(\omega) - t^2 G(\omega), \tag{2}$$

and the imaginary part of the above equation reads

$$\mathrm{Im}\Sigma(\omega) = \mathrm{Im}G(\omega)(|G(\omega)|^{-2} - t^2). \tag{3}$$

It is immediately obvious that $|G(\omega)| = 1/t$ yields $\mathrm{Im}\Sigma(\omega) = 0$, at any frequency. When there is an unphysical excess of QP weight, precisely this is seen, usually at the edges of the QP peak. This makes the conductivity integral divergent and the DC resistivity exactly zero.

We find that much better results are obtained by performing MEM on the spectral function

$$A(\varepsilon, i\omega_n) = \frac{1}{i\omega_n + \mu - \varepsilon - \Sigma(i\omega_n)}. \tag{4}$$

The self-energy is then easily extracted from the real-axis result

$$\Sigma(\varepsilon; \omega) = \omega + \mu - \varepsilon - A^{-1}(\varepsilon, \omega). \tag{5}$$
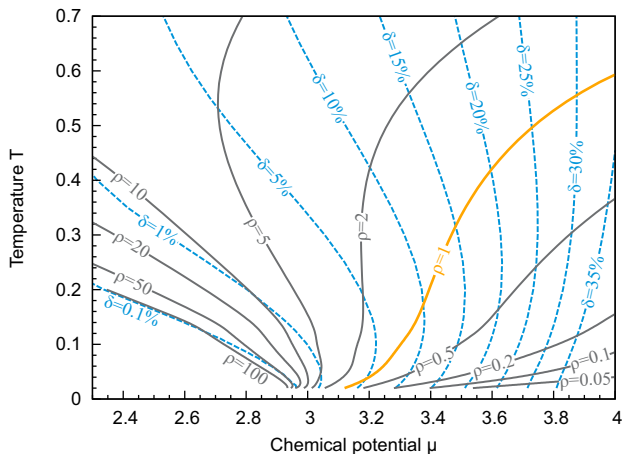

Figure 4: **Lines of constant doping intersect with the QWL (orange), along which the resistivity is equal to the MIR limit** ρ_{MIR}.
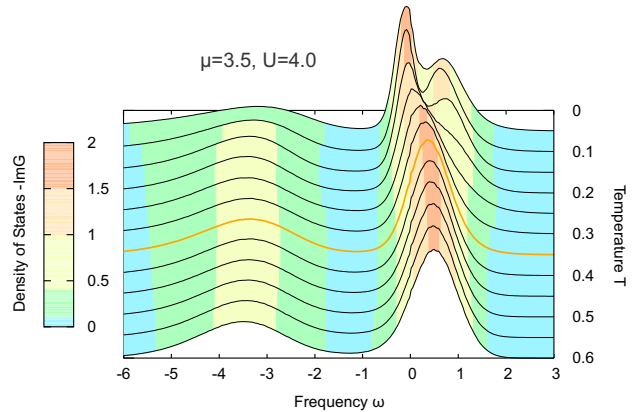

Figure 5: **Evolution of the density of states with increasing temperature.** At low temperature there is a clear quasiparticle peak in the density of states. The quasiparticle peak gradually disappears in the bad metal regime which is centered around the QWL. The orange line is the density of states at the QWL. The data are shown for the fixed chemical potential $\mu = 3.5$ and $U = 4$, which corresponds to roughly 15 % doping.

This procedure should in principle yield the same self-energy for any value of ε, but in practice this is not found to be the case. However, a good estimate of $\Sigma(\omega)$ is obtained by averaging the results of each continuation, i.e.

$$\Sigma(\omega) = \frac{1}{N}\sum_{i=1}^{N}\Sigma(\varepsilon_i; \omega). \tag{6}$$

Similarly, one could first calculate the Green's function

$$G(\omega) = \int d\varepsilon \rho_0(\varepsilon) A(\varepsilon, \omega) \tag{7}$$

and then get the self-energy from the DMFT self-consistency. In practice, we have used 40 values of ε, equally spaced within the energy range of the non-interacting band, and found that the systematic and numerical error of MEM gets canceled by the averaging. We have found that in this approach, physically meaningful solutions are always obtained, results are more consistent and have less numerical noise, but at the expense of performing a much larger number of analytical continuations. Where available, we cross-checked our results with the findings in Ref. 14 where the analytical continuation is performed via Pade approximant on the high-precision CTQMC data, and found very good agreement.

Given the self-energy on the real axis $\Sigma(\omega)$, the optical conductivity of the system can be calculated using the Kubo formula [2]

$$\sigma(\omega) = \sigma_o \iint d\varepsilon d\nu \Phi(\varepsilon) A(\varepsilon, \nu) A(\varepsilon, \nu+\omega)\frac{f(\nu) - f(\nu+\omega)}{\omega}, \tag{8}$$

where $A(\varepsilon, \nu) = -(1/\pi)\text{Im}(\varepsilon + \mu - \nu - \Sigma(\varepsilon))^{-1}$, f denotes the Fermi function, $\Phi(\varepsilon) = \Phi(0)[1 - (\varepsilon/D)^2]^{3/2}$, and $\sigma_o = 2\pi e^2/\hbar$. We present the resistivity results in the units of $\rho_{\text{MIR}} = \hbar D/e^2 \Phi(0)$, consistently with Ref. 14. We have calculated the resistivity $\rho_{\text{DC}} = \sigma^{-1}(\omega \to 0)$ in the whole (μ, T) plane. In Supplementary Figure 4 we show the lines of constant resistivity and constant doping in the (μ, T) plane. An example of the evolution of the density of states with temperature is shown in Supplementary Figure 5.

V. CHARGE COMPRESSIBILITY

The QWL is defined in purely thermodynamic terms, from the free energy functional, and as such can be examined for any model. In fact, it does not even require the presence of a first order transition line with finite T_c. It is therefore important to explore physical properties other than the resistivity along and near the QWL. It is striking that the charge compressibility is nearly constant along the QWL, and has intermediate value between the one in almost incompressible Mott insulator and Fermi liquid, see Fig. 6.
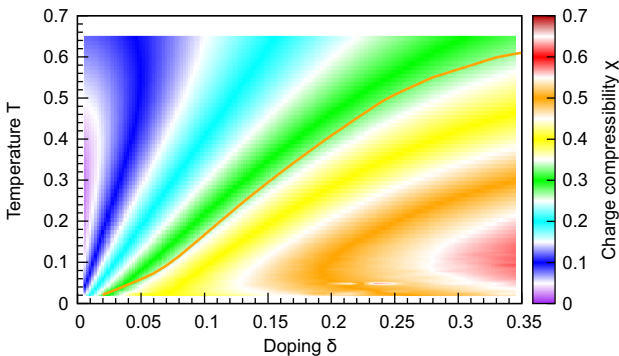

Figure 6: **Color plot of the charge compressibility has the "fan-like" form, as generally expected for quantum criticality.** The compressibility is approximately constant along the QWL.

VI. BOUNDARIES OF THE QC SCALING REGION

Around the quantum Widom line the resistivity is well approximated by a function of only one argument, such that

$$\rho(\mu, T) = \rho^*(T) F\left(\frac{T}{d\mu^{z\nu}}\right), \qquad (9)$$

where $\rho^*(T) = \rho(\mu^*(T), T)$ is the resistivity along the QWL. This behavior, typical for the quantum criticality,

is shown in Fig. 2 in the Main Text, where the resistivity curves are collapsed on the metallic and insulating branch. The explicit form of the scaling function can be obtained from an equivalent scaling equation

$$\rho(\mu, T) = \rho^*(T)\tilde{F}\left(\frac{d\mu}{T^{1/z\nu}}\right). \qquad (10)$$

with the advantage of $\tilde{F}(x)$ being a smooth analytical function in x. Then, the scaling function $\tilde{F}(x)$ can be obtained by plotting the DMFT resistivity data versus the argument $x = \frac{d\mu}{T^{1/z\nu}}$ and performing a numerical fit. This is shown in Supplementary Figure 7a. $\tilde{F}(x)$ is approximately linear on the logarithmic scale which implies that $\tilde{F}(x) \approx 10^{Bx}$, where $B \approx -0.33$. This analytical form is consistent with the mirror symmetry of the scaling formula near the QWL, $\tilde{F}(x) = 1/\tilde{F}(-x)$. We can see that the scaling region goes beyond the mirror symmetry of the scaled resistivity curves, especially on the metallic side of the QC region.

The scaling region can be estimated from the color plot of the relative error $r = |\rho_{DMFT} - 10^{Bx}|/\rho_{DMFT}$, which is shown in Supplementary Figure 7b. The boundaries of the QC scaling region defined by $r < 10\%$ are shown with gray dashed lines and correspond to the values $x_{\min} = -1.0$ and $x_{\max} = 1.5$. Note that they coincide with the $\mu = 3.0$ line (red dashed; it corresponds to chemical potential being at the lower edge of the upper Hubbard band), and the knee-like feature in $\rho(T)|_\delta$ curves (blue dashed; it corresponds to the boundary of the linear resistivity bad metal region). It is obvious from this plot that the QC scaling region completely matches the region of typically bad metallic temperature dependence of the resistivity.

The boundaries of the QC scaling region can alternatively be estimated simply by looking at Fig. 7a and observing the maximum and minimum values of x for which the DMFT results fall on a single well defined curve. This yields $x_{\min} = -1.0$ and $x_{\max} = 1.5$. These lines are also shown in Fig. 7b (gray dashed) and are in good agreement with the independent estimate based on relative error r.

Finally, the region of mirror-symmetry can be estimated by plotting the DMFT resistivity data $|\log\frac{\rho}{\rho^*}|$ as a function of $y = T/d\mu^{z\nu}$ (shown in Fig. 7c) and observing the lowest y at which the two branches of data are found to coincide. This analysis yields $y_{\min} = 1 = |x_{\min/\max}|^{-1}$, in agreement with other approaches.
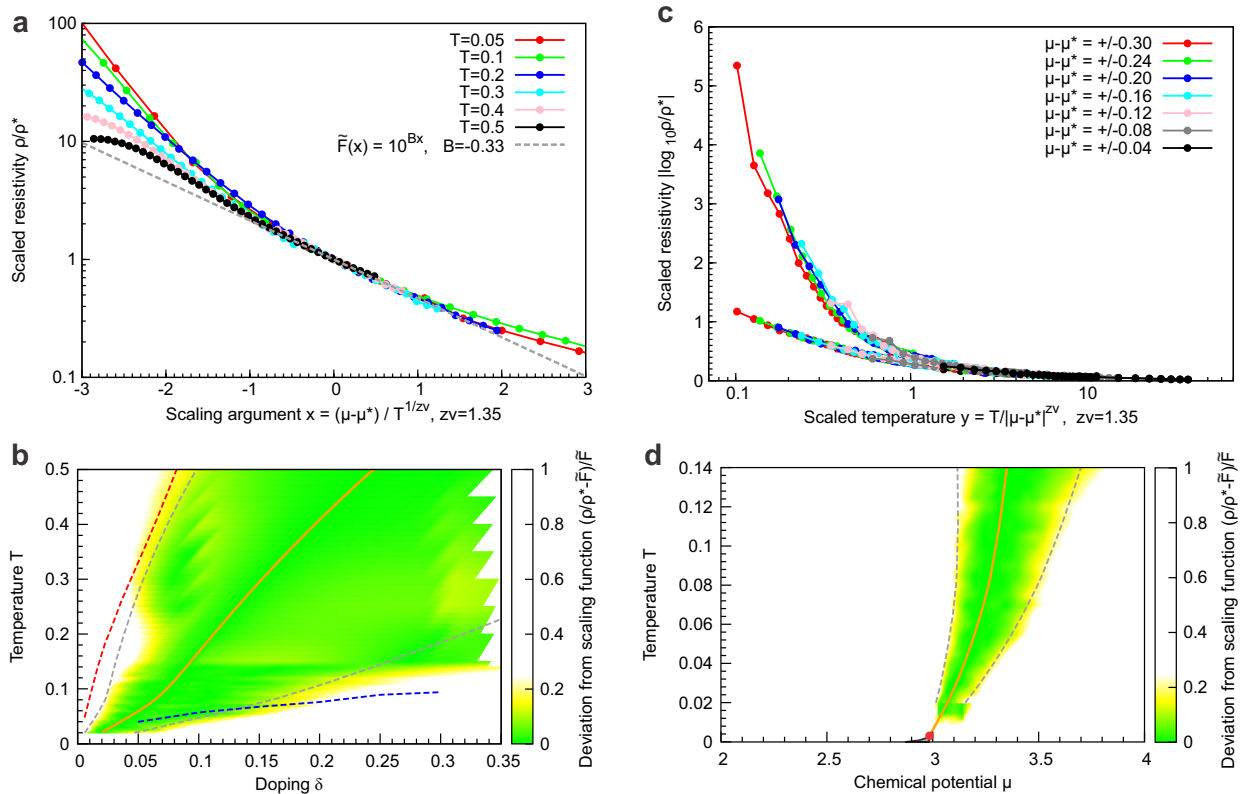
Figure 7: **The extent of the scaling region.** (a) The DMFT data are plotted as a function of the scaling argument x to obtain a fit for the scaling function. The range of x where DMFT data points fall on a single, well defined curve can be used as an estimate of the scaling region. (b) Between $x = -1.0$ and $x = 1.5$ (gray dashed lines), the relative error of the scaling formula is below 10%. The boundaries of the scaling region coincide with the $\mu = 3.0$ line (dashed red) and the knee-like feature in resistivity $\rho(T)|_\delta$ which marks the boundary of the linear resistivity bad metal region (blue line). (c) The mirror symmetry is found where the two branches of $|\log F(y)|$ coincide. (d) The scaling region in the $\mu - T$ plane; the scaling is valid for $T \gtrsim 4T_c$.

[1] K. Haule, Phys. Rev. B **75**, 155113 (2007).

[2] A. Georges, G. Kotliar, W. Krauth, and M. J. Rozenberg, Rev. Mod. Phys. **68**, 13 (1996).

[3] R. Žitko, D. Hansen, E. Perepelitsky, J. Mravlje, and A. Georges, Phys. Rev. B **88**, 235132 (2013).

[4] D. S. Fisher, G. Kotliar, and G. Moeller, Phys. Rev. B **52**, 17112 (1995).

[5] G. Kotliar, S. Murthy, and M. J. Rozenberg, Phys. Rev. Lett. **89**, 046401 (2002).

[6] P. Werner and A. J. Millis, Phys. Rev. B **75**, 085108 (2007).

[7] M. J. Rozenberg, R. Chitra, and G. Kotliar, Phys. Rev. Lett. **83**, 3498 (1999).

[8] J. Vučičević, H. Terletska, D. Tanasković, and D. Dobrosavljević, Phys. Rev. B **88**, 075143 (2013).

[9] G. G. Simeoni, T. Bryk, F. A. Gorelli, M. Krisch, G. Ruocco, M. Santoro, and T. Scopigno, Nature Physics **6**, 503 (2010).

[10] H. Terletska, J. Vučičević, D. Tanasković, and V. Dobrosavljević, Phys. Rev. Lett. **107**, 026401 (2011).

[11] M. J. Case and V. Dobrosavljević, Phys. Rev. Lett. **99**, 147204 (2007).

[12] M. Jarrell and J. E. Gubernatis, Physics Reports **269**, 133 (1996).

[13] A. W. Sandvik, Phys. Rev. B **57**, 10287 (1998).

[14] X. Deng, J. Mravlje, R. Žitko, M. Ferrero, G. Kotliar, and A. Georges, Phys. Rev. Lett. **110**, 086401 (2013).

Magnetic impurities in spin-split superconductors

W.-V. van Gerven Oei,[1] D. Tanasković,[1] and R. Žitko[2]

[1]*Scientific Computing Laboratory, Center for the Study of Complex Systems, Institute of Physics Belgrade,*
University of Belgrade, Pregrevica 118, 11080 Belgrade, Serbia
[2]*Jožef Stefan Institute, Jamova 39, SI-1000 Ljubljana, Slovenia*

Hybrid semiconductor-superconductor quantum dot devices are tunable physical realizations of quantum impurity models for a magnetic impurity in a superconducting host. The binding energy of the localized subgap Shiba states is set by the gate voltages and external magnetic field. In this work we discuss the effects of the Zeeman spin splitting, which is generically present both in the quantum dot and in the (thin-film) superconductor. The unequal g factors in semiconductor and superconductor materials result in respective Zeeman splittings of different magnitude. We consider both classical and quantum impurities. In the first case we analytically study the spectral function and the subgap states. The energy of bound states depends on the spin-splitting of the Bogoliubov quasiparticle bands as a simple rigid shift. For the case of collinear magnetization of impurity and host, the Shiba resonance of a given spin polarization remains unperturbed when it overlaps with the branch of the quasiparticle excitations of the opposite spin polarization. In the quantum case, we employ numerical renormalization group calculations to study the effect of the Zeeman field for different values of the g factors of the impurity and of the superconductor. We find that in general the critical magnetic field for the singlet-doublet transition changes nonmonotonically as a function of the superconducting gap, demonstrating the existence of two different transition mechanisms: Zeeman splitting of Shiba states or gap closure due to Zeeman splitting of Bogoliubov states. We also study how in the presence of spin-orbit coupling, modeled as an additional noncollinear component of the magnetic field at the impurity site, the Shiba resonance overlapping with the quasiparticle continuum of the opposite spin gradually broadens and then merges with the continuum.

I. INTRODUCTION

The interest in bound states induced by magnetic impurities in superconductors, predicted in the early works of Yu, Shiba, and Rusinov [1–3], has been recently revived by the advances in the synthesis and characterization of semiconductor-superconductor nanostructures [4–9] and in the tunneling spectroscopy of magnetic adsorbates on superconductor surfaces [10–15]. In particular, hybrid devices based on quantum dots can be used as fully controllable physical realizations of quantum impurity models with gapped conduction bands [16–27]. The ground state of the quantum dot can be tuned to be either a spin singlet or a spin doublet depending on the impurity level and the hybridization with the bulk superconductor [5,6,28–31]. The Coulomb interaction on the quantum dot favors the spin doublet ground state, while the spin singlet can be stabilized by the Kondo effect or by pairing due to the superconducting proximity effect [32–36]. The position of the in-gap (Shiba) resonances, as determined from the tunneling conductance, agrees even quantitatively with the calculations based on the simple single-orbital Anderson impurity model [37,38].

Very recently, research has focused on the effects of the magnetic field on the in-gap states [39–48] because systems of this class have been proposed as possible building blocks for topologically ordered systems exhibiting Majorana edge states [49–52]. These are significant for fundamental reasons and might also find application in quantum computation [53–55]. When an external magnetic field is applied to a thin-film superconductor in the parallel (in-plane) direction, the superconducting state persists to relatively large fields. The quasiparticle states become, however, strongly spin polarized

and the coherence peaks in the density of states become Zeeman split [56–60]: Systems in this regime are known as spin-split or Zeeman-split superconductors, and play a key role in the emerging field of superconducting spintronics [61]. The spectral function of a spin-split superconductor has two band edges with diverging coherence peaks separated by the bulk Zeeman energy, reflecting the fact that the Bogoliubov excitations have spin-dependent energies $E_{k\sigma} = \sqrt{\xi_k^2 + \Delta^2} + g_{\mathrm{bulk}}\mu_B B\sigma$. Here $\xi_k = \epsilon_k - \mu$ is the energy level ϵ_k of electron with momentum k measured with respect to the chemical potential μ, Δ is the gap, g_{bulk} is the g factor of the superconductor, μ_B is the Bohr magneton, B is the magnetic field, and $\sigma = \pm 1/2$ is the quasiparticle spin. Since the Shiba states can be considered as bound states of Bogoliubov quasiparticles, the spectral properties of magnetic impurities in spin-split superconductors are modified.

The theoretical work has, so far, mainly focused on the effect of a local magnetic field applied on the position of the impurity only [45,46]. For bulk electrons in the normal state, this approximation is usually justified because the impurity magnetic susceptibility is typically much larger ($\chi_{\mathrm{imp}} \propto 1/T_K$, where T_K is the Kondo temperature) than that of the bulk electrons (Pauli susceptibility, $\chi_{\mathrm{bulk}} \propto \rho \propto 1/D$, where ρ is the density of states at the Fermi level and D is the bandwidth). In superconductors, however, the Zeeman splitting of the Bogoliubov quasiparticle bands and the Zeeman splitting of the doublet subgap states are of comparable magnitude: The splitting of the first is simply the Zeeman energy $g_{\mathrm{bulk}}\mu_B B$, while the splitting of the second is $\tilde{g}_{\mathrm{imp}}\mu_B B$, where $\tilde{g}_{\mathrm{imp}}$ is the impurity g factor g_{imp} renormalized by the coupling with the bulk. Generically, both splittings are comparable with

the possible exception of nanowire quantum dots made of materials with extremely strong spin-orbit (SO) coupling and hence very high bare g_{imp}. For this reason, it is important to include the Zeeman terms both in the impurity and in the bulk part of the Hamiltonian.

We introduce the ratio r of the Landé g factors which describe the magnitude of the Zeeman splittings:

$$r = g_{bulk}/g_{imp}. \tag{1}$$

For many elemental superconductors the g factor is close to the free electron value, $g_{bulk} \approx 2$. In semiconductors the g factor usually differs strongly from this value due to SO coupling. The effective g factors are quite variable [62]: They can be very large positive, as well as very large negative, or can even be tuned close to 0. The control of g can be achieved through strain engineering [63], nanostructuring [64], or by electrical tuning in quantum dots [62,65–67]. In the $r = 0$ limit, the Zeeman term is only present on the impurity site: This limit is appropriate for materials with very large positive or negative g factor, where the Zeeman splitting in the superconductor is indeed negligible. Another special limit is $r = 1$, where all sites (bulk and impurity) have the same g factor. In general, however, the value of r is essentially unconstrained.

Here we study, using analytical calculations for a classical impurity (with no internal dynamics) and with the numerical renormalization group (NRG) method [22,68–74] for a quantum impurity (which incorporates the effect of spin flips), the spectral properties of the Shiba states. In the classical case we perform a calculation along the lines of Refs. [1–3], but include the effect of the Zeeman term in the superconductor. In the quantum case we focus on the single-orbital Anderson impurity and discuss the changes in the singlet-doublet phase transition as the ratio of the g factors of the impurity and the bulk is varied. We study the fate of a subgap resonance when it approaches the continuum of the Bogoliubov quasiparticles with the opposite spin, with and without the additional transverse magnetic field that mimics noncollinearity in the presence of SO coupling.

II. CLASSICAL IMPURITY

Initially, the impurity is described using a quantum mechanical spin-S operator, which is exchange coupled with the spin density of the conduction band electrons at the position of the impurity at $\mathbf{r} = 0$. The corresponding Hamiltonian is $H = H_{BCS} + H_{imp}$ with

$$H_{BCS} = \sum_{k\sigma} \xi_k c^\dagger_{\mathbf{k},\sigma} c_{\mathbf{k},\sigma} - \Delta \sum_k (c^\dagger_{\mathbf{k},\uparrow} c^\dagger_{-\mathbf{k},\downarrow} + \text{H.c.})$$
$$+ \sum_k b_{bulk} s_{z,\mathbf{k}} \tag{2}$$

and

$$H_{imp} = J\mathbf{S} \cdot \mathbf{s}(\mathbf{r} = 0), \tag{3}$$

where $b_{bulk} = g_{bulk}\mu_B B$ is the magnetic field expressed in the energy units (i.e., the Zeeman splitting), $s_{z,\mathbf{k}} = \frac{1}{2}(n_{\uparrow,\mathbf{k}} - n_{\downarrow,\mathbf{k}})$, and $\mathbf{s}(\mathbf{r} = 0) = \frac{1}{N} \sum_\mathbf{k} \mathbf{s}_\mathbf{k}$. J is the exchange coupling between the impurity and the host. All other quantities have already been defined in the previous section. The classical impurity

limit consists of taking the $S \to \infty$ limit while keeping $JS = \text{const}$. In this limit, the longitudinal component of the exchange interaction persists, while the transverse (spin-flip) components decrease as $1/S$ and hence drop out of the problem. The Hamiltonian then becomes noninteracting. We introduce the effective local field

$$h = JS \tag{4}$$

and the dimensionless impurity coupling parameter

$$\alpha = \pi\rho h/2 = \pi\rho JS/2, \tag{5}$$

where ρ is the density of states (DOS) at the Fermi level in the normal state. We will first assume that the bulk field b_{bulk} and the effective local field h are collinear and of the same sign. To be specific, we choose $b_{bulk} > 0, h > 0$.

The nonperturbed Green's function of the Zeeman-split superconductor is

$$G^0_k(z) = \frac{(z - b_{bulk}/2)\tau_0 + \epsilon_k\tau_3 - \Delta\tau_1}{(z - b_{bulk}/2)^2 - (\epsilon_k^2 + \Delta^2)}. \tag{6}$$

Here τ_1, τ_2, τ_3 are the Pauli matrices, τ_0 is the identity matrix, and z is the frequency argument. To obtain the local Green's function at the origin, G^0_{loc}, we sum over the momenta k and switch over to an integral over energies assuming a flat DOS in the normal state. In the wide-band limit we find

$$G^0(z) = -\pi\rho \frac{(z - b_{bulk}/2)\tau_0 - \Delta\tau_1}{\sqrt{\Delta^2 - (z - b_{bulk}/2)^2}}. \tag{7}$$

The Dyson's equation to include the impurity effect can be written as [1–3]

$$[G(z)]^{-1} = [G^0(z)]^{-1} - h\tau_0. \tag{8}$$

We have

$$[G^0(z)]^{-1} = -\frac{\sqrt{\Delta^2 - \left(z - \frac{b_{bulk}}{2}\right)^2}}{\pi\rho\left[\left(z - \frac{b_{bulk}}{2}\right)^2 - \Delta^2\right]}[(z - b_{bulk}/2)\tau_0 + \Delta\tau_1], \tag{9}$$

and finally

$$G(z) = -\pi\rho \frac{1}{D}\begin{pmatrix} a & \Delta \\ \Delta & a \end{pmatrix}, \tag{10}$$

where

$$D = 2\alpha\left(\frac{b_{bulk}}{2} - z\right) + (\alpha^2 - 1)\sqrt{\Delta^2 - \left(\frac{b_{bulk}}{2} - z\right)^2},$$

$$a = b_{bulk}/2 - z + \alpha\sqrt{\Delta^2 - (b_{bulk}/2 - z)^2}. \tag{11}$$

The spin-up spectral function is $A_\uparrow(\omega) = -(1/\pi)\text{Im}G_{11}(\omega + i\delta)$, while the spin-down spectral function is $A_\downarrow(\omega) = -(1/\pi)\text{Im}[-G_{22}(-\omega - i\delta)] = -(1/\pi)\text{Im}G_{22}(-\omega + i\delta)$.

The 11 (spin-up) matrix component of $G(z)$ has two poles:

$$\omega_{1,2} = b_{bulk}/2 \pm \Delta\frac{1 - \alpha^2}{1 + \alpha^2}. \tag{12}$$
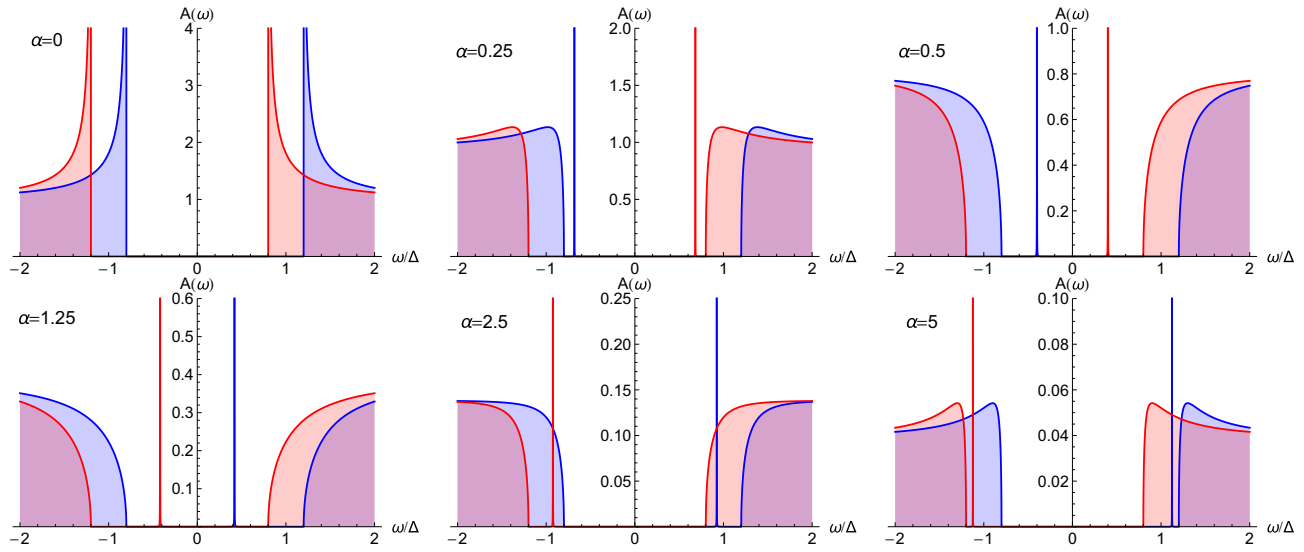
FIG. 1. Spin-projected spectral functions (blue for spin-up, red for spin-down) for a range of the dimensionless impurity coupling $\alpha = \pi \rho J S/2$ in a Zeeman-split superconductor with $b_{\text{bulk}}/\Delta = 0.4$.

Only one pole has a finite residue. For $h > 0$ (hence $\alpha > 0$) we find a subgap resonance in the spin-up spectral function at

$$\omega_\uparrow = b_{\text{bulk}}/2 - \Delta \frac{1 - \alpha^2}{1 + \alpha^2}. \tag{13}$$

Conversely, the spin-down spectral function has a resonance at $\omega_\downarrow = -\omega_\uparrow$:

$$\omega_\downarrow = -b_{\text{bulk}}/2 + \Delta \frac{1 - \alpha^2}{1 + \alpha^2}. \tag{14}$$

We emphasize that the spin-projected spectral functions have a single subgap resonance, one for each spin. This is to be contrasted with the behavior of the quantum model discussed in the following section which has (in the spin-singlet regime for finite magnetic field) two resonances in each spin-projected spectral function. This is a clear indication of the different degeneracies of states in the classical and quantum impurity models.

Some representative spectra are plotted in Fig. 1. The $\alpha = 0$ case corresponds to the limit of a clean Zeeman-split superconductor. Each quasiparticle continuum branch has a characteristic inverse square root divergence at its edge.

For small $\alpha = 0.25$, the Shiba bound states emerge out of the quasiparticle continuum, the spin-up resonance in the negative part of the spectrum, and the spin-down resonance in the positive part, in line with Eqs. (13) and (14) for small α. The shift by $b_{\text{bulk}}/2$ is expected, since the spin-up Shiba state is generated by the Bogoliubov states with spin up, which are themselves shifted by the same amount. Conversely, the spin-down Shiba state is generated as a linear superposition of Bogoliubov states with spin down, which are shifted by $-b_{\text{bulk}}/2$. We observe that *all four* branches of the quasiparticle band lose their inverse square-root singularity and contribute spectral weight to the nascent Shiba state (see also Ref. [48]), not only the "inner" ones (spin-up occupied and spin-down unoccupied).

With increasing α, the Shiba states move toward the gap center (chemical potential) and they cross when the condition

$$b_{\text{bulk}}/2 = \Delta \frac{1 - \alpha^2}{1 + \alpha^2} \tag{15}$$

is met, i.e., at

$$\alpha^* = \frac{\sqrt{1 - b_{\text{bulk}}/2\Delta}}{\sqrt{1 + b_{\text{bulk}}/2\Delta}}. \tag{16}$$

For $b_{\text{bulk}}/\Delta = 0.4$, as used here, this happens at $\alpha^* \approx 0.82 < 1$. This signals the occurrence of the quantum phase transition in which the fermion parity of the (sub)system changes. We also note that alternatively, for constant $\alpha < 1$, the transition can be driven by the external magnetic field.

For still larger $\alpha = 2.5$, the spin-up Shiba resonance overlaps with the spin-down quasiparticle continuum (and vice versa for the spin-down Shiba resonance), but since the spin is assumed to be a good quantum number there is no broadening of the Shiba resonances. (See below, Sec. III B, for a discussion of the SO effects in the case of a quantum impurity.)

For very large values of α, the Shiba states eventually merge with the continuum again. This trend is accompanied by the reappearance of the inverse square-root resonances, an indication of which is visible for $\alpha = 5$ in Fig. 1.

We now discuss the case of antialigned fields, taking $b_{\text{bulk}} > 0$ and $h < 0$. In this case, for small $|\alpha|$ the spin-up Shiba state occurs at

$$\omega_\uparrow = b_{\text{bulk}}/2 + \Delta \frac{1 - \alpha^2}{1 + \alpha^2}, \tag{17}$$

and hence overlaps with the continuum of spin-down quasiparticles for $|\alpha| < 1/\sqrt{2\Delta/b_{\text{bulk}} - 1}$. The quantum phase transition occurs for

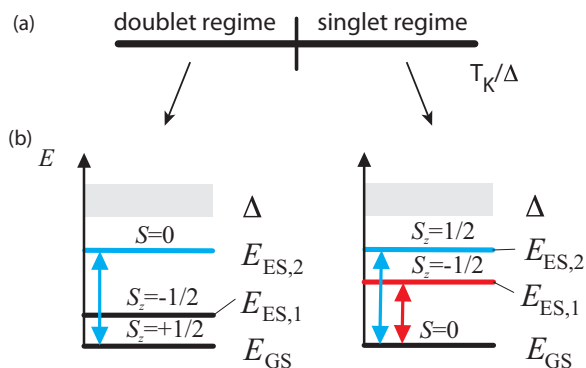$$|\alpha^*| = \frac{\sqrt{1 + b_{\text{bulk}}/2\Delta}}{1 - b_{\text{bulk}}/2\Delta} > 1. \tag{18}$$

FIG. 2. (a) Schematic phase diagram for $B = 0$. (b) Subgap splitting for finite field B.

For large $|\alpha|$ the Shiba states again merge with the continuum at the inner edges of the Bogoliubov bands. The regimes that the system goes through for $\alpha < 0$ are thus in the opposite order to those for $\alpha > 0$.

The main deficiency of the impurity model in the classical limit is the reduced multiplicity of the subgap states. Physically, this is due to the fact that in the classical limit the effective impurity potential for particle-like excitations is attractive for one spin orientation and repulsive for the other; hence a single bound state is generated for a given spin orientation. The spin-flip processes in the quantum model lead to a situation where the effective potential is attractive for both spin polarizations, hence twice the degeneracy. We discuss this more general situation in the following section.

III. QUANTUM IMPURITY

A. Model and method

We consider a single spin-$\frac{1}{2}$ impurity level with on-site Coulomb interaction. The Hamiltonian is given by

$$
H = \sum_{\mathbf{k},\sigma} \epsilon_{\mathbf{k}} c^\dagger_{\mathbf{k}\sigma} c_{\mathbf{k}\sigma} - \Delta \sum_{\mathbf{k}} (c^\dagger_{\mathbf{k}\uparrow} c^\dagger_{-\mathbf{k}\downarrow} + \text{H.c.})
$$
$$
+ V \sum_{\mathbf{k},\sigma} (d^\dagger_\sigma c_{\mathbf{k}\sigma} + \text{H.c.}) + \epsilon_d \sum_\sigma n_\sigma + U n_\uparrow n_\downarrow
$$
$$
+ g_{\text{imp}} \mu_B (B S_z + B_x S_x) + g_{\text{bulk}} \mu_B B \sum_{\mathbf{k}} s_{z,\mathbf{k}}. \quad (19)
$$

$d^\dagger_\sigma$ is the creation operator on the impurity which is hybridized with the bulk by V and has the energy level ϵ_d. $n_\sigma = d^\dagger_\sigma d_\sigma$, $S_z = \frac{1}{2}(d^\dagger_\uparrow d_\uparrow - d^\dagger_\downarrow d_\downarrow)$, $S_x = \frac{1}{2}(d^\dagger_\uparrow d_\downarrow + d^\dagger_\downarrow d_\uparrow)$, $s_{z,\mathbf{k}} = \frac{1}{2}(c^\dagger_{\mathbf{k}\uparrow} c_{\mathbf{k}\uparrow} - c^\dagger_{\mathbf{k}\downarrow} c_{\mathbf{k}\downarrow})$. The magnetic field B couples with the quantum dot by the g factor equal to g_{imp} and with the superconductor by g_{bulk}. The transverse magnetic field which can flip the spin is introduced through the parameter B_x. We will consider a flat particle-hole symmetric band of half-width D so that $\rho = 1/2D$. The hybridization strength is characterized by $\Gamma = \pi \rho V^2$.

We employ the NRG method to solve the problem. There are two ways to introduce a bulk Zeeman field in the NRG: as local Zeeman terms on all sites of the Wilson chain, or through a separate discretization of spin-up and spin-down densities of states shifted by the Zeeman term [75]. The former approach is suitable for models with a spectral gap, as discussed here, while the latter has to be used for spin-polarized metals with finite DOS at the Fermi level. We use a fine discretization mesh with twist averaging over $N_z = 64$ grids so that high spectral
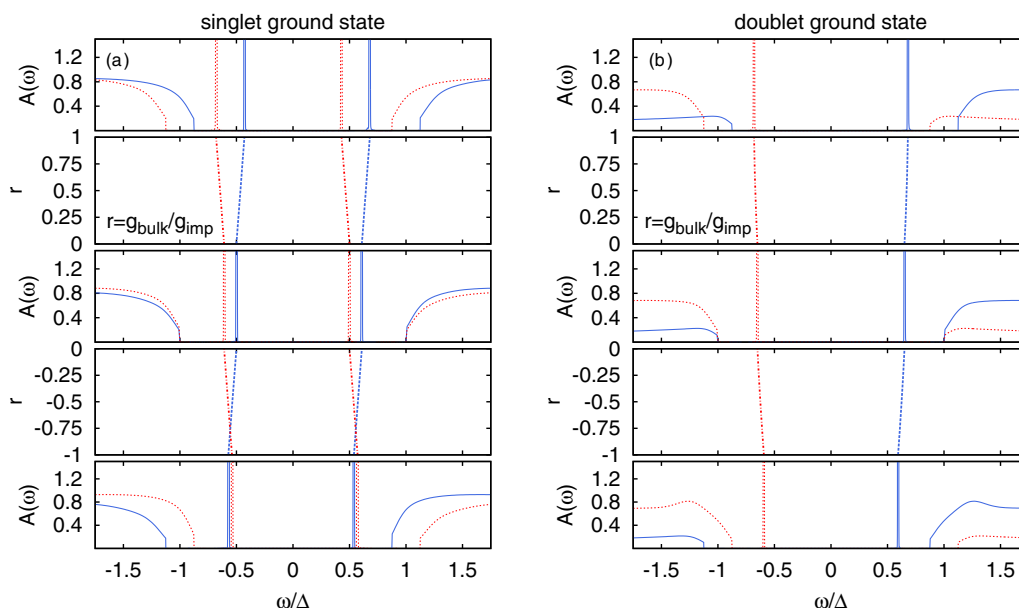

FIG. 3. Spectral function of the impurity for the spin singlet (a) and spin doublet ground state (b). The parameters are $b_{\text{imp}}/U = 0.005$ and $\Delta/U = 0.02$. For the singlet ground state $\Gamma/U = 0.2$ and for the doublet $\Gamma/U = 0.075$. The spectrum for $r = g_{\text{bulk}}/g_{\text{imp}} = 0$ is shown in central panels, the adjoining panels show the evolution of the position of the Shiba resonances as $|r|$ increases, and the top/bottom panels correspond to $r = 1$ and $r = -1$, respectively.

resolution is possible inside the gap and in the vicinity of the gap edges, which are the regions of main interest in this work. The only conserved quantum number in the presence of an external field along the z axis is the projection of total spin S_z, i.e., the problem has U(1) spin symmetry. Other parameters are $\Lambda = 2$, the NRG truncation cutoff energy is $10\epsilon_N$ where $\epsilon_N \propto \Lambda^{-N/2}$ is the energy scale at the Nth step of the iteration, and at least 200 states were used at late iterations N when the gap is opened. The spectral functions are computed with the DMNRG algorithm [70] with the $N/N+2$ scheme for patching the spectral functions. This approach allows maximal spectral resolution at zero temperature. The broadening is performed on a logarithmic mesh with a small ratio $r = 1.01$ between two energies outside the gap and on a linear mesh inside the gap. As can be seen in the figures further down, the use of these different broadening kernels leads to some artifacts at the continuum edges. All calculations are performed in the zero-temperature limit, $T = 0$.

Unless otherwise specified, the model parameters are $U/D = 1$, $\Delta/U = 0.02$, and $\epsilon_d = -U/2$.

The ground state of the Anderson impurity model, Eq. (19), in the absence of the magnetic field is either a singlet or a doublet depending on the ratio of the Kondo temperature [68,69] $T_K \approx 0.18U\sqrt{8\Gamma/\pi U}\exp(-\pi U/8\Gamma)$ and the superconducting gap Δ. The impurity spin is screened by the conduction electrons for $\Delta < \Delta_c$ forming a spin singlet, while for $\Delta > \Delta_c$ the local moment is unscreened and the ground state forms a spin doublet; here $\Delta_c \approx T_K/0.3$ [17,18,22] in the limit $U/\Gamma \ll 1$. At the quantum phase transition the energy of the excited many-particle state goes to zero, and the energy levels cross. The transition is accompanied by a jump in the spectral weight of the in-gap resonances and a change of sign of the pairing amplitude [34]. The Zeeman field B lifts the degeneracy of the doublet state [44–46,76]. For a spin singlet ground state, the in-gap resonances corresponding to the doublet state are split in the magnetic field B. In the case of doublet ground state, the positions of the singlet Shiba resonances are shifted in the Zeeman field.

Figure 2 shows a schematic phase diagram in zero magnetic field and the evolution of the energy levels of the ground and excited states with increasing Zeeman magnetic field. This evolution of the in-gap resonances with changes of the hybridization and the magnetic field has been recently observed in tunneling experiments and agrees with the theoretical predictions in the case when the field is coupled only with impurity [44–47]. Here, we explore the fate of the subgap states when the magnetic field is also Zeeman coupled with the bulk superconductor.

B. Results

We now discuss the spectral function of the impurity in different parameter regimes and identify the boundary of the singlet-doublet phase transition in the (B, Δ) parameter plane for different values of the g-factor ratio r.

We first consider the case of singlet ground state. In the magnetic field the subgap resonance (which is a spin doublet) splits to its spin-up and spin-down components. The impurity spectral function for $\Gamma/U = 0.2$, $b_{\mathrm{imp}}/U = 0.005$ is shown in Fig. 3(a) for $r = 0$ (central panel), $r = 1$ (top panel), and
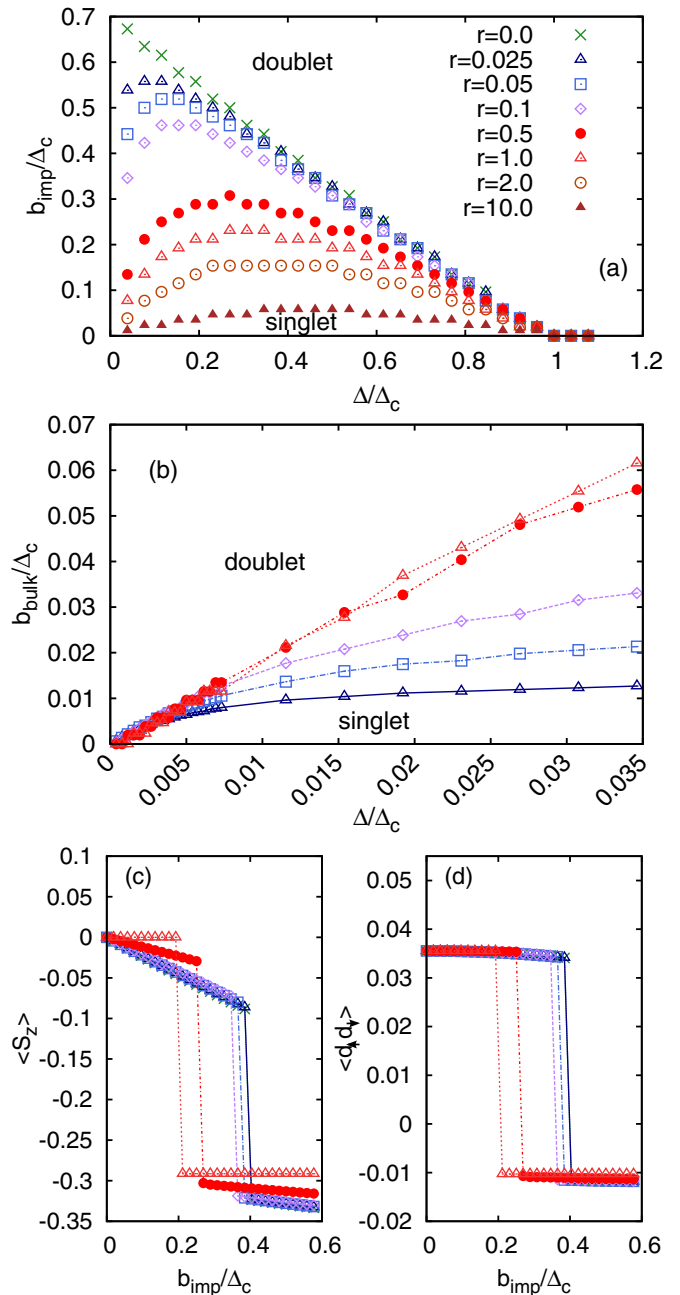

FIG. 4. (a) Phase diagram in the (B, Δ) plane for several values of $r = g_{\mathrm{bulk}}/g_{\mathrm{imp}}$. Here $\Gamma/U = 0.2$, $\Delta_c/U \approx 0.13$. (b) For small Δ the singlet-doublet transition coincides with the closure of the SC gap for $b_{\mathrm{bulk}} \approx 2\Delta$. (c) The expectation value $\langle S_z \rangle$ and (d) the pairing amplitude $\langle d_\uparrow d_\downarrow \rangle$ abruptly change across the phase transition. Here $\Delta = 0.385\Delta_c$.

$r = -1$ (bottom panel). The additional panels show how the position of the resonances shifts as the parameter r is varied. For $r = 1$ the expectation value of the spin projection $\langle S_z \rangle$ at the impurity site is $\langle S_z \rangle = 0$ [see Fig. 4(c) and the appendix]. Such compensation holds also in the particle-hole asymmetric case as long as $g_{\mathrm{imp}} = g_{\mathrm{bulk}}$. If the g factors are different, there will be net magnetization at the impurity site even if the ground state is a spin singlet and there is a finite gap to excited states.

We next consider the case of smaller hybridization, $\Gamma/U = 0.075$, so that the impurity is in the doublet ground state. The spectral functions for $r = 0$, $r = 1$, and $r = -1$, as well as the evolution between them, are shown in Fig. 3(b). A single resonance is now visible for $\omega > 0$, since the ground state has spin projection $S_z = 1/2$, and the only possible excitation is adding a spin-up particle to form a $S_z = 0$ singlet state. We also observe notable differences in the appearance of the gap edges for both spin projections, related to the strong spin polarization of the impurity state in the doublet regime. We emphasize that this distinguishing feature is not present in the classical impurity model discussed above.

The phase diagram in the (B, Δ) plane is shown in Fig. 4. This plot represents the main result of this work. In the absence of a magnetic field, the ground state changes from singlet to doublet for $\Delta = \Delta_c = 0.13U$. Here, $T_K \approx 0.018U$ and $T_K/\Delta_c = 0.138$ for the chosen value of $\Gamma/U = 0.2$. For $\Delta < \Delta_c$ the transition can be also induced by changing the magnetic field. For $r = 0$ the magnetic field is coupled only with the impurity. In this case, as shown in Ref. [45], the critical magnetic field B_c for the singlet-doublet transition linearly depends on the gap, $B_c \sim \Delta_c - \Delta$. For $r \neq 0$, however, B_c has nonmonotonic dependence on Δ: It increases approximately linearly with Δ as it gets reduced from Δ_c, reaches a maximum, and then decreases to zero as $\Delta \rightarrow 0$. For $\Delta \sim \Delta_c$ the singlet-doublet transition is a consequence of a competition of three characteristic energies: Δ, T_K, and B. For very small values of Δ (for $\Delta \ll \Delta_c$) the singlet-doublet transition coincides with the closure of the superconducting gap for $b_{\text{bulk}} = 2\Delta$. The phase boundary for small value of Δ is shown in Fig. 4(b). We note that for small Δ the transition to the normal phase would actually occur for smaller value of B, $B = B_{\text{cl}} = \sqrt{g}\Delta \approx \sqrt{2}\Delta$, known as the Clogston limit [77,78]. For $B > B_{\text{cl}}$ the normal phase has lower free energy than the superconducting one. Our main focus is, however, on larger values of the superconducting gap when it is comparable to the Kondo temperature.

The average value of the projection of the local spin $\langle S_z \rangle$ abruptly changes at the phase transition, Fig. 4(c). For
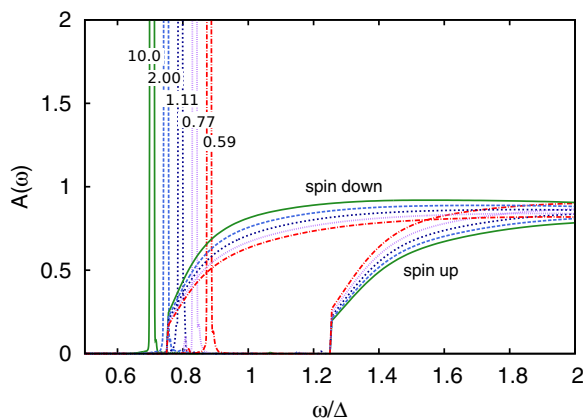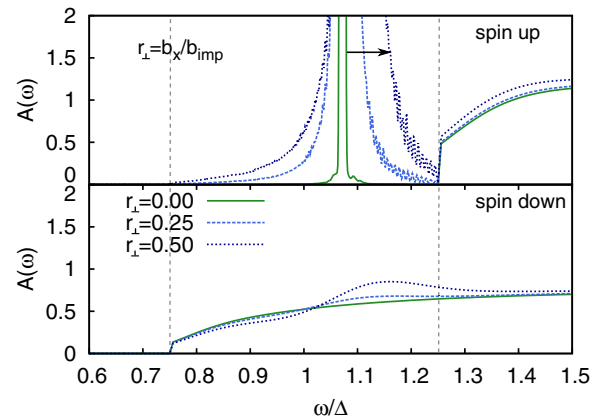

FIG. 6. Spectral function of the spin-up Shiba resonance and the quasiparticle continuum for several values of the spin-flipping transverse magnetic field. As b_x increases, the Shiba resonance broadens.

$g_{\text{imp}} = g_{\text{bulk}}$, i.e., for $r = 1$, the average value $\langle S_z \rangle = 0$ in the singlet case (see also the appendix). For $r \neq 1$, $\langle S_z \rangle$ is nonzero but small for singlet ground state, and it jumps to large absolute value by increasing the magnetic field at the transition to doublet ground state. The pairing amplitude on the impurity, $\langle d_\uparrow d_\downarrow \rangle$, shows a characteristic sign change at the transition, Fig. 4(d).

When the spin-up Shiba state begins to overlap with the spin-down branch of Bogoliubov excitations, it remains unperturbed, as in the classical impurity model. This is the case in spite of the spin-flip processes in the quantum model and is a simple consequence of the conservation of the spin projection S_z quantum number. In other words, the spin-up Shiba state is a bound state of spin-up Bogoliubov quasiparticles, which are orthogonal to and do not mix with the spin-down Bogoliubov quasiparticles. This is illustrated in Fig. 5. Here g_{bulk} and B were kept constant, while the position of the spin-up resonance was changed by changing g_{imp}. A transverse magnetic field, however, flips the spin and the Shiba resonances broaden, as illustrated in Fig. 6. Such broadening effects are expected in realistic systems due to SO coupling.

IV. CONCLUSION

We have analyzed the behavior of magnetic impurities coupled to superconductors subject to an applied magnetic field that does not fully suppress the superconducting order but strongly spin splits the Bogoliubov quasiparticle continua because of the Zeeman coupling. This situation commonly occurs when the field is applied in the plane of a superconducting thin layer and leads to clearly observable effects.

For a classical impurity, approximated as a static local pointlike magnetic field (and aligned with the external field), we find that the position of the Shiba state is shifted linearly with the external field as a simple consequence of the shifting edges of the quasiparticle bands. In fact, the only effect of the spin splitting of the Bogoliubov states is that the frequency

FIG. 5. Spin up in-gap resonances and continuum of excitations for several values of r. Here $b_{\text{bulk}}/U = 0.01$ was kept constant. The finite width of the Shiba resonances is a broadening artifact: These resonances are true δ peaks at zero temperature.

argument in the impurity Green's function is shifted as $\omega \to \omega + b_{\text{bulk}}/2$ for spin-up and $\omega \to \omega - b_{\text{bulk}}/2$ for spin-down particles. The parity-changing quantum phase transition no longer occurs at $\alpha = \pi\rho J S/2 = 1$, but rather when the condition $b_{\text{bulk}} = g_{\text{bulk}}\mu_B B/2 = \Delta(1-\alpha^2)/(1+\alpha^2)$ is met. This occurs for $\alpha = \alpha^* < 1$. We observed that for large α the Shiba state of a given spin may overlap with the quasiparticle continuum of the opposite spin and still remain a sharp resonance (a δ peak). This remains true as long as there is no matrix element linking the quasiparticles of both spins.

We then turned to the case of a quantum impurity with far more complex behavior. The Zeeman coupling is present both in the bulk and on the impurity site, and generically the corresponding g factors are different: This is typically indeed the case in the nanoscale hybrid superconductor-semiconductor devices. We find a very significant effect of the Zeeman splitting of the quasiparticle continua: The phase diagram of the possible many-particle ground states (singlet or doublet) in the (Δ, B) plane actually has two very different regimes. In the $\Delta \to \Delta_c$ limiting regime, the transition occurs because a strong enough field decreases the energy of spin-down doublet state below that of the singlet state. In this regime, the phase boundary in the (Δ, B) plane has a negative slope: The closer Δ is to Δ_c, the smaller the separation between the singlet and doublet states in the absence of the field and hence a smaller Zeeman splitting is necessary to induce the transition. We have established that for finite $r = g_{\text{bulk}}/g_{\text{imp}}$ the splitting between the doublet subgap states is larger than for $r = 0$ and hence the separation between the singlet and the spin-down doublet is smaller; thus the transition occurs for a smaller value of the magnetic field. In the other limiting regime of small Δ, the transition occurs because the gap between the spin-polarized Bogoliubov bands closes and the transition line is given asymptotically as $b_{\text{bulk}}/2 = \Delta$; hence the transition line has a positive slope. In reality, such transition is of course preempted by a bulk transition to the normal state (Clogston limit). Nevertheless, even in the physically accessible regime we observe that the actual behavior is determined by a competition of both trends and that the slope of the transition line changes at some intermediate point where the system crosses over from one limiting behavior to another. The actual transition line is therefore bell-shaped and depends on the value of r. The straight line found in the limit $r \to 0$ is, in fact, highly anomalous, and for realistic values of the ratio r there will be a significant degree of curvature.

We have confirmed the possibility of a sharp Shiba resonance overlapping with the continuum of opposite-spin Bogoliubov quasiparticles. In addition, we have considered the gradual widening of the Shiba resonance if local spin-flip processes are allowed (generated, e.g., by SO coupling leading to noncollinear effective magnetic fields): Such processes lead to the hybridization of the Shiba state and its gradual engulfing in the continuum.

In conclusion, we have established the importance of including the Zeeman splitting in the bulk of the superconductor when discussing the effect of the external magnetic field on the subgap states induced by magnetic impurities in superconductors.

APPENDIX: NONINTERACTING MODEL

For completeness, in this appendix we define the analytical expression for the noninteracting Anderson impurity model ($U = 0$); see also Ref. [79]. We work in the Nambu space, $D^\dagger = (d_\uparrow^\dagger, d_\downarrow)$, $C_k^\dagger = (c_{k\uparrow}^\dagger, c_{-k\downarrow})$. The Hamiltonian can be written as

$$H_{SC} = \sum_k C_k^\dagger A_k C_k, \quad (A1)$$

where

$$A_k = \begin{pmatrix} \epsilon_k + b_{\text{bulk}}/2 & -\Delta \\ -\Delta & -\epsilon_k + b_{\text{bulk}}/2 \end{pmatrix}. \quad (A2)$$

The Green's function is given by $g_k(z) = (z - A_k)^{-1}$,

$$g_k(z)^{-1} = (z - b_{\text{bulk}}/2)\sigma_0 - \epsilon_k \sigma_3 + \Delta \sigma_1, \quad (A3)$$

with $\sigma_{1,2,3}$ being Pauli matrices and σ_0 being the identity matrix, so that

$$g_k(z) = \frac{(z - b_{\text{bulk}}/2)\sigma_0 + \epsilon_k \sigma_3 - \Delta \sigma_1}{(z - b_{\text{bulk}}/2)^2 - (\epsilon_k^2 + \Delta^2)}. \quad (A4)$$

The impurity Green's function is

$$G(z)^{-1}(z) = z\sigma_0 - \epsilon_d \sigma_3 - (b_{\text{imp}}/2)\sigma_0 - V^2 \sigma_3 \frac{1}{N} \sum_k g_k(z)\sigma_3. \quad (A5)$$

In the wide-band limit

$$-V^2 \frac{1}{N}\sigma_3 \sum_k g_k(z)\sigma_3 = \Gamma \frac{(z - b_{\text{bulk}}/2)\sigma_0 + \Delta \sigma_1}{E(z - b_{\text{bulk}}/2)}, \quad (A6)$$

where $\Gamma = \pi\rho_0 V^2$. $T \to 0$, on real axis, $z = x + i\delta$:

$$E(x) = -i\,\text{sgn}(x)\sqrt{x^2 - \Delta^2}, \quad \text{for } |x| > \Delta,$$
$$E(x) = \sqrt{\Delta^2 - x^2}, \quad \text{for } |x| < \Delta. \quad (A7)$$

Finally, we have

$$G^{-1}(\omega) = (\omega - b_{\text{imp}}/2)\sigma_0 - \epsilon_d \sigma_3$$
$$+ \Gamma \frac{(\omega - b_{\text{bulk}}/2)\sigma_0 + \Delta \sigma_1}{E(\omega - b_{\text{bulk}}/2)}. \quad (A8)$$

Matrix inversion yields

$$G(\omega) = \frac{1}{D(\omega)}\left\{ (\omega - b_{\text{imp}}/2)\left[1 + \frac{\Gamma}{E(\omega - b_{\text{bulk}}/2)}\right]\sigma_0 \right.$$
$$\left. - \frac{\Gamma\Delta}{E(\omega - b_{\text{bulk}}/2)}\sigma_1 + \epsilon_d \sigma_3 \right\}, \quad (A9)$$

with

$$D(\omega) = (\omega - b_{\text{imp}}/2)^2 \left[1 + \frac{\Gamma}{E(\omega - b_{\text{bulk}}/2)}\right]^2$$
$$- \frac{\Gamma^2 \Delta^2}{E(\omega - b_{\text{bulk}}/2)^2} - \epsilon_d^2. \qquad (A10)$$

Now assume $b \equiv b_{\text{imp}} = b_{\text{bulk}}$. We consider two functions $G_\uparrow(\omega) = G_{11}(\omega + b/2)$ and $G_\downarrow(\omega) = -G_{22}(-\omega - b/2)^*$.

Taking into account the symmetry properties of $E(x)$, it is easily shown that $G_\uparrow = G_\downarrow$ both inside and outside the gap. This shows that as long as the system is in the singlet ground state, it is possible to shift the spectral functions of spin-up and spin-down subsystems to make them overlap; thus their integrals over the negative energies (occupied states) are equal and hence $\langle S_z \rangle = 0$. This is also the case in the interacting case. For $b_{\text{imp}} \neq b_{\text{bulk}}$, $\langle S_z \rangle$ in the singlet regime will be nonzero but small. In the doublet regime, irrespective of the value of $r = b_{\text{bulk}}/b_{\text{imp}}$, $\langle S_z \rangle$ is large.

[1] L. Yu, Bound state in superconductors with paramagnetic impurities, Acta Phys. Sin. **21**, 75 (1965).

[2] H. Shiba, Classical spins in superconductors, Prog. Theor. Phys. **40**, 435 (1968).

[3] A. I. Rusinov, Superconductivity near a paramagnetic impurity, Zh. Eksp. Teor. Fiz. Pisma Red. **9**, 146 (1968) [JETP Lett. **9**, 85 (1969)].

[4] M. F. Goffman, R. Cron, A. Levy Yeyati, P. Joyez, M. H. Devoret, D. Esteve, and C. Urbina, Supercurrent in Atomic Point Contacts and Andreev States, Phys. Rev. Lett. **85**, 170 (2000).

[5] J.-D. Pillet, C. H. L. Quay, P. Morin, C. Bena, A. Levy Yeyati, and P. Joyez, Andreev bound states in supercurrent-carrying carbon nanotubes revealed, Nat. Phys. **6**, 965 (2010).

[6] R. S. Deacon, Y. Tanaka, A. Oiwa, R. Sakano, K. Yoshida, K. Shibata, K. Hirakawa, and S. Tarucha, Interplay of Kondo and Superconducting Correlations in the Nonequilibrium Andreev Transport Through a Quantum Dot, Phys. Rev. Lett. **104**, 076805 (2010).

[7] S. De Franceschi, L. Kouwenhoven, C. Schönenberger, and W. Wernsdorfer, Hybrid superconductor-quantum dot devices, Nat. Nanotechnol. **5**, 703 (2010).

[8] L. Bretheau, C. O. Girit, C. Urbina, D. Esteve, and H. Pothier, Supercurrent Spectroscopy of Andreev States, Phys. Rev. X **3**, 041034 (2013).

[9] C. Janvier, L. Tosi, L. Bretheau, C. O. Girit, M. Stern, P. Bertet, P. Joyez, D. Vion, D. Esteve, M. F. Goffman, H. Pothier, and C. Urbina, Coherent manipulation of Andreev states in superconducting atomic contacts, Science **349**, 1199 (2015).

[10] A. Yazdani, B. A. Jones, C. P. Lutz, M. F. Crommie, and D. M. Eigler, Probing the local effects of magnetic impurities on superconductivity, Science **275**, 1767 (1997).

[11] S. H. Ji, T. Zhang, Y. S. Fu, X. Chen, X.-C. Ma, J. Li, W.-H. Duan, J.-F. Jia, and Q.-K. Xue, High-Resolution Scanning Tunneling Spectroscopy of Magnetic Impurity Induced Bound States in the Superconducting Gap of Pb Thin Films, Phys. Rev. Lett. **100**, 226801 (2008).

[12] K. J. Franke, G. Schulze, and J. I. Pascual, Competition of superconductivity phenomena and Kondo screening at the nanoscale, Science **332**, 940 (2011).

[13] M. Ruby, F. Pientka, Y. Peng, F. von Oppen, B. W. Heinrich, and K. J. Franke, Tunneling Processes into Localized Subgap States in Superconductors, Phys. Rev. Lett. **115**, 087001 (2015).

[14] M. T. Randeria, B. E. Feldman, I. K. Drozdov, and A. Yazdani, Scanning Josephson spectroscopy on the atomic scale, Phys. Rev. B **93**, 161115 (2016).

[15] N. Hatter, B. W. Heinrich, M. Ruby, J. I. Pascual, and K. J. Franke, Magnetic anisotropy in Shiba bound states across a quantum phase transition, Nat. Commun. **6**, 8988 (2015).

[16] A. Sakurai, Comments on superconductors with magnetic impurities, Prog. Theor. Phys. **44**, 1472 (1970).

[17] K. Satori, H. Shiba, O. Sakai, and Y. Shimizu, Numerical renormalization group study of magnetic impurities in superconductors, J. Phys. Soc. Jpn. **61**, 3239 (1992).

[18] O. Sakai, Y. Shimizu, H. Shiba, and K. Satori, Numerical renormalization group study of magnetic impurities in supercoductors, II: Dynamical excitations spectra and spatial variation of the order parameter, J. Phys. Soc. Jpn. **62**, 3181 (1993).

[19] M. I. Salkola, A. V. Balatsky, and J. R. Schrieffer, Spectral properties of quasiparticle excitations induced by magnetic moments in superconductors, Phys. Rev. B **55**, 12648 (1997).

[20] M. E. Flatté and J. M. Byers, Local Electronic Structure of a Single Magnetic Impurity in a Superconductor, Phys. Rev. Lett. **78**, 3761 (1997).

[21] M. E. Flatté and J. M. Byers, Local electronic structure of defects in superconductors, Phys. Rev. B **56**, 11213 (1997).

[22] T. Yoshioka and Y. Ohashi, Numerical renormalization group studies on single impurity Anderson model in superconductivity: A unified treatment of magnetic, nonmagnetic impurities, and resonance scattering, J. Phys. Soc. Jpn. **69**, 1812 (2000).

[23] D. K. Morr and N. A. Stavropoulos, Quantum interference between impurities: Creating novel many-body states in s-wave superconductors, Phys. Rev. B **67**, 020502(R) (2003).

[24] A. V. Balatsky, I. Vekhter, and J.-X. Zhu, Impurity-induced states in conventional and unconventional superconductors, Rev. Mod. Phys. **78**, 373 (2006).

[25] J. Bauer, A. Oguri, and A. C. Hewson, Spectral properties of locally correlated electrons in a Bardeen-Cooper-Schrieffer superconductor, J. Phys.: Condens. Matter **19**, 486211 (2007).

[26] A. Martín-Rodero and A. Levy Yeyati, Josephson and Andreev transport through quantum dots, Adv. Phys. **60**, 899 (2011).

[27] T. Dirks, T. L. Hughes, S. Lal, B. Uchoa, Y.-F. Chen, C. Chialvo, P. M. Goldbart, and N. Mason, Transport through Andreev bound states in a graphene quantum dot, Nat. Phys. **7**, 386 (2011).

[28] M. R. Buitelaar, T. Nussbaumer, and C. Schonenberger, Quantum Dot in the Kondo Regime Coupled to Superconductors, Phys. Rev. Lett. **89**, 256801 (2002).

[29] R. Maurand, T. Meng, E. Bonet, S. Florens, L. Marty, and W. Wernsdorfer, First-Order 0-π Quantum Phase Transition in the Kondo Regime of a Superconducting Carbon-Nanotube Quantum Dot, Phys. Rev. X **2**, 011009 (2012).

[30] A. Martín-Rodero and A. L. Yeyati, The Andreev states of a superconducting quantum dot: Mean field versus exact numerical results, J. Phys.: Condens. Matter **24**, 385303 (2012).

[31] M. Jarrell, D. S. Sivia, and B. Patton, Gap states in dilute-magnetic-alloy superconductors: A quantum Monte Carlo study, Phys. Rev. B **42**, 4804 (1990).

[32] E. Vecino, A. Martín-Rodero, and A. Yeyati, Josephson current through a correlated quantum level: Andreev states and π junction behavior, Phys. Rev. B **68**, 035105 (2003).

[33] A. Oguri, Y. Tanaka, and A. C. Hewson, Quantum phase transition in a minimal model for the Kondo effect in a Josephson junction, J. Phys. Soc. Jpn. **73**, 2494 (2004).

[34] M.-S. Choi, M. Lee, K. Kang, and W. Belzig, Kondo effect and Josephson current through a quantum dot between two superconductors, Phys. Rev. B **70**, 020502 (2004).

[35] C. Karrasch, A. Oguri, and V. Meden, Josephson current through a single Anderson impurity coupled to BCS leads, Phys. Rev. B **77**, 024517 (2008).

[36] T. Meng, S. Florens, and P. Simon, Self-consistent description of Andreev bound states in Josephson quantum dot devices, Phys. Rev. B **79**, 224521 (2009).

[37] J.-D. Pillet, P. Joyez, R. Žitko, and M. F. Goffman, Tunneling spectroscopy of a single quantum dot coupled to a superconductor: From Kondo ridge to Andreev bound states, Phys. Rev. B **88**, 045101 (2013).

[38] E. J. H. Lee, X. Jiang, R. Žitko, C. M. Lieber, and S. De Franceschi, Scaling of sub-gap excitations in a superconductor-semiconductor nanowire quantum dot, arXiv:1609.07582.

[39] V. Mourik, K. Zuo, S. M. Frolov, S. R. Plissard, E. P. A. A. Bakkers, and L. P. Kouwenhoven, Signatures of Majorana fermions in hybrid superconductor-semiconductor nanowire devices, Science **336**, 1003 (2012).

[40] E. J. H. Lee, X. Jiang, R. Aguado, G. Katsaros, C. M. Lieber, and S. De Franceschi, Zero-Bias Anomaly in a Nanowire Quantum Dot Coupled to Superconductors, Phys. Rev. Lett. **109**, 186802 (2012).

[41] A. Das, Y. Ronen, Y. Most, Y. Oreg, M. Heiblum, and H. Shtrikman, Zero-bias peaks and splitting in an Al-InAs nanowire topological superconductor as a signature of Majorana fermions, Nat. Phys. **8**, 887 (2012).

[42] M. T. Deng, C. L. Yu, G. Y. Huang, M. Larsson, P. Caroff, and H. Q. Xu, Anomalous zero-bias conductance peak in a Nb-InSb nanowire-Nb hybrid device, Nano Lett. **12**, 6414 (2012).

[43] W. Chang, V. E. Manucharyan, T. S. Jespersen, J. Nygård, and C. M. Marcus, Tunneling Spectroscopy of Quasiparticle Bound States in a Spinful Josephson Junction, Phys. Rev. Lett. **110**, 217005 (2013).

[44] E. J. H Lee, X. Jiang, M. Houzet, R. Aguado, C. M. Lieber, and S. De Franceschi, Spin-resolved Andreev levels and parity crossings in hybrid superconductor-semiconductor nanostructures, Nat. Nanotechnol. **9**, 79 (2014).

[45] R. Žitko, J. S. Lim, R. Lopez, and R. Aguado, Shiba states and zero-bias anomalies in the hybrid normal-superconductor Anderson model, Phys. Rev. B **91**, 045441 (2015).

[46] N. Wentzell, S. Florens, T. Meng, V. Meden, and S. Andergassen, Magneto-electric spectroscopy of Andreev bound states in Josephson quantum dots, Phys. Rev. B **94**, 085151 (2016).

[47] A. Jellinggaard, K. Grove-Rasmussen, M. H. Madsen, and J. Nygård, Tuning Yu-Shiba-Rusinov states in a quantum dot, Phys. Rev. B **94**, 064520 (2016).

[48] B. Bujnowski, D. Bercioux, F. Konschelle, J. Cayssol, and F. S. Bergeret, Andreev spectrum of a Josephson junction with spin-split superconductors, Europhys. Lett. **115**, 67001 (2016).

[49] A. Y. Kitaev, Unpaired Majorana fermions in quantum wires, Phys.-Usp. **44**, 131 (2001).

[50] S. Nadj-Perge, I. K. Drozdov, B. A. Bernevig, and A. Yazdani, Proposal for realizing Majorana fermions in chains of magnetic atoms on a superconductor, Phys. Rev. B **88**, 020407 (2013).

[51] S. Nadj-Perge, I. K. Drozdov, J. Li, H. Chen, S. Jeon, J. Seo, A. H. MacDonald, B. A. Bernevig, and A. Yazdani, Observation of Majorana fermions in ferromagnetic atomic chains on a superconductor, Science **346**, 602 (2014).

[52] M. Ruby, F. Pientka, Y. Peng, F. von Oppen, B. W. Heinrich, and K. J. Franke, End States and Subgap Structure in Proximity-Coupled Chains of Magnetic Adatoms, Phys. Rev. Lett. **115**, 197204 (2015).

[53] J. D. Sau, R. M. Lutchyn, S. Tewari, and S. Das Sarma, Generic New Platform for Topological Quantum Computation using Semiconductor Heterostructures, Phys. Rev. Lett. **104**, 040502 (2010).

[54] J. Alicea, Y. Oreg, G. Refael, F. van Oppen, and M. P. A. Fischer, Non-Abelian statistics and topological quantum information processing in 1D wire networks, Nat. Phys. **7**, 412 (2011).

[55] S. Das Sarma, M. Freedman, and C. Nayak, Majorana zero modes and topological quantum computation, npj Quantum Inform. **1**, 15001 (2015).

[56] R. Meservey, P. M. Tedorow, and P. Fulde, Magnetic Field Splitting of the Quasiparticle States in Superconducting Aluminum Films, Phys. Rev. Lett. **25**, 1270 (1970).

[57] P. M. Tedrow and R. Meservey, Spin-Dependent Tunneling into Ferromagnetic Nickel, Phys. Rev. Lett. **26**, 192 (1971).

[58] P. M. Tedrow and R. Meservey, Spin polarization of electrons tunneling from films of Fe, Co, Ni, and Gd, Phys. Rev. B **7**, 318 (1973).

[59] R. Meservey and P. M. Tedrow, Spin-polarized electron tunneling, Phys. Rep. **238**, 173 (1994).

[60] M. Eltschka, B. Jäck, M. Assig, O. V. Kondrashov, M. A. Skvortsov, M. Etzkorn, C. R. Ast, and K. Kern, Probing absolute spin polarization at the nanoscale, Nano Lett. **14**, 7171 (2014).

[61] J. Linder and J. W. A. Robinson, Superconducting spintronics, Nat. Phys. **11**, 307 (2015).

[62] C. Csonka, L. L. Hofstetter, F. Freitag, S. Oberholzer, C. Schönberger, T. S. Jespersen, M. Aegesen, and J. Nygard, Giant fluctuations and gate control of the g-factor in InAs nanowire quantum dots, Nano Lett. **8**, 3932 (2008).

[63] T. Nakaoka, T. Saito, J. Tatebayashi, S. Hirose, T. Usuki, N. Yokoyama, and Y. Arakawa, Tuning of g-factor in self-assembled In(Ga)As quantum dots through strain engineering, Phys. Rev. B **71**, 205301 (2005).

[64] J. van Bree, A. Y. Silov, M. L. van Maasakkers, C. E. Pryor, M. E. Flatté, and P. M. Koenraad, Anisotropy of electron and hole gtensors of quantum dots: An intuitive picture based on spin-correlated orbital currents, Phys. Rev. B **93**, 035311 (2016).

[65] M. D. Schroer, K. D. Petersson, M. Jung, and J. R. Petta, Field Tuning the g Factor in Inas Nanowire Double Quantum Dots, Phys. Rev. Lett. **107**, 176811 (2011).

[66] R. S. Deacon, Y. Kanai, S. Takahashi, A. Oiwa, K. Yoshida, K. Shibata, K. Hirakawa, Y. Tokura, and S. Tarucha, Electrically tuned g tensor in an InAs self-assembled quantum dot, Phys. Rev. B **84**, 041302 (2011).

[67] N. Ares, V. N. Golovach, G. Katsaros, M. Stoffel, F. Fournel, L. I. Glazman, O. G. Schmidt, and S. De Franceschi, Nature of Tunable Hole *g* Factors in Quantum Dots, Phys. Rev. Lett. **110**, 046602 (2013).

[68] K. G. Wilson, The renormalization group: Critical phenomena and the Kondo problem, Rev. Mod. Phys. **47**, 773 (1975).

[69] H. R. Krishna-murthy, J. W. Wilkins, and K. G. Wilson, Renormalization-group approach to the Anderson model of dilute magnetic alloys, I: Static properties for the symmetric case, Phys. Rev. B **21**, 1003 (1980).

[70] W. Hofstetter, Generalized Numerical Renormalization Group for Dynamical Quantities, Phys. Rev. Lett. **85**, 1508 (2000).

[71] R. Žitko and T. Pruschke, Energy resolution and discretization artefacts in the numerical renormalization group, Phys. Rev. B **79**, 085106 (2009).

[72] R. Žitko, Adaptive logarithmic discretization for numerical renormalization group methods, Comput. Phys. Commun. **180**, 1271 (2009).

[73] T. Hecht, A. Weichselbaum, J. von Delft, and R. Bulla, Numerical renormalization group calculation of near-gap peaks in spectral functions of the Anderson model with superconducting leads, J. Phys.: Condens. Matter **20**, 275213 (2008).

[74] R. Bulla, T. Costi, and T. Pruschke, The numerical renormalization group method for quantum impurity systems, Rev. Mod. Phys. **80**, 395 (2008).

[75] M. Höck and J. Schnack, Numerical renormalization group calculations of the magnetization of Kondo impurities with and without uniaxial anisotropy, Phys. Rev. B **87**, 184408 (2013).

[76] R. Žitko, R. Peters, and T. Pruschke, Properties of anisotropic magnetic impurities on surfaces, Phys. Rev. B **78**, 224404 (2008).

[77] A. M. Clogston, Upper Limit for the Critical Field in Hard Superconductors, Phys. Rev. Lett. **9**, 266 (1962).

[78] B. S. Chandrasekhar, A note on the maximum critical field of high-field superconductors, Appl. Phys. Lett. **1**, 7 (1962).

[79] K. Machida and F. Shibata, Bound states due to resonance scattering in superconductor, Prog. Theor. Phys. **47**, 1817 (1972).

Raman spectroscopy of K$_x$Co$_{2-y}$Se$_2$ single crystals near the ferromagnet–paramagnet transition

M Opačić[1], N Lazarević[1], M M Radonjić[2,3], M Šćepanović[1], Hyejin Ryu[4,5,6], Aifeng Wang[4], D Tanasković[3], C Petrovic[4,5] and Z V Popović[1]

[1] Center for Solid State Physics and New Materials, Institute of Physics Belgrade, University of Belgrade, Pregrevica 118, 11080 Belgrade, Serbia
[2] Center for Electronic Correlations and Magnetism, Theoretical Physics III, Institute of Physics, University of Augsburg, D-86135 Augsburg, Germany
[3] Scientific Computing Laboratory, Institute of Physics Belgrade, University of Belgrade, Pregrevica 118, 11080 Belgrade, Serbia
[4] Condensed Matter Physics and Materials Science Department, Brookhaven National Laboratory, Upton, NY 11973-5000, USA
[5] Department of Physics and Astronomy, Stony Brook University, Stony Brook, NY 11794-3800, USA

E-mail: nenad.lazarevic@ipb.ac.rs

Abstract

Polarized Raman scattering spectra of the K$_x$Co$_{2-y}$Se$_2$ single crystals reveal the presence of two phonon modes, assigned as of the A_{1g} and B_{1g} symmetry. The absence of additional modes excludes the possibility of vacancy ordering, unlike in K$_x$Fe$_{2-y}$Se$_2$. The ferromagnetic (FM) phase transition at $T_c \approx 74$ K leaves a clear fingerprint on the temperature dependence of the Raman mode energy and linewidth. For $T > T_c$ the temperature dependence looks conventional, driven by the thermal expansion and anharmonicity. The Raman modes are rather broad due to the electron–phonon coupling increased by the disorder and spin fluctuation effects. In the FM phase the phonon frequency of both modes increases, while an opposite trend is seen in their linewidth: the A_{1g} mode narrows in the FM phase, whereas the B_{1g} mode broadens. We argue that the large asymmetry and anomalous frequency shift of the B_{1g} mode is due to the coupling of spin fluctuations and vibration. Our density functional theory (DFT) calculations for the phonon frequencies agree rather well with the Raman measurements, with some discrepancy being expected since the DFT calculations neglect the spin fluctuations.

Keywords: Raman spectroscopy, electron–phonon, lattice dynamics

(Some figures may appear in colour only in the online journal)

1. Introduction

In the last few years considerable attention was focused on the iron-based superconductors in an effort to gain deeper insight into their physical properties and to determine the origin of high-T_c superconductivity [1–4]. Discovery of superconductivity in alkali-doped iron chalcogenides, together with its uniqueness among the iron based superconductors, challenged the physical picture of the superconducting mechanism in iron pnictides [5]. The absence of hole pockets even suggested the possibility for the different type of pairing mechanism [6]. Another striking feature in K$_x$Fe$_{2-y}$Se$_2$ was the presence of the intrinsic nano to mesoscale phase separation between an insulating phase and a metallic/superconducting phase [7–10]. The insulating phase hosts antiferromagnetically, $\sqrt{5} \times \sqrt{5}$ ordered iron vacancies, whereas the superconducting stripe-like phase is free of vacancies [7]. The theoretical study of

Huang *et al* [11] revealed that proximity effects of the two phases result in the Fermi surface deformation due to interlayer hopping and, consequently, suppression of superconductivity. On the other hand, a large antiferromagnetic order protects the superconductivity against interlayer hopping, thus explaining relatively high T_c in $K_xFe_{2-y}Se_2$ [11]. However, the correlation between the two phases and its impact on superconductivity are still not fully understood.

Although the absolute values of resistivity are much smaller for the Ni-member of the $K_xM_{2-y}Se_2$ (M = transition metal) series than for the iron member, this material does not exhibit superconductivity down to $0.3\,K$ [12]. As opposed to $K_xFe_{2-y}Se_2$, vacancy ordering has not been observed in the $K_xNi_{2-y}Se_2$ single crystal [13]. These materials, together with the Co- and Ni-doped $K_xFe_{2-y}Se_2$ single crystals, have very rich structural, magnetic and transport phase diagrams. This opens a possibility for fine tuning of their physical properties by varying the sample composition [14, 15]. First results obtained on $K_xCo_{2-y}Se_2$ single crystal revealed the ferromagnetic ordering below $T_c \sim 74\,K$, as well as the absence of the superconducting phase [16].

Raman spectroscopy is a valuable tool not only for measuring vibrational spectra, but it also helps in the analysis of structural, electronic and magnetic properties, and phase transitions. There are several recent studies of the influence of the antiferromagnetic order, [17, 18] ferromagnetism, [19, 20] and magnetic fluctuations [21] on the Raman spectra.

In this paper the Raman scattering study of the $K_xCo_{2-y}Se_2$ single crystal ($x = 0.3$, $y = 0.1$), together with the lattice dynamics calculations of KCo_2Se_2, is presented. The polarized Raman scattering measurements were performed in the temperature range from $20\,K$ up to $300\,K$. The observation of only two Raman active modes when measuring from the $(0\,0\,1)$-oriented samples suggests that the $K_xCo_{2-y}Se_2$ single crystal has no ordered vacancies. The temperature dependence of the energy and linewidth of the observed Raman modes reveals a clear fingerprint of the phase transition. A large linewidth of the B_{1g} mode and its Fano line shape indicate the importance of spin fluctuations.

The rest of the manuscript is organized as follows. Section 2 contains a brief description of the experimental and numerical methods, section 3 are the results, and section 4 contains a discussion of the phonon frequencies and linewidths and their temperature dependencies. Section 5 summarizes the results.

2. Experiment and numerical method

Single crystals of $K_xCo_{2-y}Se_2$ were grown by the self-flux method, as described in [12]. The elemental analysis was performed using energy-dispersive x-ray spectroscopy (EDX) in a JEOL JSM-6500 scanning electron microscope. Raman scattering measurements were performed on freshly cleaved $(0\,0\,1)$-oriented samples with size up to $3 \times 3 \times 1\,mm^3$, using a TriVista 557 Raman system equipped with a nitrogen-cooled CCD detector, in a backscattering micro-Raman configuration. The $514.5\,nm$ line of an Ar^+/Kr^+ ion gas laser was used as an excitation source. A microscope objective with $50 \times$ magnification was used for focusing the laser beam. All
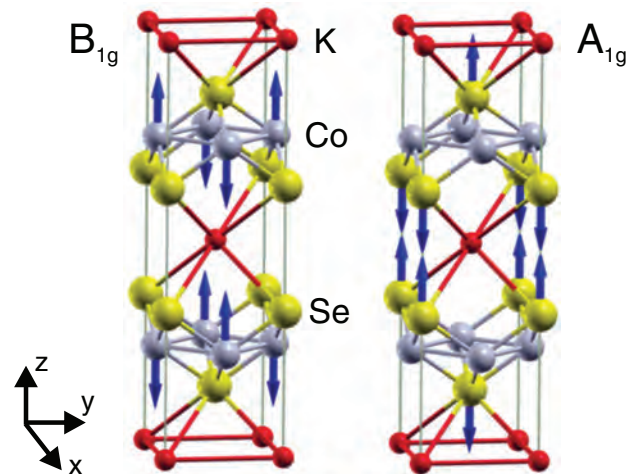
Figure 1. Unit cell of KCo_2Se_2 single crystal, together with the displacement patterns of the A_{1g} and B_{1g} Raman modes.

measurements were carried out at low laser power, in order to minimize local heating of the sample. Low temperature measurements were performed using KONTI CryoVac continuous flow cryostat with $0.5\,mm$ thick window. Spectra were corrected for the Bose factor.

The electronic structure of the ferromagnetic (FM) and paramagnetic (PM) phases is calculated within the density functional theory (DFT), and the phonon frequencies at the Γ-point are obtained within the density functional perturbation theory (DFPT) [22]. All calculations are performed using the QUANTUM ESPRESSO package [23]. We have used projector augmented-wave (PAW) pseudo-potentials with Perdew–Burke–Ernzerhof (PBE) exchange-correlation functional with nonlinear core correction and Gaussian smearing of $0.005\,Ry$. The electron wave-function and the density energy cutoffs are $40\,Ry$ and $500\,Ry$, respectively. The Brillouin zone is sampled with a $16 \times 16 \times 8$ Monkhorst–Pack k-space mesh. The phonon frequencies were calculated with relaxed unit cell parameters and, for comparison, with the unit cell size taken from the experiments and the relaxed positions of only Se atoms. The forces acting on individual atoms in the relaxed configuration were smaller than $10^{-4}\,Ry/a.u.$ and the pressure smaller than $0.5\,kbar$.

3. Results

KCo_2Se_2 crystallizes in the tetragonal crystal structure of $ThCr_2Si_2$-type, $I4/mmm$ space group, which is shown in figure 1. The experimental values of the unit cell parameters are $a = 3.864(2)$ Å and $c = 13.698(2)$ Å [24]. The potassium atoms are at $2a$: $(0, 0, 0)$, Co atoms at $4d$: $(0, \frac{1}{2}, \frac{1}{4})$, and Se atoms at $4e$: $(0, 0, z)$ Wyckoff positions, with the experimental value $z = 0.347$.

The KCo_2Se_2 single crystal consists of alternatively stacked K ions and CoSe layers, isostructural to the KFe_2Se_2 [25]. Factor group analysis for the $I4/mmm$ space group yields a normal mode distribution at the Brillouin-zone center, which is shown in table 1. According to the selection rules, when measuring from the $(0\,0\,1)$-plane of the sample, only two

Table 1. Atomic types with their Wyckoff positions and the contribution of the each site to the Γ-point phonons, the Raman tensors and the selection rules for the $K_xCo_{2-y}Se_2$ single crystal (*I4/mmm* space group).

Atoms	Wyckoff positions	Irreducible representations
K	2a	$A_{2u} + E_u$
Co	4d	$A_{2u} + B_{1g} + E_g + E_u$
Se	4e	$A_{1g} + A_{2u} + E_g + E_u$

Raman tensors

$$\hat{R}_{A_{1g}} = \begin{pmatrix} |a|\exp i\varphi_a & 0 & 0 \\ 0 & |a|\exp i\varphi_a & 0 \\ 0 & 0 & |b|\exp i\varphi_b \end{pmatrix} \qquad \hat{R}_{B_{1g}} = \begin{pmatrix} |c|\exp i\varphi_c & 0 & 0 \\ 0 & -|c|\exp i\varphi_c & 0 \\ 0 & 0 & 0 \end{pmatrix}$$

$$\hat{R}_{E_g} = \begin{pmatrix} 0 & 0 & |e|\exp i\varphi_e \\ 0 & 0 & 0 \\ |e|\exp i\varphi_e & 0 & 0 \end{pmatrix} \qquad \hat{R}_{E_g} = \begin{pmatrix} 0 & 0 & 0 \\ 0 & 0 & |f|\exp i\varphi_f \\ 0 & |f|\exp i\varphi_f & 0 \end{pmatrix}$$

Activity and selection rules

$$\Gamma_{Raman} = A_{1g}(\alpha_{xx+yy}, \alpha_{zz}) + B_{1g}(\alpha_{xx-yy}) + 2E_g(\alpha_{xz}, \alpha_{yz})$$

$$\Gamma_{IR} = 2A_{2u}(\mathbf{E}\|\mathbf{z}) + 2E_u(\mathbf{E}\|\mathbf{x}, \mathbf{E}\|\mathbf{y})$$

$$\Gamma_{acoustic} = A_u + E_u$$

modes (A_{1g} and B_{1g}) are expected to be observed in the Raman scattering experiment. Displacement patterns of the experimentally observable Raman modes are illustrated in figure 1. The A_{1g} (B_{1g}) mode represents the vibrations of the Se (Co) ions along the c-axis, whereas the E_g modes (which are not observable for our scattering configuration) involve the vibration of both Co and Se ions within the (0 0 1)-plane.

Figure 2 shows polarized Raman scattering spectra of the $K_xCo_{2-y}Se_2$ single crystal, measured from the (0 0 1)-plane of the sample at room temperature, in different sample orientations. Only two modes, at about 187 and 198 cm^{-1}, are observed, which is in agreement with the selection rules for (0 0 1)-oriented samples. In some iron-chalcogenide compounds, the appearance of additional Raman active modes due to the iron vacancy ordering and, consequently, symmetry lowering, has been observed [8, 26]. The absence of additional phonon modes in figure 2 suggests that in $K_xCo_{2-y}Se_2$ single crystals vacancy ordering does not occur in our samples.

Selection rules imply that the A_{1g} mode may be observed for any sample orientation, provided that the polarization vector of the incident light $\mathbf{e}_i$ is parallel to the scattered light polarization vector $\mathbf{e}_s$, whereas it vanishes if these vectors are perpendicular. On the other hand, the intensity of the B_{1g} mode strongly depends on the sample orientation ($I_{B_{1g}} \sim |c|^2 \cos^2(\theta + 2\beta)$), where $\theta = \angle(\mathbf{e}_i, \mathbf{e}_s)$ and $\beta = \angle(\mathbf{e}_i, \mathbf{x})$ [8]. This implies that, in parallel polarization configuration ($\theta = 0°$), the intensity of the B_{1g} mode is maximal when the sample is oriented so that $\mathbf{e}_i\|\mathbf{x}$, gradually decreases with increasing β and finally vanishes for $\beta = 45°$. In crossed polarization configuration ($\theta = 90°$), B_{1g} mode intensity decreases from its maximal value for $\beta = 45°$ to zero, which reaches when $\beta = 0°$. From figure 2 it can be seen that the intensity of the Raman mode at about 187 cm^{-1} coincides with theoretically predicted behavior for the B_{1g} mode; thereby, this phonon mode is assigned accordingly. The phonon mode at $\sim$198 cm^{-1}, which is present in Raman spectra only for the parallel polarization configuration ($\theta = 0°$) and whose intensity is independent on
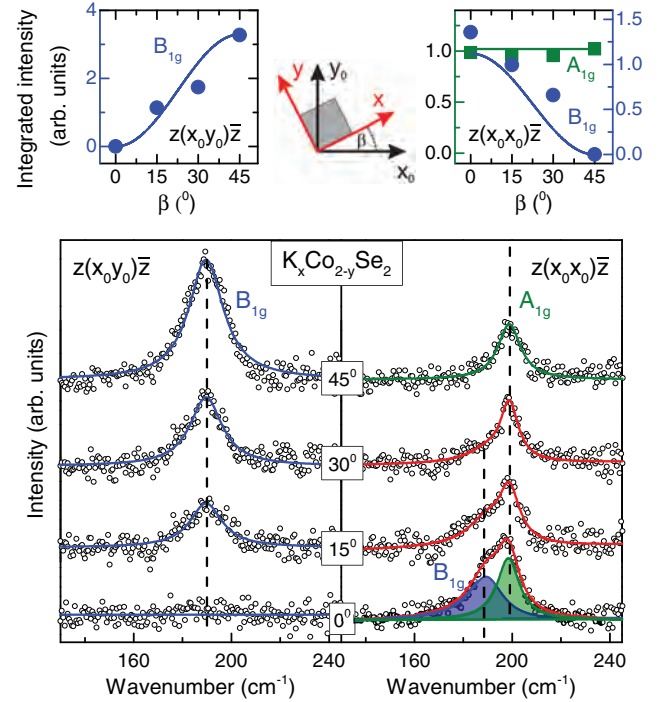
Figure 2. Upper panel: integrated intensity of the observed Raman modes as a function of the crystal orientation with respect to the laboratory axes $\mathbf{x_0}$ and $\mathbf{y_0}$. In order to estimate the intensity of the modes, phonon at 198 cm^{-1} was fitted with Lorentzian, whereas an asymmetric Raman mode appearing at 187 cm^{-1} was fitted with Fano line shape. Lower panel: Raman scattering spectra of $K_xCo_{2-y}Se_2$ single crystal measured at room temperature, in various sample orientations ($\mathbf{x} = (1\,0\,0)$, $\mathbf{y} = (0\,1\,0)$).

the sample orientation, can be assigned as the A_{1g} mode. The intensity ratio of the two Raman modes can be obtained from the spectrum measured in ($\theta = 0°, \beta = 0°$) scattering geometry as $I_{B_{1g}}/I_{A_{1g}} \approx 1.38$. Having in mind that the A_{1g} mode intensity is given by [8] $I_{A_{1g}} \sim |a|^2 \cos^2 \theta$, the ratio of the appropriate Raman tensor components can be estimated as $|c|/|a| \approx 1.17$.

Table 2. Optimized lattice constants and internal coordinate z_{Se} in the FM and PM solution.

	a (Å)	c (Å)	z_{Se}
FM^{rel}	3.893	13.269	0.350
PM^{rel}	3.766	13.851	0.368
FM^{fixed}	3.864	13.698	0.3486
PM^{fixed}	3.864	13.698	0.3496
Exper.	3.864	13.698	0.347

Note: The next two rows give the relaxed z_{Se} when the unit cell size is taken from the experiment, and the last row contains the atomic positions from the experiment [24].

The experimentally determined frequencies are compared with those obtained with DFT numerical calculations. The experimental lattice constants [24] are shown in table 2, together with their values from the DFT calculation which relaxes or keeps fixed the unit cell size. The DFPT phonon frequencies obtained using the fully relaxed atomic positions in both FM and PM phases are given in table 3, with the corresponding values obtained with the fixed unit cell size and relaxed only fractional coordinate z_{Se} given in the parenthesis. The equilibrium atomic positions in the FM solution are given by $a = 3.893$ Å, $c = 13.269$ Å, and $z_{Se} = 0.350$. The corresponding phonon frequencies are 199.5 cm^{-1} for A_{1g} mode and 171.2 cm^{-1} for B_{1g} mode. When we enforce the PM solution, we obtain $a = 3.766$ Å, $c = 13.851$ Å, and $z_{Se} = 0.368$, and 212.6 cm^{-1}, 176.6 cm^{-1} for the frequencies of the A_{1g} and B_{1g} mode, respectively. These values agree rather well with the experimental data, and agree with recently published numerical results [27][7]. They can be used to confirm the experimental assignment of the modes, but cannot resolve subtle changes of the phonon frequencies near the FM–PM transition. This level of discrepancy is expected for metallic materials with magnetic ordering since the DFT calculations neglect spin fluctuations, as discussed in some detail in the next section (see also [21]). A rather large difference between the calculated frequencies in the two phases is due to the relatively large change in the unit cell size. This difference between the unit cell sizes in the FM and PM phases is overestimated in the calculation which neglects spin fluctuations. For comparison, we also calculated the frequencies keeping the experimental values of the unit cell size, and relaxing just the coordinate z_{Se} of the Se atoms, which is often done in the case of iron based superconductors and related compounds [21]. This gives $z_{Se} = 0.3486$ in the FM solution and $z_{Se} = 0.3496$ in the PM solution, while the change in the phonon frequencies between the two solutions is much smaller, see table 3 and a discussion in section 4.

Polarized Raman scattering spectra of $K_xCo_{2-y}Se_2$ single crystals, measured at various temperatures from the (0 0 1)-plane of the sample, are presented in figure 3. The orientation of the sample is chosen so that each of the observable modes appears in a different polarization configuration. A pronounced feature in the spectra is an asymmetric Fano profile of the B_{1g} mode, persisting down to low temperatures, as well as its large linewidth compared to isostructural $K_xFe_{2-y}Se_2$ [8, 28]. This feature should by mainly due to the spin

[7] There is typo in table 3 of [27] in the frequency of the B_{1g} mode.

fluctuations influencing the B_{1g} vibrational mode which modulates the distances between the magnetic Co atoms. A detailed discussion of the frequency and linewidth temperature dependence is given in the next section.

4. Discussion

There are several factors that affect the phonon frequencies (energies) and linewidths, and their changes across the FM–PM transition. In general, the temperature dependence of the phonon frequency of the mode i, $\omega_i(T)$, is influenced by thermal expansion and magnetostriction, anharmonicity effects, electron–phonon and magnetic exchange interaction (spin-phonon coupling) [29, 30]

$$\omega_i(T) - \omega_i(T_0) = \Delta\omega_i(T) = (\Delta\omega_i)_{latt} + (\Delta\omega_i)_{anh} + (\Delta\omega_i)_{el-ph} + (\Delta\omega_i)_{sp-ph}. \quad (1)$$

The first term is the frequency shift due to the change of the unit cell size caused by the thermal effects and magnetostriction. $(\Delta\omega_i)_{anh}$ is the anharmonic frequency shift. $(\Delta\omega_i)_{el-ph}$ appears due to the change in the electron–phonon interaction primarily influenced by changes in the electronic spectrum near the Fermi level, and $(\Delta\omega_i)_{sp-ph}$ is the spin-phonon contribution caused by the modulation of exchange interaction by lattice vibrations.

In our case of $K_xCo_{2-y}Se_2$, for temperatures above T_c, $\omega_i(T)$ decreases and $\Gamma_i(T)$ (full width at half-maximum, FWHM) increases with increasing temperature for A_{1g} and B_{1g} modes, similar as in the Raman spectra of many other materials. However, they show anomalous behavior near T_c, see figure 4. In the following, we analyze $\omega_i(T)$ and $\Gamma_i(T)$ more closely.

4.1. Phonon frequencies

The frequencies of the A_{1g} and B_{1g} modes change by less than 2 percent in the temperature range between 20 K and 250 K. The red solid lines in figures 4(a)–(c) represent the fits of the phonon energy temperature dependence (see below), following the frequencies of the two modes in the high-temperature PM phase. The red dotted line is the extrapolation to $T = 0$. For $T > T_c$, the temperature dependence of the frequency looks conventional for both modes: the frequency decreases with increasing temperature. This behavior is expected both due to the thermal expansion and the anharmonicity. These two effects can be standardly analyzed as follows.

The temperature dependent frequency of the vibrational mode i is given by

$$\omega_i(T) = \omega_{0,i} + \Delta_i(T), \quad (2)$$

where $\omega_{0,i}$ denotes the temperature independent term and $\Delta_i(T)$ can be decomposed as [19, 31, 32]

$$\Delta_i(T) = \Delta_i^V + \Delta_i^A. \quad (3)$$

Δ_i^V describes a change of the Raman mode energy as a consequence of the lattice thermal expansion and can be expressed with [31]

Table 3. The experimental phonon energies measured at 20 K in the FM phase and the extrapolated value to 0 K from the PM phase (see the text).

Symmetry	Activity	Experiment FM (cm^{-1})	Experiment PM (cm^{-1})	Calculation FM (cm^{-1})	Calculation PM (cm^{-1})	Main atomic displacements
A_{1g}	Raman	201.9	201.3	199.5 (193.2)	212.6 (193.1)	Se(z)
B_{1g}	Raman	195.3	194.2	171.2 (172.7)	176.6 (168.1)	Co(z)
E_g^1	Raman			93.1 (100.7)	92.7 (99.0)	Co(xy), Se(xy)
E_g^2	Raman			237.9 (237.6)	257.2 (235.6)	Co(xy), Se(xy)
A_{2u}^1	IR			115.1 (99.0)	113.7 (102.9)	K(z), Se(-z)
A_{2u}^2	IR			246.7 (241.4)	250.9 (241.4)	Co(z), K(-z)
E_u^1	IR			97.9 (95.0)	100.1 (95.0)	K(xy)
E_u^2	IR			239.0 (229.7)	231.0 (229.9)	Co(xy), Se(-xy)

Note: The phonon frequencies at the Γ point are calculated with fully relaxed atomic positions. The frequencies obtained with only relaxed internal coordinate are given in parenthesis.
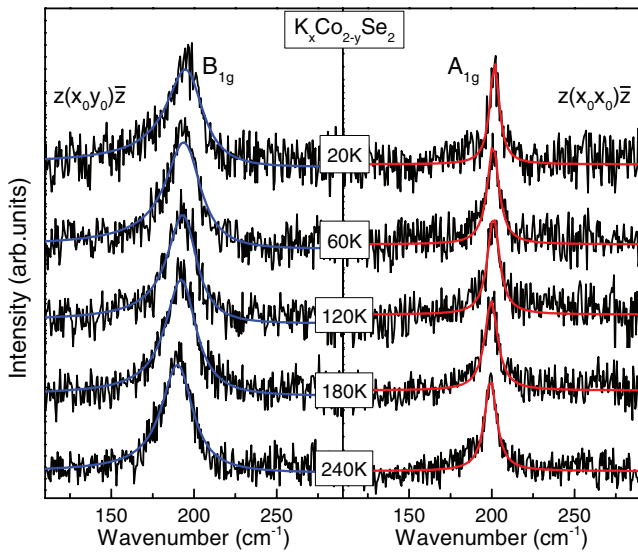
Figure 3. Temperature dependent Raman spectra of K$_x$Co$_{2-y}$Se$_2$ single crystal in parallel (left panel) and crossed (right panel) polarization configuration ($\mathbf{x_0} = \frac{1}{\sqrt{2}}(1\,1\,0)$, $\mathbf{y_0} = \frac{1}{\sqrt{2}}(\bar{1}\,1\,0)$). The solid lines represent fits of the experimental spectra with the Lorentzian (A_{1g} mode) and the Fano profile (B_{1g} mode).

$$\Delta_i^V = \omega_{0,i}\left(e^{-3\gamma_i \int_0^T \alpha(T')dT'} - 1 \right), \qquad (4)$$

where γ_i is the Grüneisen parameter of the Raman mode i and $\alpha(T)$ is the thermal expansion coefficient of a considered single crystal. Δ_i^A represents the anharmonic contribution to the Raman mode energy. If we assume, for simplicity, that anharmonic effects are described by three-phonon processes, this term is given by [31, 33]

$$\Delta_i^A = -C_i\left(1 + \frac{2\lambda_{p-p,i}}{e^{\hbar\omega_{0,i}/2k_BT} - 1}\right), \qquad (5)$$

where C is the anharmonic constant and $\lambda_{p-p,i}$ is a fitting parameter which describes the phonon–phonon coupling, including the nonsymmetric phonon decay processes.

The relative importance of the thermal expansion and anharmonicity to frequency changes is, to the best of our knowledge, not yet firmly established for pnictides and

chalcogenides. In several cases [13, 17] the anharmonic formula, equation (5), is used for the $\omega(T)$ fit. We follow here the arguments from [19, 28, 34] that $\omega(T)$ is dominated by the thermal expansion. To the best of our knowledge, the thermal expansion coefficient $\alpha(T)$ of the K$_x$Co$_{2-y}$Se$_2$ single crystal is unknown. For estimating the lattice thermal expansion contribution to the phonon energy change, the coefficient $\alpha(T)$ for FeSe, given in [35], is used. The best fit shown in our figure 4 is obtained with $\omega_{0,A_{1g}} = 201.3$ cm^{-1}, $\gamma_{A_{1g}} = 1.23$ and $\omega_{0,B_{1g}} = 194.2$ cm^{-1}, $\gamma_{B_{1g}} = 1.7$.

There exists a shift in phonon frequencies as the temperature is lowered below T_c. This shift does not show clear discontinuity (as well as the corresponding shift in the linewidths) and no additional modes are registered in the Raman spectra, which suggest that the FM–PM transition is continuous, without structural changes. There are several causes of the sudden frequency change as the sample gets magnetized. It can change due to the magnetostriction, modulation of the magnetic exchange by lattice vibrations (spin-phonon coupling), and due to the changes in the electron–phonon interaction due to spin polarization and changes in the electronic spectrum.

The effect of spin-phonon interactions, caused by the modulation of magnetic exchange interaction by lattice vibrations, may be quantitatively examined within the framework developed in [29] for insulating magnets, and recently applied also to several itinerant ferromagnets [36–39]. In this model, the shift of the Raman mode energy due to the spin-phonon interaction is proportional to the spin–spin correlation function $\langle S_i|S_j\rangle$ between nearest magnetic ions. This term should have the same temperature dependence as $(M(T)/M_0)^2$, where $M(T)$ is the magnetization per magnetic ion at a temperature T and M_0 is the saturation magnetization,

$$\Delta\omega(T) = \omega_{\text{exp}}(T) - \omega_{\text{fit}}(T) \propto \pm\left(\frac{M(T)}{M_0}\right)^2, \qquad (6)$$

where $\omega_{\text{fit}}(T)$ is the extrapolation from the high-temperature data. This model does not predict the sign of the phonon energy shift—softening or hardening. From the inset in figure 4(c) it can be seen that the B_{1g} mode energy renormalization scales well with the $(M(T)/M_0)^2$ curve. However, the effect of the
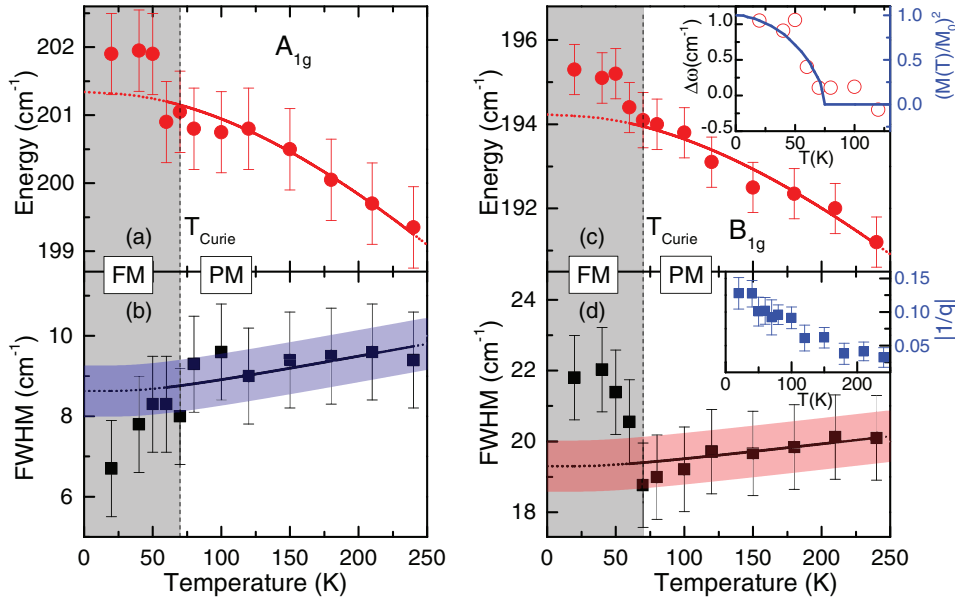
Figure 4. Temperature dependence of the energy and linewidth for the A_{1g} (a), (b) and B_{1g} (c), (d) Raman modes of the $K_xCo_{2-y}Se_2$ single crystal. Solid lines are a theoretical fit (see the text) and the dotted lines are the extrapolation to the FM phase. Upper inset: temperature dependence of the B_{1g} mode frequency, compared with the $(M(T)/M(0))^2$ curve. Lower inset: measure of the electron-mediated photon–phonon coupling ($1/q$) of the B_{1g} mode as a function of temperature.

magnetostriction (change of the unit cell size due to the magnetization) cannot be excluded based just on this plot, especially since the A_{1g} mode corresponding to the vibrations of nonmagnetic Se ions also shows a similar shift in frequency.

The DFT calculations can give us some guidance for understanding of the changes of the phonon frequencies and linewidths, but one has to be aware of its limitations. The DFT calculations (see table 2) give a rather large magnetostriction, i.e. rather large change in the size of the unit cell between the FM and PM phases (*a* changes by 3.2% and *c* by 4.3%). This leads to very large changes in the phonon frequencies, see table 3. The calculated frequencies are lower in the FM phase, as opposed to the experimental data. This already points to the limitations of the DFT calculations, which is expected near the phase transition. A similar conclusion is also present in [21]. The DFT ignores spin fluctuations which often leads to quantitative discrepancy in various physical quantities [40] and, in some cases, even predicts wrong phases. In the case of $K_xCo_{2-y}Se_2$, the DFT calculations correctly predict the FM ground state, but the calculated magnetic moment $m = 0.947\ \mu_B$ is much larger than the experimental value $m \approx 0.72\ \mu_B$ [16]. This already shows the importance of correlations and quantum fluctuations which are neglected within the DFT. Strong correlation effects can be captured using screened hybrid functional [41] or within the dynamical mean field theory combined with DFT (LDA+DMFT) [42], which is beyond our present work.

Since the magnetostriction effects are overestimated in the DFT calculations with relaxed unit cell size, we repeated the DFT (DFPT) calculations keeping the experimental value for the unit cell size and relaxing only the fractional coordinate (positions of the Se atoms). This is often done in the literature on iron based superconductors and related compounds [21]. Our calculated frequencies are given in the parenthesis

in table 3. We see that the frequency changes between the two phases are small, in better agreement with the experiment.

4.2. Phonon linewidths

The phonon linewidths of the A_{1g} and B_{1g} modes are very large, $\Gamma_{i,A_{1g}} \sim 10$ cm^{-1} and $\Gamma_{i,B_{1g}} \sim 20$ cm^{-1}, which implies the importance of disorder (impurities, nonstoichiometry, lattice imperfections) in measured samples. In general, the broadening of the phonon lines can be a consequence of the electron–phonon interaction, disorder, spin fluctuations and anharmonicity effects. The temperature dependence of the linewidth in the PM phase is, however, very weak, which indicates that the anharmonicity effects are small. The DFT calculation of the linewidth is usually based on the Allen's formula, [43] $\Gamma_{q,i} = \pi N(E_F)\lambda_{q,i}\omega^2_{q,i}$. Here, $N(E_F)$ is the density of states (DOS) at the Fermi level, $\lambda_{q,i}$ is the electron–phonon coupling constant, and $\omega^2_{q,i}$ is the phonon frequency of the mode i and wavevector $\mathbf{q}$. A straightforward implementation of Allen's formula in the $\mathbf{q} \to 0$ limit corresponding to the Γ point is, however, unjustified, as explained for example in [44, 45]. In addition, structural disorder and impurities break the conservation of the momentum, which means that phonons with finite wave vectors also contribute to the Raman scattering spectra. The standard DFT calculation for the Brillouin zone averaged electron–phonon coupling constant λ gives too small value to explain the large width of the Raman lines in pnictides and chalcogenides, [33] and several other metallic systems like MgB_2 [44] and fullerides [46]. A correct estimate of the phonon linewidth can be obtained only by explicitly taking into account the disorder and electron scattering which enhances the electron–phonon interaction, [44, 46] which is beyond the standard DFT approach and scope of the present work.

The Raman mode linewidth is not directly affected by the lattice thermal expansion. Assuming that the three-phonon processes represent the leading temperature dependent term in the paramagnetic phase, full width at half-maximum, $\Gamma_i(T)$, is given by

$$\Gamma_i(T) = \Gamma_{0,i}\left(1 + \frac{2\lambda_{p-p,i}}{e^{\hbar\omega_{0,i}/2k_\mathrm{B}T} - 1}\right) + A_i. \tag{7}$$

The first term represents the anharmonicity induced effects, where $\Gamma_{0,i}$ is the anharmonic constant. The second term A_i includes the contributions from other scattering channels, i.e. structural disorder and/or coupling of phonons with other elementary excitations, like particle-hole and spin excitations. These effects, typically, depend very weakly on temperature, but can become important near the phase transition. The best fit parameters are $\lambda_{p-p,i} = 0.2$ for both modes, $A_{A_{1g}} = 6.6$ cm^{-1} and $A_{B_{1g}} = 17.3$ cm^{-1}. The value $\Gamma_{0,i} = 2$ cm^{-1} is adopted from [28] for related compound $K_xFe_{2-y}Se_2$, where the anharmonic effects dominate the temperature dependence. We see that $\lambda_{p-p,i}$ assumes values much smaller than 1. Small and sometimes irregular changes in $\Gamma_i(T)$ are also observed in other materials whose Raman spectra are considered to be dominated by spin fluctuations [21, 33]. Therefore, we believe that a simple separation of $\Gamma_i(T)$ to the anharmonic and temperature independent term, which works well in many systems, is not appropriate for itinerant magnetic systems like $K_xCo_{2-y}Se_2$. We conclude that the spin fluctuations and electron–phonon coupling are likely to affect the linewidth even above T_c.

The electron–phonon interaction strength is proportional to the density of states at the Fermi level $N(E_\mathrm{F})$. Our DFT calculations for the DOS agree with those in [47]. The calculated DOS in the FM phase, $N(E_\mathrm{F}) = 3.69$ eV^{-1}, is smaller than, $N(E_\mathrm{F}) = 5.96$ eV^{-1}, in the PM phase. (Though, in reality, it is possible that the DOS significantly differs from the one given by the DFT calculations due to the spin fluctuations and disorder effects.) Therefore, one expects that the phonon line is narrower in the FM phase than in the PM phase. This is indeed the case for the A_{1g} mode, but the opposite is observed for the B_{1g} mode.

It is also interesting to note that the B_{1g} mode is much more asymmetric than the A_{1g} mode and almost twice broader. These two observations are in striking similarity with the Raman spectra in the quasi-one-dimensional superconductor $K_2Cr_3As_3$ [21]. In this material the vibrational mode that modulates the distance between the magnetic Cr atoms also features large asymmetry and linewidth. In our case, the distances between the magnetic Co ions are modulated by the vibrations of the B_{1g} mode, see figure 1. This leads us to the conclusion that the anomalous features of the B_{1g} mode are the consequence of spin fluctuations coupled to the electronic structure via lattice vibrations (in addition to the magnetostriction and spin polarization, which change the electronic spectrum near the Fermi level and, therefore, affect the electron–phonon interaction for both modes). It should be noted that similar anomalous properties of B_{1g} phonon were experimentally observed in the cuprate high-temperature superconductor $YBa_2Cu_3O_7$ [48, 49], and

explained as a consequence of the out-of-phase nature of this mode which couples to oxygen-oxygen in-plane charge fluctuations [50–52]. In the case of iron-based superconductors and related compounds, the chalcogen atoms and Fe (or Co) are not in the same plane and phonons of A_{1g} symmetry can also directly couple with the electrons. A satisfactory agreement of theory and Raman experiments remains to be established [53].

The asymmetric B_{1g} phonon line can be described by the Fano profile [21, 36, 54, 55]

$$I(\omega) = I_0\frac{(\epsilon + q)^2}{1 + \epsilon^2}, \tag{8}$$

where $\epsilon = 2(\omega - \omega_0)/\Gamma$, ω_0 is the bare phonon frequency, Γ is the linewidth. I_0 is a constant and q is the Fano asymmetry parameter. It serves as a measure of a strength of the electron–phonon coupling: an increase in $|1/q|$ indicates an increase in the electron–phonon interaction, more precisely, an increase in the electron-mediated photon–phonon coupling function [51, 53]. From the inset of figure 4(d) it can be seen that $|1/q|$ increases as the temperature is lowered and reaches the highest values around T_c, when the spin fluctuations are the strongest. Spin fluctuations increase the electron–phonon scattering, similarly does the disorder. Technically, the electronic Green function acquires an imaginary component of the self energy due to the spin fluctuations, and this implies the increase in the damping term in the phonon self-energy, as explained in, e.g. [44]. This leads us to conclude that the spin fluctuations strongly enhance the electron–phonon interaction for the B_{1g} vibrational mode affecting its frequency and linewidth near T_c.

5. Conclusion

In summary, the Raman scattering study of the $K_xCo_{2-y}Se_2$ ($x = 0.3, y = 0.1$) single crystals and lattice dynamics calculations of the KCo_2Se_2, have been presented. Two out of four Raman active phonons are experimentally observed and assigned. The lack of any additional modes indicates the absence of vacancy ordering. The Raman spectra show sudden changes in the phonon energy and linewidth near the FM–PM phase transition. Above T_c the energy and linewidth temperature dependence of the A_{1g} and B_{1g} modes look conventional, as expected from the thermal expansion and anharmonicity effects. The linewidth, though, has very weak temperature dependence even above T_c which may be the consequence of the proximity of the phase transition and spin fluctuations. The B_{1g} vibrational mode has particularly large linewidth and features a Fano profile, which is likely the consequence of the magnetic exchange coupled to the vibrations of the Co atoms. Interestingly, the A_{1g} mode linewidth decreases below T_c, whereas the linewidth of the B_{1g} mode increases. The DFT calculations generally agree with the measured phonon frequencies. However, fine frequency differences in the two phases cannot be correctly predicted since the DFT calculations do not account for the spin fluctuation effects.

Acknowledgments

References

[1] Stewart G R 2011 *Rev. Mod. Phys.* **83** 1589–652
[2] Wei B, Qing-Zhen H, Gen-Fu C, Green M A, Du-Ming W, Jun-Bao H and Yi-Ming Q 2011 *Chin. Phys. Lett.* **28** 086104
[3] Liu R H *et al* 2011 *Europhys. Lett.* **94** 27008
[4] Ma L, Ji G F, Dai J, Lu X R, Eom M J, Kim J S, Normand B and Yu W 2012 *Phys. Rev. Lett.* **109** 197002
[5] Dagotto E 2013 *Rev. Mod. Phys.* **85** 849–67
[6] Zhang Y M *et al* 2011 *Nat. Mater.* **10** 273–7
[7] Li W *et al* 2012 *Nat. Phys.* **8** 126–30
[8] Lazarević N, Abeykoon M, Stephens P W, Lei H, Bozin E S, Petrovic C and Popović Z V 2012 *Phys. Rev.* B **86** 054503
[9] Ding X, Fang D, Wang Z, Yang H, Liu J, Deng Q, Ma G, Meng C, Hu Y and Wen H-H 2013 *Nat. Commun.* **4** 1897
[10] Louca D, Park K, Li B, Neuefeind J and Yan J 2013 *Sci. Rep.* **3** 2047
[11] Huang S-M, Mou C-Y and Lee T-K 2013 *Phys. Rev.* B **88** 174510
[12] Lei H, Abeykoon M, Wang K, Bozin E S, Ryu H, Graf D, Warren J B and Petrovic C 2014 *J. Phys.: Condens. Matter* **26** 015701
[13] Lazarević N, Radonjić M, Šćepanović M, Lei H, Tanasković D, Petrovic C and Popović Z V 2013 *Phys. Rev.* B **87** 144305
[14] Ryu H, Wang K, Opacic M, Lazarevic N, Warren J B, Popovic Z V, Bozin E S and Petrovic C 2015 *Phys. Rev.* B **92** 174522
[15] Ryu H, Abeykoon M, Wang K, Lei H, Lazarevic N, Warren J B, Bozin E S, Popovic Z V and Petrovic C 2015 *Phys. Rev.* B **91** 184503
[16] Yang J, Chen B, Wang H, Mao Q, Imai M, Yoshimura K and Fang M 2013 *Phys. Rev.* B **88** 064406
[17] Um Y J *et al* 2012 *Phys. Rev.* B **85** 064519
[18] Popović Z V, Lazarević N, Bogdanović S, Radonjić M M, Tanasković D, Hu R, Lei H and Petrovic C 2014 *Solid State Commun.* **193** 51–5
[19] Eiter H-M, Jaschke P, Hackl R, Bauer A, Gangl M and Pfleiderer C 2014 *Phys. Rev.* B **90** 024411

[20] Kirillov D, Suzuki Y, Antognazza L, Char K, Bozovic I and Geballe T H 1995 *Phys. Rev.* B **51** 12825–8
[21] Zhang W-L, Li H, Xia D, Liu H W, Shi Y-G, Luo J L, Hu J, Richard P and Ding H 2015 *Phys. Rev.* B **92** 060502
[22] Baroni S, de Gironcoli S, Dal Corso A and Giannozzi P 2001 *Rev. Mod. Phys.* **73** 515–62
[23] Gianozzi P *et al* 2009 *J. Phys.: Condens. Matter* **21** 395502
[24] Huan G and Greenblatt M 1989 *J. Less-Common Met.* **156** 247–57
[25] Guo J, Jin S, Wang G, Wang S, Zhu K, Zhou T, He M and Chen X 2010 *Phys. Rev.* B **82** 180520
[26] Lazarević N, Lei H, Petrovic C and Popović Z V 2011 *Phys. Rev.* B **84** 214305
[27] Wdowik U D, Jaglo G and Piekarz P 2015 *J. Phys.: Condens. Matter* **27** 415403
[28] Opačić M, Lazarević N, Šćepanović M, Ryu H, Lei H, Petrovic C and Popović Z V 2015 *J. Phys.: Condens. Matter* **27** 485701
[29] Granado E, García A, Sanjurjo J A, Rettori C, Torriani I, Prado F, Sánchez R D, Caneiro A and Oseroff S B 1999 *Phys. Rev.* B **60** 11879–82
[30] Gupta R, Sood A K, Metcalf P and Honig J M 2002 *Phys. Rev.* B **65** 104430
[31] Menéndez J and Cardona M 1984 *Phys. Rev.* B **29** 2051–9
[32] Haro E, Balkanski M, Wallis R F and Wanser K H 1986 *Phys. Rev.* B **34** 5358–67
[33] Rahlenbeck M, Sun G L, Sun D L, Lin C T, Keimer B and Ulrich C 2009 *Phys. Rev.* B **80** 064509
[34] Gnezdilov V, Pashkevich Y G, Lemmens P, Wulferding D, Shevtsova T, Gusev A, Chareev D and Vasiliev A 2013 *Phys. Rev.* B **87** 144508
[35] Böhmer A E, Hardy F, Eilers F, Ernst D, Adelmann P, Schweiss P, Wolf T and Meingast C 2013 *Phys. Rev.* B **87** 180505
[36] Kumar A, Chaudhary S, Pandya D K and Sharma S K 2014 *Phys. Rev.* B **90** 024302
[37] Iliev M N, Abrashev M V, Litvinchuk A P, Hadjiev V G, Guo H and Gupta A 2007 *Phys. Rev.* B **75** 104118
[38] Laverdière J, Jandl S, Mukhin A A, Ivanov V Y, Ivanov V G and Iliev M N 2006 *Phys. Rev.* B **73** 214301
[39] Kumar D, Kumar S and Sathe V G 2014 *Solid State Commun.* **194** 59–64
[40] Yin Z P, Haule K and Kotliar G 2011 *Nat. Mater.* **10** 932–5
[41] Yin Z P, Kutepov A and Kotliar G 2013 *Phys. Rev.* X **3** 021011
[42] Haule K, Shim J H and Kotliar G 2008 *Phys. Rev. Lett.* **100** 226402
[43] Allen P B 1972 *Phys. Rev.* B **6** 2577–9
[44] Cappelluti E 2006 *Phys. Rev.* B **73** 140505
[45] Calandra M and Mauri F 2005 *Phys. Rev.* B **71** 064501
[46] Aksenov V L and Kabanov V V 1998 *Phys. Rev.* B **57** 608–12
[47] Bannikov V V, Shein I R and Ivanovskii A L 2012 *Phys. B: Condens. Matter* **407** 271–5
[48] Ruf T, Thomsen C, Liu R and Cardona M 1988 *Phys. Rev.* B **38** 11985–7
[49] Macfarlane R M, Rosen H and Seki H 1987 *Solid State Commun.* **63** 831–4
[50] Barišić S, Kupčić I and Batistić I 1989 *Int. J. Mod. Phys.* B **03** 2051–63
[51] Devereaux T P, Virosztek A and Zawadowski A 1995 *Phys. Rev.* B **51** 505–14
[52] Kupčić I and Barišić S 2007 *Phys. Rev.* B **75** 094508
[53] García-Martínez N A, Valenzuela B, Ciuchi S, Cappelluti E, Calderón M J and Bascones E 2013 *Phys. Rev.* B **88** 165106
[54] Iliev M N, Jandl S, Popov V N, Litvinchuk A P, Cmaidalka J, Meng R L and Meen J 2005 *Phys. Rev.* B **71** 214305
[55] Lazarević N, Popović Z V, Hu R and Petrovic C 2010 *Phys. Rev.* B **81** 144302

Anderson localization effects near the Mott metal-insulator transition

Helena Bragança,[1] M. C. O. Aguiar,[1] J. Vučičević,[2] D. Tanasković,[2] and V. Dobrosavljević[3]

[1]*Departamento de Física, Universidade Federal de Minas Gerais, Belo Horizonte, MG, Brazil*
[2]*Scientific Computing Laboratory, Institute of Physics Belgrade, University of Belgrade, Pregrevica 118, 11080 Belgrade, Serbia*
[3]*Department of Physics and National High Magnetic Field Laboratory, Florida State University, Tallahassee, Florida 32306, USA*

The interplay between Mott and Anderson routes to localization in disordered interacting systems gives rise to different transitions and transport regimes. Here, we investigate the phase diagram at finite temperatures using dynamical mean-field theory combined with typical medium theory, which is an effective theory of the Mott-Anderson metal-insulator transition. We mainly focus on the properties of the coexistence region associated with the Mott phase transition. For weak disorder, the coexistence region is found to be similar to that in the clean case. However, as we increase disorder, Anderson localization effects are responsible for shrinking the coexistence region, and at sufficiently strong disorder (approximately equal to twice the bare bandwidth) it drastically narrows, the critical temperature T_c abruptly goes to zero, and we observe a phase transition in the absence of a coexistence of the metallic and insulating phases. In this regime, the effects of interaction and disorder are found to be of comparable importance for charge localization.

I. INTRODUCTION

The Mott mechanism of localization [1] is an emergent phenomenon in which a large local Coulomb repulsion suppresses double occupation, which prevents charge transport in a half-filled system. Strongly correlated electron materials, such as transition-metal oxides [2–5] and some organic salts [6–10], exhibit a Mott metal-insulator transition due to the effectively strong Coulomb repulsion that exists between electrons occupying a narrow valence band. Below the critical temperature T_c, this transition is of first-order and one observes a region where metal and insulator coexist [4–6,8].

The presence of disorder also leads to localization of electron wave functions, a phenomenon known as Anderson localization [11,12]. In this case, the energetic mismatch between neighboring sites prevents charge transport in the lattice. These two mechanisms of localization—Mott and Anderson—combine in nontrivial ways, sometimes reducing, sometimes enhancing each other's effects. Recently, the interplay between interaction and disorder has received much attention, mainly through three different perspectives. First, due to the investigation of the many-body localization [13], a novel paradigm arose for understanding localization in disordered and interacting quantum systems at nonzero temperature. Second, very recently, models of disordered and interacting systems have been simulated with cold atoms in optical lattices [14,15]. Finally, the disorder and the effective interaction strength can be systematically tuned by doping [3,5,9,16,17], or even x-ray irradiation [10,18].

Over the past few decades, considerable progress has been made in the description of strongly correlated materials and the Mott metal-insulator transition (MIT) through dynamical mean-field theory (DMFT) [19]. In this method, a lattice model of interacting electrons is mapped to the Anderson impurity model with a conduction bath that needs to be calculated self-consistently. To describe disorder, the simplest treatment is within the coherent potential approximation (CPA) [20]. The CPA can be easily combined with the DMFT [21–28] by considering an ensemble of impurities surrounded by an average bath, which is the same for each electron. This approach thus does not describe the spatial fluctuations associated with the Anderson localization. Near the Anderson transition, the distribution of the local density of states (DOS) changes from Gaussian to log-normal [29,30], implying that its arithmetic average value does not provide a proper description of the system. The typical medium theory (TMT) [31] provides a simple method that can effectively describe the Anderson localization. The central quantity in TMT is the typical density of states, defined as the geometric average of the local DOS [32], which plays the role of the order parameter for the Anderson localization. The TMT method was carefully tested for the noninteracting system [31,33,34], and it was successfully applied to the interacting case within the TMT-DMFT approach [35], elucidating the full nonmagnetic phase diagram for the disordered half-filled Hubbard model and the precise nature of the Mott-Anderson critical point [36]. The TMT-DMFT approach also allows for a spin-dependence analysis of the DOS, which enables one to include the effects of long-range magnetic order in disordered and interacting systems [37].

In this paper, we perform a TMT-DMFT calculation at finite temperatures. We explore the entire nonmagnetic phase diagram, with a particular focus on the effects of disorder on the Mott metal-insulator coexistence region. We carefully compare the TMT-DMFT and CPA-DMFT results with the goal of precisely determining the Anderson localization effects, described only within the former method. We find that the TMT-DMFT coexistence region is at comparatively lower values of the interaction U, while the critical temperature T_c is higher than in CPA-DMFT. The width of the coexistence region, however, quickly decreases with disorder. At disorder strength $W \sim 2B$, where B is the bandwidth in the clean noninteracting system, TMT-DMFT predicts T_c to abruptly go to zero, as opposed to the CPA-DMFT solution, where the coexistence region asymptotically shrinks to a single point as disorder is increased to infinity. In the regime $W \gtrsim 2B$, the MIT takes place at $U \approx W$, which causes Anderson and Mott mechanisms to become equally important for the properties of the system.

The paper is organized as follows. In Sec. II we briefly present the TMT-DMFT method for the solution of the disordered Hubbard model, and the (U, W) phase diagram is shown is Sec. III. Sections IV and V show details of the metal-insulator transition in the presence of weak, moderate, and strong disorder. Section VI contains conclusions.

II. TMT-DMFT METHOD

We consider the Hubbard model with random site energies, given by the Hamiltonian

$$H = -t \sum_{\langle ij \rangle \sigma} (c_{i\sigma}^\dagger c_{j\sigma} + \text{H.c.}) + U \sum_i n_{i\uparrow} n_{i\downarrow} + \sum_{i\sigma} (\varepsilon_i - \mu) n_{i\sigma},$$

where $c_{i\sigma}^\dagger$ ($c_{i\sigma}$) creates (destroys) an electron with spin σ on site i, $n_{i\sigma} = c_{i\sigma}^\dagger c_{i\sigma}$, t is the hopping amplitude for nearest-neighbor sites, U is the on-site repulsion, and ε_i is the random on-site energy, which follows a uniform distribution $P(\varepsilon)$ of width W, centered in $\varepsilon_i = 0$. We study the half-filled particle-hole symmetric lattice by setting the chemical potential μ equal to $U/2$. In general, transition-metal oxides and organic salts described by the Hubbard model can exhibit both antiferromagnetic and paramagnetic Mott insulating phases. In this work, we focus on the paramagnetic solution, which is present even at zero temperature in frustrated lattices.

Within TMT-DMFT, the lattice model describing a disordered correlated system is mapped onto an ensemble of single-impurity problems, corresponding to sites with different values of the on-site energy, each being embedded in a typical effective medium that needs to be calculated self-consistently. The TMT-DMFT self-consistent procedure can be summarized as follows [31,36]: By considering an initial guess for the (typical) bath $\Delta(\omega)$ surrounding the impurities, we solve an ensemble of impurity problems, which give us local Green's functions $G(\omega, \varepsilon_i)$ from which local spectra $\rho(\omega, \varepsilon_i) = -\frac{1}{\pi} \text{Im} G(\omega, \varepsilon_i)$ are obtained. The typical DOS is then calculated by the geometric average of the local spectra,

$$\rho_{\text{typ}}(\omega) = \exp \left[\int d\varepsilon \, P(\varepsilon) \ln \rho(\omega, \varepsilon) \right],$$

and the typical Green's function is obtained through the Hilbert transform, $G_{\text{typ}}(\omega) = \int_{-\infty}^{\infty} d\omega \frac{\rho_{\text{typ}}(\omega')}{\omega - \omega'}$. For lattices with semicircular DOS, $\rho_0(\omega) = \frac{4}{\pi B} \sqrt{1 - \left(\frac{2\omega}{B}\right)^2}$, in the clean non-interacting limit (Bethe lattice with infinite coordination number), the self-consistent loop is closed by calculating a new bath according to $\Delta(\omega) = t^2 G_{\text{typ}}(\omega)$. To solve the single-impurity problems, in this work we use the iterative perturbation theory (IPT) on the real axis [38,39]. In this case, we do not need analytic continuation. This is an important advantage of this method since the TMT self-consistency relation is based on the local DOS.

III. PHASE DIAGRAM

Figure 1 presents the TMT-DMFT phase diagram of the disordered Hubbard model obtained at a small temperature, $T = 0.008$. Here and throughout the paper, we define the noninteracting bandwidth $B = 4t$ as the unit of energy. In the phase diagram, the black and pink circles correspond to
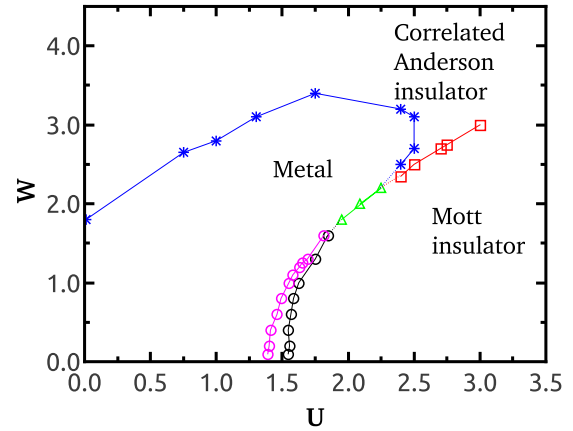

FIG. 1. (Color online) (U, W) phase diagram obtained within TMT-DMFT for the disordered Hubbard model at $T = 0.008$. The description of the different symbols/colors used is given in the text.

the metallic and the insulating spinodal lines of the first-order Mott phase transition; these two lines delimit the metal-insulator coexistence region. The green triangles indicate a transition between a metal and a Mott insulator in the absence of a well-defined coexistence region (see Sec. V for details), while the blue stars indicate a transition between a metal and a correlated Anderson insulator. Finally, the red squares correspond to a crossover between the two insulators, which takes place at $W \approx U$.

To differentiate the phases and build the phase diagram, we have analyzed the behavior of the typical DOS at the Fermi level [$\rho_{\text{typ}}(0)$], the frequency-integrated typical DOS (N), and the site occupation as a function of the on-site energy. As an example, these quantities are presented in Fig. 2 for the particular case of $U = 1.75$ and $T = 0.008$. For this set of parameters, as disorder W increases, the system goes from the Mott insulator to the Anderson insulator, crossing an intermediate metallic phase (see Ref. [40], for example, for a discussion about the presence of an intermediate metallic phase when disorder increases). The Mott insulator is characterized by a gap in the typical DOS [$\rho_{\text{typ}}(0) = 0$] and a finite frequency-integrated typical-DOS N [see panel (a)], as well as a single occupation of all sites [see panel (b)]. The metallic phase, on the other hand, features a quasiparticle peak in the typical DOS, nonzero integrated DOS N, and a variable site occupation n_i. Finally, the correlated Anderson insulator shows a vanishing typical DOS, indicating that all the states are localized and as such do not contribute with spectral weight to the typical DOS [31,35]. For this reason, the frequency-integrated typical DOS goes to zero when the system approaches the Anderson insulator, and thus it can be used as an order parameter that signalizes this transition. Furthermore, within the TMT-DMFT, the Anderson insulating phase corresponds to a two-fluid phase [36]: it consists of empty and doubly occupied sites, characteristic of noninteracting Anderson insulators, as well as singly occupied sites, characterizing Mott localized states [see the results for $W = 4$ in panel (b)].

We find good agreement between our diagram and others known in the literature at $T = 0$ [35,36]. The most relevant effects of finite but small temperature are over the Mott
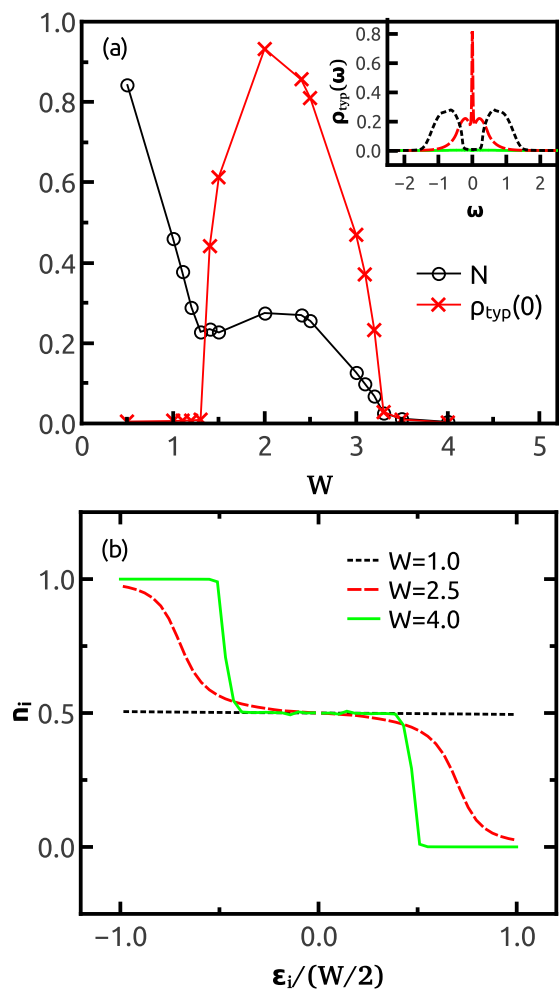
FIG. 2. (Color online) TMT-DMFT results for $U = 1.75$ and $T = 0.008$. According to the phase diagram of Fig. 1, as disorder W increases, the system goes from the Mott insulating phase to the metallic phase and finally to the Anderson insulating phase. These transitions are identified (and the phase diagram is built) by looking at the behavior of the quantities shown in the two panels of the present figure: (a) frequency-integrated typical DOS, N, and typical DOS at the Fermi level, $\rho_{typ}(0)$, as a function of W, and (b) site occupation per spin as a function of the site energy, normalized by the disorder distribution width, W. The inset shows an example of the typical DOS in the metallic phase (red long-dashed line), as well as in the Mott (black dashed line) and the Anderson (green solid line) insulating phases.

coexistence region, which spans a smaller range of U in comparison with the $T = 0$ case. The real axis IPT impurity solver makes it possible to solve TMT-DMFT equations for a broad range of parameters and several temperatures. In the following, we concentrate on the range of parameters near the phase transition, and, in particular, near the coexistence region of metallic and insulating solutions.

IV. MOTT TRANSITION FOR WEAK AND MODERATE DISORDER $W < 2B$

In this section, we analyze the coexistence region for weak and moderate disorder, which corresponds to
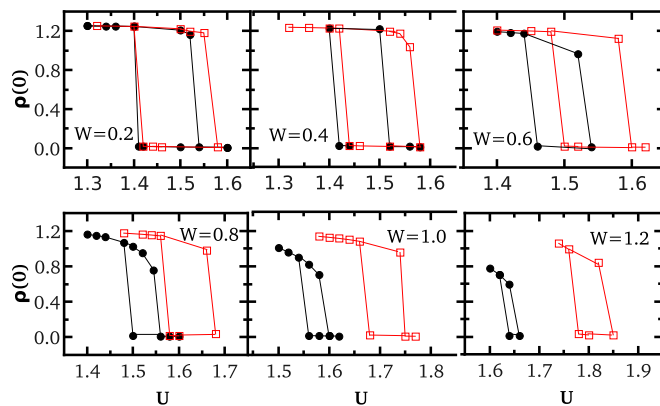
FIG. 3. (Color online) Hysteresis curves for the DOS at the Fermi level obtained by increasing and decreasing U at a fixed temperature $T = 0.01$. The curves enclose the coexistence region. The open squares were obtained within CPA-DMFT, while the filled circles correspond to TMT-DMFT results.

$W < W^*$, $W^* \approx 1.7$. At this regime, the critical U for the Mott transition is greater than the disorder strength. Although the phase transition described within TMT-DMFT is qualitatively similar to that of CPA-DMFT, some Anderson localization effects are already observed.

A. Coexistence region

To obtain the coexistence region within CPA-DMFT or TMT-DMFT for a fixed temperature $T < T_c$, we start from a metallic initial bath and increase U to find U_{c2}, which corresponds to the interaction value at which $\rho(0)$ goes to zero, indicating the disappearance of the quasiparticle peak in the DOS. Alternatively, when starting from an insulator, by decreasing U we find U_{c1}, where $\rho(0)$ becomes finite, indicating the closure of the gap at the Fermi level. This procedure allows us to obtain hysteresis curves of $\rho(0)$ as a function of U, which enclose the coexistence region (see Fig. 3 for examples of these hysteresis curves). For a given W, we can repeat this procedure for different temperatures and determine the two spinodal lines, $U_{c1}(T)$ and $U_{c2}(T)$, defining the coexistence region. The temperature at which the two spinodal lines merge gives the critical temperature, T_c, which corresponds to a second order critical end point.

Figure 4 shows the coexistence region obtained as described above for the clean case ($W = 0$) and for a disordered system ($W = 0.8$), both within TMT-DMFT and CPA-DMFT. According to our results, when disorder is added to the system, the critical U at which the transition occurs increases in comparison with the clean case. This happens because the general effect of disorder is to broaden the bands, as shown in Fig. 5, when the CPA-DMFT calculation is performed inside both the metallic and the insulating phases. Another general effect of disorder seen in the results of Fig. 4 is that the temperature of the second-order critical point decreases with disorder, in agreement with previous CPA-DMFT calculations [26]. These general consequences of disorder do not depend on the inclusion of Anderson localization effects, since they are observed even within the CPA-DMFT approach.
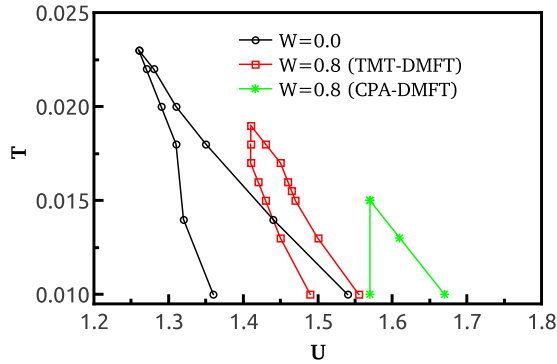
FIG. 4. (Color online) Spinodal lines enclosing the coexistence region for the clean system ($W = 0$) and the disordered case ($W = 0.8$) obtained within both TMT-DMFT and CPA-DMFT.
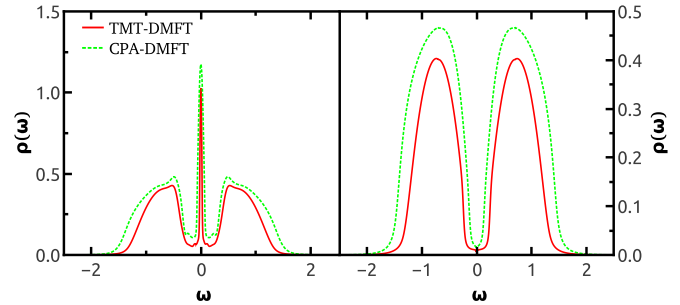

FIG. 6. (Color online) Typical (TMT-DMFT) and average (CPA-DMFT) values of the DOS as a function of frequency showing that Anderson localization effects start at the band edges, since both localized and extended states contribute to the average DOS, while only extended ones contribute to the typical DOS. The left panel shows results for $U = 1.5$, while those in the right panel are for $U = 1.6$, both at $T = 0.01$.

To carefully study the effects of Anderson localization, we compare the results obtained within TMT-DMFT with those of CPA-DMFT. As can be seen in Fig. 4 for $W = 0.8$, the critical U at which the transition occurs is smaller within TMT-DMFT than within CPA-DMFT. Moreover, a narrower coexistence region is observed within the former. To understand these results, one should consider that the wave-function localization starts at the band edges and that localized states do not contribute with spectral weight to the typical DOS. For these reasons, in the presence of Anderson localization, narrower bands are observed in comparison with CPA-DMFT results, both in the metallic and the insulating phase, as can be seen in Fig. 6. This is the opposite effect to that described in the previous paragraph regarding the effects of adding disorder to a clean system. As a consequence, the coexistence region within TMT-DMFT is seen in between that of a clean system and that obtained within CPA-DMFT for the same value of disorder.

From the TMT-DMFT and the CPA-DMFT hysteresis curves shown in Fig. 3, we see that the Anderson localization effects over the coexistence region become more important as the disorder increases. As W approaches $W^* \approx 1.7$, the width of the TMT-DMFT coexistence region vanishes, and we were not able to observe the hysteresis even at the lowest temperatures $T = 0.005$ (see Sec. V). In contrast, in the CPA-DMFT solution [26], the coexistence region with finite small T_c is observed even for very large W.

B. Crossover regime and the critical temperature T_c

As seen in Fig. 3, the coexistence region shrinks as disorder increases, making it difficult to obtain the critical temperature T_c from the merging of the two spinodal lines. One alternative is to determine T_c from the results obtained above it, that is, in the crossover region between metal and insulator. This was shown to be possible in the clean case, and in the present work we extend this analysis to the disordered system.

The quantum Widom line (QWL) associated with the Mott transition is defined in Refs. [41–44] in analogy with the classical Widom line [45] as the instability (crossover) line above the critical end point (U_c, T_c). It starts at the critical end point and goes to higher temperatures (above the coexistence region) as a continuation of the first-order phase-transition line. It is associated with the (zero-temperature) quantum critical point, which is masked by the coexistence region in the case of the Mott transition. The QWL can be defined from the free-energy functional $F_L[G(i\omega_n)]$, and it can be used to determine T_c from the behavior at higher temperatures, as explained (for the clean case) in Refs. [41,42]. With the objective of applying the QWL analysis to obtain T_c in the disordered case, here we review this procedure.

The Landau free-energy functional of the Hubbard model as a functional of $G(i\omega_n)$ is given by

$$F_L[G(i\omega_n)] = -Tt^2 \sum_n G^2(i\omega_n) + F_{\text{imp}}[G(i\omega_n)],$$

where the first term represents the energy needed to form the bath around a given site, and the second term describes the energy of the electron at the impurity level surrounded by the bath, that is, the free energy of the single-impurity problem. The DMFT (TMT-DMFT) equations are obtained by minimizing $F_L[G(i\omega_n)]$ with respect to $G(i\omega_n)$.

The curvature λ of the above free-energy functional with respect to U is finite and minimal along the crossover line and is zero at the second-order critical point. This curvature can be identified with the convergence rate of the iterative DMFT calculation [41,42], that is, $\lambda(U,T)$ corresponds to the slope of the convergence rate $\ln\{\text{Im}[G^{(\text{it})}(0) - G^{(\text{it}-1)}(0)]\}$ as a function of the step "it" of the iterative calculation. Repeating

FIG. 5. (Color online) Average DOS obtained within CPA-DMFT for different values of disorder at fixed temperature $T = 0.01$. Disorder broadens the bands in both the metallic (left panel, for $U = 1$) and the insulating (right panel, for $U = 3$) phase.
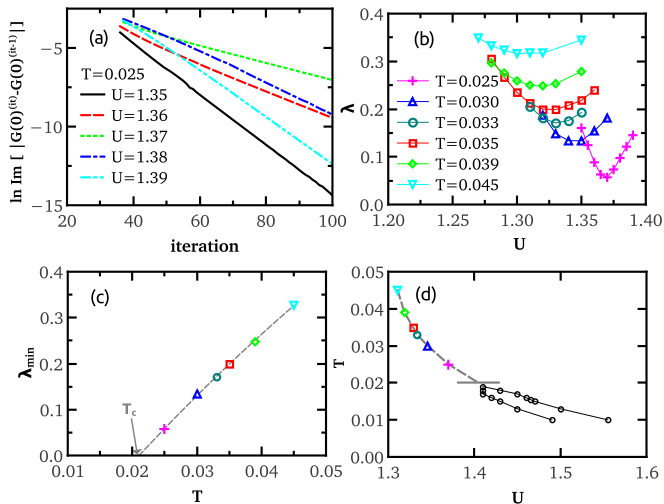
FIG. 7. (Color online) QWL analysis for the disordered system with $W = 0.8$ described by TMT-DMFT. See the text for the explanation of the results in each panel.
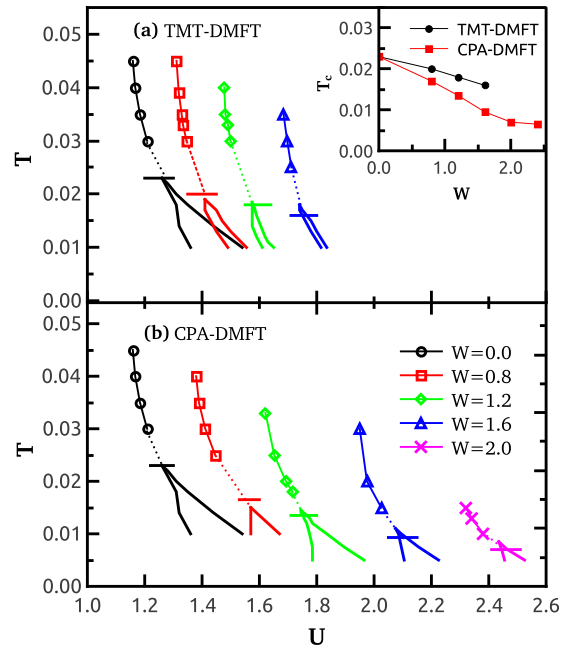

FIG. 8. (Color online) QWL and coexistence regions obtained within TMT-DMFT (a) and CPA-DMFT (b) for different values of disorder (CPA-DMFT coexistence regions for $W \geqslant 1.2$ were obtained from Ref. [26]). The horizontal lines represent T_c obtained from the corresponding QWL, calculated as exemplified in Fig. 7 (c). The inset shows these T_c values as a function of disorder.

the calculation for different values of T, we obtain the curve $\lambda_{\min} = \lambda(T)|_{U^*}$, where U^* is the point at which λ is minimum for a given T. This line can be extrapolated, to $\lambda_{\min}|_{T=T_c} = 0$, since the curvature of the free-energy functional is zero at the second-order critical point.

The procedure is illustrated in Fig. 7 for the disordered system with $W = 0.8$. For each value of U, we obtain the free-energy curvature λ from the convergence rate of the typical Green's function through the iterative steps, as presented in (a) for $T = 0.025$. For a fixed temperature and different values of U, we obtain the corresponding $\lambda(U)|_T$ curve. Repeating this procedure for different temperatures, we obtain the set of curves $\lambda(U)|_T$ presented in Fig. 7(b). The minima $\lambda_{\min}$ of these curves are shown in panel (c), and we obtain T_c as the temperature at which $\lambda_{\min} = 0$. Finally, panel (d) shows the crossover line obtained from data in panel (b), T_c obtained through the QWL analysis (gray horizontal line), and the two spinodal lines. We conclude that the T_c calculated from the QWL analysis coincides with the T_c obtained from the merging of the two spinodal lines that define the coexistence region.

In Fig. 8, we show the QWL and the critical temperatures obtained from them as we vary the system disorder, both within TMT-DMFT and CPA-DMFT. For disorder strengths $W \gtrsim 1.6$, we find a nonlinear behavior of the TMT-DMFT convergence rate as a function of the iteration step; we were thus unable to use the QWL analysis discussed above to evaluate T_c for very large disorder. For $W < 1.7$, both methods predict that T_c decreases when W increases [see also the inset in Fig. 8(a)]. The critical temperature T_c is higher within TMT-DMFT than within CPA-DMFT, although the coexistence region becomes (very) narrow in the presence of Anderson localization effects (TMT-DMFT results). However, T_c always remains finite within CPA-DMFT even for very large disorder strength [26], whereas we do not observe the coexistence region for $W \gtrsim 1.7$ in TMT-DMFT (see the next section). Our numerical TMT-DMFT solution indicates that

T_c abruptly drops to zero as the coexistence region disappears for $W \approx 1.7$.

V. MOTT-ANDERSON TRANSITION FOR STRONG DISORDER $W \gtrsim 2B$

Within the TMT-DMFT calculation, as we increase disorder, the value of the critical U becomes closer to the disorder width W. For $U \sim W \sim 2B$ both Mott and Anderson routes to localization become equally relevant, and it becomes the most difficult to precisely understand the mechanism of the MIT. In Fig. 9, we show the results for $W = 2.0$ at $T = 0.01$. The transition is seen to take place at $U \approx 2.09$. Moreover, if we look at the results for the typical DOS at the Fermi level when U increases, as well as when U decreases [see panel (a)], we observe no hysteresis, even if we decrease the temperature down to $T = 0.005$, in contrast to the results shown in Fig. 3. Since $\rho_{\text{typ}}(0)$ becomes zero, the system certainly goes through a MIT—but to what type of insulator does the system go?

To answer this question, we first look at the frequency-integrated typical DOS N, which can be considered an order parameter in the case of the Anderson transition, as discussed in the beginning of the paper. As can be seen in Fig. 9(a), N becomes very small but is still finite when $\rho_{\text{typ}}(0) \to 0$, suggesting that the transition is *not* of the Anderson type. The nature of the transition can finally be confirmed by analyzing the occupation number per spin n_i as a function of the site energy close to the transition, which can be seen in panel (b). As U increases toward the MIT, all sites become singly occupied, which is a characteristic of the Mott insulator. Although of the Mott type, the Hubbard subbands are strongly
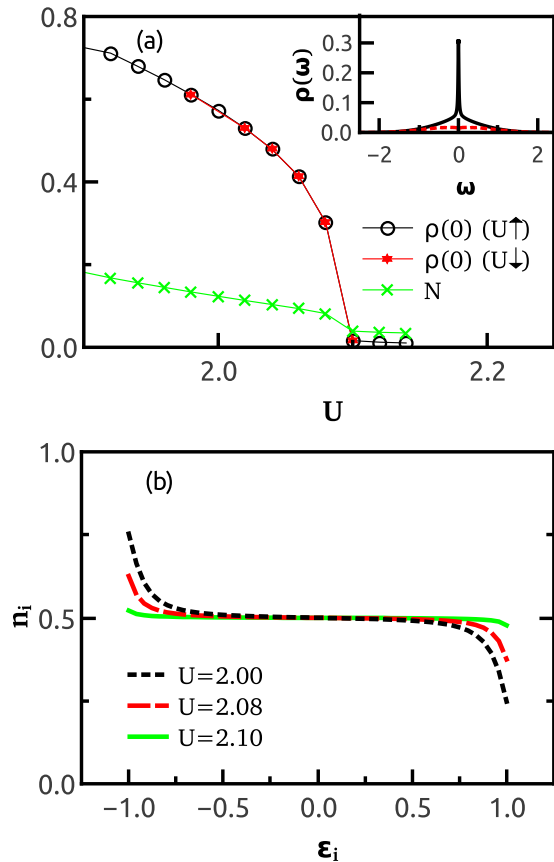
FIG. 9. (Color online) Results obtained within TMT-DMFT for $W = 2.0$ at $T = 0.01$. Panel (a) presents the typical DOS at the Fermi level obtained by increasing U (black circles) and decreasing U (red stars); no coexistence region is observed. In the same panel, we can also see the frequency-integrated typical DOS N as a function of U. The inset shows the typical DOS as a function of frequency for $U = 2.08$ (black solid line) and $U = 2.10$ (red dashed line). Finally, panel (b) presents the occupation number per spin as a function of the site energy as the transition is approached.

reduced for this value of W, as can be seen in the DOS presented in the inset, which is consistent with our expectation that both Mott and Anderson routes to localization are relevant in this regime of $U \approx W$.

Interestingly, our analysis of Fig. 9 suggests that for $W = 2.0$ there exists a transition between a metal and a Mott insulator in the *absence* of a coexistence region. Indeed, according to the phase diagram (Fig. 1), the same behavior is observed in a small range around $U \approx W \approx 2$. According to Figs. 3 and 8, TMT-DMFT predicts that the coexistence region will become (very) narrow when the system is in the $U < W$ regime and disorder increases. When the system enters the $U \sim W$ regime, the two spinodal lines seem to merge and no coexistence is observed, suggesting that T_c abruptly goes to zero due to the Anderson localization effects. Our results are in general agreement with the $T = 0$ phase diagram of Ref. [35] while presenting a much more detailed analysis of the MIT with the vanishing coexistence region.

For $W \gtrsim 2.3$, one can find a direct crossover between the two insulators, Mott and correlated Anderson, without

an intermediate metallic phase; this crossover is represented by red squares in our diagram of Fig. 1. To distinguish between the two insulators, we have looked at the occupation number as a function of site energy, as exemplified in Fig. 2. Our results show that when $W < U$, all the sites are singly occupied, characterizing a Mott insulator; when $W > U$, on the other hand, there are sites with energy larger than $U/2$, which are empty, sites with energy smaller than $-U/2$, which have double occupancy, and also sites occupied with one electron, characterizing the two-fluid behavior of the correlated Anderson insulator. According to these results, as might have been expected from the two-fluid picture of the Mott-Anderson insulator [36], the crossover between the two insulators is seen to take place at $W \approx U$.

VI. CONCLUSIONS

In this work, we studied Mott and Anderson routes to localization by using a combination of dynamical mean-field theory (DMFT) and typical medium theory (TMT) to solve the disordered Hubbard model. According to our TMT-DMFT results, Anderson localization has important effects near the Mott transition, especially on the coexistence region of metallic and insulating phases that exists below a critical temperature T_c. In the presence of small and moderate disorder W, the TMT-DMFT transition is qualitatively similar to that in the CPA-DMFT case (which does not describe localization due to disorder), and the main precursors of Anderson localization are seen in the narrowing of the coexistence region in comparison with CPA-DMFT. As the disorder increases further, for $W \gtrsim 2B$ (where B is the bandwidth for $U = W = 0$), the transition occurs at $U \approx W$ and our results indicate that Anderson and Mott routes to localization become equally important. The critical temperature T_c abruptly goes to zero for $W = W^* \approx 1.7B$. For $1.7B < W \sim U < 2.3B$, the typical DOS at the metal-insulator transition is strongly reduced, but the states are nearly half-filled irrespective of the on-site energy, indicating dominantly Mott character of the MIT, although no coexistence region is observed. For even larger disorder, $W > 2.3$, there is a crossover between the Mott and the correlated Anderson insulator.

The observation of a Mott transition without a coexistence region suggests that the nature of the transition has changed from first to second order as disorder increases. For the clean system, it has been shown [41] that at T just above T_c the resistivity as a function of temperature shows a scaling behavior that is compatible with an assumption of quantum criticality. In other words, despite the presence of a coexistence region between the metallic and the Mott insulating phases at small temperatures, at intermediate temperatures the system seems to be controlled by a hidden quantum critical point. Very recently, an experimental work on κ-organics confirmed the presence of this quantum critical regime at intermediate temperatures [44]. In this respect, it will be very important to compare the TMT-DMFT phase diagram and charge transport with the experiments on disordered correlated systems. Preliminary results [46] on introducing disorder by x-ray irradiation show that U_c indeed increases with disorder while T_c also decreases and seems to vanish at some finite disorder.

[1] N. F. Mott, *Metal-Insulator Transitions* (Taylor and Francis, London, 1974).

[2] M. Imada, A. Fujimori, and Y. Tokura, Rev. Mod. Phys. **70**, 1039 (1998).

[3] D. B. McWhan, T. M. Rice, and J. P. Remeika, Phys. Rev. Lett. **23**, 1384 (1969); D. B. McWhan, A. Menth, J. P. Remeika, W. F. Brinkman, and T. M. Rice, Phys. Rev. B **7**, 1920 (1973).

[4] P. Limelette, A. Georges, D. Jérome, P. Wzietek, P. Metcalf, and J. M. Honig, Science **302**, 89 (2003).

[5] S. Lupi, L. Baldassarre, B. Mansart, A. Perucchi, A. Barinov, P. Dudin, E. Papalazarou, F. Rodolakis, J.-P. Rueff, J.-P. Itié, S. Ravy, D. Nicoletti, P. Postorino, P. Hansmann, N. Parragh, A. Toschi, T. Saha-Dasgupta, O. K. Andersen, G. Sangiovanni, K. Held, and M. Marsi, Nat. Commun. **1**, 105 (2010).

[6] F. Kagawa, K. Miyagawa, and K. Kanoda, Nature (London) **436**, 534 (2005).

[7] J. Merino, M. Dumm, N. Drichko, M. Dressel, and R. H. McKenzie, Phys. Rev. Lett. **100**, 086404 (2008).

[8] P. Limelette, P. Wzietek, S. Florens, A. Georges, T. A. Costi, C. Pasquier, D. Jérome, C. Mézière, and P. Batail, Phys. Rev. Lett. **91**, 016401 (2003).

[9] M. Dumm, D. Faltermeier, N. Drichko, M. Dressel, C. Mézière, and P. Batail, Phys. Rev. B **79**, 195106 (2009).

[10] T. Sasaki, Crystals **2**, 374 (2012).

[11] P. W. Anderson, Phys. Rev. **109**, 1492 (1958).

[12] P. A. Lee and T. V. Ramakrishnan, Rev. Mod. Phys. **57**, 287 (1985).

[13] D. M. Basko, I. L. Aleiner, and B. L. Altshuler, Ann. Phys. (N.Y.) **321**, 1126 (2006).

[14] S. Murmann, A. Bergschneider, V. M. Klinkhamer, G. Zurn, T. Lompe, and S. Jochim, Phys. Rev. Lett. **114**, 080402 (2015).

[15] S. S. Kondov, W. R. McGehee, W. Xu, and B. DeMarco, Phys. Rev. Lett. **114**, 083002 (2015).

[16] Y. Sekine, H. Takahashi, N. Môri, T. Matsumoto, and T. Kosaka, Physica B **237-238**, 148 (1997).

[17] M. Matsuura, H. Hiraka, K. Yamada, and Y. Endoh, J. Phys. Soc. Jpn. **69**, 1503 (2000).

[18] J. G. Analytis, A. Ardavan, S. J. Blundell, R. L. Owen, E. F. Garman, C. Jeynes, and B. J. Powell, Phys. Rev. Lett. **96**, 177002 (2006).

[19] A. Georges, G. Kotliar, W. Krauth, and M. J. Rozenberg, Rev. Mod. Phys. **68**, 13 (1996).

[20] E. N. Economou, *Green's Functions in Quantum Physics*, 3rd ed. (Springer, Berlin, 2005).

[21] V. Janiš and D. Vollhardt, Phys. Rev. B **46**, 15712 (1992).

[22] M. Ulmke, V. Janiš, and D. Vollhardt, Phys. Rev. B **51**, 10411 (1995).

[23] M. S. Laad, L. Craco, and E. Müller-Hartmann, Phys. Rev. B **64**, 195114 (2001).

[24] K. Byczuk, M. Ulmke, and D. Vollhardt, Phys. Rev. Lett. **90**, 196403 (2003).

[25] K. Byczuk, W. Hofstetter, and D. Vollhardt, Phys. Rev. B **69**, 045112 (2004).

[26] M. C. O. Aguiar, V. Dobrosavljević, E. Abrahams, and G. Kotliar, Phys. Rev. B **71**, 205115 (2005).

[27] M. M. Radonjić, D. Tanasković, V. Dobrosavljević, and K. Haule, Phys. Rev. B **81**, 075118 (2010).

[28] A. I. Poteryaev, S. L. Skornyakov, A. S. Belozerov, and V. I. Anisimov, Phys. Rev. B **91**, 195141 (2015).

[29] G. Schubert, J. Schleede, K. Byczuk, H. Fehske, and D. Vollhardt, Phys. Rev. B **81**, 155106 (2010).

[30] S. Mahmoudian and V. Dobrosavljević, arXiv:1503.00420.

[31] V. Dobrosavljević, A. A. Pastor, and B. K. Nikolic, Europhys. Lett. **62**, 76 (2003).

[32] M. Janssen, Phys. Rep. **295**, 1 (1998).

[33] C. E. Ekuma, H. Terletska, Z.-Y. Meng, J. Moreno, M. Jarrell, S. Mahmoudian, and V. Dobrosavljevic, J. Phys.: Condens. Matter **26**, 274209 (2014).

[34] C. E. Ekuma, H. Terletska, K.-M. Tam, Z.-Y. Meng, J. Moreno, and M. Jarrell, Phys. Rev. B **89**, 081107(R) (2014).

[35] K. Byczuk, W. Hofstetter, and D. Vollhardt, Phys. Rev. Lett. **94**, 056404 (2005).

[36] M. C. O. Aguiar, V. Dobrosavljević, E. Abrahams, and G. Kotliar, Phys. Rev. Lett. **102**, 156402 (2009).

[37] K. Byczuk, W. Hofstetter, and D. Vollhardt, Phys. Rev. Lett. **102**, 146403 (2009).

[38] H. Kajueter and G. Kotliar, Phys. Rev. Lett. **77**, 131 (1996).

[39] M. Potthoff, T. Wegner, and W. Nolting, Phys. Rev. B **55**, 16132 (1997).

[40] D. Heidarian and N. Trivedi, Phys. Rev. Lett. **93**, 126401 (2004).

[41] H. Terletska, J. Vučičević, D. Tanasković, and V. Dobrosavljević, Phys. Rev. Lett. **107**, 026401 (2011).

[42] J. Vučičević, H. Terletska, D. Tanasković, and V. Dobrosavljević, Phys. Rev. B **88**, 075143 (2013).

[43] J. Vučičević, D. Tanasković, M. J.. Rozenberg, and V. Dobrosavljević, Phys. Rev. Lett. **114**, 246402 (2015).

[44] T. Furukawa, K. Miyagawa, H. Taniguchi, R. Kato, and K. Kanoda, Nat. Phys. **11**, 221 (2015).

[45] G. G. Simeoni, T. Bryk, F. A. Gorelli, M. Krisch, G. Ruocco, M. Santoro, and T. Scopigno, Nat. Phys. **6**, 503 (2010).

[46] K. Kanoda (private communication).

Lattice dynamics of BaFe$_2X_3$(X = S, Se) compounds

Z. V. Popović, M. Šćepanović, N. Lazarević, and M. Opačić

Center for Solid State Physics and New Materials, Institute of Physics Belgrade, University of Belgrade,
Pregrevica 118, 11080 Belgrade, Serbia

M. M. Radonjić

Scientific Computing Laboratory, Institute of Physics Belgrade, University of Belgrade, Pregrevica 118, 11080 Belgrade, Serbia,
and Center for Electronic Correlations and Magnetism, Theoretical Physics III, Institute of Physics, University of Augsburg,
D-86135 Augsburg, Germany

D. Tanasković

Scientific Computing Laboratory, Institute of Physics Belgrade, University of Belgrade, Pregrevica 118, 11080 Belgrade, Serbia

Hechang Lei (雷和畅)[*] and C. Petrovic

Condensed Matter Physics and Materials Science Department, Brookhaven National Laboratory, Upton, New York 11973-5000, USA

We present the Raman scattering spectra of the BaFe$_2$X$_3$ (X = S, Se) compounds in a temperature range between 20 and 400 K. Although the crystal structures of these two compounds are both orthorhombic and very similar, they are not isostructural. The unit cell of BaFe$_2$S$_3$(BaFe$_2$Se$_3$) is base-centered *Cmcm* (primitive *Pnma*), giving 18 (36) modes to be observed in the Raman scattering experiment. We have detected almost all Raman active modes, predicted by factor group analysis, which can be observed from the cleavage planes of these compounds. Assignment of the observed Raman modes of BaFe$_2$S(Se)$_3$ is supported by the lattice dynamics calculations. The antiferromagnetic long-range spin ordering in BaFe$_2$Se$_3$ below T_N = 255 K leaves a fingerprint both in the A_{1g} and B_{3g} phonon mode linewidth and energy.

I. INTRODUCTION

Iron-based compounds are one of the top research fields in condensed matter physics [1]. These materials are not only superconducting [2] but also form low-dimensional magnetic structures—spin chains, spin ladders, or spin dimers [3], similar to the cases of cuprates [4] or vanadates [5]. Properties of iron-based selenide superconductors and other low-dimensional magnetic phases of iron-chalcogenides are reviewed in Ref. [6].

BaFe$_2$S$_3$ and BaFe$_2$Se$_3$ belong to the family of the iron-based $S = 2$ two-leg spin-ladder compounds. The crystal structure of these materials can be described as alternate stacking of Fe-S(Se) layers and Ba cations along the crystallographic a axis (b axis). In the Fe-S(Se) plane, only one-dimensional (1D) double chains of edge-shared [FeS(Se)]$_4$ tetrahedra propagate along the a axis (b axis), as shown in Fig. 1. Although the crystal structures of the BaFe$_2$S$_3$ and BaFe$_2$Se$_3$ are isomorphic, they are not isostructural. BaFe$_2$S$_3$ crystalizes in a base-centered orthorhombic structure with *Cmcm* space group [7]. The unit cell of BaFe$_2$Se$_3$ is also orthorhombic but primitive of the *Pmna* space group. The main crystal structure difference of these compounds is an alternation of the Fe-Fe distances in BaFe$_2$Se$_3$ along the chain direction which does not exist in BaFe$_2$S$_3$, where all distances between Fe atoms along the chain direction are the same;

see Figs. 1(b) and 1(c). This difference probably leads to the diverse magnetic properties of these two compounds at low temperatures.

BaFe$_2$S$_3$ is a quasi-one-dimensional semiconductor. The magnetic susceptibility of BaFe$_2$S$_3$, measured at 100 Oe, showed the divergence of the field-cooled susceptibility and zero-field-cooled susceptibility with the cusp at 25 K (freezing temperature) [8], indicating the presence of short-range magnetic correlations and spin-glass-like behavior below 25 K. On the basis of these observations Gönen *et al.* [8] proposed that each [Fe$_2$S$_3$]$^{2-}$ chain possess strong intrachain antiferromagnetic coupling of Fe ions that is mediated through the sulfide ions. The combination of antiferromagnetic coupling, additional crystal field splitting due to neighboring Fe atoms, and direct Fe-Fe interactions presumably give rise to $S = 0$ ground states in this compound [8].

BaFe$_2$Se$_3$ is an insulator down to the lowest measured temperature with a long-range antiferromagnetic (AFM) order with T_N around 255 K and short-range AFM order at higher temperatures [9–12]. It was shown that a dominant order involves 2×2 blocks of ferromagnetically aligned four iron spins, whereas these blocks order antiferromagnetically in the same manner as the block AFM $\sqrt{5} \times \sqrt{5}$ state of the iron vacancy ordered A$_2$Fe$_4$Se$_5$ [13–15].

To the best of our knowledge there are no data about the phonon properties of these compounds. In this paper we have measured polarized Raman scattering spectra of BaFe$_2X_3$(X = S, Se) in the temperature range between 20 and 400 K. We have observed the Raman active optical phonons, which are assigned using polarized measurements and the lattice dynamical calculations. At temperatures below

---

[*]Present address: Department of Physics, Renmin University of China, 59 Zhongguancun Street, Haidian District, Beijing 100872, China.
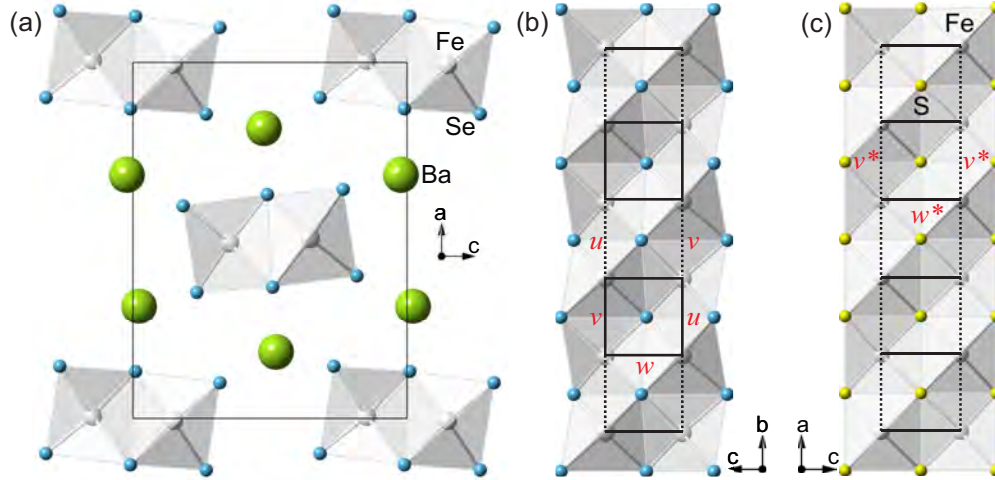
FIG. 1. (Color online) Schematic representation of the $BaFe_2X_3(X = S, Se)$ crystal structure. (a) Projection of the $BaFe_2Se_3$ crystal structure in the (ac) plane. (b) The double chain of Fe-Se tetrahedra connected via common edges along the *b* axis. (c) The Fe-S double chain in the (010) projection. w, u, v represents Fe-Fe distances of ladder rungs ($w = 0.2697$ nm; $w* = 0.2698$ nm) and legs ($u = 0.2688$ nm, $v = 0.2720$ nm; $v* = 0.2643$ nm). Note that in the case of $BaFe_2S_3$ the Fe atoms form an "ideal" ladder (all Fe-Fe distances along the ladder legs are equivalent, which is not the case in $BaFe_2Se_3$).

$T_N = 255$ K in $BaFe_2Se_3$ the Raman modes shows an abrupt change of energy and linewidth due to the antiferromagnetic spin ordering.

II. EXPERIMENT AND NUMERICAL METHOD

Single crystals of $BaFe_2X_3(X = S, Se)$ were grown using self-flux method with nominal composition $Ba:Fe:X = 1:2:3$. Details were described in Ref. [16]. Raman scattering measurements were performed on (110)(sulfide) [(100) (selenide)]-oriented samples in the backscattering micro-Raman configuration. Low-temperature measurements were performed using KONTI CryoVac continuous flow cryostat coupled with JY T64000 and TriVista 557 Raman systems. The 514.5-nm line of an Ar^+/Kr^+ mixed gas laser was used as excitation source. The Raman scattering measurements at higher temperatures were done using a LINKAM THMS600 heating stage.

We calculated phonon energies of the nonmagnetic $BaFe_2S(Se)_3$ single crystals at the center of the Brillouin zone. Calculations were performed within the theory of linear response using the density functional perturbation theory (DFPT) [17] as implemented in the QUANTUM ESPRESSO package [18]. In the first step, we obtained the electronic structure by applying the pseudopotentials based on the projected augmented waves method with the Perdew-Burke-Ernzerhof exchange-correlation functional and nonlinear core correction. Used energy cutoffs for the wave functions and electron densities were 80 (64) Ry and 960 (782) Ry for $BaFe_2S(Se)_3$, respectively. We have carried out the calculation with experimental values of the $BaFe_2S(Se)_3$ unit cell parameters $a = 0.878\,35$ nm, $b = 1.1219$ nm, $c = 0.5286$ nm [7] ($a = 1.188\,34$ nm, $b = 0.541\,41$ nm, $c = 0.914\,09$ nm [11]), and the relaxed fractional coordinates; see Table I. Relaxation was applied to place atoms in their equilibrium positions in respect to used pseudopotentials (all forces acting on every atom were smaller than 10^{-4} Ry/a.u.). The difference between experimental and relaxed coordinates is less than 3% for almost

all atom coordinates, except for the *x* direction of the Ba atoms in $BaFe_2Se_3$, which is 6%. Reduction of the *x* coordinate of Ba atoms by relaxation leads to an increase of the distance between the Ba layers. The Brillouin zone was sampled with $8 \times 8 \times 8$ Monkhorst-Pack **k**-space mesh. Calculated Γ point phonon energies of the $BaFe_2S_3$ and $BaFe_2Se_3$ are listed in Tables II and Table IV, respectively.

The DFPT calculation of the phonon-mode energies is performed assuming the paramagnetic solution and the comparison of energies is performed with the experimental results at room temperature. The paramagnetic density functional theory (DFT) solution is metallic, whereas $BaFe_2Se_3$ is AFM insulator at low temperatures. Therefore, we have performed also the spin-polarized DFT calculations, assuming AFM ordering of 2×2 ferromagnetic iron blocks [10–12]. We find the AFM solution and opening of the gap at the Fermi level in agreement with earlier DFT calculations by Saparov *et al.* [10]. Accordingly, we attempted to calculate the phonon

TABLE I. Experimental and relaxed (in square brackets) fractional coordinates of $BaFe_2S_3$ (Ref. [7]) and $BaFe_2Se_3$ (Ref. [11]) crystal structures.

Atom	Site	x	y	z
$BaFe_2S_3$				
Ba	(4c)	0.50 [0.50]	0.1859 [0.1817]	0.25 [0.25]
Fe	(8e)	0.3464 [0.3553]	0.50 [0.50]	0.00 [0.00]
S1	(4c)	0.50 [0.50]	0.6147 [0.6051]	0.25 [0.25]
S2	(8g)	0.2074 [0.2108]	0.3768 [0.3945]	0.25 [0.25]
$BaFe_2Se_3$				
Ba	(4c)	0.186 [0.175]	0.25 [0.25]	0.518 [0.513]
Fe	(8d)	0.493 [0.490]	0.002 [−0.001]	0.353 [0.358]
Se1	(4c)	0.355 [0.366]	0.25 [0.25]	0.233 [0.230]
Se2	(4c)	0.630 [0.613]	0.25 [0.25]	0.491 [0.485]
Se3	(4c)	0.402 [0.415]	0.25 [0.25]	0.818 [0.809]

TABLE II. Calculated and experimentally observed values of Raman active phonon mode energies (in cm^{-1}) of BaFe$_2$S$_3$ single crystal.

Symmetry	Calculation relax. (unrelax.)	Experiment 300 K	Experiment 100 K	Activity	Symmetry	Calculation relax. (unrelax.)	Experiment 300 K	Experiment 100 K	Activity
A_g^1	42.3 (51.2)		39	(xx,yy,zz)	B_{1g}^1	16.7 (63)			(xy)
A_g^2	154.2 (156)		157	(xx,yy,zz)	B_{1g}^2	55.1 (81.8)	44	48	(xy)
A_g^3	201.9 (167.4)	152	165	(xx,yy,zz)	B_{1g}^3	138.8 (153.1)	127	133	(xy)
A_g^4	366.9 (294.8)	295	301	(xx,yy,zz)	B_{1g}^4	243.5 (221.9)	203	214	(xy)
A_g^5	385.8 (307.1)	365	372	(xx,yy,zz)	B_{1g}^5	337.8 (241.6)		332(?)	(xy)
					B_{1g}^6	400.2 (330)	374	381	(xy)
B_{2g}^1	107.8 (113.7)	107	109	(xz)	B_{3g}^1	55.1 (66.8)			(yz)
B_{2g}^2	224.1 (180.8)	181	193	(xz)	B_{3g}^2	201.1 (171.1)	181	193	(yz)
B_{2g}^3	347.8 (283.6)			(xz)	B_{3g}^3	311.2 (308.7)	297	307	(yz)
					B_{3g}^4	369.3 (351.7)			(yz)

energies in the spin-polarized case. However, having now 48 atoms in the unit cell, this calculation turned out to be computationally too demanding. Furthermore, we do not believe that such a calculations would gives us in this case important new insights since the number of phonon modes becomes $2 \times 72 - 1 = 143$ (one mode is degenerate), and it is not likely that small splitting of the modes could be compared with the experiments. Also, the phonon frequencies are not particularly sensitive on the precise form of the density of states near the Fermi level (or gap opening) if the overall spectral function remains similar. Therefore, we believe that the usage of the nonmagnetic DFT is a reasonable method for identification of vibrational modes and comparison with the experimental data.

III. RESULTS AND DISCUSSION

A. BaFe$_2$S$_3$

The BaFe$_2$S$_3$ crystal symmetry is orthorhombic, space group $Cmcm$ and $Z = 4$ [7]. The site symmetries of atoms in $Cmcm$ space group are C_{2v}^y (Ba, S1), C_2^x(Fe), and C_s^{xy} (S2). Factor group analysis yields

$$\left(C_{2v}^y\right): \Gamma = A_g + B_{1g} + B_{3g} + B_{1u} + B_{2u} + B_{3u},$$

$$\left(C_2^x\right): \Gamma = A_g + 2B_{1g} + 2B_{2g} + B_{3g}$$
$$+ A_u + 2B_{1u} + 2B_{2u} + B_{3u}.$$

$$\left(C_s^{xy}\right): \Gamma = 2A_g + 2B_{1g} + B_{2g} + B_{3g} + A_u$$
$$+ B_{1u} + 2B_{2u} + 2B_{3u}.$$

Summarizing these representations and subtracting the acoustic ($B_{1u} + B_{2u} + B_{3u}$) and silent ($2A_u$) modes, we obtained the following irreducible representations of BaFe$_2$S$_3$ vibrational modes:

$$\Gamma_{\text{BaFe}_2\text{S}_3}^{\text{optical}} = 5A_g(xx,yy,zz) + 6B_{1g}(xy) + 3B_{2g}(xz)$$
$$+ 4B_{3g}(yz) + 4B_{1u}(E \parallel z) + 5B_{2u}(E \parallel y)$$
$$+ 4B_{3u}(E \parallel x).$$

Thus 18 Raman and 13 infrared active modes are expected to be observed in the BaFe$_2$S$_3$ infrared and Raman spectra. Because

our BaFe$_2$S$_3$ single-crystal samples have (110) orientation, we were able to observe all symmetry modes in the Raman scattering experiment.

The polarized Raman spectra of BaFe$_2$S$_3$, measured from the (110) plane at 100 K, are given in Fig. 2. Five A_g symmetry modes at about 39, 157, 165, 301, and 373 cm^{-1} (100 K) are clearly observed for the $x'(zz)x'$ polarization configuration ($x' = [110]$, $y' = [1\bar{1}0]$, $z = [001]$). For parallel polarization along the y' axis, the A_g and B_{1g} symmetry modes may be observed. By comparison $(y'y')$ with (zz) polarized spectrum we assigned the modes at 48, 133, 214, 332, and 381 cm^{-1} as the B_{1g} ones. The intensity of the 332 cm^{-1} mode is at a level of noise. Because of that, assignment of this mode as B_{1g}^5 should be taken as tentative.

For the $x'(y'z)x'$ polarization configuration both the B_{2g} and the B_{3g} symmetry modes can be observed. Because we cannot distinguish the B_{2g} and B_{3g} by selection rules from the (110) plane, the assignment of these modes was done with help of the lattice dynamics calculation; see Table II. Features between 40 and 100 cm^{-1} come after subtracting of nitrogen
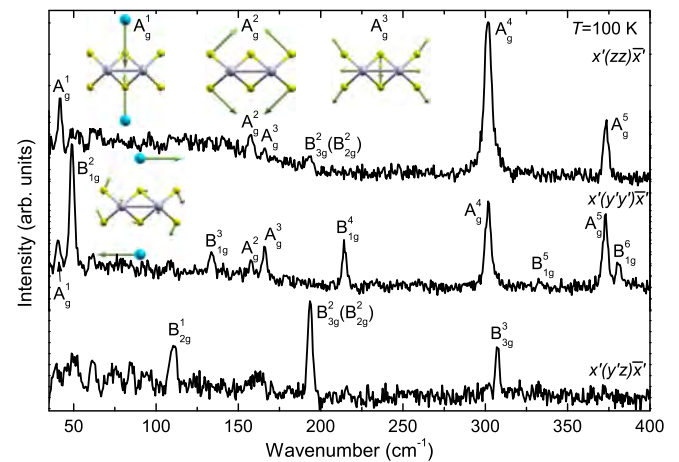

FIG. 2. (Color online) The polarized Raman scattering spectra of BaFe$_2$S$_3$ single crystal measured at 100 K. Insets are the normal modes of the A_g^1, A_g^2, A_g^3, and B_{1g}^2 vibrations. $x' = [110]$, $y' = [1\bar{1}0]$, and $z = [001]$.
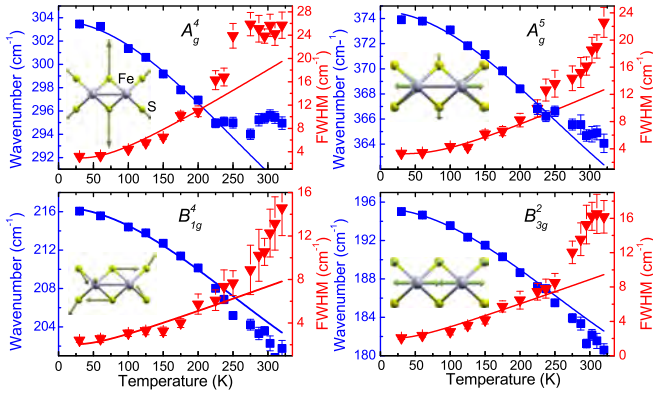
FIG. 3. (Color online) Experimental values (symbols) and calculated temperature dependence (solid lines) of the $BaFe_2S_3$ Raman mode energies and broadenings. Insets represent the normal modes of the A_g^4, A_g^5, B_{1g}^4, and B_{3g}^2 vibrations.

vibration modes. Bump at about 160 cm^{-1} is a leakage of A_g^2 and A_g^3 modes from parallel polarization.

The normal modes of some of A_g, B_{1g}, and B_{3g} vibrations, obtained by the lattice dynamics calculations, are given as insets in Figs. 2 and 3. According to these representations the lowest energy A_g^1 mode (39 cm^{-1}) originates from the Ba atom vibrations along the y axis, and the A_g^2 mode (157 cm^{-1}) represents dominantly S atom vibrations, which tend to elongate $[Fe_2S_3]^{2-}$ chains along the y axis. The A_g^3 mode originates from both the sulfur and the iron atom vibrations, which tend to stretch ladders along the x axis. The A_g^4 mode (Fig. 3) is sulfur atoms breathing vibrations, and the A_g^5 symmetry mode represents the S and Fe atom vibrations with the opposite tendency. The Fe atoms vibrate in opposite directions along the x axis, elongating the ladder, together with S atom vibrations, which tend to compress ladder structure.

Temperature dependence of the A_g^4, A_g^5, B_{1g}^4, and B_{3g}^2 mode energy and linewidth are given in Fig. 3.

In general, temperature dependance of Raman mode energy can be described with [19]

$$\omega(T) = \omega_0 + \Delta(T), \qquad (1)$$

where ω_0 is temperature-independent contribution to the energy of the phonon mode, whereas $\Delta(T)$ can be decomposed in

$$\Delta(T) = \Delta^V + \Delta^A. \qquad (2)$$

The first term in Eq. (2) represents change of phonon energy due to the thermal expansion of the crystal lattice, and is given by [20]

$$\Delta^V = -\omega_0 \gamma \frac{\Delta V(T)}{V_0}, \qquad (3)$$

where γ is the Grüneisen parameter of a given mode.

The second term in Eq. (2) is a contribution to the Raman mode energy from phonon-phonon scattering. By taking into account only three-phonon processes,

$$\Delta^A = -C\left(1 + \frac{4\lambda_{\text{ph-ph}}}{e^{\hbar\omega_0/2k_BT} - 1}\right). \qquad (4)$$

TABLE III. The best fit parameters of $BaFe_2S_3$ and $BaFe_2Se_3$.

Mode symmetry	ω_0(cm^{-1})	γ	Γ_0(cm^{-1})	λ
$BaFe_2S_3$				
A_g^4	303.7(2)	3.7(2)	2.9(2)	2.8(5)
A_g^5	374.6(2)	2.6(2)	3.3(2)	1.9(3)
B_{1g}^4	216.5(2)	4.8(2)	2.0(3)	0.9(3)
B_{3g}^2	195.3(1)	5.2(2)	2.0(3)	1.0(1)
$BaFe_2Se_3$				
A_g^8	200.0(1)	1.6(2)	2.3(1)	0.4(1)
A_g^9	272.6(2)	1.4(1)	2.3(1)	0.6(1)
A_g^{10}	288.1(3)	1.8(2)	5.2(1)	0.3(1)
A_g^{11}	297.1(4)	1.4(2)	5.6(2)	0.4(1)

C and $\lambda_{\text{ph-ph}}$ are the anharmonic constant and phonon-phonon interaction constant, respectively.

Temperature dependence of Raman mode linewidth is caused only by phonon anharmonicity:

$$\Gamma(T) = \Gamma_0\left(1 + \frac{2\lambda_{\text{ph-ph}}}{e^{\hbar\omega_0/2k_BT} - 1}\right), \qquad (5)$$

where Γ_0 is the anharmonic constant.

Parameter C is connected with ω_0 and Γ_0 via relation [19]

$$C = \frac{\Gamma_0^2}{2\omega_0}. \qquad (6)$$

ω_0 and Γ_0 can be determined by extrapolation of the corresponding experimental data to 0 K. With these parameters known, we can fit the phonon mode linewidth, using Eq. (5), to obtain $\lambda_{\text{ph-ph}}$. Then, by determining parameter C via Eq. (6), Raman mode energy can be properly fitted, with γ as the only unknown parameter. Using data from Ref. [12] for the temperature change of the lattice constants of $BaFe_2Se_3$ one can perform the corresponding analysis of the Raman mode energies' temperature dependance.

The best-fit parameters are collected in Table III. Because the Γ_0 is very small in comparison to ω_0, for all modes of both compounds (Table III), according to Eq. (6) the C anharmonic parameter becomes very small. Thus, contribution to the Raman mode energy from the phonon-phonon interaction can be neglected. In fact, a change of Raman mode energy with temperature is properly described only with the thermal expansion term Δ^V, Eq. (3).

The most intriguing finding in Fig. 3 is a dramatic change of slope of the A_g^4 mode linewidth (energy) temperature dependence at about 275 K. Because a hump in the inverse molar magnetic susceptibility [8] and a change of slope of the electrical resistivity [21] temperature dependence are observed in $BaFe_2S_3$ at about the same temperature we concluded that the deviation from anharmonic behavior for A_g^4 mode could be related to spin and charge. In fact, many of iron-based spin-ladder materials have the 3D-antiferromagnetic phase transition at about 260 K. We believe that in the case of $BaFe_2S_3$ the antiferromagnetic ordering of spins within the ladder legs changes from short-range to the long-range state, without 3D antiferromagnetic spin ordering (the Néel state) of the whole crystal. This transition is followed with change
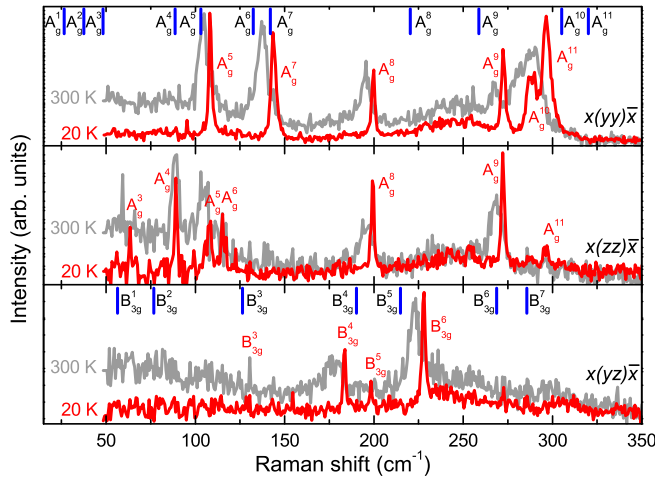
FIG. 4. (Color online) The $x(yy)\bar{x}$, $x(zz)\bar{x}$, and $x(yz)\bar{x}$ polarized Raman scattering spectra of BaFe$_2$Se$_3$ single crystals measured at room temperature and at 20 K. Vertical bars are calculated values of the A_g and the B_{3g} symmetry Raman active vibrations.

of the electronic structure, which could explain the abrupt increase of the resistivity at this temperature [21]. A lack of the BaFe$_2$S$_3$ low-temperature crystallographic and transport properties measurements did not allow a more detailed study of a possible origin of the phonon energy and linewidth deviation from the anharmonic picture at about 275 K.

B. BaFe$_2$Se$_3$

The BaFe$_2$Se$_3$ unit cell consists of four formula units comprising of 24 atoms. The site symmetries of atoms in

Pnma space group are C_s^{xz} (Ba, Se1, Se2, Se3) and C_1 (Fe). Factor group analysis yields

$$\left(C_s^{xz}\right): \Gamma = 2A_g + 1B_{1g} + 2B_{2g} + 1B_{3g}$$
$$+ A_u + 2B_{1u} + 1B_{2u} + 2B_{3u},$$
$$(C_1): \Gamma = 3A_g + 3B_{1g} + 3B_{2g} + 3B_{3g}$$
$$+ 3B_{1u} + 3B_{2u} + 3B_{3u}.$$

Summarizing these representations and subtracting the acoustic ($B_{1u} + B_{2u} + B_{3u}$) and silent ($4A_u$) modes, we obtained the following irreducible representations of BaFe$_2$Se$_3$ vibrational modes:

$$\Gamma_{\text{BaFe}_2\text{Se}_3}^{\text{optical}} = 11A_g + 7B_{1g} + 11B_{2g} + 7B_{3g}$$
$$+ 11B_{1u} + 7B_{2u} + 11B_{3u}$$

Thus 36 Raman and 29 infrared active modes are expected to be observed in the BaFe$_2$Se$_3$ vibrational spectra. Because the BaFe$_2$Se$_3$ single crystals have the (100) orientation (the crystallographic a axis is perpendicular to the plane of the single crystal), we were able to access only the A_g and the B_{3g} symmetry modes in the Raman scattering experiment.

The polarized Raman spectra of BaFe$_2$Se$_3$, measured from (100) plane at room temperature and 20 K, for the parallel and crossed polarization configurations, are given in Fig. 4. The spectra measured for parallel polarization configurations consist of the A_g symmetry modes. Six modes at about 108, 143.5, 200, 272, 288.7, and 296.5 cm^{-1} (20 K) are clearly observed for the $x(yy)\bar{x}$ polarization configuration and three additional modes are observed at about 63.4, 89, and 115 cm^{-1} for the $x(zz)\bar{x}$ polarization configuration. For the $x(yz)\bar{x}$ polarization configuration, three Raman active B_{3g} symmetry

TABLE IV. Calculated and experimentally observed values of Raman active phonon mode energies (in cm^{-1}) of BaFe$_2$Se$_3$ single crystal.

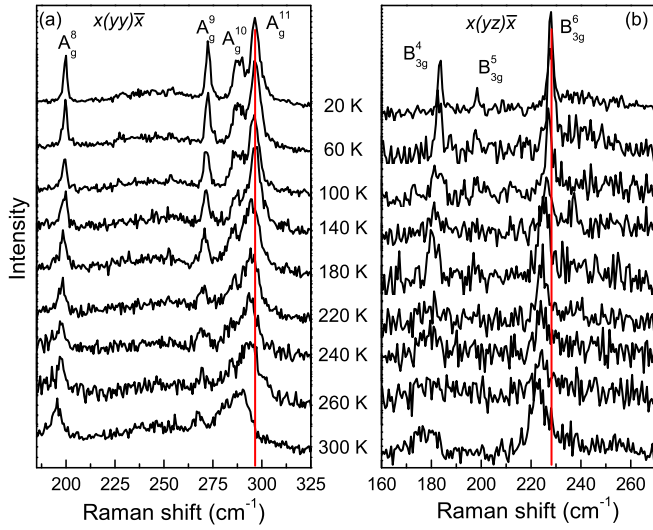| Symmetry	Calc.	Experiment 300 K	Experiment 20 K	Activity	Symmetry	Calc.	Experiment 300 K	Experiment 20 K	Activity
A_g^1	26.5			(xx,yy,zz)	B_{2g}^1	25.8			(xz)
A_g^2	37.5			(xx,yy,zz)	B_{2g}^2	48.0			(xz)
A_g^3	48.3	59	63.4	(xx,yy,zz)	B_{2g}^3	68.7			(xz)
A_g^4	88.6	88	89	(xx,yy,zz)	B_{2g}^4	88.8			(xz)
A_g^5	103.0	104.3	108	(xx,yy,zz)	B_{2g}^5	100.4			(xz)
A_g^6	132.4	111	115	(xx,yy,zz)	B_{2g}^6	138.2			(xz)
A_g^7	142.0	137	143	(xx,yy,zz)	B_{2g}^7	144.5			(xz)
A_g^8	220.4	195.6	200	(xx,yy,zz)	B_{2g}^8	212.9			(xz)
A_g^9	258.8	267	272	(xx,yy,zz)	B_{2g}^9	261.7			(xz)
A_g^{10}	305.2	280	288.7	(xx,yy,zz)	B_{2g}^{10}	303.9			(xz)
A_g^{11}	320.2	290	296.5	(xx,yy,zz)	B_{2g}^{11}	321.5			(xz)
B_{1g}^1	56.4			(xy)	B_{3g}^1	56.4			(yz)
B_{1g}^2	72.8			(xy)	B_{3g}^2	76.7			(yz)
B_{1g}^3	126.2			(xy)	B_{3g}^3	126.4			(yz)
B_{1g}^4	191.4			(xy)	B_{3g}^4	190.2	177	183.8	(yz)
B_{1g}^5	210.5			(xy)	B_{3g}^5	214.9		198	(yz)
B_{1g}^6	267.1			(xy)	B_{3g}^6	268.8	222.8	228	(yz)
B_{1g}^7	285.2			(xy)	B_{3g}^7	285.7			(yz)

FIG. 5. (Color online) The polarized Raman spectra of BaFe$_2$Se$_3$ single crystals measured at various temperatures. (a) $x(yy)\bar{x}$ polarization configuration; (b) $x(yz)\bar{x}$ polarization configuration.
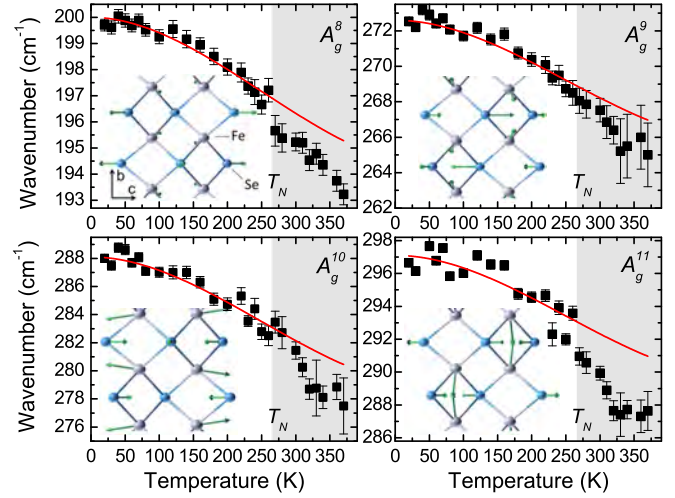

FIG. 6. (Color online) Experimental values (symbols) and calculated temperature dependence (solid lines) of BaFe$_2$Se$_3$ Raman mode energies. The best-fit parameters, for the temperature range below T_N, are given in Table III. Insets represent normal modes of the A_g^8, A_g^9, A_g^{10}, and A_g^{11} vibrations.

modes at 183.8, 198, and 228 cm^{-1} (20 K) are observed. Vertical bars in Fig. 4 denote the calculated energies of the A_g and B_{3g} symmetry modes, which are in rather good agreement with experimentally observed ones. The results of the lattice dynamics calculations, together with the experimental data, are summarized in Table IV.

According to the lattice dynamics calculations the lowest energy A_g^1 mode is dominated by Ba atom vibrations along the $\langle 101 \rangle$ directions and the A_g^2 mode represents vibrations of Fe and Se atoms which tend to rotate [Fe$_2$Se$_3$]$^{2-}$ chains around of the b axis. The A_g^3 mode involves all atom vibrations, which tend to stretch crystal structure along the $\langle 101 \rangle$ directions, whereas the A_g^4 mode originates from Se atom vibrations along the c axis and the Fe atom vibrations along the $\langle 101 \rangle$ directions. The A_g^5 mode represents vibration of Fe and Se atoms, which leads to [Fe$_2$Se$_3$]$^{2-}$-chain compression along the c axis. The A_g^6 mode originates from Se and Fe atom vibrations which stretch [Fe$_2$Se$_3$]$^{2-}$ chains along the c axis. Finally, the A_g^7 mode originates from Fe atom vibrations toward each other along the chain direction together with vibrations of the Se atoms along the c axis. The normal coordinates of the A_g^8, A_g^9, A_g^{10}, and A_g^{11} modes are given as insets in Fig. 6. As can be seen from Fig. 6 the A_g^8 mode originates dominantly from Se atom stretching vibrations, whereas the A_g^9, A_g^{10}, and A_g^{11} modes represent vibrations of both the Se and Fe atoms. In fact, the A_g^9 mode represents mostly Se atom vibrations along the c axis, and the A_g^{10} mode consists of Fe and Se vibrations along the c axis, which tend to elongate ladder structure along the b axis. Finally, the A_g^{11} mode represents the Fe atom vibrations toward each other along the chain axis, together with Se atom vibrations perpendicular to the chain direction.

By lowering the temperature, the lattice parameters of BaFe$_2$Se$_3$ decrease continuously without the crystal symmetry change around the magnetic ordering temperature [11,12] $T_N = 255$ K. Consequently we should expect the Raman mode hardening, without any abrupt change. Contrary to

expectations, the A_g and B_{3g} modes (see Figs. 5, 6, and 7) sharply increase their energies below the phase transition temperature T_N, as shown in details in Fig. 6. Because a significant local lattice distortion (Fe atom displacement along
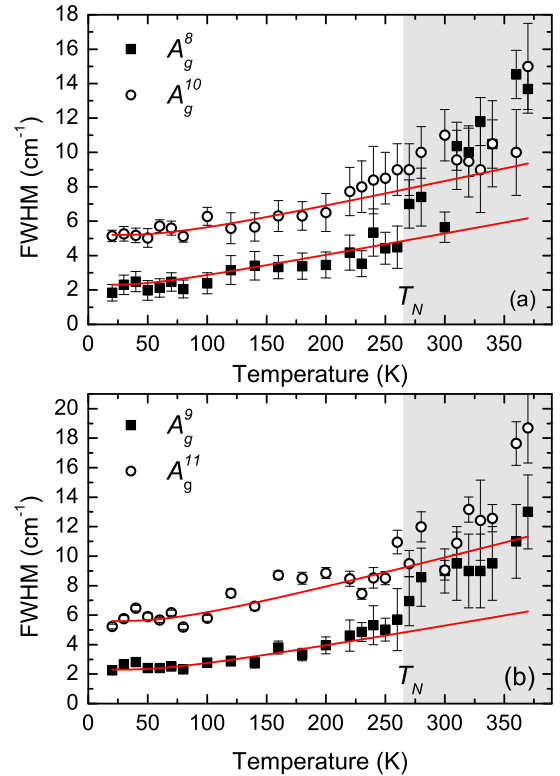

FIG. 7. (Color online) Linewidth vs temperature dependence of (a) A_g^8 and A_g^{10} modes and (b) A_g^9 and A_g^{11} modes of BaFe$_2$Se$_3$. Solid lines are calculated using Eq. (5). The best-fit parameters for a temperature range below T_N are given in Table III.

the b axis is as large as approximately 0.001 nm) [11,12] exists, driven by the magnetic order, we concluded that spin-phonon (magnetoelastic) coupling is responsible for Raman mode energy and linewith change in the antiferromagnetic phase. In fact, the existence of local displacements in the Fe atoms at T_N have a significant impact on the electronic structure due to rearrangement of electrons near the Fermi level [11] and consequently the change in the phonon energy and broadening. Raman mode linewidth change at about T_N is clearly observed as deviation from the usual anharmonicity temperature dependence (solid lines in Fig. 7) for all modes presented in Fig. 6.

IV. CONCLUSION

We have measured the polarized Raman scattering spectra of the BaFe$_2$S$_3$ and BaFe$_2$Se$_3$ single crystals in a temperature range between 20 and 400 K. Almost all Raman-active modes predicted by factor-group analysis to be observed from the cleavage planes of BaFe$_2$S$_3$ (110) and BaFe$_2$Se$_3$ (100) single crystals are experimentally detected and assigned.

Energies of these modes are in rather good agreement with the lattice dynamics calculations. The BaFe$_2$Se$_3$ Raman modes linewidth and energy change substantially at temperatures below $T_N = 255$ K, where this compound becomes antiferromagneticaly long-range ordered.

[1] C. King and D. A. Pendlebury, Web of knowledge research fronts 2013: 100 top-ranked specialties in the sciences and social sciences, http://sciencewatch.com/sites/sw/files/sw-article/media/research-fronts-2013.pdf

[2] Y. Kamihara, T. Watanabe, M. Hirano, and H. Hosono, J. Am. Chem. Soc. **130**, 3296 (2008).

[3] Z. V. Popović, M. Šćepanović, N. Lazarević, M. M. Radonjić, D. Tanasković, H. Lei, and C. Petrovic, Phys. Rev. B **89**, 014301 (2014).

[4] Z. V. Popović, M. J. Konstantinović, V. A. Ivanov, O. P. Khuong, R. Gajić, A. Vietkin, and V. V. Moshchalkov, Phys. Rev. B **62**, 4963 (2000).

[5] M. J. Konstantinović, Z. V. Popović, M. Isobe, and Y. Ueda, Phys. Rev. B **61**, 15185 (2000).

[6] E. Dagotto, Rev. Mod. Phys. **85**, 849 (2013).

[7] H. Hong and H. Steinfink, J. Solid State Chem. **5**, 93 (1972).

[8] Z. S. Gönen, P. Fournier, V. Smolyaninova, R. Greene, F. M. Araujo-Moreira, and B. Eichhorn, Chem. Mater. **12**, 3331 (2000).

[9] H. Lei, H. Ryu, A. I. Frenkel, and C. Petrovic, Phys. Rev. B **84**, 214511 (2011).

[10] B. Saparov, S. Calder, B. Sipos, H. Cao, S. Chi, D. J. Singh, A. D. Christianson, M. D. Lumsden, and A. S. Sefat, Phys. Rev. B **84**, 245132 (2011).

[11] J. M. Caron, J. R. Neilson, D. C. Miller, A. Llobet, and T. M. McQueen, Phys. Rev. B **84**, 180409 (2011).

[12] Y. Nambu, K. Ohgushi, S. Suzuki, F. Du, M. Avdeev, Y. Uwatoko, K. Munakata, H. Fukazawa, S. Chi, Y. Ueda, and T. J. Sato, Phys. Rev. B **85**, 064413 (2012).

[13] F. Ye, S. Chi, W. Bao, X. F. Wang, J. J. Ying, X. H. Chen, H. D. Wang, C. H. Dong, and M. Fang, Phys. Rev. Lett. **107**, 137003 (2011).

[14] N. Lazarević, M. Abeykoon, P. W. Stephens, H. Lei, E. S. Bozin, C. Petrovic, and Z. V. Popović, Phys. Rev. B **86**, 054503 (2012).

[15] N. Lazarević, H. Lei, C. Petrovic, and Z. V. Popović, Phys. Rev. B **84**, 214305 (2011).

[16] H. Lei, H. Ryu, V. Ivanovski, J. B. Warren, A. I. Frenkel, B. Cekic, W.-G. Yin, and C. Petrovic, Phys. Rev. B **86**, 195133 (2012).

[17] S. Baroni, S. de Gironcoli, A. Dal Corso, and P. Giannozzi, Rev. Mod. Phys. **73**, 515 (2001).

[18] P. Giannozzi, S. Baroni, N. Bonini, M. Calandra, R. Car, C. Cavazzoni, D. Ceresoli, G. L. Chiarotti, M. Cococcioni, I. Dabo, A. D. Corso, S. de Gironcoli, S. Fabris, G. Fratesi, R. Gebauer, U. Gerstmann, C. Gougoussis, A. Kokalj, M. Lazzeri, L. Martin-Samos, N. Marzari, F. Mauri, R. Mazzarello, S. Paolini, A. Pasquarello, L. Paulatto, C. Sbraccia, S. Scandolo, G. Sclauzero, A. P. Seitsonen, A. Smogunov, P. Umari, and R. M. Wentzcovitch, J. Phys.: Condens. Matter **21**, 395502 (2009).

[19] H.-M. Eiter, P. Jaschke, R. Hackl, A. Bauer, M. Gangl, and C. Pfleiderer, Phys. Rev. B **90**, 024411 (2014).

[20] V. Gnezdilov, Y. Pashkevich, P. Lemmens, A. Gusev, K. Lamonova, T. Shevtsova, I. Vitebskiy, O. Afanasiev, S. Gnatchenko, V. Tsurkan, J. Deisenhofer, and A. Loidl, Phys. Rev. B **83**, 245127 (2011).

[21] W. Reiff, I. Grey, A. Fan, Z. Eliezer, and H. Steinfink, J. Solid State Chem. **13**, 32 (1975).

Lattice dynamics of BaFe$_2$X$_3$(X = S, Se) compounds

Z. V. Popović, M. Šćepanović, N. Lazarević, and M. Opačić

Center for Solid State Physics and New Materials, Institute of Physics Belgrade, University of Belgrade,
Pregrevica 118, 11080 Belgrade, Serbia

M. M. Radonjić

Scientific Computing Laboratory, Institute of Physics Belgrade, University of Belgrade, Pregrevica 118, 11080 Belgrade, Serbia,
and Center for Electronic Correlations and Magnetism, Theoretical Physics III, Institute of Physics, University of Augsburg,
D-86135 Augsburg, Germany

D. Tanasković

Scientific Computing Laboratory, Institute of Physics Belgrade, University of Belgrade, Pregrevica 118, 11080 Belgrade, Serbia

Hechang Lei (雷和畅)* and C. Petrovic

Condensed Matter Physics and Materials Science Department, Brookhaven National Laboratory, Upton, New York 11973-5000, USA

We present the Raman scattering spectra of the BaFe$_2$X$_3$ (X = S, Se) compounds in a temperature range between 20 and 400 K. Although the crystal structures of these two compounds are both orthorhombic and very similar, they are not isostructural. The unit cell of BaFe$_2$S$_3$(BaFe$_2$Se$_3$) is base-centered *Cmcm* (primitive *Pnma*), giving 18 (36) modes to be observed in the Raman scattering experiment. We have detected almost all Raman active modes, predicted by factor group analysis, which can be observed from the cleavage planes of these compounds. Assignment of the observed Raman modes of BaFe$_2$S(Se)$_3$ is supported by the lattice dynamics calculations. The antiferromagnetic long-range spin ordering in BaFe$_2$Se$_3$ below T_N = 255 K leaves a fingerprint both in the A_{1g} and B_{3g} phonon mode linewidth and energy.

I. INTRODUCTION

Iron-based compounds are one of the top research fields in condensed matter physics [1]. These materials are not only superconducting [2] but also form low-dimensional magnetic structures—spin chains, spin ladders, or spin dimers [3], similar to the cases of cuprates [4] or vanadates [5]. Properties of iron-based selenide superconductors and other low-dimensional magnetic phases of iron-chalcogenides are reviewed in Ref. [6].

BaFe$_2$S$_3$ and BaFe$_2$Se$_3$ belong to the family of the iron-based $S = 2$ two-leg spin-ladder compounds. The crystal structure of these materials can be described as alternate stacking of Fe-S(Se) layers and Ba cations along the crystallographic *a* axis (*b* axis). In the Fe-S(Se) plane, only one-dimensional (1D) double chains of edge-shared [FeS(Se)]$_4$ tetrahedra propagate along the *a* axis (*b* axis), as shown in Fig. 1. Although the crystal structures of the BaFe$_2$S$_3$ and BaFe$_2$Se$_3$ are isomorphic, they are not isostructural. BaFe$_2$S$_3$ crystalizes in a base-centered orthorhombic structure with *Cmcm* space group [7]. The unit cell of BaFe$_2$Se$_3$ is also orthorhombic but primitive of the *Pnma* space group. The main crystal structure difference of these compounds is an alternation of the Fe-Fe distances in BaFe$_2$Se$_3$ along the chain direction which does not exist in BaFe$_2$S$_3$, where all distances between Fe atoms along the chain direction are the same;

see Figs. 1(b) and 1(c). This difference probably leads to the diverse magnetic properties of these two compounds at low temperatures.

BaFe$_2$S$_3$ is a quasi-one-dimensional semiconductor. The magnetic susceptibility of BaFe$_2$S$_3$, measured at 100 Oe, showed the divergence of the field-cooled susceptibility and zero-field-cooled susceptibility with the cusp at 25 K (freezing temperature) [8], indicating the presence of short-range magnetic correlations and spin-glass-like behavior below 25 K. On the basis of these observations Gönen *et al.* [8] proposed that each [Fe$_2$S$_3$]$^{2-}$ chain possess strong intrachain antiferromagnetic coupling of Fe ions that is mediated through the sulfide ions. The combination of antiferromagnetic coupling, additional crystal field splitting due to neighboring Fe atoms, and direct Fe-Fe interactions presumably give rise to $S = 0$ ground states in this compound [8].

BaFe$_2$Se$_3$ is an insulator down to the lowest measured temperature with a long-range antiferromagnetic (AFM) order with T_N around 255 K and short-range AFM order at higher temperatures [9–12]. It was shown that a dominant order involves 2×2 blocks of ferromagnetically aligned four iron spins, whereas these blocks order antiferromagnetically in the same manner as the block AFM $\sqrt{5} \times \sqrt{5}$ state of the iron vacancy ordered A$_2$Fe$_4$Se$_5$ [13–15].

To the best of our knowledge there are no data about the phonon properties of these compounds. In this paper we have measured polarized Raman scattering spectra of BaFe$_2$X$_3$(X = S, Se) in the temperature range between 20 and 400 K. We have observed the Raman active optical phonons, which are assigned using polarized measurements and the lattice dynamical calculations. At temperatures below

---

*Present address: Department of Physics, Renmin University of China, 59 Zhongguancun Street, Haidian District, Beijing 100872, China.
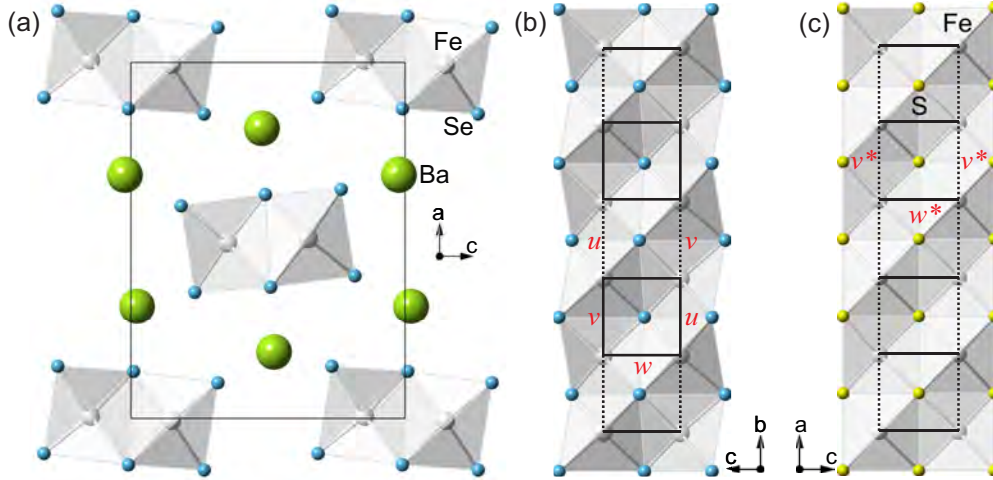
FIG. 1. (Color online) Schematic representation of the BaFe$_2$X$_3$(X = S, Se) crystal structure. (a) Projection of the BaFe$_2$Se$_3$ crystal structure in the (ac) plane. (b) The double chain of Fe-Se tetrahedra connected via common edges along the *b* axis. (c) The Fe-S double chain in the (010) projection. *w*, *u*, *v* represents Fe-Fe distances of ladder rungs (*w* = 0.2697 nm; *w*∗ = 0.2698 nm) and legs (*u* = 0.2688 nm, *v* = 0.2720 nm; *v*∗ = 0.2643 nm). Note that in the case of BaFe$_2$S$_3$ the Fe atoms form an "ideal" ladder (all Fe-Fe distances along the ladder legs are equivalent, which is not the case in BaFe$_2$Se$_3$).

$T_N = 255$ K in BaFe$_2$Se$_3$ the Raman modes shows an abrupt change of energy and linewidth due to the antiferromagnetic spin ordering.

II. EXPERIMENT AND NUMERICAL METHOD

Single crystals of BaFe$_2$X$_3$(X = S, Se) were grown using self-flux method with nominal composition Ba:Fe:X = 1:2:3. Details were described in Ref. [16]. Raman scattering measurements were performed on (110)(sulfide) [(100) (selenide)]-oriented samples in the backscattering micro-Raman configuration. Low-temperature measurements were performed using KONTI CryoVac continuous flow cryostat coupled with JY T64000 and TriVista 557 Raman systems. The 514.5-nm line of an Ar$^+$/Kr$^+$ mixed gas laser was used as excitation source. The Raman scattering measurements at higher temperatures were done using a LINKAM THMS600 heating stage.

We calculated phonon energies of the nonmagnetic BaFe$_2$S(Se)$_3$ single crystals at the center of the Brillouin zone. Calculations were performed within the theory of linear response using the density functional perturbation theory (DFPT) [17] as implemented in the QUANTUM ESPRESSO package [18]. In the first step, we obtained the electronic structure by applying the pseudopotentials based on the projected augmented waves method with the Perdew-Burke-Ernzerhof exchange-correlation functional and nonlinear core correction. Used energy cutoffs for the wave functions and electron densities were 80 (64) Ry and 960 (782) Ry for BaFe$_2$S(Se)$_3$, respectively. We have carried out the calculation with experimental values of the BaFe$_2$S(Se)$_3$ unit cell parameters $a = 0.87835$ nm, $b = 1.1219$ nm, $c = 0.5286$ nm [7] ($a = 1.18834$ nm, $b = 0.54141$ nm, $c = 0.91409$ nm [11]), and the relaxed fractional coordinates; see Table I. Relaxation was applied to place atoms in their equilibrium positions in respect to used pseudopotentials (all forces acting on every atom were smaller than 10^{-4} Ry/a.u.). The difference between experimental and relaxed coordinates is less than 3% for almost

all atom coordinates, except for the *x* direction of the Ba atoms in BaFe$_2$Se$_3$, which is 6%. Reduction of the *x* coordinate of Ba atoms by relaxation leads to an increase of the distance between the Ba layers. The Brillouin zone was sampled with $8 \times 8 \times 8$ Monkhorst-Pack **k**-space mesh. Calculated Γ point phonon energies of the BaFe$_2$S$_3$ and BaFe$_2$Se$_3$ are listed in Tables II and Table IV, respectively.

The DFPT calculation of the phonon-mode energies is performed assuming the paramagnetic solution and the comparison of energies is performed with the experimental results at room temperature. The paramagnetic density functional theory (DFT) solution is metallic, whereas BaFe$_2$Se$_3$ is AFM insulator at low temperatures. Therefore, we have performed also the spin-polarized DFT calculations, assuming AFM ordering of 2×2 ferromagnetic iron blocks [10–12]. We find the AFM solution and opening of the gap at the Fermi level in agreement with earlier DFT calculations by Saparov *et al.* [10]. Accordingly, we attempted to calculate the phonon

TABLE I. Experimental and relaxed (in square brackets) fractional coordinates of BaFe$_2$S$_3$ (Ref. [7]) and BaFe$_2$Se$_3$ (Ref. [11]) crystal structures.

Atom	Site	x	y	z
BaFe$_2$S$_3$				
Ba	(4c)	0.50 [0.50]	0.1859 [0.1817]	0.25 [0.25]
Fe	(8e)	0.3464 [0.3553]	0.50 [0.50]	0.00 [0.00]
S1	(4c)	0.50 [0.50]	0.6147 [0.6051]	0.25 [0.25]
S2	(8g)	0.2074 [0.2108]	0.3768 [0.3945]	0.25 [0.25]
BaFe$_2$Se$_3$				
Ba	(4c)	0.186 [0.175]	0.25 [0.25]	0.518 [0.513]
Fe	(8d)	0.493 [0.490]	0.002 [−0.001]	0.353 [0.358]
Se1	(4c)	0.355 [0.366]	0.25 [0.25]	0.233 [0.230]
Se2	(4c)	0.630 [0.613]	0.25 [0.25]	0.491 [0.485]
Se3	(4c)	0.402 [0.415]	0.25 [0.25]	0.818 [0.809]

TABLE II. Calculated and experimentally observed values of Raman active phonon mode energies (in cm^{-1}) of BaFe$_2$S$_3$ single crystal.

Symmetry	Calculation relax. (unrelax.)	Experiment 300 K	Experiment 100 K	Activity	Symmetry	Calculation relax. (unrelax.)	Experiment 300 K	Experiment 100 K	Activity
A_g^1	42.3 (51.2)		39	(xx,yy,zz)	B_{1g}^1	16.7 (63)			(xy)
A_g^2	154.2 (156)		157	(xx,yy,zz)	B_{1g}^2	55.1 (81.8)	44	48	(xy)
A_g^3	201.9 (167.4)	152	165	(xx,yy,zz)	B_{1g}^3	138.8 (153.1)	127	133	(xy)
A_g^4	366.9 (294.8)	295	301	(xx,yy,zz)	B_{1g}^4	243.5 (221.9)	203	214	(xy)
A_g^5	385.8 (307.1)	365	372	(xx,yy,zz)	B_{1g}^5	337.8 (241.6)		332(?)	(xy)
					B_{1g}^6	400.2 (330)	374	381	(xy)
B_{2g}^1	107.8 (113.7)	107	109	(xz)	B_{3g}^1	55.1 (66.8)			(yz)
B_{2g}^2	224.1 (180.8)	181	193	(xz)	B_{3g}^2	201.1 (171.1)	181	193	(yz)
B_{2g}^3	347.8 (283.6)			(xz)	B_{3g}^3	311.2 (308.7)	297	307	(yz)
					B_{3g}^4	369.3 (351.7)			(yz)

energies in the spin-polarized case. However, having now 48 atoms in the unit cell, this calculation turned out to be computationally too demanding. Furthermore, we do not believe that such a calculations would gives us in this case important new insights since the number of phonon modes becomes $2 \times 72 - 1 = 143$ (one mode is degenerate), and it is not likely that small splitting of the modes could be compared with the experiments. Also, the phonon frequencies are not particularly sensitive on the precise form of the density of states near the Fermi level (or gap opening) if the overall spectral function remains similar. Therefore, we believe that the usage of the nonmagnetic DFT is a reasonable method for identification of vibrational modes and comparison with the experimental data.

III. RESULTS AND DISCUSSION

A. BaFe$_2$S$_3$

The BaFe$_2$S$_3$ crystal symmetry is orthorhombic, space group $Cmcm$ and $Z = 4$ [7]. The site symmetries of atoms in $Cmcm$ space group are C_{2v}^y (Ba, S1), C_2^x(Fe), and C_s^{xy} (S2). Factor group analysis yields

$$\left(C_{2v}^y\right): \Gamma = A_g + B_{1g} + B_{3g} + B_{1u} + B_{2u} + B_{3u},$$

$$\left(C_2^x\right): \Gamma = A_g + 2B_{1g} + 2B_{2g} + B_{3g}$$
$$+ A_u + 2B_{1u} + 2B_{2u} + B_{3u}.$$

$$\left(C_s^{xy}\right): \Gamma = 2A_g + 2B_{1g} + B_{2g} + B_{3g} + A_u$$
$$+ B_{1u} + 2B_{2u} + 2B_{3u}.$$

Summarizing these representations and subtracting the acoustic ($B_{1u} + B_{2u} + B_{3u}$) and silent ($2A_u$) modes, we obtained the following irreducible representations of BaFe$_2$S$_3$ vibrational modes:

$$\Gamma_{\text{BaFe}_2\text{S}_3}^{\text{optical}} = 5A_g(xx,yy,zz) + 6B_{1g}(xy) + 3B_{2g}(xz)$$
$$+ 4B_{3g}(yz) + 4B_{1u}(E \parallel z) + 5B_{2u}(E \parallel y)$$
$$+ 4B_{3u}(E \parallel x).$$

Thus 18 Raman and 13 infrared active modes are expected to be observed in the BaFe$_2$S$_3$ infrared and Raman spectra. Because

our BaFe$_2$S$_3$ single-crystal samples have (110) orientation, we were able to observe all symmetry modes in the Raman scattering experiment.

The polarized Raman spectra of BaFe$_2$S$_3$, measured from the (110) plane at 100 K, are given in Fig. 2. Five A_g symmetry modes at about 39, 157, 165, 301, and 373 cm^{-1} (100 K) are clearly observed for the $x'(zz)x'$ polarization configuration ($x' = [110]$, $y' = [1\bar{1}0]$, $z = [001]$). For parallel polarization along the y' axis, the A_g and B_{1g} symmetry modes may be observed. By comparison ($y'y'$) with (zz) polarized spectrum we assigned the modes at 48, 133, 214, 332, and 381 cm^{-1} as the B_{1g} ones. The intensity of the 332 cm^{-1} mode is at a level of noise. Because of that, assignment of this mode as B_{1g}^5 should be taken as tentative.

For the $x'(y'z)x'$ polarization configuration both the B_{2g} and the B_{3g} symmetry modes can be observed. Because we cannot distinguish the B_{2g} and B_{3g} by selection rules from the (110) plane, the assignment of these modes was done with help of the lattice dynamics calculation; see Table II. Features between 40 and 100 cm^{-1} come after subtracting of nitrogen
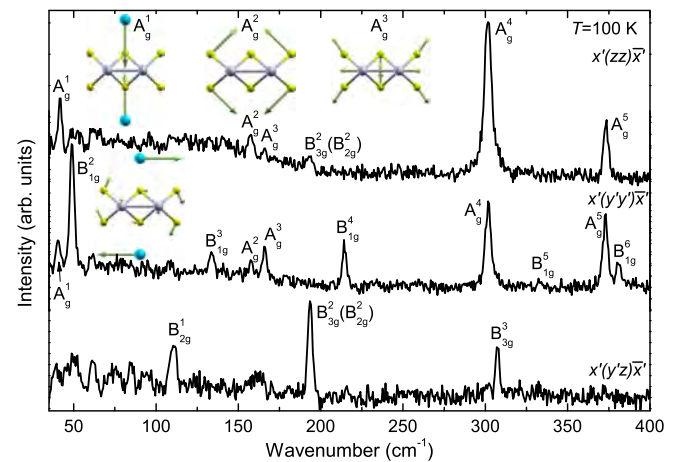

FIG. 2. (Color online) The polarized Raman scattering spectra of BaFe$_2$S$_3$ single crystal measured at 100 K. Insets are the normal modes of the A_g^1, A_g^2, A_g^3, and B_{1g}^2 vibrations. $x' = [110]$, $y' = [1\bar{1}0]$, and $z = [001]$.
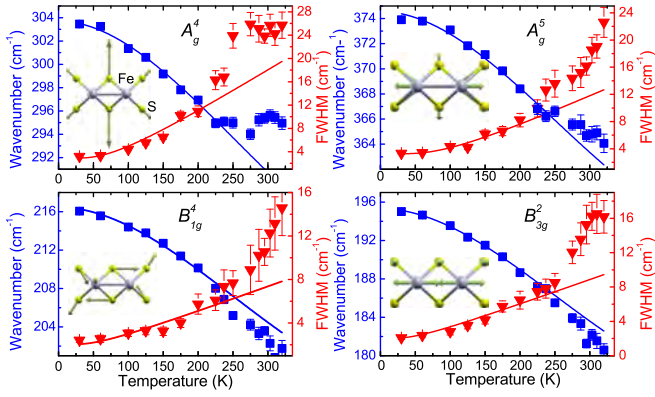
FIG. 3. (Color online) Experimental values (symbols) and calculated temperature dependence (solid lines) of the $BaFe_2S_3$ Raman mode energies and broadenings. Insets represent the normal modes of the A_g^4, A_g^5, B_{1g}^4, and B_{3g}^2 vibrations.

vibration modes. Bump at about 160 cm^{-1} is a leakage of A_g^2 and A_g^3 modes from parallel polarization.

The normal modes of some of A_g, B_{1g}, and B_{3g} vibrations, obtained by the lattice dynamics calculations, are given as insets in Figs. 2 and 3. According to these representations the lowest energy A_g^1 mode (39 cm^{-1}) originates from the Ba atom vibrations along the y axis, and the A_g^2 mode (157 cm^{-1}) represents dominantly S atom vibrations, which tend to elongate $[Fe_2S_3]^{2-}$ chains along the y axis. The A_g^3 mode originates from both the sulfur and the iron atom vibrations, which tend to stretch ladders along the x axis. The A_g^4 mode (Fig. 3) is sulfur atoms breathing vibrations, and the A_g^5 symmetry mode represents the S and Fe atom vibrations with the opposite tendency. The Fe atoms vibrate in opposite directions along the x axis, elongating the ladder, together with S atom vibrations, which tend to compress ladder structure.

Temperature dependence of the A_g^4, A_g^5, B_{1g}^4, and B_{3g}^2 mode energy and linewidth are given in Fig. 3.

In general, temperature dependance of Raman mode energy can be described with [19]

$$\omega(T) = \omega_0 + \Delta(T), \qquad (1)$$

where ω_0 is temperature-independent contribution to the energy of the phonon mode, whereas $\Delta(T)$ can be decomposed in

$$\Delta(T) = \Delta^V + \Delta^A. \qquad (2)$$

The first term in Eq. (2) represents change of phonon energy due to the thermal expansion of the crystal lattice, and is given by [20]

$$\Delta^V = -\omega_0 \gamma \frac{\Delta V(T)}{V_0}, \qquad (3)$$

where γ is the Grüneisen parameter of a given mode.

The second term in Eq. (2) is a contribution to the Raman mode energy from phonon-phonon scattering. By taking into account only three-phonon processes,

$$\Delta^A = -C\left(1 + \frac{4\lambda_{\text{ph-ph}}}{e^{\hbar\omega_0/2k_BT} - 1}\right). \qquad (4)$$

TABLE III. The best fit parameters of $BaFe_2S_3$ and $BaFe_2Se_3$.

Mode symmetry	ω_0(cm^{-1})	γ	Γ_0(cm^{-1})	λ
$BaFe_2S_3$				
A_g^4	303.7(2)	3.7(2)	2.9(2)	2.8(5)
A_g^5	374.6(2)	2.6(2)	3.3(2)	1.9(3)
B_{1g}^4	216.5(2)	4.8(2)	2.0(3)	0.9(3)
B_{3g}^2	195.3(1)	5.2(2)	2.0(3)	1.0(1)
$BaFe_2Se_3$				
A_g^8	200.0(1)	1.6(2)	2.3(1)	0.4(1)
A_g^9	272.6(2)	1.4(1)	2.3(1)	0.6(1)
A_g^{10}	288.1(3)	1.8(2)	5.2(1)	0.3(1)
A_g^{11}	297.1(4)	1.4(2)	5.6(2)	0.4(1)

C and $\lambda_{\text{ph-ph}}$ are the anharmonic constant and phonon-phonon interaction constant, respectively.

Temperature dependence of Raman mode linewidth is caused only by phonon anharmonicity:

$$\Gamma(T) = \Gamma_0\left(1 + \frac{2\lambda_{\text{ph-ph}}}{e^{\hbar\omega_0/2k_BT} - 1}\right), \qquad (5)$$

where Γ_0 is the anharmonic constant.

Parameter C is connected with ω_0 and Γ_0 via relation [19]

$$C = \frac{\Gamma_0^2}{2\omega_0}. \qquad (6)$$

ω_0 and Γ_0 can be determined by extrapolation of the corresponding experimental data to 0 K. With these parameters known, we can fit the phonon mode linewidth, using Eq. (5), to obtain $\lambda_{\text{ph-ph}}$. Then, by determining parameter C via Eq. (6), Raman mode energy can be properly fitted, with γ as the only unknown parameter. Using data from Ref. [12] for the temperature change of the lattice constants of $BaFe_2Se_3$ one can perform the corresponding analysis of the Raman mode energies' temperature dependance.

The best-fit parameters are collected in Table III. Because the Γ_0 is very small in comparison to ω_0, for all modes of both compounds (Table III), according to Eq. (6) the C anharmonic parameter becomes very small. Thus, contribution to the Raman mode energy from the phonon-phonon interaction can be neglected. In fact, a change of Raman mode energy with temperature is properly described only with the thermal expansion term Δ^V, Eq. (3).

The most intriguing finding in Fig. 3 is a dramatic change of slope of the A_g^4 mode linewidth (energy) temperature dependence at about 275 K. Because a hump in the inverse molar magnetic susceptibility [8] and a change of slope of the electrical resistivity [21] temperature dependence are observed in $BaFe_2S_3$ at about the same temperature we concluded that the deviation from anharmonic behavior for A_g^4 mode could be related to spin and charge. In fact, many of iron-based spin-ladder materials have the 3D-antiferromagnetic phase transition at about 260 K. We believe that in the case of $BaFe_2S_3$ the antiferromagnetic ordering of spins within the ladder legs changes from short-range to the long-range state, without 3D antiferromagnetic spin ordering (the Néel state) of the whole crystal. This transition is followed with change
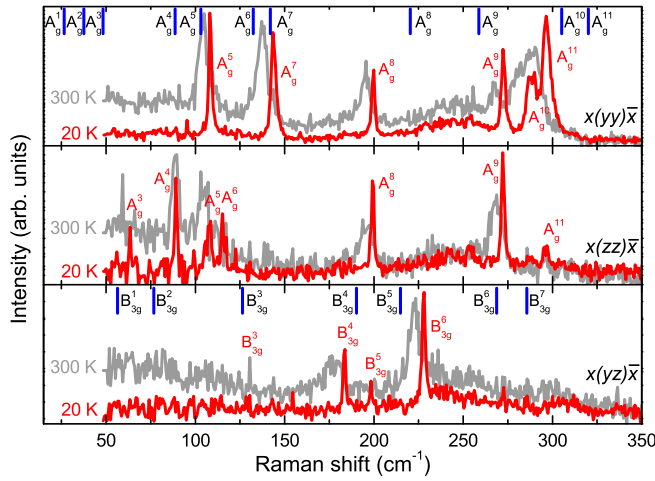
FIG. 4. (Color online) The $x(yy)\overline{x}$, $x(zz)\overline{x}$, and $x(yz)\overline{x}$ polarized Raman scattering spectra of BaFe$_2$Se$_3$ single crystals measured at room temperature and at 20 K. Vertical bars are calculated values of the A_g and the B_{3g} symmetry Raman active vibrations.

of the electronic structure, which could explain the abrupt increase of the resistivity at this temperature [21]. A lack of the BaFe$_2$S$_3$ low-temperature crystallographic and transport properties measurements did not allow a more detailed study of a possible origin of the phonon energy and linewidth deviation from the anharmonic picture at about 275 K.

B. BaFe$_2$Se$_3$

The BaFe$_2$Se$_3$ unit cell consists of four formula units comprising of 24 atoms. The site symmetries of atoms in

Pnma space group are C_s^{xz} (Ba, Se1, Se2, Se3) and C_1 (Fe). Factor group analysis yields

$$\left(C_s^{xz}\right): \Gamma = 2A_g + 1B_{1g} + 2B_{2g} + 1B_{3g}$$
$$+ A_u + 2B_{1u} + 1B_{2u} + 2B_{3u},$$
$$\left(C_1\right): \Gamma = 3A_g + 3B_{1g} + 3B_{2g} + 3B_{3g}$$
$$+ 3B_{1u} + 3B_{2u} + 3B_{3u}.$$

Summarizing these representations and subtracting the acoustic ($B_{1u} + B_{2u} + B_{3u}$) and silent ($4A_u$) modes, we obtained the following irreducible representations of BaFe$_2$Se$_3$ vibrational modes:

$$\Gamma_{\text{BaFe}_2\text{Se}_3}^{\text{optical}} = 11A_g + 7B_{1g} + 11B_{2g} + 7B_{3g}$$
$$+ 11B_{1u} + 7B_{2u} + 11B_{3u}$$

Thus 36 Raman and 29 infrared active modes are expected to be observed in the BaFe$_2$Se$_3$ vibrational spectra. Because the BaFe$_2$Se$_3$ single crystals have the (100) orientation (the crystallographic a axis is perpendicular to the plane of the single crystal), we were able to access only the A_g and the B_{3g} symmetry modes in the Raman scattering experiment.

The polarized Raman spectra of BaFe$_2$Se$_3$, measured from (100) plane at room temperature and 20 K, for the parallel and crossed polarization configurations, are given in Fig. 4. The spectra measured for parallel polarization configurations consist of the A_g symmetry modes. Six modes at about 108, 143.5, 200, 272, 288.7, and 296.5 cm^{-1} (20 K) are clearly observed for the $x(yy)\overline{x}$ polarization configuration and three additional modes are observed at about 63.4, 89, and 115 cm^{-1} for the $x(zz)\overline{x}$ polarization configuration. For the $x(yz)\overline{x}$ polarization configuration, three Raman active B_{3g} symmetry

TABLE IV. Calculated and experimentally observed values of Raman active phonon mode energies (in cm^{-1}) of BaFe$_2$Se$_3$ single crystal.

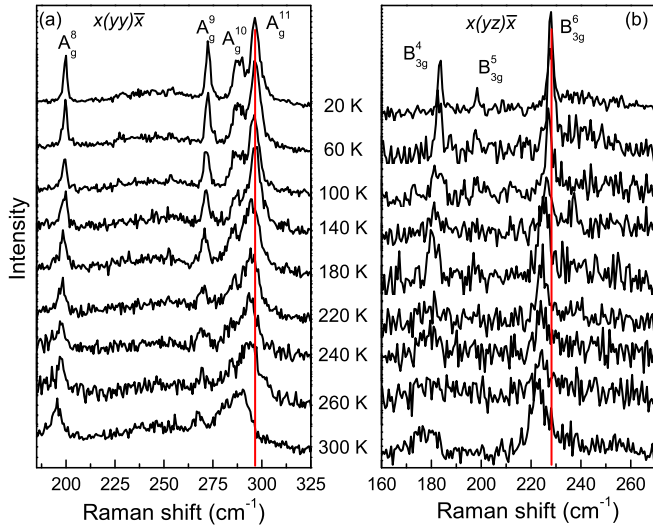| Symmetry	Calc.	Experiment 300 K	Experiment 20 K	Activity	Symmetry	Calc.	Experiment 300 K	Experiment 20 K	Activity
A_g^1	26.5			(xx,yy,zz)	B_{2g}^1	25.8			(xz)
A_g^2	37.5			(xx,yy,zz)	B_{2g}^2	48.0			(xz)
A_g^3	48.3	59	63.4	(xx,yy,zz)	B_{2g}^3	68.7			(xz)
A_g^4	88.6	88	89	(xx,yy,zz)	B_{2g}^4	88.8			(xz)
A_g^5	103.0	104.3	108	(xx,yy,zz)	B_{2g}^5	100.4			(xz)
A_g^6	132.4	111	115	(xx,yy,zz)	B_{2g}^6	138.2			(xz)
A_g^7	142.0	137	143	(xx,yy,zz)	B_{2g}^7	144.5			(xz)
A_g^8	220.4	195.6	200	(xx,yy,zz)	B_{2g}^8	212.9			(xz)
A_g^9	258.8	267	272	(xx,yy,zz)	B_{2g}^9	261.7			(xz)
A_g^{10}	305.2	280	288.7	(xx,yy,zz)	B_{2g}^{10}	303.9			(xz)
A_g^{11}	320.2	290	296.5	(xx,yy,zz)	B_{2g}^{11}	321.5			(xz)
B_{1g}^1	56.4			(xy)	B_{3g}^1	56.4			(yz)
B_{1g}^2	72.8			(xy)	B_{3g}^2	76.7			(yz)
B_{1g}^3	126.2			(xy)	B_{3g}^3	126.4			(yz)
B_{1g}^4	191.4			(xy)	B_{3g}^4	190.2	177	183.8	(yz)
B_{1g}^5	210.5			(xy)	B_{3g}^5	214.9		198	(yz)
B_{1g}^6	267.1			(xy)	B_{3g}^6	268.8	222.8	228	(yz)
B_{1g}^7	285.2			(xy)	B_{3g}^7	285.7			(yz)

FIG. 5. (Color online) The polarized Raman spectra of $BaFe_2Se_3$ single crystals measured at various temperatures. (a) $x(yy)\bar{x}$ polarization configuration; (b) $x(yz)\bar{x}$ polarization configuration.

FIG. 6. (Color online) Experimental values (symbols) and calculated temperature dependence (solid lines) of $BaFe_2Se_3$ Raman mode energies. The best-fit parameters, for the temperature range below T_N, are given in Table III. Insets represent normal modes of the A_g^8, A_g^9, A_g^{10}, and A_g^{11} vibrations.

modes at 183.8, 198, and 228 cm^{-1} (20 K) are observed. Vertical bars in Fig. 4 denote the calculated energies of the A_g and B_{3g} symmetry modes, which are in rather good agreement with experimentally observed ones. The results of the lattice dynamics calculations, together with the experimental data, are summarized in Table IV.

According to the lattice dynamics calculations the lowest energy A_g^1 mode is dominated by Ba atom vibrations along the $\langle 101 \rangle$ directions and the A_g^2 mode represents vibrations of Fe and Se atoms which tend to rotate $[Fe_2Se_3]^{2-}$ chains around of the b axis. The A_g^3 mode involves all atom vibrations, which tend to stretch crystal structure along the $\langle 101 \rangle$ directions, whereas the A_g^4 mode originates from Se atom vibrations along the c axis and the Fe atom vibrations along the $\langle 101 \rangle$ directions. The A_g^5 mode represents vibration of Fe and Se atoms, which leads to $[Fe_2Se_3]^{2-}$-chain compression along the c axis. The A_g^6 mode originates from Se and Fe atom vibrations which stretch $[Fe_2Se_3]^{2-}$ chains along the c axis. Finally, the A_g^7 mode originates from Fe atom vibrations toward each other along the chain direction together with vibrations of the Se atoms along the c axis. The normal coordinates of the A_g^8, A_g^9, A_g^{10}, and A_g^{11} modes are given as insets in Fig. 6. As can be seen from Fig. 6 the A_g^8 mode originates dominantly from Se atom stretching vibrations, whereas the A_g^9, A_g^{10}, and A_g^{11} modes represent vibrations of both the Se and Fe atoms. In fact, the A_g^9 mode represents mostly Se atom vibrations along the c axis, and the A_g^{10} mode consists of Fe and Se vibrations along the c axis, which tend to elongate ladder structure along the b axis. Finally, the A_g^{11} mode represents the Fe atom vibrations toward each other along the chain axis, together with Se atom vibrations perpendicular to the chain direction.

By lowering the temperature, the lattice parameters of $BaFe_2Se_3$ decrease continuously without the crystal symmetry change around the magnetic ordering temperature [11,12] $T_N = 255$ K. Consequently we should expect the Raman mode hardening, without any abrupt change. Contrary to
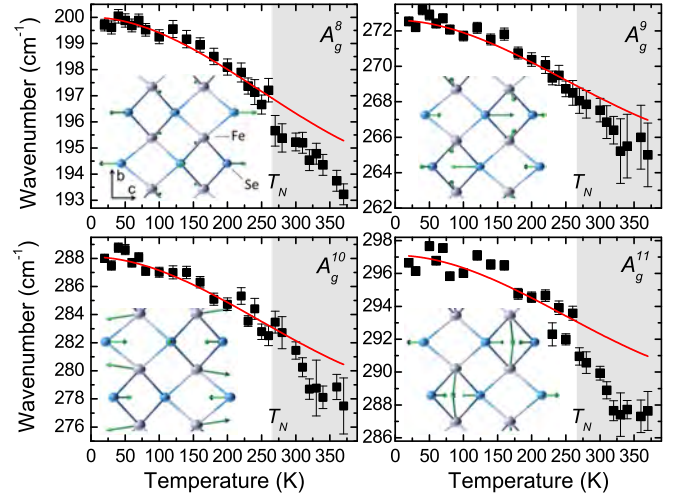
expectations, the A_g and B_{3g} modes (see Figs. 5, 6, and 7) sharply increase their energies below the phase transition temperature T_N, as shown in details in Fig. 6. Because a significant local lattice distortion (Fe atom displacement along
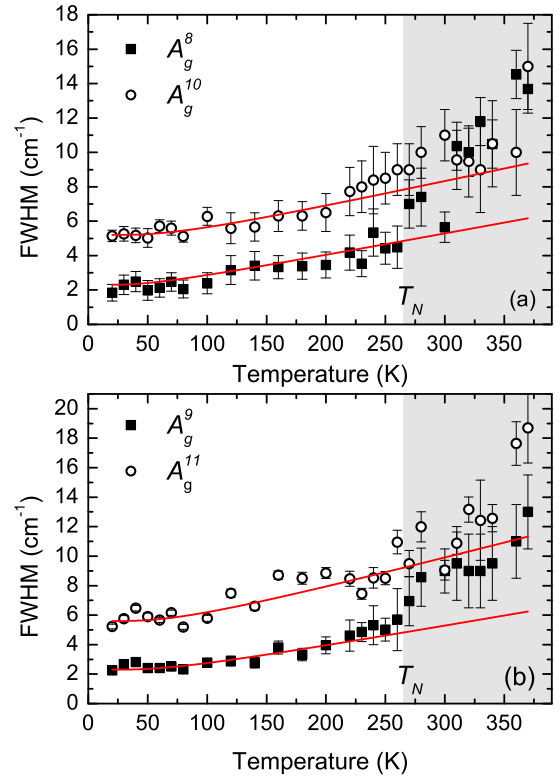

FIG. 7. (Color online) Linewidth vs temperature dependence of (a) A_g^8 and A_g^{10} modes and (b) A_g^9 and A_g^{11} modes of $BaFe_2Se_3$. Solid lines are calculated using Eq. (5). The best-fit parameters for a temperature range below T_N are given in Table III.

the b axis is as large as approximately 0.001 nm) [11,12] exists, driven by the magnetic order, we concluded that spin-phonon (magnetoelastic) coupling is responsible for Raman mode energy and linewith change in the antiferromagnetic phase. In fact, the existence of local displacements in the Fe atoms at T_N have a significant impact on the electronic structure due to rearrangement of electrons near the Fermi level [11] and consequently the change in the phonon energy and broadening. Raman mode linewidth change at about T_N is clearly observed as deviation from the usual anharmonicity temperature dependence (solid lines in Fig. 7) for all modes presented in Fig. 6.

IV. CONCLUSION

We have measured the polarized Raman scattering spectra of the BaFe$_2$S$_3$ and BaFe$_2$Se$_3$ single crystals in a temperature range between 20 and 400 K. Almost all Raman-active modes predicted by factor-group analysis to be observed from the cleavage planes of BaFe$_2$S$_3$ (110) and BaFe$_2$Se$_3$ (100) single crystals are experimentally detected and assigned.

Energies of these modes are in rather good agreement with the lattice dynamics calculations. The BaFe$_2$Se$_3$ Raman modes linewidth and energy change substantially at temperatures below $T_N = 255$ K, where this compound becomes antiferromagneticaly long-range ordered.

[1] C. King and D. A. Pendlebury, Web of knowledge research fronts 2013: 100 top-ranked specialties in the sciences and social sciences, http://sciencewatch.com/sites/sw/files/sw-article/media/research-fronts-2013.pdf

[2] Y. Kamihara, T. Watanabe, M. Hirano, and H. Hosono, J. Am. Chem. Soc. **130**, 3296 (2008).

[3] Z. V. Popović, M. Šćepanović, N. Lazarević, M. M. Radonjić, D. Tanasković, H. Lei, and C. Petrovic, Phys. Rev. B **89**, 014301 (2014).

[4] Z. V. Popović, M. J. Konstantinović, V. A. Ivanov, O. P. Khuong, R. Gajić, A. Vietkin, and V. V. Moshchalkov, Phys. Rev. B **62**, 4963 (2000).

[5] M. J. Konstantinović, Z. V. Popović, M. Isobe, and Y. Ueda, Phys. Rev. B **61**, 15185 (2000).

[6] E. Dagotto, Rev. Mod. Phys. **85**, 849 (2013).

[7] H. Hong and H. Steinfink, J. Solid State Chem. **5**, 93 (1972).

[8] Z. S. Gönen, P. Fournier, V. Smolyaninova, R. Greene, F. M. Araujo-Moreira, and B. Eichhorn, Chem. Mater. **12**, 3331 (2000).

[9] H. Lei, H. Ryu, A. I. Frenkel, and C. Petrovic, Phys. Rev. B **84**, 214511 (2011).

[10] B. Saparov, S. Calder, B. Sipos, H. Cao, S. Chi, D. J. Singh, A. D. Christianson, M. D. Lumsden, and A. S. Sefat, Phys. Rev. B **84**, 245132 (2011).

[11] J. M. Caron, J. R. Neilson, D. C. Miller, A. Llobet, and T. M. McQueen, Phys. Rev. B **84**, 180409 (2011).

[12] Y. Nambu, K. Ohgushi, S. Suzuki, F. Du, M. Avdeev, Y. Uwatoko, K. Munakata, H. Fukazawa, S. Chi, Y. Ueda, and T. J. Sato, Phys. Rev. B **85**, 064413 (2012).

[13] F. Ye, S. Chi, W. Bao, X. F. Wang, J. J. Ying, X. H. Chen, H. D. Wang, C. H. Dong, and M. Fang, Phys. Rev. Lett. **107**, 137003 (2011).

[14] N. Lazarević, M. Abeykoon, P. W. Stephens, H. Lei, E. S. Bozin, C. Petrovic, and Z. V. Popović, Phys. Rev. B **86**, 054503 (2012).

[15] N. Lazarević, H. Lei, C. Petrovic, and Z. V. Popović, Phys. Rev. B **84**, 214305 (2011).

[16] H. Lei, H. Ryu, V. Ivanovski, J. B. Warren, A. I. Frenkel, B. Cekic, W.-G. Yin, and C. Petrovic, Phys. Rev. B **86**, 195133 (2012).

[17] S. Baroni, S. de Gironcoli, A. Dal Corso, and P. Giannozzi, Rev. Mod. Phys. **73**, 515 (2001).

[18] P. Giannozzi, S. Baroni, N. Bonini, M. Calandra, R. Car, C. Cavazzoni, D. Ceresoli, G. L. Chiarotti, M. Cococcioni, I. Dabo, A. D. Corso, S. de Gironcoli, S. Fabris, G. Fratesi, R. Gebauer, U. Gerstmann, C. Gougoussis, A. Kokalj, M. Lazzeri, L. Martin-Samos, N. Marzari, F. Mauri, R. Mazzarello, S. Paolini, A. Pasquarello, L. Paulatto, C. Sbraccia, S. Scandolo, G. Sclauzero, A. P. Seitsonen, A. Smogunov, P. Umari, and R. M. Wentzcovitch, J. Phys.: Condens. Matter **21**, 395502 (2009).

[19] H.-M. Eiter, P. Jaschke, R. Hackl, A. Bauer, M. Gangl, and C. Pfleiderer, Phys. Rev. B **90**, 024411 (2014).

[20] V. Gnezdilov, Y. Pashkevich, P. Lemmens, A. Gusev, K. Lamonova, T. Shevtsova, I. Vitebskiy, O. Afanasiev, S. Gnatchenko, V. Tsurkan, J. Deisenhofer, and A. Loidl, Phys. Rev. B **83**, 245127 (2011).

[21] W. Reiff, I. Grey, A. Fan, Z. Eliezer, and H. Steinfink, J. Solid State Chem. **13**, 32 (1975).

Lattice dynamics of KNi$_2$Se$_2$

N. Lazarević,[1] M. Radonjić,[2] M. Šćepanović,[1] Hechang Lei (雷和畅),[3,*] D. Tanasković,[2] C. Petrovic,[3] and Z. V. Popović[1]

[1]*Center for Solid State Physics and New Materials, Institute of Physics Belgrade, University of Belgrade,*
Pregrevica 118, 11080 Belgrade, Serbia

[2]*Scientific Computing Laboratory, Institute of Physics Belgrade, University of Belgrade, Pregrevica 118, 11080 Belgrade, Serbia*

[3]*Condensed Matter Physics and Materials Science Department, Brookhaven National Laboratory, Upton, New York 11973-5000, USA*

We report first-principles calculations of the lattice dynamics of KNi$_2$Se$_2$ together with Raman scattering study. We have observed three out of four Raman-active modes predicted by factor group analysis. Calculated phonon frequencies are in good agreement with experimental findings. Contrary to its iron counterpart (K$_x$Fe$_{2-y}$Se$_2$), K$_{0.95}$Ni$_{1.86}$Se$_2$ does not show vacancy ordering.

I. INTRODUCTION

The discovery of superconductivity in the iron materials has aroused great interest among researches to study the physical properties of these materials which are dominated by the layers of Fe atoms surrounded by the elements of pnictogen (As, P) or the chalcogen group (Se, Te).[1–5] The recently discovered superconductivity in the alkali-doped iron selenide layered compounds with $T_c \sim 33$ K brings forth some unique characteristics that are absent in the other iron-based superconductors.[6] These include the presence of the iron vacancies and their ordering, the antiferromagnetically ordered insulating phases, and a very high Néel transition temperature.[7–11]

Nickel pnictides have recently attracted a lot of attention,[12] despite the low critical superconducting temperature, much lower than in iron-based pnictides. The cause of such significant distinction in T_c value is not clear. It could be the consequence of the different superconducting mechanisms, or different values of the material parameters responsible for superconductivity. Typically, these materials display a very rich phase diagram including phases with magnetic ordering, or heavy-fermion phase, which is typically accompanied by a superconducting phase at low temperatures. KNi$_2$Se$_2$ shows a putative local charge density wave (LCDW) state which persists up to 300 K, followed by the magnetic-field-independent heavy-fermion phase below 40 K and a superconducting phase below $T_c = 0.8$ K.[12] The superconducting phase is very sensitive to stoichiometry.[13] Even a small deficiency of K and Ni atoms leads to the absence of superconducting phase down to 0.3 K. Therefore, in order to understand the low-temperature transport and thermodynamic properties of this material, a full knowledge of the lattice dynamics is necessary. To the best of our knowledge phonon properties of this compound are unknown.

In this paper we address the lattice dynamics of KNi$_2$Se$_2$. The first-principles lattice dynamics calculations were performed within density functional perturbation theory[14] (DFPT) using the QUANTUM ESPRESSO[15] package. The polarized Raman scattering measurements were performed in a wide temperature range. Three out of four Raman-active modes predicted by the symmetry considerations are observed and assigned.

II. EXPERIMENT AND NUMERICAL CALCULATIONS

Single-crystal growth and characterization of the K$_{0.95}$Ni$_{1.86}$Se$_2$ samples were described in a previous report.[13] Raman scattering measurements were performed on freshly cleaved samples using JY T64000 and TriVista 557 Raman systems in backscattering micro-Raman configuration. The 514.5 nm line of a mixed Ar$^+$/Kr$^+$ gas laser was used as an excitation source. The corresponding excitation power density was less than 0.2 kW/cm^2. Low-temperature measurements were performed using the KONTI CryoVac continuous flow cryostat with 0.5 mm thick window. Measurements in the optical phonon region of K$_{0.95}$Ni$_{1.86}$Se$_2$ (30–350 cm^{-1}) were performed using the 1800/1800/1800 grooves/mm gratings configuration of the JY T64000 system and the 900/900/2400 grooves/mm gratings configuration of the TriVista 557 system.

We have performed calculations of the lattice dynamics of the KNi$_2$Se$_2$ within the DFPT[14] using the QUANTUM ESPRESSO[15] package. KNi$_2$Se$_2$ crystallizes in the tetragonal ThCr$_2$Si$_2$-type of crystal structure [$I4/mmm$ space group with the unit cell parameters $a = 3.9089(8)$ Å, $c = 13.4141(5)$ Å, $z = 0.35429(2)$].[12,13] Potassium atoms are at $2a : (0,0,0)$, Ni atoms at $4d : (0,\frac{1}{2},\frac{1}{4})$, and Se atoms at $4e : (0,0,z)$ Wyckoff positions. In our calculations we have used the ultrasoft projector augmented wave (PAW) pseudopotentials calculated with the Perdew-Burke-Ernzerhof (PBE) exchange-correlation functional and nonlinear core correction. We carried out the relaxation of the structural parameters until all forces acting on the individual atom in the unit cell became smaller than 5×10^{-6} Ry/a.u. and all the stresses to the unit cell were smaller than 0.01 kbar. The relaxed structural parameters are $a = 3.9490$ Å, $c = 13.0552$ Å, $z = 0.35250$, and they are in good agreement (within a few percent) with the experimentally measured values. The electronic calculations are performed on a $16 \times 16 \times 16$ Monkhorst-Pack **k**-space mesh, with a kinetic-energy cutoff of 41 Ry, a charge-density cutoff of 236 Ry, and a Gaussian smearing of 0.005. The obtained Γ-point phonon energies are listed in Table I. The normal modes of all four Raman-active phonons are shown in Fig. 1. As can be seen from Fig. 1 the A_{1g} (B_{1g}) mode represents the vibrations of the Se (Ni) ions along the c axis, whereas the E_g

TABLE I. Top panel gives the types of atoms together with their Wyckoff positions and each site's contribution to the Γ-point phonons, as well as Raman tensors, phonon activities, and selection rules for KNi_2Se_2 ($I4/mmm$ space group). Lower panel of the table lists experimental (at room temperature) and calculated phonon mode frequencies and their activity.

Atoms	Wyckoff position	Irreducible representations
K	2a	$A_{2u} + E_u$
Ni	4d	$A_{2u} + B_{1g} + E_g + E_u$
Se	4e	$A_{1g} + A_{2u} + E_g + E_u$

Raman tensors

$$\hat{R}_{A_{1g}} = \begin{pmatrix} a & 0 & 0 \\ 0 & a & 0 \\ 0 & 0 & b \end{pmatrix} \quad \hat{R}_{B_{1g}} = \begin{pmatrix} c & 0 & 0 \\ 0 & -c & 0 \\ 0 & 0 & 0 \end{pmatrix} \quad \hat{R}_{E_g} = \begin{pmatrix} 0 & 0 & e \\ 0 & 0 & 0 \\ e & 0 & 0 \end{pmatrix} \quad \hat{R}_{E_g} = \begin{pmatrix} 0 & 0 & 0 \\ 0 & 0 & f \\ 0 & f & 0 \end{pmatrix}$$

Activity and selection rules

$$\Gamma_{\text{Raman}} = A_{1g}(\alpha_{xx+yy}, \alpha_{zz}) + B_{1g}(\alpha_{xx-yy}) + 2E_g(\alpha_{xz}, \alpha_{yz})$$
$$\Gamma_{\text{infrared}} = 2A_{2u}(\mathbf{E} \parallel \mathbf{z}) + 2E_u(\mathbf{E} \parallel \mathbf{x}, \mathbf{E} \parallel \mathbf{y})$$
$$\Gamma_{\text{acoustic}} = A_u + E_u$$

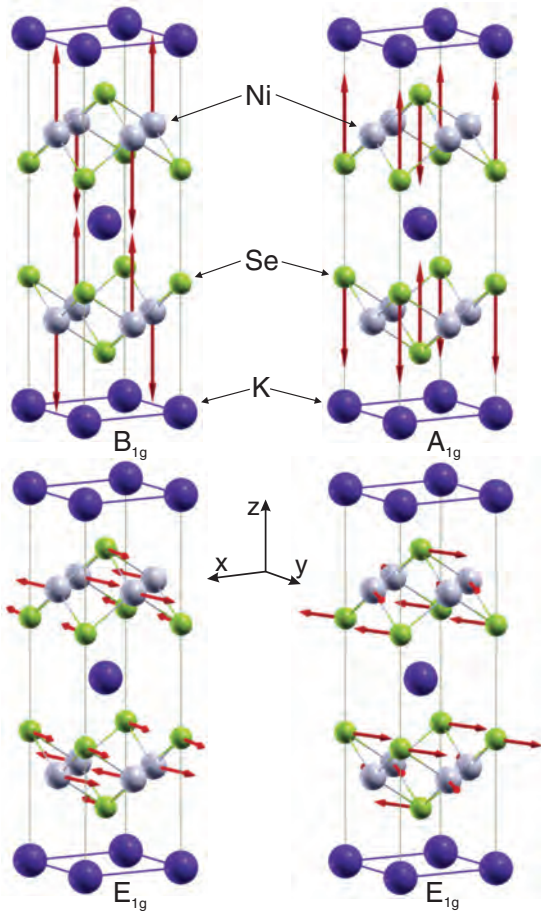| Symmetry	Activity	Experiment (cm^{-1})	Calculations (cm^{-1})	Main atomic displacements
A_{1g}	Raman	179	189.4	Se(z)
B_{1g}	Raman	134	133.8	Ni(z)
E_g^1	Raman	63	35.4	Ni(xy), Se(xy)
E_g^2	Raman	(201)	203.9	Ni(xy), Se(xy)
A_{2u}^1	IR		116.4	K(z), Se($-z$)
A_{2u}^2	IR		220.8	Ni(z), K($-z$)
E_u^1	IR		105.1	K(xy)
E_u^2	IR		208.3	Ni(xy), Se($-xy$)

FIG. 1. (Color online) Displacement patterns of the Raman-active vibrational modes of KNi_2Se_2.

modes involve the vibration of both Ni and Se ions within the *ab* plane.

III. RESULTS AND DISCUSSION

Symmetry considerations predict four Raman-active phonons: A_{1g}, B_{1g}, and $2E_g$ (Table I) for KNi_2Se_2. However, ordering of the vacancies may reduce the symmetry to $I4/m$. This results in an increase of the number of Raman-active modes as was shown for $K_xFe_{2-y}Se_2$[16] and $K_xFe_{2-y}S_2$.[17] Figure 2 shows room temperature polarized Raman scattering spectra of $K_{0.95}Ni_{1.86}Se_2$ single crystals. Only three Raman-active modes are observed in the Raman spectra for different sample orientations. This finding supports the high symmetry ($I4/mmm$ space group) of the $K_{0.95}Ni_{1.86}Se_2$ structure without the Ni vacancy ordering as opposed to the $K_xFe_{2-y}Se_2$ case.[16]

According to the selection rules, the Raman scattering spectra measured from the *ab* plane of the sample may contain only A_{1g} and B_{1g} modes. The A_{1g} mode can be observed for any orientation of the incident light polarization $\mathbf{e}_i$ provided that the scattered light polarization $\mathbf{e}_s$ is parallel to it ($\mathbf{e}_s \parallel \mathbf{e}_i$) and will vanish in any crossed polarization configuration ($\mathbf{e}_s \perp \mathbf{e}_i$). On the other hand, the intensity of the B_{1g} mode strongly depends on the sample orientation [$I_{B_{1g}}(\Theta) \sim |c|^2 \cos^2(\Theta + 2\beta)$ where $\Theta = \angle(\mathbf{e}_i, \mathbf{e}_s)$ and $\beta = \angle(\mathbf{e}_i, \mathbf{x})$].[16] When the sample is oriented so that $\mathbf{e}_i \parallel \mathbf{x}$ [see Fig. 2(a)], one can expect the appearance of both the A_{1g} and B_{1g} modes in the parallel and their absence for a cross polarization. In order to separate the A_{1g} from the B_{1g} symmetry mode, incident light polarization should be parallel to the $\mathbf{x}' = 1/\sqrt{2}[110]$ axis of the crystal [see Fig. 2(b)]. The Raman mode at about 179 cm^{-1} has been observed in the parallel, but not in the cross polarization configuration, and consequently it is
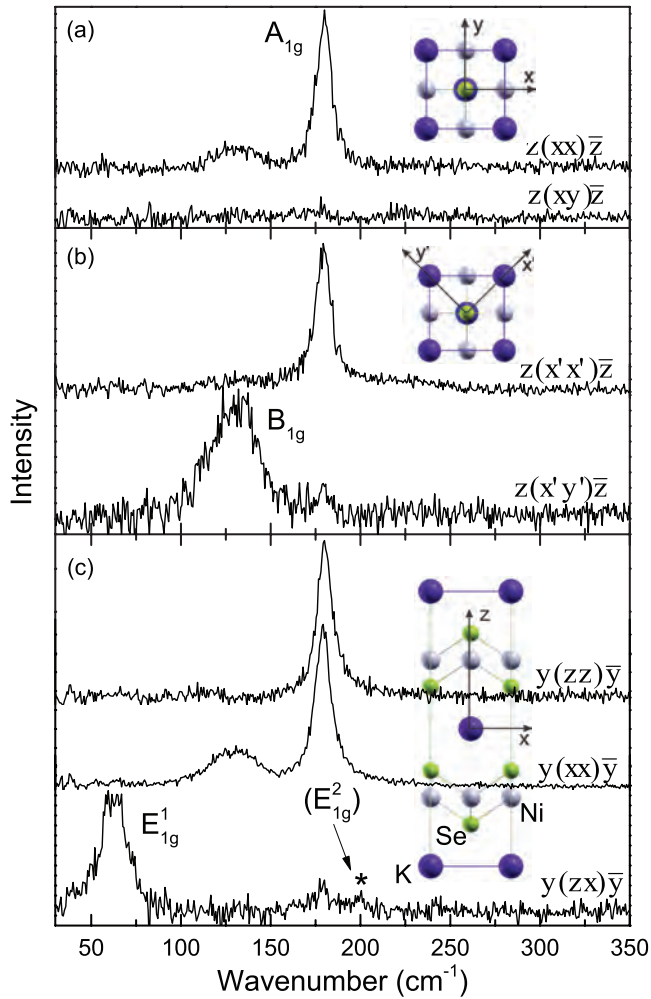
FIG. 2. (Color online) Raman scattering spectra of K$_{0.95}$Ni$_{1.86}$Se$_2$ single crystals measured at room temperature using the JY T64000 Raman system in various scattering configurations (**x** = [100], **y** = [010], **x**$'$ = $1/\sqrt{2}$[110], **y**$'$ = $1/\sqrt{2}$[1$\bar{1}$0], **z** = [001]).

FIG. 3. (Color online) (a) Temperature-dependent unpolarized Raman scattering spectra of the K$_{0.95}$Ni$_{1.86}$Se$_2$ single crystals measured from the *ab* plane of the sample using the TriVista 557 Raman system. (b) Energy and linewidth of A_{1g} and B_{1g} modes as a function of temperature. Solid lines show the expected behavior due to anharmonic phonon decay (see the text).

assigned as the A_{1g} mode. The mode at about 134 cm^{-1} has been observed in the cross but not in the parallel polarization configuration and consequently is assigned as the B_{1g} mode.

Observation of the E_g symmetry modes, in the case of the tetragonal crystal symmetry, requires performing measurements in the *ac* plane of the sample. According to the selection rules, for the parallel polarization configuration with $\mathbf{e}_i \parallel \mathbf{z}$ the A_{1g} mode appearance is the only one to be expected, whereas both the A_{1g} and B_{1g} modes are expected to be observable in the case of $\mathbf{e}_i \parallel \mathbf{x}$ [see Fig. 2(c)]. In the cross polarization configuration only the E_g modes can be observed. Consequently, the mode at around 63 cm^{-1} [see Fig. 2(c)] has been assigned as the E_g^1 symmetry one. In addition, a weak peak-like feature has been observed at around 201 cm^{-1} [denoted by the asterisk in Fig. 2(c)]. However, assignment of this feature cannot be unambiguously performed because of the extremely low intensity, although it falls in the region where the appearance of the E_g^2 mode is expected (see Table I). The frequencies of the observed modes are in good agreement with our calculations (see Table I).
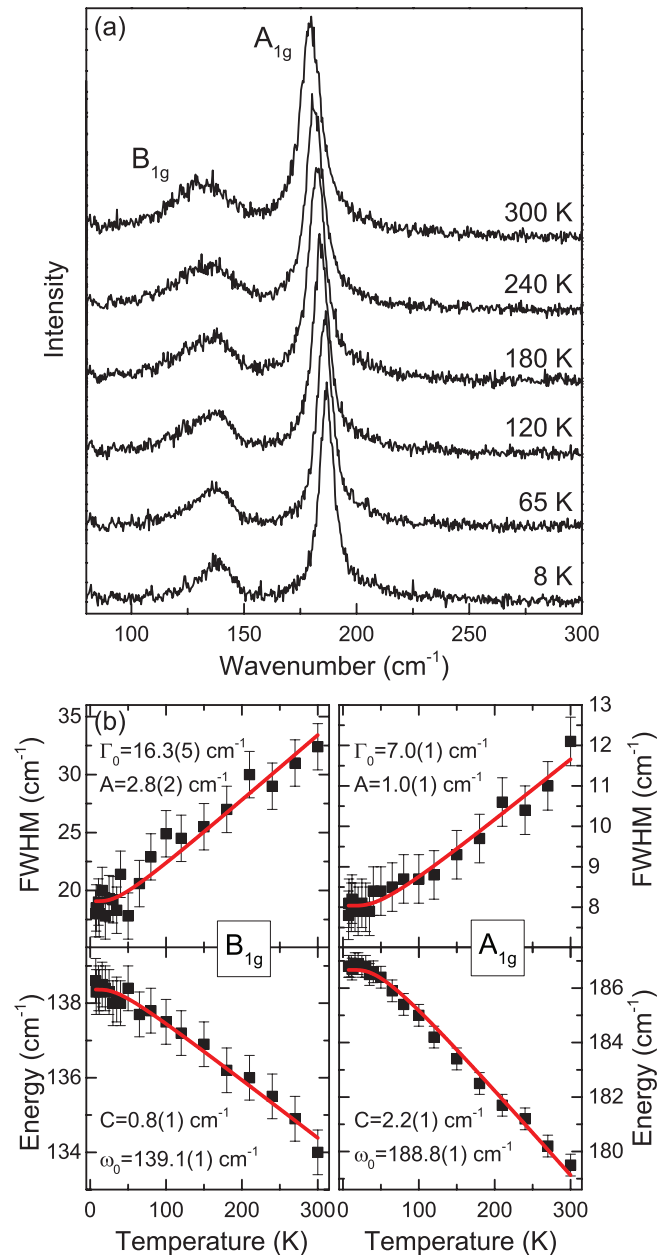
Figure 3(a) shows unpolarized Raman spectra of the K$_{0.95}$Ni$_{1.86}$Se$_2$ single crystal, measured from the *ab* plane of the sample at various temperatures. No observable change has been observed in the spectra near the local CDW to heavy-fermion transition temperature ($T \sim 40$ K). The A_{1g} and B_{1g} symmetry mode energies and full width at half maximum (FWHM) temperature dependance are presented in Fig. 3(b).

Temperature dependance of the phonon mode energy, $\Omega(T)$, and linewidth, $\Gamma(T)$, are usually governed by phonon-phonon interaction (anharmonic effects). For simplicity we assume a

symmetric decay of the low-lying optical phonon into two acoustic phonons:[18]

$$\Omega(T) = \Omega_0 - C\left(1 + \frac{2}{e^x - 1}\right), \tag{1}$$

$$\Gamma(T) = \Gamma_0 + A\left(1 + \frac{2}{e^x - 1}\right), \tag{2}$$

where Ω_0 is the Raman mode energy, A and C are the anharmonic constants, and $x = \overline{h}\Omega_0/2k_B T$. In the case of semiconducting and insulating materials, A is usually the only parameter needed for describing the temperature dependence of the linewidth. Phonons may also couple with other elementary excitations i.e., electrons, in which case an additional term Γ_0 must be included. The Γ_0 term also includes the contributions from scattering on defects.

Red lines in Fig. 3(b) represent calculated spectra by using Eqs. (1) and (2). Although there is a good agreement with the experimental data, the large value of the Γ_0 parameter, especially for the B_{1g} phonon, together with the clear asymmetry of this mode, points out the possible contribution from the interaction of the phonons with some other excitations (i.e., electrons).[19] However, a clear nonstoichiometry of the studied single crystals indicates that the origin of the increased width and asymmetry of the B_{1g} mode is more likely due to disorder that breaks the conservation of the momentum during the Raman scattering process enabling contributions of finite wave vector phonons to the Raman spectra.

IV. CONCLUSION

We have performed the Raman scattering study and the lattice dynamics calculations of KNi_2Se_2. By analyzing polarized Raman scattering spectra of $K_{0.95}Ni_{1.86}Se_2$ single crystals, we have identified three out of four Raman-active modes predicted by the factor group analysis. Frequencies of these modes are in good agreement with the lattice dynamics results. Contrary to its counterpart $K_xFe_{2-y}Se_2$, $K_{0.95}Ni_{1.86}Se_2$ did not show Ni vacancy ordering. Temperature-dependent study revealed no significant changes in the Raman spectra near the local CDW to the heavy-fermion-phase transition temperature.

*Present address: Frontier Research Center, Tokyo Institute of Technology, 4259 Nagatsuta, Midori, Yokohama 226-8503, Japan.

[1] Y. Kamihara, T. Watanabe, M. Hirano, and H. Hosono, J. Am. Chem. Soc. **130**, 3296 (2008).

[2] M. Rotter, M. Tegel, and D. Johrendt, Phys. Rev. Lett. **101**, 107006 (2008).

[3] K.-W. Yeh, T.-W. Huang, Y. lin Huang, T.-K. Chen, F.-C. Hsu, P. M. Wu, Y.-C. Lee, Y.-Y. Chu, C.-L. Chen, J.-Y. Luo, D.-C. Yan, and M.-K. Wu, EPL (Europhys. Lett.) **84**, 37002 (2008).

[4] F.-C. Hsu, J.-Y. Luo, K.-W. Yeh, T.-K. Chen, T.-W. Huang, P. M. Wu, Y.-C. Lee, Y.-L. Huang, Y.-Y. Chu, D.-C. Yan, and M.-K. Wu, Proc. Natl. Acad. Sci. **105**, 14262 (2008).

[5] X. Wang, Q. Liu, Y. Lv, W. Gao, L. Yang, R. Yu, F. Li, and C. Jin, Solid State Commun. **148**, 538 (2008).

[6] J. Guo, S. Jin, G. Wang, S. Wang, K. Zhu, T. Zhou, M. He, and X. Chen, Phys. Rev. B **82**, 180520 (2010).

[7] B. Wei, H. Qing-Zhen, C. Gen-Fu, M. A. Green, W. Du-Ming, H. Jun-Bao, and Q. Yi-Ming, Chin. Phys. Lett. **28**, 086104 (2011).

[8] G. M. Zhang, Z. Y. Lu, and T. Xiang, Phys. Rev. B **84**, 052502 (2011).

[9] F. Ye, S. Chi, W. Bao, X. F. Wang, J. J. Ying, X. H. Chen, H. D. Wang, C. H. Dong, and M. Fang, Phys. Rev. Lett. **107**, 137003 (2011).

[10] D. H. Ryan, W. N. Rowan-Weetaluktuk, J. M. Cadogan, R. Hu, W. E. Straszheim, S. L. Bud'ko, and P. C. Canfield, Phys. Rev. B **83**, 104526 (2011).

[11] Z. Shermadini, A. Krzton-Maziopa, M. Bendele, R. Khasanov, H. Luetkens, K. Conder, E. Pomjakushina, S. Weyeneth, V. Pomjakushin, O. Bossen, and A. Amato, Phys. Rev. Lett. **106**, 117602 (2011).

[12] J. R. Neilson, A. Llobet, A. V. Stier, L. Wu, J. Wen, J. Tao, Y. Zhu, Z. B. Tesanovic, N. P. Armitage, and T. M. McQueen, Phys. Rev. B **86**, 054512 (2012).

[13] H. Lei, K. Wang, H. Ryu, D. Graf, J. B. Warren, and C. Petrovic, arXiv:1211.1371 [cond-mat.supr-con].

[14] S. Baroni, S. de Gironcoli, A. Dal Corso, and P. Giannozzi, Rev. Mod. Phys. **73**, 515 (2001).

[15] P. Giannozzi *et al.*, J. Phys.: Condens. Matter **21**, 395502 (2009).

[16] N. Lazarević, M. Abeykoon, P. W. Stephens, H. Lei, E. S. Bozin, C. Petrovic, and Z. V. Popović, Phys. Rev. B **86**, 054503 (2012).

[17] N. Lazarević, H. Lei, C. Petrovic, and Z. V. Popović, Phys. Rev. B **84**, 214305 (2011).

[18] M. Balkanski, R. F. Wallis, and E. Haro, Phys. Rev. B **28**, 1928 (1983).

[19] N. Lazarević, Z. V. Popović, R. Hu, and C. Petrovic, Phys. Rev. B **81**, 144302 (2010).

Finite-temperature crossover and the quantum Widom line near the Mott transition

J. Vučičević,[1] H. Terletska,[2] D. Tanasković,[1] and V. Dobrosavljević[3]

[1]*Scientific Computing Laboratory, Institute of Physics Belgrade, University of Belgrade, Pregrevica 118, 11080 Belgrade, Serbia*
[2]*Condensed Matter Physics and Materials Science Department, Brookhaven National Laboratory, Upton, New York 11973, USA*
[3]*Department of Physics and National High Magnetic Field Laboratory, Florida State University, Tallahassee, Florida 32306, USA*

The experimentally established phase diagram of the half-filled Hubbard model features the existence of three distinct finite-temperature regimes, separated by extended crossover regions. A number of crossover lines can be defined to span those regions, which we explore in quantitative detail within the framework of dynamical mean-field theory. Most significantly, the high-temperature crossover between the bad metal and Mott-insulator regimes displays a number of phenomena marking the gradual development of the Mott insulating state. We discuss the quantum critical scaling behavior found in this regime, and propose methods to facilitate its possible experimental observation. We also introduce the concept of *quantum Widom lines* and present a detailed discussion that highlights its physical meaning when used in the context of quantum-phase transitions.

I. INTRODUCTION

Strongly correlated materials exhibit a variety of phases whose properties often lack a complete microscopic understanding.[1] The most interesting new aspect of this class of materials is a possibility to tune the system through two or more different ground states separated by quantum critical points (QCPs).[2] Such QCPs are often difficult to directly approach and investigate, not only because they reside at $T = 0$, but also because various additional instabilities and orders emerge in their immediate vicinity. Nevertheless, understanding them is of chief importance, because they often control rather extended finite-temperature quantum critical regions displaying universal properties and featuring scaling behavior of all quantities.

Quantum critical points have been experimentally identified and studied in several classes of physical systems, ranging from heavy fermion metals[3,4] to conventional[5] and even high-temperature superconductors.[6] In most of these, however, the QCP is obtained when quantum fluctuations become sufficiently strong to suppress an appropriate ordering temperature—for magnetic, structural, or superconducting order—down to $T = 0$. When this happens, then concepts familiar from the very successful theory of classical critical phenomena can be utilized and naturally extended to a quantum regime.[2] Indeed, most conventional theoretical approaches follow the Landau theory paradigm[7] and examine the impact of thermal and quantum fluctuations of appropriate order parameters, as describing the corresponding patterns of spontaneous symmetry breaking.

Should most exotic phenomena, then, be regarded as manifestations of some form of (static or fluctuating) order, as Slater speculated as early as in the 1930's,[8] or should fundamentally different classes of quantum-phase transitions exist? The first viewpoint was at the origin of the Hertz (weak coupling) approach[9,10] to quantum criticality, which, despite its formal elegance, resulted in only modest successes. The latter, however, was at the core of pioneering ideas of Mott[11] and Anderson,[12] who provided a complementary perspective. According to their views, strong electronic correlations are

able destroy the metallic state even in the absence of any ordering, leading to the formation of the Mott insulating state. The existence of broad classes of Mott insulators is, of course, beyond the doubt at this time. And while most order antiferromagnetically at low temperature, they indeed remain robustly insulating (gaps often in the electron volt range) even well above the corresponding Néel temperature.[13–15]

The nature of the phase transition between the metallic and the insulating phase—the Mott transition—has, in contrast, remained highly controversial and subject to much debate. Because the two phases share the same symmetries, the clear distinction between them is apparent only at $T = 0$. Should a direct and *continuous* transition between a paramagnetic metal and a paramagnetic Mott insulator exist at $T = 0$, it would represent the most obvious example of a QCP outside the Landau paradigm, unrelated to any mechanism of spontaneous symmetry breaking. Unfortunately, in most familiar situations, the Mott metal-insulator transition is also accompanied by simultaneous magnetic, charge, structural, or orbital ordering, considerably complicating the situation and fogging the issues, both from the theoretical and the experimental perspective.

Still, it is a well established experimental fact that in all known cases, the characteristic temperature scale T_c, below which many of such "intervening" phases are found, is quite small, as compared to both basic competing energy scales: the Fermi energy E_F measuring the quantum fluctuations, and the Coulomb repulsion U that opposes the electron motion. As a result, a very sharp crossover between metallic and insulating behavior is observed even at $T \gg T_c$, for all physical quantities. The key issue thus remains: What is the main physical mechanism controlling this finite-temperature metal-insulator crossover? Should it be viewed as a quantum critical regime dominated by appropriate order-parameter fluctuations, or is it, as postulated by Mott and Anderson, a dynamical phenomenon not directly related to any ordering tendency.

To clearly and precisely address this question, one must (1) suppress all ordering tendencies, at least in the relevant temperature range, and (2) understand and describe the remaining physical processes controlling the resulting finite-temperature

crossovers, and the corresponding quantum critical region, if one exists. From the theoretical point of view, this ambitious goal is generally very difficult to achieve, at least for realistic model systems. The task is hard, because standard perturbative approaches, which are so well suited to describe Fermi-surface instabilities and the associated competing orders, are quite incapable in describing the Mott physics. The situation, however, improved with the development of dynamical mean-field theory (DMFT) method,[16] which capitalizes on performing a local approximation for appropriate self-energies and vertex functions, yet which provides a completely nonperturbative description of strong correlation effects. Its physical content is most clearly revealed by focusing at the "maximally frustrated Hubbard model" (MFHM)[16,17] with long-range and frustrating intersite hopping (see below), where the DMFT approximation becomes exact.

The MFHM, because it is maximally frustrated, displays no magnetic or any other kind of long-range order across its phase diagram. It does display, however, a precisely defined Mott metal-insulator transition at low temperature, precisely in the fashion anticipated by the early ideas of Mott and Anderson. It has been studied by many authors, ever since the beginning of the DMFT era some 20 years ago,[18] yet, surprisingly, some of its basic features have remained ill understood and even confusing. Most studies focused on characterizing the low-temperature behavior, where a strongly correlated Fermi liquid (FL) forms on the metallic side of the Mott transition.[18] At low temperatures, this FL phase is separated from the Mott insulator by an intervening phase coexistence region (see Fig. 1), and the associated first-order transition line (FOTL) terminating at the critical end point (CEP) at $T = T_c$.[19] The behavior in the immediate vicinity of the CEP has attracted much recent attention[20,21] but, unsurprisingly (as any other finite-temperature CEP), it display scaling behavior of the standard classical liquid-gas (Ising) universality class.[19] Indeed, several experiment reporting transport in this regime have successfully been interpreted[22] using these classical models.

But what about the supercritical ($T \gg T_c$) behavior? Its rough features have been investigated by many authors,[16] who identified several regimes and complicated crossovers connected to them, but no simple and plausible physical picture has emerged. Most importantly, almost no one has attempted to interpret the features of this high-temperature regime in terms of ideas or concepts of quantum criticality.[2] The complication, of course, comes from the presence of the coexistence dome at $T < T_c$, which confuses the issues, and, at least at first glance, makes the situation seem incompatible with the standard paradigm of quantum criticality.

Our very recent work,[17] however, provided a new perspective. It made two key observations. (1) The characteristic temperature scale of the coexistence dome $T_c \ll E_F, U$: The physics associated with it should, at $T \gg T_c$, be little affected by its presence, and thus behave just as if $T_c \approx 0$, and an actual QCP would exist separating the two phases. (2) To reveal the possible quantum critical scaling associated with the proposed "hidden" QCP, one must follow a judiciously chosen trajectory (sometimes called the "Widom line"[23,24]), as in almost any standard critical phenomenon. This work also demonstrated[17] remarkable scaling of the resistivity curves, displaying all features expected of quantum criticality. The resistivity around this line exhibits a characteristic "fan-shaped" form, surprisingly similar to experimental findings in several systems,[1,20,21,25–27] reflecting gradual crossover from metallic to insulating transport. The scaling behavior in this high-temperature crossover regime was thus argued to encapsulate the universal features of finite-temperature transport near the metal-insulator transition.

The work of Ref. 17 focused on behavior close to the "instability line" and the associated quantum critical scaling regime around it. It should be noted, however, that several other finite-temperature crossover lines have been discussed by other authors[16,24,28–30] to characterize the metal-insulator region. The exact relationship between these different ideas and approaches—for the same model—thus remained an open and rather confusing issue that needs to be carefully investigated and understood. This important task is the chief subject of this paper, where we present a detailed and very precise characterization of all the crossover regimes across the entire phase diagram for the maximally frustrated Hubbard model at half filling, within the paramagnetic solution of dynamical mean-field theory. We carefully characterize the relevant crossover lines employing all the various proposed criteria used for their definitions. Two fundamentally distinct crossover regions are identified: one referring to the thermal destruction of long-lived quasiparticles and the other to the gradual opening of the Mott gap. The instability line, as previously determined from a thermodynamic analysis,[17] belongs to the latter region, and is found to lie very near to the line of inflection points in the resistivity curves $\log \rho(U)$. The scaling of resistivity curves found around both of these lines is analyzed and discussed from the perspective of hidden quantum criticality and its experimental observation. In the end, we outline the generalized concept of the Widom lines, and argue that they gain a new fundamental meaning in the context of quantum-phase transitions, which opens an avenue to put our results into a more general theoretical framework.
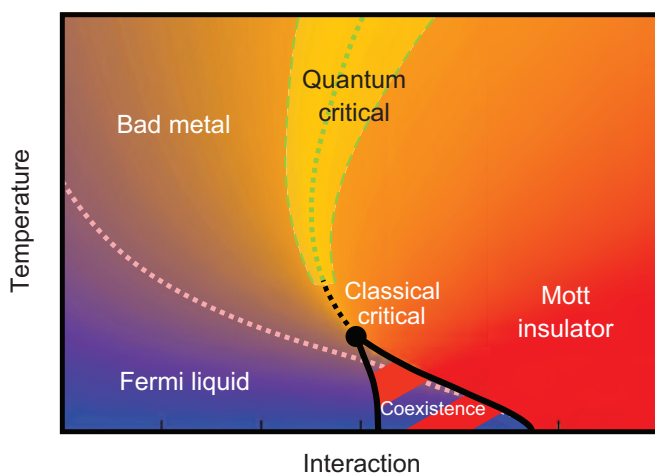

FIG. 1. (Color online) Phase diagram of the half-filled maximally frustrated Hubbard model. The background is an actual color map of the resistivity obtained using the IPT impurity solver (see the text): Blue, small resistivity; red, large resistivity.

II. PHASE DIAGRAM

We consider a single band Hubbard model at half filling,

$$H = -t \sum_{\langle i,j \rangle \sigma} (c_{i\sigma}^\dagger c_{j\sigma} + \text{H.c.}) + U \sum_i n_{i\uparrow} n_{i\downarrow}, \quad (1)$$

where $c_{i\sigma}^\dagger$ and $c_{i\sigma}$ are the electron creation and annihilation operators, $n_{i\sigma} = c_{i\sigma}^\dagger c_{i\sigma}$, t is the nearest-neighbor hopping amplitude, and U is the repulsion between two electrons on the same site. We use a semicircular density of states, and the corresponding half bandwidth $D = 2t$ is set to be our energy unit. We focus on the paramagnetic DMFT solution, which is formally exact in the limit of large coordination number, including the maximally frustrated Hubbard model.[16,17] The DMFT provides a unique theoretical framework, as it works well in the entire range of model parameters, thus treating all the relevant phases and regimes on an equal footing. It is, however, most reliable at high temperatures,[31–34] when the correlations are more local, and this is precisely the regime of primary interest of this paper. To solve the DMFT equations we utilize both the iterated perturbation theory[16] (IPT) and the numerically exact continuous time quantum Monte Carlo (CTQMC).[35,36] The results obtained with these two methods are found to be in very good agreement. In this section we concentrate on IPT results, which cover the entire phase diagram and do not suffer from numerical noise. Figures in the rest of the paper are the QMC results.

The phase diagram in the U-T plane is shown in Fig. 1. The DMFT solution reproduces the three regimes found close to the metal-insulator transition (MIT): Fermi liquid, bad metal, and Mott insulator, in qualitative agreement with experiments on various Mott systems.[16] We begin their characterization by first analyzing the behavior of the resistivity in the relevant range of parameters.

The DMFT expression for the calculation of DC resistivity, $\rho = 1/\sigma(\omega \to 0)$, is given by[16]

$$\sigma = \pi \sigma_0 \int_{-\infty}^{+\infty} d\varepsilon \, v^2(\varepsilon) D^0(\varepsilon) \int_{-\infty}^{+\infty} \left(-\frac{df}{d\omega} A^2(\varepsilon,\omega) \right), \quad (2)$$

where $A(\varepsilon,w) = -\frac{1}{\pi} \text{Im} \, G(\varepsilon,w)$, $v(\varepsilon) = \sqrt{(4t^2 - \varepsilon^2)/3}$. $D^0(\varepsilon) = \frac{1}{2\pi t^2} \sqrt{4t^2 - \varepsilon^2}$ is the noninteracting density of states (DOS), and f is the Fermi function. The calculation of resistivity from the IPT results is straightforward as this method is defined on the real axis. To calculate the resistivity from the QMC results, one first needs to perform the analytical continuation, which we carry out using the maximum entropy method.[37]

Our quantitative IPT results are replotted in Fig. 2, where the value of resistivity is color coded, with white stripes separating the consecutive orders of magnitude between 10^{-3} and 10^{13}. In this plot, as well as in the rest of the paper, the resistivity is given in the units of ρ_{Mott}, the maximal metallic resistivity in the semiclassical Boltzmann theory, defined as the resistivity of the system when the scattering length is equal to one lattice spacing.[38,39] At zero temperature, the metallic resistivity vanishes, while the Mott insulator has an infinite resistivity. With increasing temperature, the difference between the two states becomes less and less pronounced. (Between the spinodals, both metallic and insulating solutions
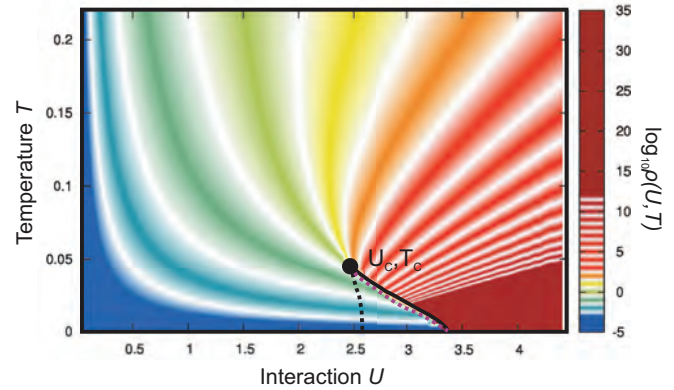

FIG. 2. (Color online) Resistivity (in units of ρ_{Mott}) calculated in the entire U-T plane. The white stripes follow the lines of equal resistivity and separate the orders of magnitude in the resistivity. Spinodals are denoted with thick black lines, and the first-order phase transition line is dashed.

are possible, but in this plot only the metallic resistivity is shown.) In the intermediate correlation, $U < U_c$, high-temperature, $T > T_c$, regime, the resistivity is comparable or even larger than ρ_{Mott}, but it still (weakly) increases with temperature, which is characteristic for the "bad metal" regime observed in several Mott systems.[38]

It is remarkable how this way of presenting the data immediately creates the familiar "fan-shape" structure, generally expected for quantum criticality.[2] At high temperatures all the white constant-resistivity stripes seem to converge almost to the same point $U \sim U_c$. The perfect convergence, however, is interrupted by the emergence of the coexistence done at $T < T_c$, but such behavior is exactly what one expects for "avoided quantum criticality,"[30] consistent with the physical picture proposed in Ref. 17.

Different regions of the phase diagram are also distinguished by the qualitatively different form for the temperature dependence of the resistivity. To make this behavior even more apparent, we follow a commonly used procedure to display the data around QCPs, compute the logarithmic derivative of resistivity with respect to the temperature, i.e., the "effective exponent"[40,41]

$$\beta(T,U) = d \log \rho(U,T)/d \log T, \quad (3)$$

which is presented in color-coded form in Fig. 3.

On the metallic side, at the lowest temperatures, one finds a typical metallic dependence of the form $\rho \sim T^2$ and here we have $\beta = 2$ (white). Far from the transition, this regime survives up to relatively high temperatures, but eventually the temperature dependence of the resistivity starts gradually slowing down, displaying behavior sometimes described as "marginal Fermi-liquid" transport (green, $\beta \sim 1$). Closer to the transition, this is preceded by an increase in the effective exponent (red), which is a reflection of the existence of the critical end point in which β diverges (yellow). Very close to the transition, a maximum of the resistivity is reached at some temperature (pink) and the trend of the resistivity increase is then reversed. On the other side of the phase diagram, deep in the Mott insulator, one finds typical activation curves which exhibit the exponential drop in the resistivity with increasing
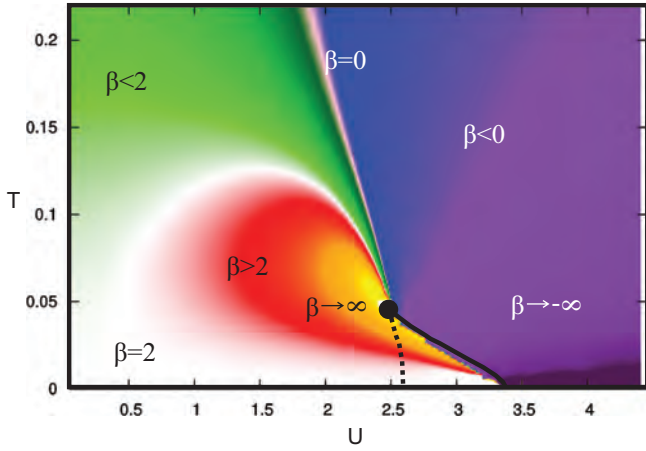
FIG. 3. (Color online) The effective resistivity exponent ($\beta = d\log\rho/d\log T$) calculated in the entire U-T plane illustrates the different transport regimes (see the text).

temperature, due to the gap in the excitation spectrum (black and purple). However, just above the coexistence dome, one finds an intermediate regime, where the behavior is generally insulating because the resistivity decreases with temperature, but the gap is not yet fully open, and the temperature dependence deviates from exponential (blue). This region is sometimes referred to as the "bad insulator."

III. CROSSOVER LINES

In the previous section we have characterized the different regimes in the vicinity of the Mott MIT: Fermi liquid, bad metal, and Mott insulator. However, apart from the coexistence region, the properties of the system change continuously in the entire phase diagram. The lines separating the different regimes are thus a matter of convention and many definitions can be found in literature proposing the criteria for their distinction.

In Fig. 4 we present the lines corresponding to various definitions of a crossover line between the Fermi-liquid and
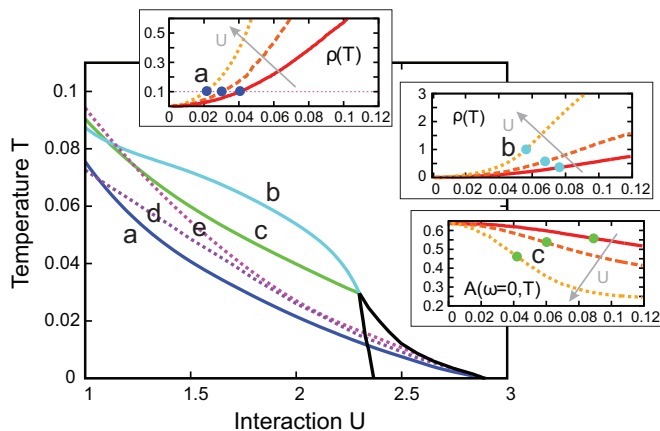
the bad metal regimes. The definition of each line is illustrated on a smaller panel on the right, where the corresponding feature in the resistivity and other relevant quantities is marked with the dots of the same color. The dark blue line (a) is defined by $\rho = 0.1\rho_{\text{Mott}}$ and it roughly corresponds to the Fermi coherence temperature T_{FL} (the temperature above which the temperature dependence of resistivity is no longer quadratic). The corresponding small panel (a) shows the resistivity as a function of temperature, plotted for three different values of U. The dotted horizontal line marks $\rho = 0.1\rho_{\text{Mott}}$. The arrow denotes the direction of increase of U. The light blue line (b) corresponds to the inflection point of the resistivity, $d^2\rho(\omega = 0)/dT^2 = 0$, and the green line (c) is determined as the inflection point of the spectral density at the Fermi level with respect to the temperature, $d^2A(\omega = 0)/dT^2 = 0$. These are illustrated on smaller panels (b) and (c) where the dc resistivity and $A(\omega = 0)$ are plotted versus the temperature, for three different values of U. The inflection points are marked with the dots of color corresponding to the (b) and (c) lines on the main panel. The additional two dotted lines are (d) the quasiparticle weight at zero temperature defined by $Z = [1 - d\,\text{Im}\,\Sigma(i\omega_n)/d\omega_n|_{\omega_n\to 0}]^{-1}$ and (e) the zero temperature local spin susceptibility χ. Both quantities are divided by 10 to fit in the temperature range of the plot and to be more easily compared to the crossover lines. It is evident that the coherence temperature is roughly proportional to the quasiparticle weight at zero temperature, but with the prefactor 0.1, $T_{\text{FL}}(U) \sim 0.1Z(U)$. As compared with the doped Hubbard model,[42,43] T_{FL} is higher but still distinct from the temperature corresponding to ρ_{Mott}, in agreement with the experiments on organic materials.[39,44,45] The quasiparticle weight Z is weakly temperature dependent and the Drude peak in the optical conductivity is still pronounced for $\rho \lesssim \rho_{\text{Mott}}$.[46]

In contrast with these lines, one can also define the lines separating the bad metal from the (bad) Mott insulator. In Fig. 5, we present several criteria for their definition. In analogy to line (a) of Fig. 4, one can use the resistivity to distinguish between the two regimes. The dark blue line (a) plotted here connects the points where the resistivity is equal

FIG. 4. (Color online) Various definitions for the crossover lines between the Fermi liquid and the bad metal. The meaning of each definition is illustrated on a smaller panel to the right. The results are obtained with the QMC.
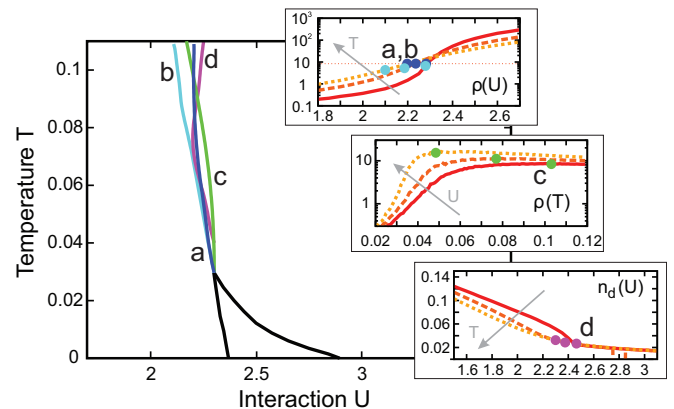

FIG. 5. (Color online) Various definitions for the crossover lines between the bad metal and the Mott insulator. The meaning of each definition is illustrated on a smaller panel to the right. The results are obtained with the QMC.

to the one found precisely at the critical end point, which we estimate to be roughly $10\rho_{\text{Mott}}$. The light blue line (b) marks the inflection point of logarithmic resistivity as a function of U $[\partial^2 \log \rho(U,T)/\partial U^2 = 0]$. It is a well pronounced feature up to high temperatures, and it is a direct consequence of the discontinuity across the FOTL at $T < T_c$. These two are illustrated on the small panel to the right, where $\log \rho(U)$ is plotted at three different temperatures. The dark blue dots are the intersections of these lines with the dotted, $10\rho_{\text{Mott}}$ line. The inflection points are marked with the light blue dots, and are found at slightly lower values of U. Another natural definition for the crossover is the $\beta = 0$ line (c), as it marks the place where the trend of resistivity growth is reversed. At its right-hand side, the resistivity decreases with temperature, which is a sign of insulating behavior. This is illustrated on the corresponding small panel, where $\log \rho(T)$ is plotted for three different values of U and the maxima are marked with the green dots. The double occupancy n_d has an obvious change in trend on crossing line (d). Here, the second derivative $\partial^2 n_d/\partial U^2$ has a sharp maximum, and separates the two distinct regimes of $n_d(U)$, both almost linear but with different slopes. This is apparent on the small panel (d), where double occupancy is plotted as a function of U at various temperatures.

It is striking that these lines almost coincide, in sharp contrast to what is seen in Fig. 4. Although the opening of the gap is very gradual, it is possible to pinpoint the boundary between the two regimes and actually divide the supercritical part of the phase diagram into metallic and insulatinglike regions. In the following section we present an overview of the instability line, another definition for a metal-insulator crossover line, and explain how it helps reveal a very peculiar property of the Hubbard model, which is very suggestive when it comes to interpreting the Mott MIT in terms of quantum-phase transitions.

IV. INSTABILITY LINE AND QUANTUM CRITICAL SCALING

It is a well established phenomenon that in the vicinity of quantum critical points, at finite temperatures, physical observables display a characteristic quantum critical scaling.[2] A very good example of this is the transport in high-mobility two-dimensional electron gases, in particular, in metal-oxide-semiconductor field-effect transistors (MOSFETs).[1] There is overwhelming evidence that they exhibit a zero temperature metal-insulator transition at a critical concentration of charge carriers.[25] It is experimentally observed in these systems that the value of resistivity at finite temperatures above the quantum critical point $(n_c, T = 0)$ is a function of only $\delta n = n - n_c$ and T, which is considered a hallmark of quantum criticality. As shown in Fig. 6(a),[47] the resistivity curves collapse onto two branches: The resistivity is first divided by the "separatrix" $\rho_c(T) = \rho(n_c, T)$ which weakly depends on the temperature, and then the temperature is scaled by $T_o(\delta n) = |\delta n|^{\nu z}$, yielding

$$\rho(\delta n, T) = \rho_c(T) f(\delta n T^{-1/\nu z}). \quad (4)$$

The mechanism behind the physical picture of MOSFETs is still elusive,[27] but a similar physical picture is seen is various spin systems, where the physics is well understood.[2]
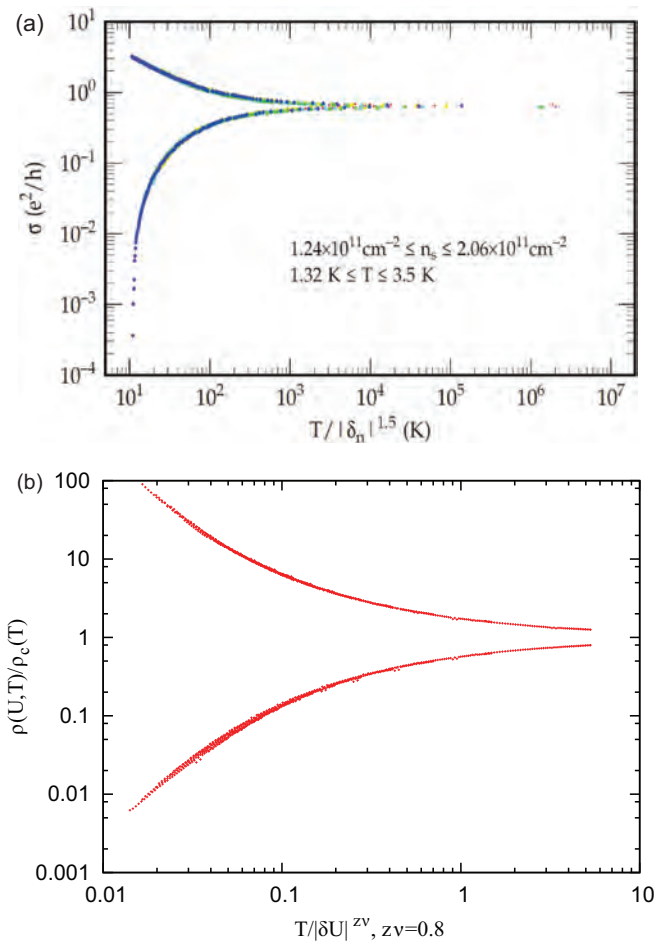

FIG. 6. (Color online) (a) Experimental results: Conductivity scaling in high-mobility Si MOSFETs presents a textbook example of quantum critical scaling (taken from Ref. 47). (b) DMFT QMC results: Resistivity scaling strongly reminiscent of what is seen in MOSFETs. After dividing $\rho(U,T)$ with the value of resistivity on the instability line $\rho_c(T)$ (see the text) and then rescaling the temperature with an appropriately chosen parameter $T_0(\delta U)$, the resistivity curves collapse onto two branches.

When there is a well defined order parameter, the separatrix corresponds to the line of zero symmetry-breaking field, which is trivially a straight vertical line emanating from the quantum critical point.

Although our model does feature a FOTL, the critical temperature is actually very low ($T_c \approx 0.03$), which makes it reasonable to pursue a description of its supercritical region from the perspective of quantum criticality. This is the approach that we have taken in a recent work,[17] where we have shown that in the Hubbard model, a quantum critical scaling of the resistivity curves does indeed hold [Fig. 6(b)]. There is an obvious analogy between the interaction U in our model and the carrier density n in MOSFETs, but it was not immediately clear what line $U_c(T)$ should correspond to the separatrix in our model. The phase transition in the Hubbard model does not break any symmetries and the first-order transition line is curved, which indicated that U_c has possibly a nontrivial temperature dependence.

A. The instability line

Starting from the thermodynamic arguments,[19,48] we have defined the instability line $U^*(T)$ as the line which corresponds to the minimum curvature of the free-energy functional $\mathcal{F}[G(i\omega_n)]$ with respect to U.[49] Above T_c the system has a unique ground state which corresponds to the minimum of $\mathcal{F}[G(i\omega_n)]$. In this minimum, the curvature of $\mathcal{F}[G(i\omega_n)]$ is determined by the lowest eigenvalue λ of the fluctuation matrix

$$M_{mn} = \frac{1}{2Tt^2} \left. \frac{\partial^2 \mathcal{F}[G]}{\partial G(i\omega_m)\partial G(i\omega_n)} \right|_{G=G_{\mathrm{DMFT}}}, \qquad (5)$$

where $\delta G(i\omega_n) \equiv G(i\omega_n) - G_{\mathrm{DMFT}}(i\omega_n)$, and G_{DMFT} is the self-consistent solution of the DMFT equations. As explained in detail in the Supplemental Material of Ref. 17, λ can be obtained by monitoring the rate of convergence in the DMFT iteration loop. Close to the self-consistent solution, the difference between the consecutive solutions drops exponentially, with an exponent proportional to λ. We have

$$\mathbf{G}^{(n+1)} - \mathbf{G}^{(n)} = \delta\mathbf{G}^{(n)} = e^{-n\lambda}\mathbf{G}_\lambda(i\omega_n), \qquad (6)$$

where $\mathbf{G}_\lambda$ is the eigenvector of $\hat{M}$ corresponding to its lowest eigenvalue λ.

The curvature λ is actually a very general quantity that describes the response of the system to an infinitesimal external perturbation, which may be a time-dependent field of an arbitrary form. As such, λ is very important in describing a thermodynamical state close to the Mott MIT, since it has a fundamentally dynamic nature. Indeed, λ vanishes precisely at the critical end point, as the free-energy functional becomes flat around G_{DMFT}. This is directly connected to the critical slowing down of dynamics, which manifests as the vanishing of a characteristic frequency scale. Above T_c, λ is related to the local stability of a given thermodynamic state and has a minimum precisely where the system is the least stable, or where its proximity to either competing phase is equal. Therefore, the instability line which connects the minima of λ vs U is the closest analogy to the lines of the zero symmetry-breaking field in systems with an order parameter.

The instability line is presented in Fig. 1 and indeed it represents a boundary between a metallic and insulating transport. It lies among the other crossover lines from Fig. 5 (see also Sec. V). Its physical meaning is illustrated in Fig. 7. The middle column shows the DOS along the instability line for three different temperatures. While the DOS at the Fermi level is strongly suppressed, the gap is not yet fully open. The left column shows the density of states in the metallic phase following a trajectory parallel to the instability line: There is a clear quasiparticle peak at low temperatures, which gradually disappears as the bad metal region is reached by increasing the temperature. At larger U (right column) the system is in the insulating phase with a fully open Mott gap, featuring activated transport.

B. Free-energy calculation

To further illustrate the physical meaning of the instability line, we explore the free-energy landscape in the Hilbert space of Green's functions. For this we closely follow the procedure described in Ref. 49. The iterative self-consistency procedure used to solve the DMFT equations converges towards a local
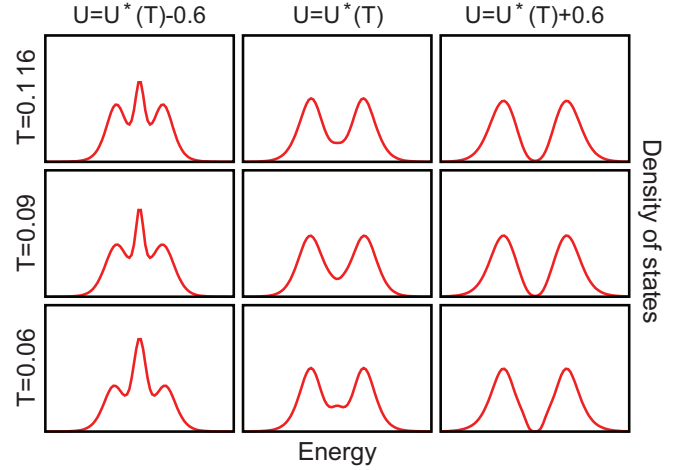

FIG. 7. (Color online) Density of states (QMC results) along the instability line $U^*(T)$ (middle column), and along the parallel trajectory for smaller (left column) and larger U (right column).

minimum of the corresponding Ginzburg-Landau free-energy functional $\mathcal{F}[\mathbf{G}]$, which, in the Hilbert space of the Matsubara Green's functions $G(i\omega_n)$, takes the form

$$\mathcal{F}[\mathbf{G}] = \mathcal{F}_{\mathrm{imp}}[\mathbf{G}] + \mathcal{F}_{\mathrm{bath}}[\mathbf{G}]$$
$$= \mathcal{F}_{\mathrm{imp}}[\mathbf{G}] - t^2 T \sum_n G^2(i\omega_n), \qquad (7)$$

where the first term is the free energy of the impurity site in the presence of the Weiss field $\Delta = t^2\mathbf{G}$, while the second term is the energy cost of forming the Weiss field around a given site.

The DMFT self-consistency condition, typically reached via an iterative procedure, is then regarded as a saddle-point equation derived from the extremum condition of such a Ginzburg-Landau functional. The physical DMFT solution corresponds to the local stationary point of $\mathcal{F}[\mathbf{G}]$, where a gradient vector $\mathbf{g} = \partial \mathcal{F}[\mathbf{G}]/\partial\mathbf{G}$ becomes zero. However, in the coexistence region below T_c, two such local minima are found. They correspond to physical solutions (metallic $\mathbf{G}_M$ and insulating $\mathbf{G}_I$), and are separated by an unstable solution (a local maximum or a saddle point).

We can visualize the shape of the infinitely dimensional free-energy surface by calculating $F[\mathbf{G}]$ along a single direction going through the self-consistent $\mathbf{G}_{\mathrm{DMFT}}$. Below T_c, we do this along the direction connecting the two solutions, which can be parametrized as $\mathbf{G}(l) = (1-l)\mathbf{G}_M - l\mathbf{G}_I$. Above T_c, where there is only one solution, we follow the eigenvector $\mathbf{G}_\lambda$ with $\mathbf{G}(l) = \mathbf{G}_{\mathrm{DMFT}} + l\mathbf{G}_\lambda$. The relative change of the free energy is calculated[49] as an integral $\Delta\mathcal{F}(l) = \mathcal{F}[\mathbf{G}(l)] - \mathcal{F}[\mathbf{G}_{M/\mathrm{DMFT}}] = t^2 T \int_0^l dl' \mathbf{e}_l \cdot \mathbf{g}[\mathbf{G}(l')]$, where $\mathbf{e}_l$ is the unit vector of the followed direction [$\mathbf{e}_l = (\mathbf{G}_M - \mathbf{G}_I)/|\mathbf{G}_M - \mathbf{G}_I|$ below T_c and $\mathbf{e}_l = \mathbf{G}_\lambda/|\mathbf{G}_\lambda|$ above T_c]. The gradient vector takes the form $\mathbf{g} = \mathbf{G}_{\mathrm{imp}}(\mathbf{G}) - \mathbf{G}$, with $\mathbf{G}_{\mathrm{imp}}(\mathbf{G})$ the output of the impurity solver used in the DMFT procedure, and $\mathbf{G}$ is the input–effective medium (hybridization bath) Green's function.

Figure 8(a) shows the free-energy landscape around $\mathbf{G}_{\mathrm{DMFT}}$, precisely at the instability line. The curvature of the global minimum vanishes as one approaches T_c, which is consistent with eigenvalue λ being zero at this point. Below T_c there are two minima and the instability line is no longer well defined,
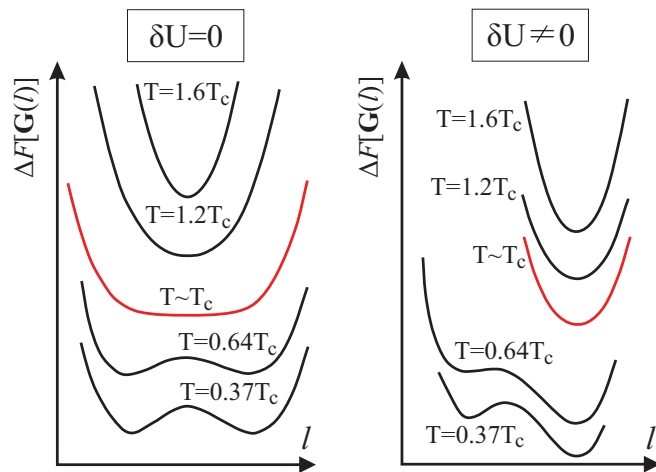
FIG. 8. (Color online) Free-energy landscape (IPT results): (a) Along the "zero field" line ($\delta U = 0$). At $T > T_c$, the curvature of the free energy increases with temperature, and it is zero at $T = T_c$. Below T_c, at the first-order transition line, metallic and insulating solutions have the same free energy. (b) Along the "finite field" line ($\delta U = -0.05$). At $T > T_c$, the curvature of the free energy is greater than in the "zero field" case. In the coexistence region one of the minima is energetically favored. Note that the spacing between $\Delta\mathcal{F}$ curves for different temperatures is arbitrary.

but it is logically continued to the line of the first-order phase transition, where two possible solutions are of the same energy. On Fig. 8(b), we move along a parallel trajectory, defined by $\delta U \neq 0$. It is immediately obvious that λ never reaches zero and that in the coexistence region one of the solutions is energetically favored. This physical picture is common to various models. For example, it is seen in the Ising model in an external field, where the analogy is between the strength of the magnetic field and δU in our case.

C. Quantum critical scaling

While the instability line is determined from the free-energy analysis, a novel physical perspective is obtained by looking at the transport properties in its vicinity. We have demonstrated[17] that around this line, all resistivity curves can be collapsed onto two branches: We first divide each resistivity curve by the resistivity along the instability line (the "separatrix") $\rho_c(T) = \rho(T, \delta U = 0)$, and then rescale the temperature for each curve with an appropriately chosen parameter $T_0(\delta U)$ to collapse the data onto two branches [Fig. 6(b)]. The family of resistivity curves displays characteristic quantum critical scaling of the form

$$\rho(T, \delta U) = \rho_c(T) f(T/T_o(\delta U)), \qquad (8)$$

with $T_o(\delta U) \sim |\delta U|^{z\nu}$. The scaling parameter T_o displays power-law scaling with the same exponents for both scaling branches and falls sharply as $U \to U^*$, which is consistent with the quantum critical scenario. The resistivity scaling holds in the temperature range roughly between $2T_c$ and $4T_c$, as depicted in Fig. 1. We estimate the exponent $z\nu$ to be around 0.6 when IPT is used to solve the DMFT equations. The scaling procedure with the data obtained with the CTQMC impurity solver gives a slightly larger critical exponent with an error
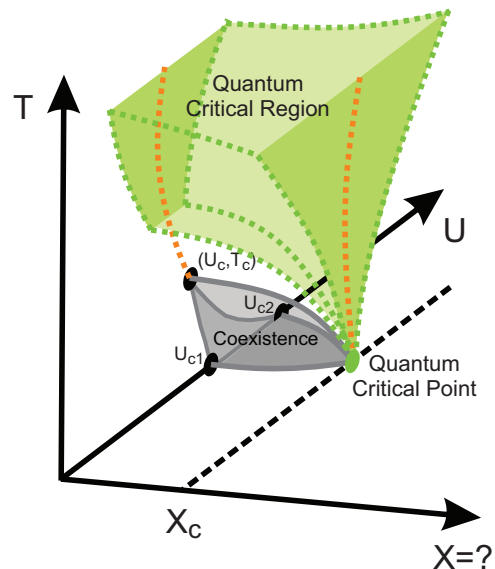

FIG. 9. (Color online) Possible phase diagram of a generalized Hubbard model. The observed scaling (valid in the green region) may be due to a quantum critical point that is unreachable by the simple two-parameter half-filled Hubbard model. An additional, third parameter (here marked with X) could drive T_c to zero at some critical value and extend the region of validity of the scaling formula in the U-T plane.

bar due to numerical noise of the data and due to the analytical continuation.

We emphasize the difference in the proposed quantum critical scaling and classical scaling in the immediate vicinity of the critical end point (classical critical region in Fig. 1). It has been already carefully studied theoretically,[19,50] and even observed in experiments,[20] revealing the classical Ising scaling in this regime. In contrast, the scaling parameter in our formula is T rather than $|T - T_c|$ and the value of the exponent does not fit any of the known universality classes. The scaling region in our analysis is significantly broader and the collapse of the resistivity curves is observed in a large temperature region above the critical end point.

A stringent test of the proposed quantum critical transport scenario would be on systems with reduced critical temperature T_c. Figure 9 presents a schematic phase diagram with an additional parameter driving T_c to zero at some critical value X_c and merging U_{c1}, U_{c2}, and U_c into a single, quantum critical point. If this were the case, the quantum critical region would extend down to zero temperature. For a simple half-filled Hubbard model, the critical temperature can be reduced, e.g., by the disorder[51] or particle-hole asymmetry, but still remains finite. Therefore, other models should be considered, also away from half filling,[52,53] which have a significantly reduced coexistence region and where the proposed scaling may give a more direct evidence of the quantum criticality. In some of these models the coexistence region was not even detected, and then the eigenvalue analysis can also be used as an ultimate test for its existence. It would be also very interesting to explore a possible quantum critical scaling in the external electric field within the nonlinear I-V regime,[5] similar as in the experiments on Si MOSFETs.[54] This seems especially important in light

of the recent discovery of devices displaying novel resistive switching in narrow gap Mott insulators.[55] Finally, the concept of the instability line above the quantum critical point, which is based on the thermodynamic analysis, is very general and can be applied to other physical systems (e.g., interacting spins in an external field), and the scaling analysis can be tested on physical quantities other than the resistivity.

V. SCALING AROUND THE INFLECTION-POINT LINE

As stated in the previous section, the curvature λ must be directly related to an appropriate relaxation rate of a system perturbed away from the equilibrium, a quantity that in principle should be possible to measure on any system. However, it is currently very hard to make such measurements on the Mott systems and precisely determine the instability line. Our calculations, however, show that it lies just among the crossover lines that separate the bad metal and the Mott insulator, so it might not be necessary to know its exact position to observe quantum criticality. In the following, we present a scaling analysis that can be performed around the resistivity inflection-point line (or any of the other crossover lines) to test the scaling hypothesis. As it turns out, the scaling is a robust feature, not particularly sensitive to the choice of $U_c(T)$, as already tested in experiments on various organic Mott systems.[56]

We first observe that the resistivity curves display almost a perfect mirror symmetry when plotted on the log scale [Fig. 6(b)]. This puts a strong constraint on the functional form of the scaling function f (as we show below) and also indicates that the resistivity curve along the inflection-point line, $\partial \log \rho(U)/\partial U = 0$, could also serve as the separatrix. The mirror symmetry requires that

$$f(y) = 1/f(-y). \tag{9}$$

For the above to be satisfied, the function f must be of the form

$$f(y) = e^{h(y)}, \tag{10}$$

where h is an antisymmetric function of y. It is clear that $f(0) = 1$ and therefore $h(0) = 0$. h must also be smooth, so it can be represented as a Taylor series with only odd terms,

$$h(y) = ay + by^3 + \cdots. \tag{11}$$

In our calculations, it turns out that only the linear term is significant, and here we show how this can be tested. First we make a substitution of variables $T/\delta U^{z\nu} \rightarrow \delta U T^{-1/z\nu}$ and then take the logarithm of both sides of the scaling formula to obtain

$$\log\left(\frac{\rho(U_c(T) + \delta U, T)}{\rho(U_c(T), T)}\right) = \log\left(f(\delta U T^{-1/z\nu})\right). \tag{12}$$

If the mirror symmetry is satisfied, then

$$\log\left(\frac{\rho(U_c(T) + \delta U, T)}{\rho(U_c(T), T)}\right) = h(\delta U T^{-1/z\nu}), \tag{13}$$

which means that the precise form of $h(y)$ can be deduced by plotting the left-hand side of the above equation as a function of $y = \delta U T^{-1/z\nu}$ and then making a fit of a polynomial curve to the data. This is possible because in the region where the
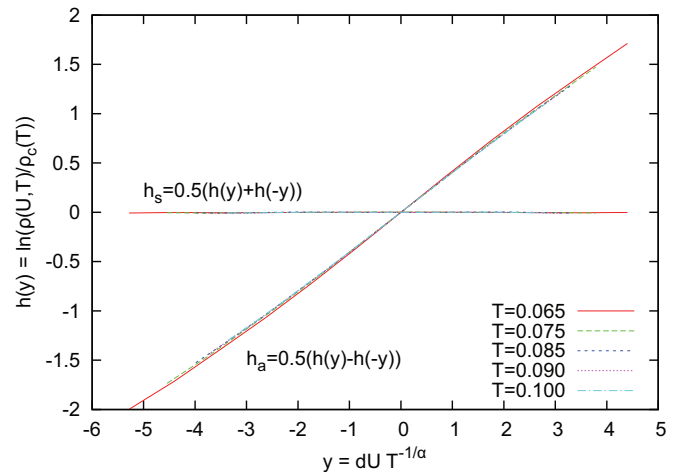

FIG. 10. (Color online) The symmetric and asymmetric part of the scaling function, h_s and h_a, at various temperatures. The small value of $h_s(y)$ shows that the mirror symmetry of resistivity curves is present. The $h_a(y)$ curves collapse around the inflection-point line, which shows that the exponent, $z\nu = 0.953$, is well evaluated. Fitting a third-order polynomial to $h_a(y)$ in the range where these curves collapse can reveal the exact form of the scaling formula. In our calculations only the linear term is significant.

scaling formula is valid, all the data points should collapse onto a single curve. To test whether $h(y)$ is truly antisymmetric, it is convenient to first split it into symmetric and antisymmetric parts, $h(y) = h_s(y) + h_a(y)$, where $h_s(y) = \frac{1}{2}[h(y) + h(-y)]$ and $h_a(y) = \frac{1}{2}[h(y) - h(-y)]$. If the resistivity is mirror symmetric, h_s should be 0 and h_a should be equal to h. In Fig. 10 we plot these functions around the inflection-point line and find h_s to be negligible. Also, it is easily seen that $h(y)$ is purely linear in the region where the data points perfectly collapse on a single curve.

Now it is clear that there are two conditions that $U_c(T)$ has to satisfy for the scaling with mirror symmetry to be possible. First, if we take the partial derivative over U at both sides of the equation, we get

$$\frac{\partial \log \rho(U,T)}{\partial U} = aT^{-\frac{1}{z\nu}} + b\delta U^2 T^{-\frac{3}{z\nu}} + \cdots. \tag{14}$$

If $h(y)$ is a linear function, then only the first term in the above equation remains, which means that the logarithm of resistivity is a linear function of U in the entire region in which the scaling formula holds. Even if there are higher terms in $h(y)$, the above has to be true at least close to U_c (small δU), where the linear term is dominant in any case. This imposes a constraint on $U_c(T)$, such that it has to be in a region where the second derivative of logarithmic resistivity is zero, or at least small,

$$\frac{\partial^2 \log \rho(U,T)}{\partial U^2} \approx 0. \tag{15}$$

This derivative is color coded in the (U,T) plane in Fig. 11 so that yellow color corresponds to a small absolute value. As it is readily verified, the above condition is not fulfilled anywhere exactly [except precisely at the log $\rho(U)$ inflection-point line by its definition], but all of the crossover lines lie in the region where this condition is approximately satisfied. There is an additional requirement for $U_c(T)$ which is not in
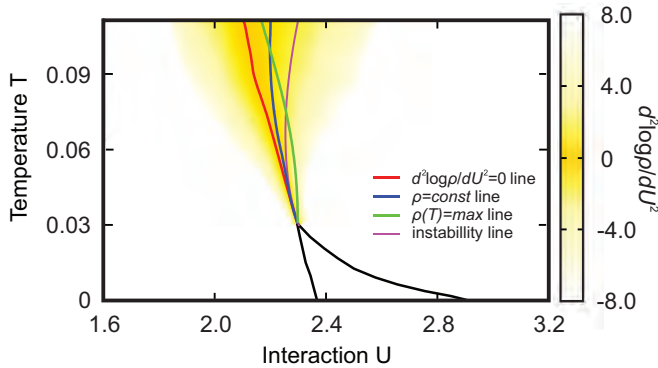
FIG. 11. (Color online) The instability line lies among the other crossover lines. $\log \rho(U)$ is linear in this crossover region, which allows for the scaling formula to be valid.

FIG. 13. (Color online) Relative error of the scaling formula color coded in the U-T plane. The dotted lines are the boundary of the scaling region. The two green filaments below $2T_c$ are where the scaling formula intersects with the actual DMFT result.

any way implied by definition of any of the crossover lines. Namely, the first derivative of the logarithmic resistivity has to be decreasing along $U_c(T)$ as a power law of temperature. This can be shown by taking the limit $\delta U \to 0$ in Eq. (14),

$$\frac{\partial \log \rho(U,T)}{\partial U}\bigg|_{U_c} \propto T^{-\frac{1}{z\nu}}. \tag{16}$$

The above holds regardless of the value of the cubic (or any higher) term coefficient. One can even use this to give a good assessment of the exponent $z\nu$, by fitting such an experimental (or theoretical) curve to a power law as shown in Fig. 12. As it is seen here, the derivative Eq. (16) calculated along the inflection-point line fits well to a power-law curve of exponent -0.95, but only above roughly $2T_c$. The same analysis of the IPT results yields a slightly lower value of $z\nu = 0.63$.

Finally, an estimate of how well the scaling works can be made by comparing the value of resistivity obtained by the scaling formula and the one measured in experiment or, as it

is in our case, calculated from the DMFT solution. In Fig. 13 it is shown how the scaling formula works within the 5% error bar in a large region, for the inflection-point line. This result is qualitatively the same for the other crossover lines. It is important to note that in the case of the instability line (and all the other crossover lines other than the inflection-point line), one is able to improve the quality of scaling by using different exponents $z\nu$ depending on $\text{sgn}(\delta U)$, and that way compensate for the lack of exact mirror symmetry. Also, when only the linear term in $h(y)$ is used, slightly lowering the value of $z\nu$ obtained from the power-law fitting procedure typically broadens the region of validity of such a scaling formula.

In conclusion, the $\log \rho(U)$ inflection-point line is easily observable in experiment and our calculations show that it lies very close to the instability line. The analysis presented here indicates that the quantum critical scaling previously found to hold around the instability line should also be observable around the inflection-point line. We show that the scaling formula that is valid around this line displays almost a perfect mirror symmetry of resistivity curves. In general, mirror symmetry, or "duality," should not be considered a necessary ingredient for a quantum critical scaling. In fact, we find that the scaling is of better quality around the instability line, although it is slightly less symmetric.

It is also very important to examine how the resistivity changes along the separatrix, and our results are presented in Fig. 14. In this crossover region, the resistivity far exceeds the Mott limit and is only weakly dependent on temperature. We find that along the instability line, the resistivity is roughly a linear, increasing function of T. Along the inflection-point line and $\rho(T) = \text{max}$ lines, the resistivity is slowly decreasing. We note that these results, however, must be model specific. Above the critical end point, the resistivity is strongly dependent on U, and a small change in the shape or position of these lines can cause a significant change in the temperature dependences of resistivity presented in Fig. 14.

FIG. 12. (Color online) The derivative of resistivity with respect to U $[\partial \rho(U,T)/\partial U|_{U_{\text{infl}}}]$ along the inflection-point line. Above roughly $2T_c$, it fits well to a power-law curve of exponent -0.95. This can be used to evaluate the value of the scaling formula exponent. At lower temperatures the decrease in resistivity is faster, and the behavior deviates from the power law, and the scaling formula fails at temperatures below $2T_c$.
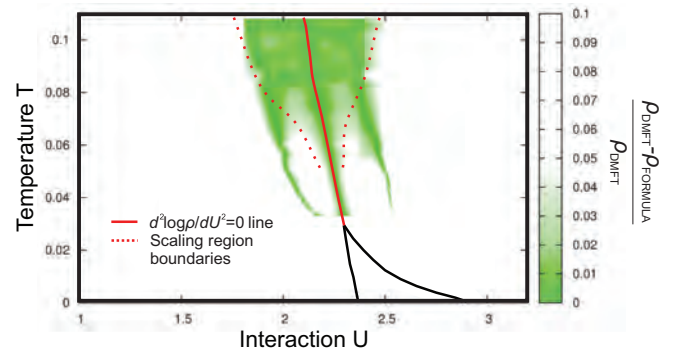
VI. WIDOM LINES

The notion of a crossover line is very general and different physical motivations can be used for its precise definition. The concept of the Widom crossover line is, however, more strict and relies on one fundamental principle.
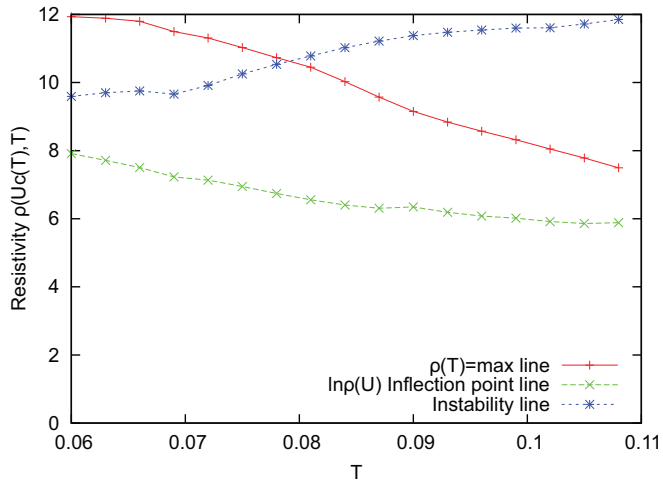
FIG. 14. (Color online) Resistivity (in units of ρ_{Mott}) along the crossover lines is weakly dependent on temperature and much larger than the Mott limit.

The Widom line was originally defined in the context of liquid-gas phase transition,[57] and as the line connecting the maxima of the isobaric specific heat as a function of pressure $(\partial C_p/\partial p = 0)$, above T_c. It was conceived as a logical continuation of the first-order phase transition line to supercritical temperatures. C_p is divergent along the first-order transition line, which directly causes the maxima in C_p present above the critical temperature. This concept is easily generalized to include all the lines that mark features directly caused by nonanalyticities due to a phase transition.[58] As such, a Widom line can be defined for any quantity that exhibits either a divergence or a discontinuity because of a phase transition, and thus a maximum or an inflection point above T_c.

Very recently,[23] in the supercritical region of an argon liquid-gas phase diagram, an unexpected nonanalyticity has been found in sound velocity dispersion curves, precisely at the Widom line. The authors give a new depth and physical meaning to the concept, by observing that there is no single supercritical fluid phase, and that the Widom line actually separates two regimes of fluidlike and gaslike dynamical behavior. This finding makes it clear that the Widom lines should not be exclusively connected with the thermodynamics of the system. The changes in transport that follow certain features in thermodynamic quantities can also be used for making a meaningful and possibly even equivalent definition of the Widom line. The significance of this concept was recognized once more[24,59] in the context of hole-doped high-T_c superconductors, where the characteristic temperature T^* of the pseudogap phase is shown to correspond to the Widom line arising above a first-order transition at critical doping.

In the above sense, we emphasize that the quantum critical scaling observed in our model can also be easily connected with the concept of Widom lines, giving them new physical importance in the context of quantum-phase transitions. One can immediately recognize that the log $\rho(U)$ inflection-point line and the instability line both qualify as generalized Widom lines—they emanate from the critical end point, separate regions of metallic and insulating behavior,

and mark features that are directly caused by nonanalyticities due to the phase transition. The quality of the scaling and the close proximity of these two lines may even indicate a profound connection between them. As the proposed physical concept may well surpass the scope of the Hubbard model and Mott physics, a definition of the instability line can be very useful. Contrary to the inflection-point line, it is based on a purely thermodynamical quantity, i.e., the free energy, and can be defined for an arbitrary model. It does not require the presence of the finite-temperature critical point (which makes a conceptual difference with the work[24,59] on hole-doped cuprates) and can be used to introduce the Widom line concept to exclusively zero temperature quantum-phase transitions.

VII. CONCLUSIONS

In this paper we carefully investigated the finite-temperature crossover behavior around the Mott transition, with the goal to provide both theoretical insight and experimental guidance for the search for quantum criticality in this regime. To obtain quantitative and reliable results that allow direct comparison with experiments, we performed these studies within the framework of single-site dynamical mean-field theory. From the conceptual point of view, this approach offers an immediate advantage—it is physically very clear what kinds of mechanisms and processes are captured by such a theory, and which are not. Most importantly, such an approach explicitly excludes all mechanisms directly or indirectly associated with any ordering tendencies, in agreement with the physical pictures for the Mott transition introduced by early pioneering ideas of Mott and Anderson.

More specifically, we focused on a single band half-filled Hubbard model, which, within DMFT, maps to solving a Kondo-Anderson magnetic impurity model in a self-consistently determined bath. The formation of the heavy Fermi liquid on the metallic side of the Mott transition is described as a formation of a Kondo-like singlet in the ground state, similarly as in the early work of Brinkmann and Rice.[60] In contrast to the Brinkmann-Rice theory, the DMFT approach is able to quantitatively and accurately describe the thermal destruction of such a correlated Fermi liquid, and the resulting coherence-incoherence crossover. The possibility to systematically and quantitatively describe this incoherent regime is especially important to properly characterize the high-temperature crossover behavior above the coexistence dome, where we obtained clear and precise signatures of quantum critical behavior. Our results show remarkable agreement with several experimental systems,[56] but future experiments should provide even more precise tests for our predictions. We expect that close enough to the quantum critical point all quantities should display appropriate scaling behaviors. Our work has, so far, focused mostly on the transport properties, and sufficiently detailed results for thermodynamic and other quantities are not available at this time to permit a scaling analysis. The investigation of these interesting questions is beyond the scope of the present work, and is left for future studies.

We should mention that ideas closely related to ours have also been discussed in a series of papers by Senthil

and collaborators,[61–63] who also seek a description of Mott quantum criticality unrelated to any ordering phenomena. This approach, however, focuses on capturing the possible effects of gapless "spinon" excitations, which may exist on the insulating side of the Mott transition, but only in the presence of sufficient and specific magnetic frustration, preventing the familiar antiferromagnetic order. Because of their gapless nature, they should remain long lived (e.g., well defined) only at the lowest temperatures, inducing long-range spatial correlations in the proposed spin liquid. The corresponding theory, therefore, focuses on long-distance spatial fluctuations, which, as in ordinary critical phenomena, are tackled by appropriate renormalization-group methods. In contrast to our DMFT approach, this theory implicitly disregards the strongly incoherent Kondo-like processes, which may play a dominant role at sufficiently high temperatures.

The key physical question thus remains: What is the crossover temperature T_{nonlocal} below which the nonlocal effects ignored by DMFT become significant? This important question can, in principle, be investigated by computing systematic nonlocal corrections to single-site DMFT, a research direction already investigated by several authors.[31–33,64] The recent work already provides some evidence that for a Hubbard model on a square lattice the nonlocal corrections are very small well above the coexistence dome (at $T \gg T_c$)[64] and are essentially negligible for a frustrated triangular lattice.[33] On the experimental side, the possible role of nonlocal effects such as spinons can be investigated by systematic studies of a series of materials with varying degrees of magnetic frustration. Such studies are accessible in organic Mott systems,[14,15] where $T_c \sim 10$–20 K, while the magnetic frustration may be varied using different crystal lattices. In some cases the magnetic ordering is completely suppressed on the insulating side,[65] while in others it remains.[66] If robust signatures of quantum criticality in transport are observed at $T \gg T_c$ in all of these materials, this finding would provide strong support for the "local quantum criticality" scenario we proposed that is based on the DMFT approach.

[1] V. Dobrosavljević, N. Trivedi, and J. M. Valles, Jr., *Conductor-Insulator Quantum Phase Transitions* (Oxford University Press, Oxford, UK, 2012).

[2] S. Sachdev, *Quantum Phase Transitions* (Cambridge University Press, Cambridge, UK, 1999).

[3] G. R. Stewart, Rev. Mod. Phys. **56**, 755 (1984).

[4] H. v. Löhneysen, A. Rosch, M. Vojta, and P. Wölfle, Rev. Mod. Phys. **79**, 1015 (2007).

[5] S. Sondhi, S. Girvin, J. Carini, and D. Shahar, Rev. Mod. Phys. **69**, 315 (1997).

[6] C. Panagopoulos and V. Dobrosavljević, Phys. Rev. B **72**, 014536 (2005).

[7] L. D. Landau, Sov. Phys. JETP **3**, 920 (1957).

[8] J. C. Slater, Rev. Mod. Phys. **6**, 209 (1934).

[9] J. A. Hertz, Phys. Rev. B **14**, 1165 (1976).

[10] A. J. Millis, Phys. Rev. B **48**, 7183 (1993).

[11] N. F. Mott, Proc. R. Soc. London, Ser. A **197**, 269 (1949).

[12] P. W. Anderson, Rev. Mod. Phys. **50**, 191 (1978).

[13] M. Imada, A. Fujimori, and Y. Tokura, Rev. Mod. Phys. **70**, 1039 (1998).

[14] K. Kanoda and R. Kato, Annu. Rev. Condens. Matter Phys. **2**, 167 (2011).

[15] B. J. Powell and R. H. McKenzie, Rep. Prog. Phys. **74**, 056501 (2011).

[16] A. Georges, G. Kotliar, W. Krauth, and M. J. Rozenberg, Rev. Mod. Phys. **68**, 13 (1996).

[17] H. Terletska, J. Vučičević, D. Tanasković, and V. Dobrosavljević, Phys. Rev. Lett. **107**, 026401 (2011).

[18] M. J. Rozenberg, X. Y. Zhang, and G. Kotliar, Phys. Rev. Lett. **69**, 1236 (1992).

[19] G. Kotliar, E. Lange, and M. J. Rozenberg, Phys. Rev. Lett. **84**, 5180 (2000).

[20] P. Limelette, A. Georges, D. Jérome, P. Wzietek, P. Metcalf, and J. M. Honig, Science **302**, 89 (2003).

[21] F. Kagawa, K. Miyagawa, and K. Kanoda, Nature (London) **436**, 534 (2005).

[22] S. Papanikolaou, R. M. Fernandes, E. Fradkin, P. W. Phillips, J. Schmalian, and R. Sknepnek, Phys. Rev. Lett. **100**, 026408 (2008).

[23] G. G. Simeoni, T. Bryk, F. A. Gorelli, M. Krisch, G. Ruocco, M. Santoro, and T. Scopigno, Nat. Phys. **6**, 503 (2010).

[24] G. Sordi, P. Sémon, and A.-M. S. Tremblay, Sci. Rep. **2**, 547 (2012).

[25] E. Abrahams, S. V. Kravchenko, and M. P. Sarachik, Rev. Mod. Phys. **73**, 251 (2001).

[26] V. Dobrosavljević, E. Abrahams, E. Miranda, and S. Chakravarty, Phys. Rev. Lett. **79**, 455 (1997).

[27] M. M. Radonjić, D. Tanasković, V. Dobrosavljević, K. Haule, and G. Kotliar, Phys. Rev. B **85**, 085133 (2012).

[28] T. Pruschke, D. L. Cox, and M. Jarrell, Phys. Rev. B **47**, 3553 (1993).

[29] M. J. Rozenberg, G. Kotliar, H. Kajueter, G. A. Thomas, D. H. Rapkine, J. M. Honig, and P. Metcalf, Phys. Rev. Lett. **75**, 105 (1995).

[30] K. Haule and G. Kotliar, Phys. Rev. B **76**, 092503 (2007).

[31] A. Georges, Ann. Phys. **523**, 672 (2011).

[32] D. Tanasković, K. Haule, G. Kotliar, and V. Dobrosavljević, Phys. Rev. B **84**, 115105 (2011).

[33] A. Liebsch, H. Ishida, and J. Merino, Phys. Rev. B **79**, 195108 (2009).

[34] J. Kokalj and R. H. McKenzie, Phys. Rev. Lett. **110**, 206402 (2013).

[35] P. Werner, A. Comanac, L. de Medici, M. Troyer, and A. J. Millis, Phys. Rev. Lett. **97**, 076405 (2006).

[36] K. Haule, Phys. Rev. B **75**, 155113 (2007).

[37] M. Jarrell and J. E. Gubernatis, Phys. Rep. **269**, 133 (1996).

[38] N. E. Hussey, K. Takenaka, and H. Takagi, Philos. Mag. **84**, 2847 (2004).

[39] J. Merino and R. H. McKenzie, Phys. Rev. B **61**, 7996 (2000).

[40] R. A. Cooper, Y. Wang, B. Vignolle, O. J. Lipscombe, S. M. Hayden, Y. Tanabe, T. Adachi, Y. Koike, M. Nohara, H. Takagi *et al.*, Science **323**, 603 (2009).

[41] P. Gegenwart, Q. Si, and F. Steglich, Nat. Phys. **4**, 186 (2008).

[42] X. Deng, J. Mravlje, R. Žitko, M. Ferrero, G. Kotliar, and A. Georges, Phys. Rev. Lett. **110**, 086401 (2013).

[43] W. Xu, K. Haule, and G. Kotliar, arXiv:1304.7486.

[44] P. Limelette, P. Wzietek, S. Florens, A. Georges, T. A. Costi, C. Pasquier, D. Jérome, C. Mézière, and P. Batail, Phys. Rev. Lett. **91**, 016401 (2003).

[45] J. Merino, M. Dumm, N. Drichko, M. Dressel, and R. H. McKenzie, Phys. Rev. Lett. **100**, 086404 (2008).

[46] M. M. Radonjić, D. Tanasković, V. Dobrosavljević, and K. Haule, Phys. Rev. B **81**, 075118 (2010).

[47] D. Popović, A. B. Fowler, and S. Washburn, Phys. Rev. Lett. **79**, 1543 (1997).

[48] J. H. Mooij, Phys. Status Solidi A **17**, 521 (1973).

[49] G. Moeller, V. Dobrosavljević, and A. E. Ruckenstein, Phys. Rev. B **59**, 6846 (1999).

[50] P. Sémon and A.-M. S. Tremblay, Phys. Rev. B **85**, 201101(R) (2012).

[51] M. C. O. Aguiar, V. Dobrosavljević, E. Abrahams, and G. Kotliar, Phys. Rev. B **71**, 205115 (2005).

[52] G. Sordi, A. Amaricci, and M. J. Rozenberg, Phys. Rev. B **80**, 035129 (2009).

[53] A. Amaricci, A. Camjayi, K. Haule, G. Kotliar, D. Tanasković, and V. Dobrosavljević, Phys. Rev. B **82**, 155102 (2010).

[54] S. V. Kravchenko, D. Simonian, M. P. Sarachik, W. Mason, and J. E. Furneaux, Phys. Rev. Lett. **77**, 4938 (1996).

[55] V. Guiot, L. Cario, E. Janod, B. Corraze, V. T. Phuoc, M. Rozenberg, P. Stoliar, T. Cren, and D. Roditchev, Nat. Commun. **4**, 1722 (2013).

[56] K. Kanoda (private communication).

[57] B. Widom, in *Phase Transitions and Critical Phenomena*, edited by C. Domb and M. S. Green (Academic, New York, 1972), Vol. 2.

[58] L. Xu, P. Kumar, S. V. Buldyrev, S.-H. Chen, P. H. Poole, F. Sciortino, and H. E. Stanley, Proc. Natl. Acad. Sci. USA **102**, 16558 (2005).

[59] G. Sordi, P. Sémon, K. Haule, and A.-M. S. Tremblay, Phys. Rev. B **87**, 041101 (2013).

[60] W. F. Brinkman and T. M. Rice, Phys. Rev. B **2**, 4302 (1970).

[61] T. Senthil, Phys. Rev. B **78**, 035103 (2008).

[62] T. Senthil, Phys. Rev. B **78**, 045109 (2008).

[63] W. Witczak-Krempa, P. Ghaemi, T. Senthil, and Y. B. Kim, Phys. Rev. B **86**, 245102 (2012).

[64] H. Park, K. Haule, and G. Kotliar, Phys. Rev. Lett. **101**, 186403 (2008).

[65] Y. Shimizu, K. Miyagawa, K. Kanoda, M. Maesato, and G. Saito, Phys. Rev. Lett. **91**, 107001 (2003).

[66] K. Miyagawa, A. Kawamoto, Y. Nakazawa, and K. Kanoda, Phys. Rev. Lett. **75**, 1174 (1995).

Signatures of the spin-phonon coupling in $Fe_{1+y}Te_{1-x}Se_x$ alloys

Z.V. Popović [a,*], N. Lazarević [a], S. Bogdanović [a], M.M. Radonjić [b], D. Tanasković [b], Rongwei Hu [c,1], Hechang Lei [c,2], C. Petrovic [c]

[a] Center for Solid State Physics and New Materials, Institute of Physics Belgrade, University of Belgrade, Pregrevica 118, 11080 Belgrade, Serbia
[b] Scientific Computing Laboratory, Institute of Physics Belgrade, University of Belgrade, Pregrevica 118, 11080 Belgrade, Serbia
[c] Condensed Matter Physics and Materials Science Department, Brookhaven National Laboratory, Upton, New York 11973-5000, USA

ARTICLE INFO

ABSTRACT

Raman scattering spectra of $Fe_{1+y}Te_{1-x}Se_x$ ($x=0$, $y=0.07$; $x=0.1$, $y=0.05$ and $x=0.4$, $y=0.02$) alloys are measured in a temperature range between 20 K and 300 K. The A_{1g} and B_{1g} Raman active modes have been experimentally observed at energies 156 and 198 cm^{-1}, which is in rather good agreement with the lattice dynamics calculation. The antiferromagnetic spin ordering below 70 K in $Fe_{1.07}$Te leaves a fingerprint only in the B_{1g} phonon mode linewidth and energy, whose temperature dependence follows the normalized magnetic susceptibility, indicating the presence of the spin-phonon coupling. The frequency and the linewidth of the A_{1g} mode assume a conventional anharmonic temperature dependence in all measured samples, which is also the case for the B_{1g} mode in the Se doped samples. The linewidth (energy) of the A_{1g} mode decreases (increases) with doping, whereas the opposite is seen for the B_{1g} mode.

1. Introduction

The discovery of a new $LaFeAsO_{1-x}F_x$ superconductor family with $T_c=24$ K spurred the research in the field of iron-based superconductors [1–3]. Among these compounds, iron-chalcogenides have the simplest crystal structure of the PbO type including only Fe and Ch atoms (Ch=S, Se and Te) [4,5]. This structure consists of Fe square planar sheets with Ch ions forming distorted tetrahedra around the Fe ions, analogous to the structure of the FeAs planes in LaFeAsO, $BaFe_2As_2$, and LiFeAs, which are prototypes of the known families of Fe–As based high-T_c super-conductors [6–8]. In fact, these structures match the reported structure of $K_xFe_{2-y}Se_2$ with interspersed FeSe stacked along the c-axis [9,10].

FeTe crystallizes in the tetragonal system of the $P4/nmm$ space group [11]. By lowering the temperature below 70 K, there is a structural transition from the tetragonal to the monoclinic lattice ($P2_1/m$ space group), accompanied by the antiferromagnetic spin ordering [12]. Partial substitution of Te with Se progressively suppresses the magnetic ordering temperature and structural transition

[13], and leads to the superconductivity at low temperatures [11]. The T_c of the $Fe_{1+y}Te_{1-x}Se_x$ system can reach up to 14 K at ambient pressure for $x=0.5$ [14] and 27 K at a pressure of 1.46 GPa [15].

The mechanism for superconductivity in the iron-based materials is still under debate [16]. In particular, the magnetic ordering and spin fluctuations are expected to have an important impact on the phonon dynamics and lead to the increase of the electron–phonon coupling [17] which is, however, still insufficient to explain high T_c in these compounds.

Raman scattering is an excellent tool for a study of the phonon properties of materials and its coupling to the electronic charge and spin excitations. Although the Raman scattering spectra in $Fe_{1+y}Te_{1-x}Se_x$ alloys were analyzed in Refs. [18–21], there are several features in the spectra that have not been fully resolved and understood. Two modes at about 155(± 4) and 199(± 3) cm^{-1} are experimentally observed and assigned as the A_{1g} (Te-ions vibration along the z-axis) and the B_{1g} (Fe-ions vibration along the z-axis) modes, respectively. Calculated phonon frequencies of these modes agree with the experimental data within 10%, see Table 1. The temperature dependence of the phonon mode linewidth and energy of undoped FeTe sample is, however, controversial. Gnezdilov et al. [20] found an increase of the A_{1g} mode linewidth from 28 to 31.4 cm^{-1} by lowering the temperature from 200 K to 5 K. This A_{1g} mode temperature dependence deviates from the anharmonic picture. In addition, they found the A_{1g} mode energy change about the phase transition temperature

* Corresponding author. Tel.: +381 11 3161385.
[1] Present address: Department of Physics, University of Maryland, College Park, MD 20742-4111, USA.
[2] Present address: Frontier Research Center, Tokyo Institute of Technology, 4259 Nagatsuta, Midori, Yokohama 226-8503, Japan.

Table 1
Calculated and experimentally observed values of the Raman active phonon mode energies (in cm^{-1}) of FeTe single crystal in tetragonal (upper part of the table) and monoclinic (lower part of the table) phase.

Tetragonal phase (P4/nmm)

Symmetry	Calculations				Experiment				
	Ref. [18]	Ref. [19]	Ref. [21]	This work	Ref. [18]	Ref. [21]	Ref. [19]	Ref. [20]	This work
E_g^1	59.1	120.1	–	**66.0**	–	–	–	–	–
A_{1g}	140.3	168.4	175	**141.2**	159.1	159.7	158	151	**156**
B_{1g}	215.7	216.4	197.5	**214.7**	196.3	200.5	202	197	**198**
E_g^2	196.9	274.1	–	**215.2**	–	–	–	–	–

Monoclinic phase (P2$_1$/m)

| Symmetry	Calculations		Experiment
	Ref. [20]	This work (nonmagnetic DFT)	This work
A_g^1	86.8	67.8	–
B_g^1	76.8	69.2	–
A_g^2	164.5	141.0	**160.5**
A_g^3	206.4	204.8	**200.2**
B_g^2	214.8	218.7	–
A_g^4	243.6	222.3	–

of $T_N=70$ K. Um et al. [21], on the other hand, found only minor A_{1g} mode broadening (from 19 to 21 cm^{-1} by lowering the temperature to 5 K) without the energy change at the phase transition temperature. The B_{1g} mode hardens and broadens with decreasing temperature down to T_N and then softens and narrows down to 5 K in both papers [20,21]. This feature is, however, supressed in the excess-Fe rich sample Fe$_{1.09}$Te [21]. One additional mode at about 136 cm^{-1} for undoped FeTe sample is observed in Refs. [18,21], which origin is related to the sample decomposition.

In this paper we have measured the Raman scattering spectra of Fe$_{1+y}$Te$_{1-x}$Se$_x$ ($x=0$, $y=0.07$; $x=0.1$, $y=0.05$ and $x=0.4$, $y=0.02$) alloys in the temperature range from room temperature down to 20 K in the spectral range from 90 up to 300 cm^{-1}. In the optical phonon region of FeTe we have observed two optical phonons of the A_{1g} (156 cm^{-1}) and the B_{1g} (198 cm^{-1}) symmetries. The observed frequencies are in rather good agreement with our lattice dynamics calculations. The temperature dependence of the energy and linewidth of the B_{1g} mode in Fe$_{1.07}$Te has a maximum at about T_N and follows the lineshape of the normalized magnetic susceptibility as seen in our magnetization measurements. Doping with Se suppresses T_N and a conventional temperature dependence is observed for the B_{1g} mode. We find that the energy and the linewidth of the A_{1g} mode assume a conventional anharmonic temperature dependence in all three samples. Phonon mode at 136 cm^{-1} is not observed in our samples. In Se doped samples the A_{1g} mode hardens and narrows, whereas the B_{1g} mode softens and broadens. These features cannot be simply explained just as a consequence of the substitution of Te by lighter and smaller Se ions and the disorder effect.

2. Experiment and numerical method

Single crystals of Fe$_{1+y}$Te$_{1-x}$Se$_x$ ($x=0$, $y=0.07$; $x=0.1$, $y=0.05$ and $x=0.4$, $y=0.02$) alloys were grown using self-flux method, as described in Ref. [22]. Raman scattering measurements were performed on freshly cleaved (001)-oriented samples using JY T64000 and Tri-Vista 557 Raman systems in backscattering micro-Raman configuration. The 514.5 nm line of an Ar$^+$/Kr$^+$ mixed gas laser was used as an excitation source. The corresponding excitation power density was less than 0.2 kW/cm^2. Low temperature measurements were performed using KONTI CryoVac continuous flow cryostat with 0.5 mm thick window. Magnetization measurements were carried out in Quantum Design MPMS-XL5 system.

We have calculated the lattice dynamics of both FeTe phases: the room temperature phase (tetragonal symmetry) and the low temperature phase (monoclinic symmetry). The lattice dynamics calculations are performed within the density functional perturbation theory (DFPT) [23] as implemented in the QUANTUM ESPRESSO package [24] using the generalized gradient approximation with the PW91 exchange-correlation functional which is used to obtain ultra-soft pseudo-potentials. Iron (tellurium) pseudo-potential includes 3 s^2 4 s^2 3p^6 4p^0 3d^6 (5 s^2 5p^4 4d^{10}) electron states for the valence electrons. The Brillouin zone is sampled with a Monkhorst-Pack $16 \times 16 \times 10$ **k**-space mesh for higher-symmetry phase ($P4/nmm$ space group) and $16 \times 16 \times 8$ **k**-space mesh for lower-symmetry phase ($P2_1$/m space group). Unit cell is constructed using experimental values of the lattices parameters [25] ($P4/nmm$ phase: $a=0.38219$ nm, $c=0.62851$ nm; $P2_1$/m phase: $a=0.38312$ nm, $b=0.37830$ nm, $c=0.62643$ nm and $\beta=89.17$degr). The Energy cutoffs for the wave functions and the electron densities are 64 Ry and 762 Ry, respectively, which are the highest suggested radii for the chosen pseudo-potentials. We have used Gaussian smearing of 0.001 Ry.
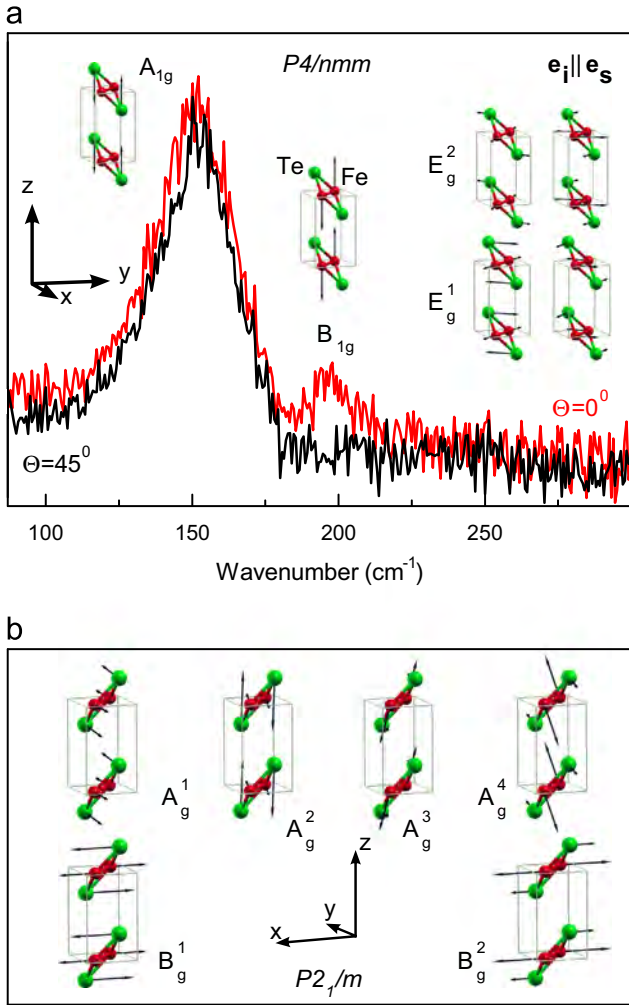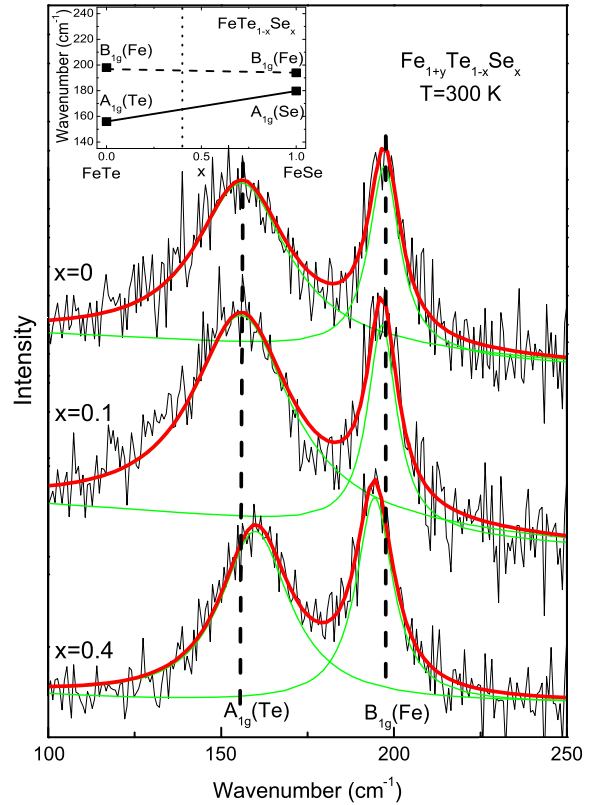
Fig. 1. (Color online) (a) Room temperature polarized Raman scattering spectra of the FeTe crystal (the tetragonal phase, space group *P4/nmm*) measured for different sample orientations together with normal modes. (b) The normal modes of lattice vibrations of the low temperature monoclinic phase of FeTe (the *P2₁/m* space group). The length of the arrows is proportional to the square roots of the vibration amplitudes.

Fig. 2. (Color online) The unpolarized Raman scattering spectra of the (001)-oriented $Fe_{1+y}Te_{1-x}Se_x$ ($x=0$, $y=0.07$; $x=0.1$, $y=0.05$ and $x=0.4$, $y=0.02$) single crystals measured at room temperature. Red lines are calculated spectra obtained by Lorentzian line (green lines) profile fit. Inset: Experimental values (■) of the A_{1g} and B_{1g} modes of $FeTe_{1-x}Se_x$ for $x=0$ (this work) and $x=1$ (Ref. [33]). Solid and dashed lines represent linear fit between mode energies of parent materials.

3. Results and discussion

The results of the lattice dynamics calculations, together with the experimental data are presented in Table 1. Normal modes of Raman active phonons of both FeTe phases are given in Fig. 1.

Fig. 1(a) shows the polarized Raman scattering spectra of $Fe_{1.07}Te$ crystal measured from the (001) plane at room temperature in the spectral range from 90 to 300 cm^{-1}. Two peaks are observed at frequencies of about 156 and 198 cm^{-1}. According to the selection rules, when Raman scattering spectrum is measured from the (001) plane of the sample, only the A_{1g} and the B_{1g} modes can be observed. In the parallel polarization configuration ($e_l \parallel e_s$), the A_{1g} could be seen for an arbitrary orientation of the sample, whereas the B_{1g} mode vanishes for the sample orientation in which $e_s \parallel \langle 110 \rangle$. By rotating the sample, we were able to find the orientation in which the peak around 198 cm^{-1} vanishes. Consequently, this peak is assigned as the B_{1g} symmetry mode, whereas the peak at around 156 cm^{-1} is assigned as the A_{1g} mode. This is in agreement with the previous assignment [18–21] and our lattice dynamics calculation (Table 1). The additional mode at about 136 cm^{-1}, as found in Ref. [21] for nearly stoichiometric $Fe_{1.02}Te$ sample, has not been observed in the spectra.

Fig. 2 shows the unpolarized Raman scattering spectra of $Fe_{1+y}Te_{1-x}Se_x$ ($x=0$, $y=0.07$; $x=0.1$, $y=0.05$ and $x=0.4$, $y=0.02$) single crystals measured at room temperature. Replacing Te with Se ions leads to the A_{1g} (the B_{1g}) mode hardening (softening), which is indicated in Fig. 2 where the vertical dashed lines denote the energies for the undoped sample. A significant reduction (for about 10 cm^{-1}) of the A_{1g} mode linewidth, as well as an increase of the B_{1g} mode linewidth (for about 2.4 cm^{-1}) is found in the $Fe_{1.02}Te_{0.6}Se_{0.4}$ sample. The A_{1g} mode hardening is a consequence of the replacement of heavier Te ions with lighter Se ions (the mass effect) and the unit-cell contraction (*c*-axis reduction) upon doping [26]. On the other hand, an introduction of substitutional impurities (disorder) should in general induce the linewidth increase in doped compounds [27], as it was observed for the B_{1g} mode. In the case of the A_{1g} mode, the phonon mode linewidth decrease can be related to the decrease of the electron–phonon interaction upon doping [28]. This assumption is also supported by the DFT calculations of the electron–phonon coupling constant λ in the nonmagnetic solution, which shows a significant decrease of λ as the Te atoms are replaced with the Se atoms ($\lambda(FeTe) = 0.30$ [29], $\lambda(FeTe_{0.5}Se_{0.5}) = 0.22$ [30], and $\lambda(FeSe) = 0.17$ [31]). At this point we can not exclude the possibility that excess Fe ions may play role in the behaviour of the A_{1g} mode. The excess Fe ions are located within Te layer [32] and may produce qualitatively different effects from those induced by the substitutional disorder.

In the case of the B_{1g} mode (Fe ions vibrations) we expected the mode hardening due to the unit cell compression with doping by the Se atoms. Instead of the hardening, we observe the mode softening in the $Fe_{1.02}Te_{0.6}Se_{0.4}$ sample, which is in accordance

with expectations for $FeTe_{1-x}Se_x$ solid solution based on a linear fit of the mode energy values of parent crystals FeTe (this work) and FeSe [33], see the inset of Fig. 2. However, one should also have in mind that the change in the excess iron concentration (decrease from $y = 0.07$ for the undoped to $y = 0.02$ for the 40% Se doped sample) may have significant impact on the B_{1g} mode energy [21].

Upon cooling, no additional Raman lines have been observed although the crystal structure and the crystal symmetry of FeTe are changed at $T < T_N$. By comparing the calculated phonon energies in both phases (see Table 1) it can be seen that the phonon energies do not differ substantially. In fact, the $E_g^1(E_g^2)$ mode of the tetragonal phase splits into $A_g^1/B_g^1(A_g^4/B_g^2)$ doublets of monoclinic symmetry, which appear at energies very close to the mode energies of tetragonal phase. In the case of the A_{1g} mode there is virtually no energy change between the A_{1g} mode of the tetragonal phase and the A_g^2 mode of the monoclinic phase (see Table 1). The B_{1g} mode of the tetragonal phase changes energy (softens) and symmetry (becomes A_g symmetry one) at the phase transition temperature. The change of the symmetry of this mode in the low temperature phase does not influence the low temperature Raman spectra because the energy of this mode (A_g^3) is far enough (40 cm^{-1}) from the (A_g^2) mode, preventing the phonon mode coupling between them [34]. The lattice vibration normal modes of the low temperature phase are given in Fig. 1(b).

Fig. 3 shows the energy and the linewidth temperature dependence for the A_{1g} and the B_{1g} modes of the $Fe_{1.07}Te$ sample, which are obtained from the Raman spectra measured at various temperatures using the Lorentzian profile fit. Solid and dashed lines in Fig. 3(c,d) are calculated curves obtained using the well known anharmonicity effect formula, [35,27] which takes into account three-phonon processes for the temperature dependent change of the phonon energy and linewidth:

$$\omega(T) = \omega_0 - C[1 + 2/(e^x - 1)], \tag{1}$$

$$\Gamma(T) = \Gamma_0 + A[1 + 2/(e^x - 1)], \tag{2}$$

where ω_0 (Γ_0) is the temperature independent energy (intrinsic linewidth), C (A) is the anharmonic constant and $x = \hbar\omega_0/(2k_BT)$. The best fit parameters are indicated in Fig. 3(c,d). A rather good agreement between the experimental data and fitted curves for the A_{1g} mode is observed in the whole temperature range (above and below $T_N = 70$ K). Large value of Γ_0 parameter in comparison to the anharmonic constant ($24.5 \gg 1$ cm^{-1}) also suggest the importance of the electron–phonon interaction for this mode [36] or the orbital degrees of freedom of Fe ions [20].

Upon cooling, the B_{1g} mode of the undoped sample shows pronounced broadening down to T_N, when it suddenly narrows (see Fig. 3(b)). This deviation from the standard anharmonic picture suggests the presence of additional scattering process. The energy and broadening temperature change of the B_{1g} mode closely follows the normalized magnetic susceptibility curve, as can be seen in Fig. 4, indicating that spin-phonon coupling leaves a
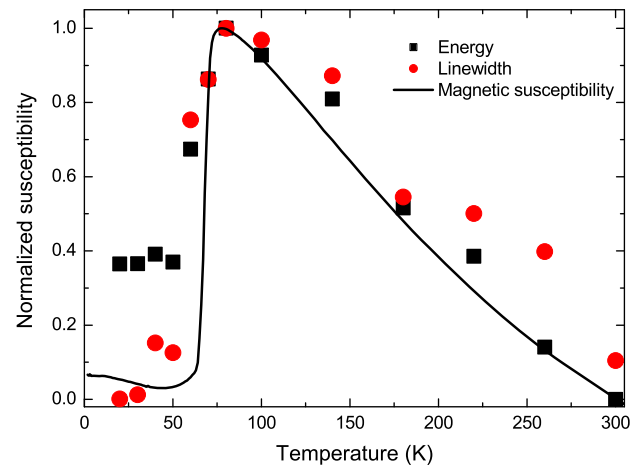

Fig. 4. (Color online) Temperature dependence of the normalized frequency and linewidth of the B_{1g} mode together with the normalized magnetic susceptibility (solid line) of $Fe_{1.07}Te$ single crystal.
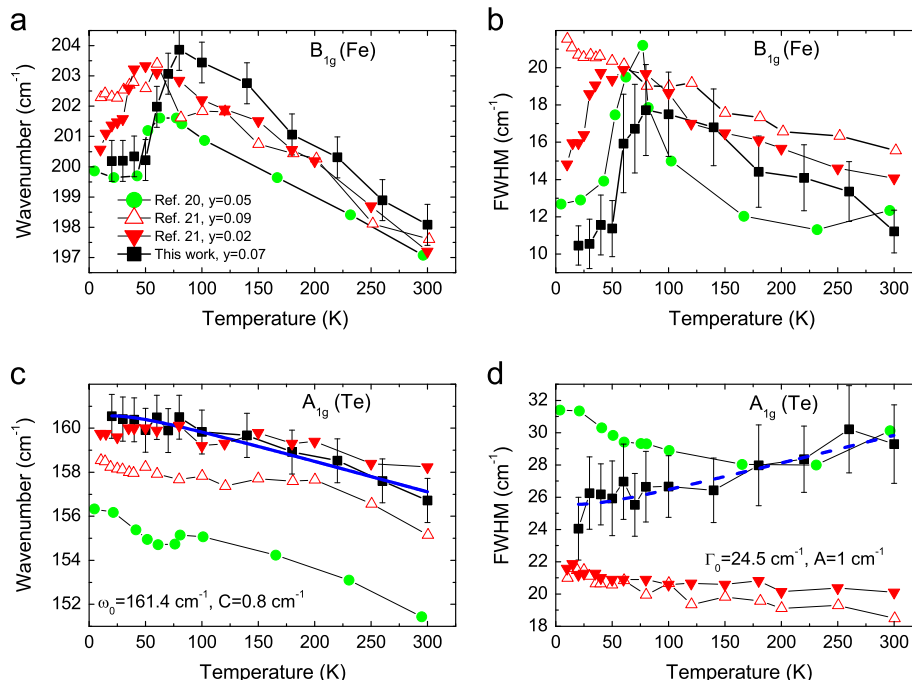

Fig. 3. (Color online) The phonon energy and the linewidth temperature dependence of the A_{1g} (c,d) and the B_{1g} (a,b) modes of $Fe_{1+y}Te$ single crystal together with existing literature data [20,21]. The solid and the dashed lines represent calculated curves using Eqs. (1) and (2), respectively.

fingerprint in the phonon dynamics of FeTe. This is to be expected because the B_{1g} mode represents vibrations of Fe-ions which carry the magnetic moments. Softening of the B_{1g} mode below T_N is a consequence of the antiferromagnetic ordering and structural change (see Table 1).

In the case of the $Fe_{1.02}Te_{0.6}Se_{0.4}$ sample, the temperature dependencies of the phonon mode energy and linewidth follow the standard anharmonic picture for both vibrational modes. The absence of the B_{1g} mode softening in this sample at temperatures below 70 K is a consequence of the suppression of antiferromagnetic ordering with doping [13].

Finally, in Fig. 3 we compared energy and linewidth vs temperature dependence of the A_{1g} and B_{1g} modes with previously published results [20,21]. The B_{1g} mode energy and linewidth (Fig. 3(a,b)) show no substantial difference from our results (taking into account that error bar in our case is $\pm 2\ cm^{-1}$; in Ref. [21] is $\pm 4\ cm^{-1}$) except of the position of *FWHM(T)* curve maximum, which is related to the sample composition, *i.e.*, T_N. The A_{1g} mode energy temperature dependencies follow the same trend (mode hardening) by the temperature lowering in Refs. [20,21] and in this work. The main difference is the linewidth change by the temperature lowering (Fig. 3(d)). We have shown that the linewidth narrows by temperature lowering, but an opposite trend is found in Refs. [20,21]. Our finding is in accordance with an anharmonic picture.

4. Conclusion

In summary, we have measured the Raman scattering spectra of the $Fe_{1+y}Te_{1-x}Se_x$ ($x=0$, $y=0.07$; $x=0.1$, $y=0.05$ and $x=0.4$, $y=0.02$) alloys at various temperatures. Two out of four Raman-active modes predicted by the factor-group analysis have been experimentally observed and assigned. Energies of these modes are in rather good agreement with our lattice dynamics calculations. The main focus of our work was the temperature and doping dependence of the phonon energies and linewidths, whose features are, to some extent, contradictory in previous works. We have shown that the A_{1g} mode (corresponding to the Te ions vibration along the *z*-axis) follows the standard anharmonic temperature dependence (which originates in the phonon–phonon interaction) both in the doped and the undoped samples. The width of the A_{1g} mode at room temperature is significantly reduced in the doped samples. In the case of the B_{1g} mode, the phonon frequency and the linewidth closely follow the magnetic susceptibility temperature dependence, indicating the presence of the spin-phonon coupling in the undoped $Fe_{1.07}Te$ sample. The antiferromagnetic ordering is suppressed by doping, and $Fe_{1.02}Te_{0.6}Se_{0.4}$ sample follows a conventional temperature dependence in both phonon modes.

Acknowledgments

References

[1] H. Okada, Y. Takahashi, K. Igawa, K. Arii, H. Takahashi, T. Watanabe, H. Yanagi, Y. Kamihara, T. Kamiya, M. Hirano, H. Hosono, S. Nakano, T. Kikegawa, J. Phys. Soc. Jpn 77SC (Suppl. C) (2008) S119–S120.
[2] M.H. Yoichi Kamihara, Takumi Watanabe, H. Hosono, J. Am. Chem. Soc. 130 (2008) 3296 130 (11) (2008) 3296–3297.
[3] G.R. Stewart, Rev. Mod. Phys. 83 (2011) 1589–1652.
[4] F.-C. Hsu, J.-Y. Luo, K.-W. Yeh, T.-K. Chen, T.-W. Huang, P.M. Wu, Y.-C. Lee, Y.-L. Huang, Y.-Y. Chu, D.-C. Yan, M.-K. Wu, Proc. Natl. Acad. Sci. U.S.A. 105 (38) (2008) 14262–14264.
[5] Y. Mizuguchi, F. Tomioka, S. Tsuda, T. Yamaguchi, Y. Takano, Appl. Phys. Lett. 94 (1) (2009) 012503.
[6] M. Rotter, M. Tegel, D. Johrendt, I. Schellenberg, W. Hermes, R. Pöttgen, Phys. Rev. B 78 (2008) 020503.
[7] M. Rotter, M. Tegel, D. Johrendt, Phys. Rev. Lett. 101 (2008) 107006.
[8] J.H. Tapp, Z. Tang, B. Lv, K. Sasmal, B. Lorenz, P.C.W. Chu, A.M. Guloy, Phys. Rev. B 78 (2008) 060505.
[9] J. Guo, S. Jin, G. Wang, S. Wang, K. Zhu, T. Zhou, M. He, X. Chen, Phys. Rev. B 82 (2010) 180520.
[10] N. Lazarević, M. Abeykoon, P.W. Stephens, H. Lei, E.S. Bozin, C. Petrovic, Z. V. Popović, Phys. Rev. B 86 (2012) 054503.
[11] K.-W. Yeh, T.-W. Huang, Y. lin Huang, T.-K. Chen, F.-C. Hsu, P.M. Wu, Y.-C. Lee, Y.-Y. Chu, C.-L. Chen, J.-Y. Luo, D.-C. Yan, M.-K. Wu, Europhys. Lett. 84 (3) 37002.
[12] S. Li, C. delaCruz, Q. Huang, Y. Chen, J.W. Lynn, J. Hu, Y.-L. Huang, F.-C. Hsu, K.-W. Yeh, M.-K. Wu, P. Dai, Phys. Rev. B 79 (2009) 054503.
[13] C.-Y. Moon, H.J. Choi, Phys. Rev. Lett. 104 (2010) 057003.
[14] M.H. Fang, H.M. Pham, B. Qian, T.J. Liu, E.K. Vehstedt, Y. Liu, L. Spinu, Z.Q. Mao, Phys. Rev. B 78 (2008) 224503.
[15] Y. Mizuguchi, F. Tomioka, S. Tsuda, T. Yamaguchi, Y. Takano, Appl. Phys. Lett. 93 (15) (2008) 152505.
[16] I.I. Mazin, Nature 464 (2010) 183–186.
[17] T. Bazhirov, M.L. Cohen, Phys. Rev. B 86 (2012) 134517.
[18] T.-L. Xia, D. Hou, S.C. Zhao, A.M. Zhang, G.F. Chen, J.L. Luo, N.L. Wang, J.H. Wei, Z.-Y. Lu, Q.M. Zhang, Phys. Rev. B 79 (2009) 140510.
[19] K. Okazaki, S. Sugai, S. Niitaka, H. Takagi, Phys. Rev. B 83 (2011) 035103.
[20] V. Gnezdilov, Y. Pashkevich, P. Lemmens, A. Gusev, K. Lamonova, T. Shevtsova, I. Vitebskiy, O. Afanasiev, S. Gnatchenko, V. Tsurkan, J. Deisenhofer, A. Loidl, Phys. Rev. B 83 (2011) 245127.
[21] Y.J. Um, A. Subedi, P. Toulemonde, A.Y. Ganin, L. Boeri, M. Rahlenbeck, Y. Liu, C. T. Lin, S.J.E. Carlsson, A. Sulpice, M.J. Rosseinsky, B. Keimer, M. Le Tacon, Phys. Rev. B 85 (2012) 064519.
[22] H. Lei, R. Hu, E.S. Choi, J.B. Warren, C. Petrovic, Phys. Rev. B 81 (2010) 094518.
[23] S. Baroni, S. de Gironcoli, A. Dal Corso, P. Giannozzi, Rev. Mod. Phys. 73 (2001) 515–562.
[24] P. Giannozzi, S. Baroni, N. Bonini, M. Calandra, R. Car, C. Cavazzoni, D. Ceresoli, G.L. Chiarotti, M. Cococcioni, I. Dabo, A.D. Corso, S. de Gironcoli, S. Fabris, G. Fratesi, R. Gebauer, U. Gerstmann, C. Gougoussis, A. Kokalj, M. Lazzeri, L. Martin-Samos, N. Marzari, F. Mauri, R. Mazzarello, S. Paolini, A. Pasquarello, L. Paulatto, C. Sbraccia, S. Scandolo, G. Sclauzero, A.P. Seitsonen, A. Smogunov, P. Umari, R.M. Wentzcovitch, J. Phys. Condens. Matter 21 (39) 395502.
[25] A. Martinelli, A. Palenzona, M. Tropeano, C. Ferdeghini, M. Putti, M. R. Cimberle, T.D. Nguyen, M. Affronte, C. Ritter, Phys. Rev. B 81 (2010) 094115.
[26] K. Horigane, H. Hiraka, K. Ohoyama, J. Phys. Soc. Jpn 78 (7) (2009) 074718.
[27] M. Cardona, T. Ruf, Solid State Commun. 117 (3) (2001) 201–212.
[28] N. Lazarević, Z.V. Popović, R. Hu, C. Petrovic, Phys. Rev. B 81 (2010) 144302.
[29] J. Li, G. Huang, X. Zhu, Physica C 492 (2013) 152–157.
[30] J. Li, G. Huang, Solid State Commun. 159 (2013) 45–48.
[31] A. Subedi, L. Zhang, D.J. Singh, M.H. Du, Phys. Rev. B 78 (2008) 134514.
[32] W. Bao, Y. Qiu, Q. Huang, M.A. Green, P. Zajdel, M.R. Fitzsimmons, M. Zhernenkov, S. Chang, M. Fang, B. Qian, E.K. Vehstedt, J. Yang, H. M. Pham, L. Spinu, Z.Q. Mao, Phys. Rev. Lett. 102 (2009) 247001.
[33] V. Gnezdilov, Y.G. Pashkevich, P. Lemmens, D. Wulferding, T. Shevtsova, A. Gusev, D. Chareev, A. Vasiliev, Phys. Rev. B 87 (2013) 144508.
[34] N. Lazarević, M.M. Radonjić, D. Tanasković, R. Hu, C. Petrovic, Z.V. Popović, J. Phys. Condens. Matter 24 (25) 255402.
[35] M. Balkanski, R.F. Wallis, E. Haro, Phys. Rev. B 28 (1983) 1928–1934.
[36] A.P. Litvinchuk, B. Lv, C.W. Chu, Phys. Rev. B 84 (2011) 092504.

Intermolecular and low-frequency intramolecular Raman scattering study of racemic ibuprofen

J.J. Lazarević [a,*], S. Uskoković-Marković [b], M. Jelikić-Stankov [b], M. Radonjić [c], D. Tanasković [c], N. Lazarević [d], Z.V. Popović [d]

[a] Innovation center, Faculty of Technology and Metallurgy, University of Belgrade, Serbia
[b] Faculty of Pharmacy, University of Belgrade, Serbia
[c] Scientific Computing Laboratory, Institute of Physics Belgrade, University of Belgrade, Pregrevica 118, 11080 Belgrade, Serbia
[d] Center for Solid State Physics and New Materials, Institute of Physics Belgrade, University of Belgrade, Pregrevica 118, 11080 Belgrade, Serbia

HIGHLIGHTS

- Racemic ibuprofen Raman scattering spectra was measured at room and low temperatures.
- First principle calculations of the ibubrofen molecule dynamics properties were performed.
- Correlations between the molecule and crystal vibrations were established.

GRAPHICAL ABSTRACT
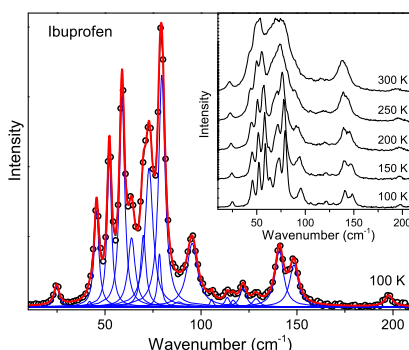
ARTICLE INFO

ABSTRACT

We report the low-temperature Raman scattering study of racemic ibuprofen. Detailed analysis of the racemic ibuprofen crystal symmetry, related to the vibrational properties of the system, has been presented. The first principle calculations of a single ibuprofen molecule dynamical properties are compered with experimental data. Nineteen, out of 26 modes expected for the spectral region below 200 cm^{-1}, have been observed.

© 2014 Elsevier B.V. All rights reserved.

Introduction

Organic molecular crystals are characterized by a pronounced contrast between the strong covalent intramolecular interactions and the weak van der Waals intermolecular attractions or the hydrogen bonding association. Whereas the intermolecular interactions are responsible for specific physical properties of the molecular compounds, the strong covalent bonds maintain the internal molecular structure. The vibrations within the molecular crystals can be of two types: internal vibrations (within the molecule) and external vibrations (between the molecules). Raman spectroscopy allows us to analyze these different kinds of motions. Consequently, external vibrations are closely related to the specific

---

* Corresponding author.
E-mail address: jasmina.lazarevic@hotmail.com (J.J. Lazarević).

physical properties of the molecular compounds, providing information on the stability of the physical state at molecular levels, and the nature of solid state transformations. Raman spectroscopy provides direct information on the phase transition from *in situ* investigations on molecular compounds exposed to a wide variety of environmental stress, since no special sample preparation is required. Thereby, Raman spectroscopy has important applications in the field of pharmaceutical sciences.

Ibuprofen (IBP), 2-(4-isobutylphenyl)propanoic acid, is a widely used non-steroidal anti-inflammatory drug having analgesic and antipyretic activities. It can be found in two enantiomeric forms: S(+)-IBP and R(−)-IBP, where the S-IBP is the pharmacologically active form. In fact, the commercial drug is the racemic mixture of these two forms and it appears at ambient temperature as a white crystalline powder. The ibuprofen racemic mixture in its crystalline phase I ((RS)-IBP) is stable up to the melting point $T_{mI} = 349$ K [1]. Recently, the existence of the second solid state phase of the racemic ibuprofen has been reported [2,3].

Although the information about the low-energy external vibrations is crucial for the identification of different solid state phases, previous Raman scattering and theoretical studies on (RS)-IBP vibration properties have been focused mainly on the internal (molecular) vibrations at energies larger than 200 cm^{-1} [4–7]. To the best of our knowledge, the low energy region of the (RS)-IBP Raman spectra has been reported only by Hédoux et al. [3]. The authors reported only three peak structures at about 20 cm^{-1}, 50 cm^{-1} and 80 cm^{-1} and assigned them as the phonon modes, whereas symmetry properties of the (RS)-IBP crystal structure suggest a large number of the external vibrations. No detailed analysis of the spectra in terms of the specific symmetry properties of (RS)-IBP has been performed. In this paper, detailed study of the low energy region of the (RS)-IBP Raman scattering spectra at various temperatures is presented. Vibrational properties of the (RS)-IBP is discussed in terms of the peculiarities of the (RS)-IBP crystal structure. Temperature dependent spectra are analysed by means of the anharmonicity model.

Experiment

Raman scattering measurements were performed using the Jobin Yvon T64000 Raman systems in backscattering micro-Raman configuration with 1800/1800/1800 grooves/mm gratings in subtractive regime. The external and second intermediate slits were set to 100 μm, whereas lateral slits were adjusted so the minimum noise is achieved. The 514.5 nm line of a mixed Ar$^+$/Kr$^+$ gas laser was used as an excitation source. The corresponding excitation power density was less than 0.3 kW/cm^2. Temperature dependent measurements were performed using LINKAM THMS 600 heating/cooling stage. All the Raman scattering spectra are corrected by the corresponding Bose factor $n(T)$.

Results and discussion

The structure of a single IBP molecule is presented in Fig. 1. Due to the low symmetry, all 93 A modes representing the vibrations of a single IBP molecule, are both infrared and Raman active. Commercially, IBP is found as a racemate in the form of the molecular crystals. (RS)-IBP crystalizes in the monoclinic type of structure with four ($Z = 4$) molecular units per unit cell [8–12]. The (RS)-IBP, R(−)- and S(+)-IBP enantiomers form a cyclic dimer across hydrogen bonds of their carboxylic groups through the center of inversion. This leads to an increase of a symmetry from the $P2_1$ for the S-IBP to $P2_1/c$ (C_{2h}^5) in the case of (RS)-IBP. The main implication of the inversion symmetry presence in the crystal is the separation of the Raman and infrared active modes.

In general, for the molecular crystals, two types of vibrations could be distinguished: external vibrations (vibrations between the molecules) and internal vibrations (vibrations within the molecules). Depending on the type of the motion, external vibrations could be translations (representing the translational motions of the molecules) or librations (representing the rotational motions of the molecules).

In order to determine the vibrational structure of the (RS)-IBP, the correlation method was applied [13]. By correlating the translational and the rotational modes of a single molecule to the site symmetry and the crystal symmetry (see Fig. 2), the external vibrational mode distribution at the Brillouin zone center (Γ point) was obtained:

$$\Gamma_{\text{Raman}} = 6A_g + 6B_g,$$
$$\Gamma_{\text{infrared}} = 5A_u + 4B_u,$$
$$\Gamma_{\text{acoustic}} = A_u + 2B_u$$

Thus one can expect 12 external modes to be observed in the Raman scattering experiment.

In the same manner, by establishing the correlation between the symmetry of the molecular vibrations, the site symmetry and the symmetry of the crystal through the peculiarities of the (RS)-IBP crystal structure (see Fig. 2), 186 internal modes ($93A_g + 93B_g$) are expected to be observed in the Raman scattering experiment. This substantial increase in the number of the observable vibrational modes for the molecular crystal in comparison to an isolated molecule is a consequence of the interactions between the molecules. Having in mind that the molecules are connected with very weak van der Waals interactions, the internal modes will usually appear as a $A_g - B_g$ doublets around the energies that correspond to the energies of the single molecule vibrations. Furthermore, the splitting within the doublets is rather small and thus they are typically observed as a single feature in the Raman scattering spectra.

Nature of the intermolecular bonds suggests that all external vibrations are expected to be found in the low energy part of the Raman spectra. However, ibuprofen is a highly flexible molecule, and thus one can also expect a number of low-lying internal doublets, each arising from a mode of the isolated molecule (see Fig. 2).

In order to determine the vibrational spectra of a single molecule, we perform first principle calculations of the IBP molecule dynamics properties, within density functional perturbation theory [14] as implemented in the QUANTUM ESPRESSO package [15]. We used scalar relativistic ultra-soft pseudopotentials, generated within general gradient approximations with Perdew–Burke–Ernzerhof exchange correlation functional. Structural parameters are relaxed so that total force acting on each atom is less than 10^{-4} Ry/a.u. In order to study the isolated molecule, the unit cell is made to be several times larger than the size of the molecule itself and all calculations are performed at the center of the Brillouin zone. Energy cut-offs for the wave functions and the electron densities are 60 Ry and 800 Ry respectively, determined to ensure a stable convergence. Calculated vibrational mode energies of a single S-IBP molecule in the low energy region are summarized in Table 1. Corresponding displacement patterns are presented in Fig. 1. We have also performed calculations on R-IBP and there are no significant changes in phonon energies between these two forms. Obtained energies of the vibrational modes at energies larger than 200 cm^{-1} are in good agreement with previously published data [4–7] and with our Raman (RS)-IBP measurements presented in Fig. 3(a).

According to the symmetry considerations for the (RS)-IBP crystal structure, 12 Raman active modes originating from the external vibrations are expected. From the single IBP molecule numerical calculations, we have found that in the spectral region under
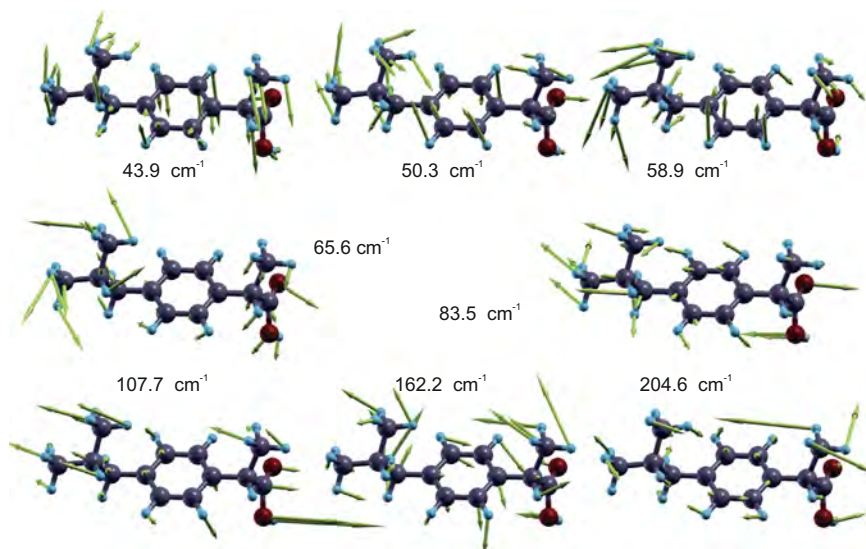
Fig. 1. Displacement patterns of the low energy Raman active vibrational modes of (RS)-IBP. The lengths of the arrows are proportional to the vibration amplitudes.
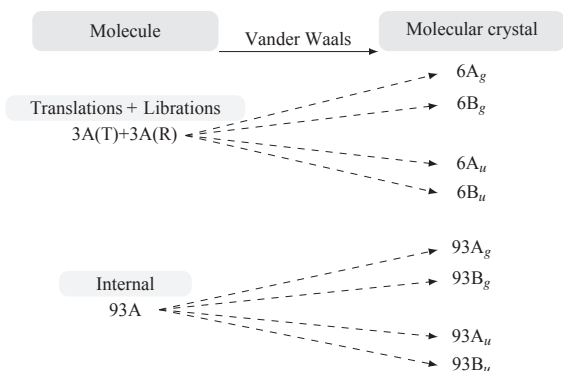

Fig. 2. Correlation diagram betwen the molecular and crystal vibrations.

Table 1
Calculated vibrational mode energies, symmetry and activity for a single S-IBP molecule in the low energy region.

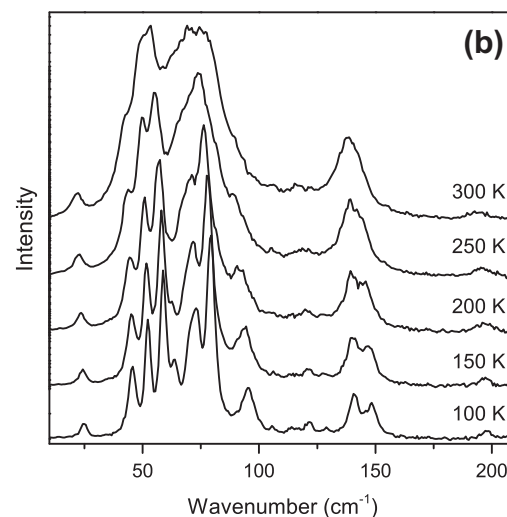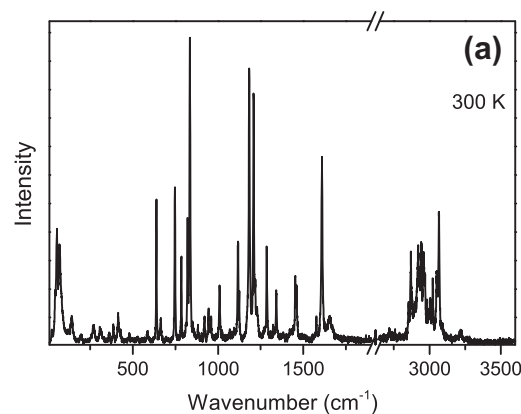| Symmetry	Calculated energy (cm^{-1})	Activity
A	43.9	IR + R
A	50.3	IR + R
A	58.9	IR + R
A	65.6	IR + R
A	83.5	IR + R
A	107.7	IR + R
A	162.2	IR + R

Fig. 3. (a) Wide range Raman scattering spectra of the (RS)-Ibuprofen. (b) The low energy region Raman scattering spectra of (RS)-Ibuprofen measured at various temperatures.

$200\ cm^{-1}$ 7 intramolecular doublets are expected, each arising from a mode of the isolated molecule. This give rise to the total of 26 Raman active modes to be observed in the spectral region under $200\ cm^{-1}$. The presence of both the internal and the external vibrational modes in the same spectral region indicates the strong mixing between the two types of vibrational modes [16–18].

Fig. 3(b) shows the low energy region Raman scattering spectra of (RS)-IBP measured at various temperatures. As one can see, at room temperature only four structures at about $21\ cm^{-1}$, $52\ cm^{-1}$, $74\ cm^{-1}$ and $138\ cm^{-1}$ can be clearly distinguished. This is in agreement with the findings of Hédoux et al. [3], where the authors observed three peaks at around $20\ cm^{-1}$, $50\ cm^{-1}$ and $80\ cm^{-1}$ and assigned them as phonon peaks. However, as already mentioned, symmetry of the system predicts a much larger number of peaks and thus we should consider these structure to be multi-peak structures. In order to analyse these multi-peaks structure, we performed the low temperature measurements. In

general, with decreasing temperature linewidth of each mode decreases due to the anharmonicity effects [19]. Consequently, a large number of modes become observable at 100 K (see Fig. 3(b)).

Fig. 4 shows unpolarized Raman scattering spectra of (RS)-Ibuprofen measured at 100 K. Solid lines represent deconvoluted spectra obtained by least-squares fitting with multiple Lorentzian line shapes. We were able to observe 19 out of 26 modes predicted by structural considerations. Energies of the observed modes are summarized in Fig. 4. Whereas all the modes below 140 cm^{-1} are expected to have mixed character to some extent, all additional modes above 140 cm^{-1} can be safely assigned as an intramolecular doublets.

Fig. 5(a) shows Raman scattering spectra of the peak structure around 145 cm^{-1} of (RS)-IBP measured at various temperatures. Although, only a single mode is predicted by the numerical calculation for the IBP molecule in this spectral region (see Table 1), two modes are clearly observed at low temperatures. Thus, this structure can be assigned as an $A_g - B_g$ doublet, as suggested by symmetry analysis (see Fig. 2). Energy separation within the doublet is related to the interaction between the molecules and the crystal structure of the sample. With increasing temperature the modes are shifted toward the lower wavenumbers and become progressively broader in accordance with anharmonicity effects (see Fig. 5(b)).

In general, temperature dependence of the vibrational mode energy, $\Omega(T)$ is usually governed by anharmonic effects. If, for the sake of simplicity, we assume a symmetric decay of the low lying optical vibration into two acoustic vibrations, the anharmonicity induced energy temperature dependence can be described with [19,20]:

$$\Omega(T) = \Omega_0 - C\left(1 + \frac{2}{e^x - 1}\right), \tag{1}$$

where Ω_0 is the Raman mode energy, C is the anharmonic constant and $x = \hbar\Omega_0/2k_BT$.

Fig. 5(c) shows the highest intensity low lying modes energy temperature dependence. Dashed lines represent calculated spectra by using Eq. (1). The best fit parameters are presented in Table 2. Good agreement between the experimental data and the calculated spectra suggest that the temperature dependence of the low energy (RS)-IBP Raman active modes is mainly driven by the anharmonicity effects. In general, knowledge about the Raman modes energy temperature dependence alone is not sufficient to separate the low lying internal from the external modes [21,22]. More complete approach for determination of the modes type
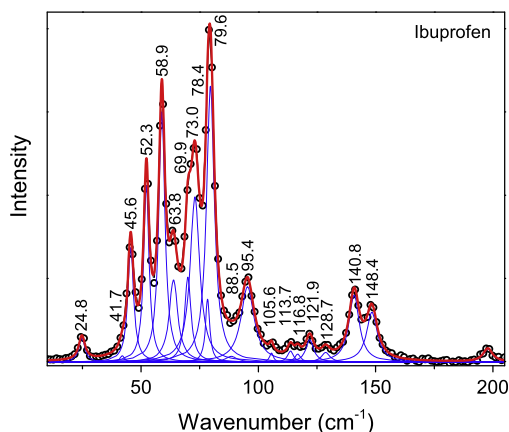

Fig. 4. Raman scattering spectra of (RS)-IBP measured at 100 K. Solid lines represent calculated spectra by using Lorentz profiles.
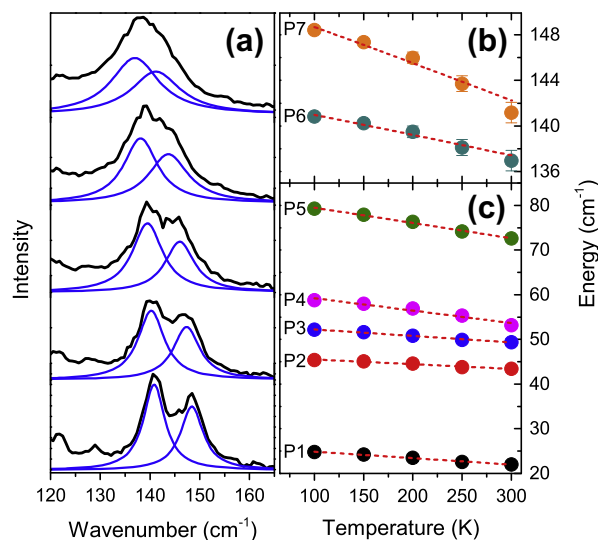

Fig. 5. (a) Raman scattering spectra of the double peak structure around 145 cm^{-1} of (RS)-IBP measured at various temperatures. (b and c) Energy temperature dependance of highest intensity Raman modes.

Table 2
Best-fitting parameters for Raman modes energy temperature dependence using Eq. (1).

	Ω (cm^{-1})	C (cm^{-1})		Ω (cm^{-1})	C (cm^{-1})
P1	26.3	0.13	P5	83.0	1.0
P2	46.6	0.18	P6	143.0	0.9
P3	53.7	0.28	P7	152.3	1.8
P4	62.0	0.6			

would require combination of pressure and temperature dependent measurements [22].

Conclusion

The Raman scattering spectra of the (RS)-IBP measured at various temperatures has been reported. Detailed analysis of the (RS)-IBP crystal symmetry, predicted 12 external modes for this system. According to the numerical calculations, appearance of internal vibrational modes is also expected in the low energy region of the spectra, mostly in terms of $A_g - B_g$ doublets, as in the case of the 141–148 cm^{-1} structure. Total of nineteen Raman active modes have been observed in the region below 200 cm^{-1}. Temperature dependance of the low energy (RS)-IBP Raman active modes is driven by anharmonicity effects.

Acknowledgments

References

[1] G.L. Perlovich, S.V. Kurkov, L.K. Hansen, A. Bauer-Brandl, Thermodynamics of sublimation, crystal lattice energies, and crystal structures of racemates and enantiomers: (+)- and (−)-ibuprofen, J. Pharm. Sci. 93 (2004) 654–666.

[2] E. Dudognon, F. Dande, M. Descamps, N. Correia, Evidence for a new crystalline phase of racemic ibuprofen, Pharm. Res. 25 (2008) 2853–2858.

[3] A. Hédoux, Y. Guinet, P. Derollez, E. Dudognon, N.T. Correia, Raman spectroscopy of racemic ibuprofen: evidence of molecular disorder in phase {II}, Int. J. Pharm. 421 (2011) 45–52.

[4] B. Rossi, P. Verrocchio, G. Viliani, I. Mancini, G. Guella, E. Rigo, G. Scarduelli, G. Mariotto, Vibrational properties of ibuprofencyclodextrin inclusion complexes investigated by Raman scattering and numerical simulation, J. Raman Spectrosc. 40 (2009) 453–458.

[5] A. Jubert, M.L. Legarto, N.E. Massa, L.L. Tvez, N.B. Okulik, Vibrational and theoretical studies of non-steroidal anti-inflammatory drugs ibuprofen [2-(4-isobutylphenyl)propionic acid]; naproxen [6-methoxy–methyl-2-naphthalene acetic acid] and tolmetin acids [1-methyl-5-(4-methylbenzoyl)-1h-pyrrole-2-acetic acid], J. Mol. Struct. 783 (2006) 34–51.

[6] M. Vueba, M. Pina, L. Batista de Carvalho, Conformational stability of ibuprofen: assessed by dft calculations and optical vibrational spectroscopy, J. Pharm. Sci. 97 (2008) 845–859.

[7] L. Bondesson, K.V. Mikkelsen, Y. Luo, P. Garberg, H. gren, Hydrogen bonding effects on infrared and Raman spectra of drug molecules, Spectrochim. Acta Part A: Mol. Biomol. Spectrosc. 66 (2007) 213–224.

[8] N. Shankland, C.C. Wilson, A.J. Florence, P.J. Cox, Refinement of ibuprofen at 100 K by single-crystal pulsed neutron diffraction, Acta Crystallogr. Section C 53 (1997) 951–954.

[9] A.A. Freer, J.M. Bunyan, N. Shankland, D.B. Sheen, Structure of (S)-(+)-ibuprofen, Acta Crystallogr. Section C 49 (1993) 1378–1380.

[10] L.K. Hansen, G.L. Perlovich, A. Bauer-Brandl, Redetermination and H-atom refinement of (S)-(+)-ibuprofen, Acta Crystallogr. Section E 59 (2003) o1357–o1358.

[11] K. Shankland, W. David, T. Csoka, L. McBride, Structure solution of ibuprofen from powder diffraction data by the application of a genetic algorithm combined with prior conformational analysis, Int. J. Pharm. 165 (1998) 117–126.

[12] N. Shankland, A.J. Florence, P.J. Cox, C.C. Wilson, K. Shankland, Conformational analysis of ibuprofen by crystallographic database searching and potential energy calculation, Int. J. Pharm. 165 (1998) 107–116.

[13] W.G. Fateley, Infrared and Raman selection rules for molecular and lattice vibrations: the correlation method, Wiley Interscience, New York, 1972.

[14] S. Baroni, S. de Gironcoli, A. Dal Corso, P. Giannozzi, Phonons and related crystal properties from density-functional perturbation theory, Rev. Mod. Phys. 73 (2001) 515–562.

[15] P. Giannozzi, S. Baroni, N. Bonini, M. Calandra, R. Car, C. Cavazzoni, D. Ceresoli, G.L. Chiarotti, M. Cococcioni, I. Dabo, A.D. Corso, S. de Gironcoli, S. Fabris, G. Fratesi, R. Gebauer, U. Gerstmann, C. Gougoussis, A. Kokalj, M. Lazzeri, L. Martin-Samos, N. Marzari, F. Mauri, R. Mazzarello, S. Paolini, A. Pasquarello, L. Paulatto, C. Sbraccia, S. Scandolo, G. Sclauzero, A.P. Seitsonen, A. Smogunov, P. Umari, R.M. Wentzcovitch, Quantum espresso: a modular and open-source software project for quantum simulations of materials, J. Phys.: Condens. Matter 21 (2009) 395502.

[16] G. Filippini, C.M. Gramaccioli, Lattice-dynamical calculations for tetracene and pentacene, Chem. Phys. Lett. 104 (1984) 50–53.

[17] R.G. Della Valle, E. Venuti, L. Farina, A. Brillante, M. Masino, A. Girlando, Intramolecular and low-frequency intermolecular vibrations of pentacene polymorphs as a function of temperature, J. Phys. Chem. B 108 (2004) 1822–1826.

[18] N. Lazarevic, M.M. Radonjic, D. Tanaskovic, R. Hu, C. Petrovic, Z.V. Popovic, Lattice dynamics of fesb 2, J. Phys.: Condens. Matter 24 (2012) 255402.

[19] M. Balkanski, R.F. Wallis, E. Haro, Anharmonic effects in light scattering due to optical phonons in silicon, Phys. Rev. B 28 (1983) 1928–1934.

[20] N. Lazarević, Z.V. Popović, R. Hu, C. Petrovic, Evidence for electron–phonon interaction in $Fe_{1-x}M_xSb_2$ (M = Co and Cr; $0 \leqslant x \leqslant 0.5$) single crystals, Phys. Rev. B 81 (2010) 144302.

[21] P.N. Prasad, R. Kopelman, External, internal and semi-internal vibrations in molecular solids: spectroscopic criteria for identification, Chem. Phys. Lett. 21 (1973) 505–510.

[22] R. Zallen, M.L. Slade, Influence of pressure and temperature on phonons in molecular chalcogenides: crystalline As 4 S 4 and S 4 N 4, Phys. Rev. B 18 (1978) 5775–5798.

Mott quantum criticality and bad metal behavior

<u>Darko Tanasković</u>[a], Jakša Vučičević[a] and Vladimir Dobrosavljević[b]

[a]*Scientific Computing Laboratory, Institute of Physics Belgrade, University of Belgrade, Pregrevica 118, 11080 Belgrade, Serbia*
[b]*Department of Physics and National High Magnetic Field Laboratory, Florida State University, Tallahassee, Florida 32306, USA*

Abstract. "Bad metal" behavior featuring linear temperature dependence of the resistivity extending to well above the Mott-Ioffe-Regel limit is often viewed as one of the key unresolved signatures of strong correlation. Here we associate the bad metal behavior with the Mott quantum criticality by examining a fully frustrated Hubbard model where all long-range magnetic orders are suppressed, and the Mott problem can be rigorously solved through dynamical mean field theory. We show that for the doped Mott insulator regime, the coexistence dome and the associated first-order Mott metal-insulator transition are confined to extremely low temperatures, while clear signatures of Mott quantum criticality emerge across much of the phase diagram. Remarkable scaling behavior is identified for the entire family of resistivity curves, with a quantum critical region covering the entire bad metal regime, providing not only new insight, but also quantitative understanding around the Mott-Ioffe-Regel limit, in agreement with the available experiments.
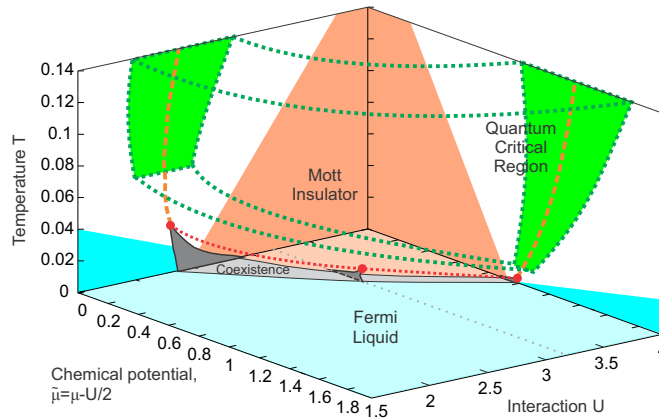
REFERENCES

1. Vučičević, J., Tanasković, D., Rozenberg, M., and Dobrosavljević, V., arXiv:1412.7960.
2. Vučičević, J., Terletska H., Tanasković, D., and Dobrosavljević, V., *Phys. Rev. B* **88**, 075143 (2013).
3. Terletska H., Vučičević, J., Tanasković, D., and Dobrosavljević, V., *Phys. Rev. Lett.* **107**, 026401 (2011).

Bulletin of the American Physical Society

APS March Meeting 2015
Volume 60, Number 1
Monday–Friday, March 2–6, 2015; San Antonio, Texas

<u>Session Q21: Metal Insulator Transitions</u>
2:30 PM–5:18 PM, Wednesday, March 4, 2015
Room: 201

Sponsoring Unit: DCMP
Chair: Dragana Popovic, National High Magnetic Field Laboratory

Abstract ID: BAPS.2015.MAR.Q21.11

Abstract: Q21.00011 : Unstable Domain-Wall Solution in the Metal-Mott Insulator Coexisting Regime
4:30 PM–4:42 PM

Preview Abstract   *MathJax **On** | Off*   ← *Abstract* →

Authors:
  Tsung-Han Lee
    (Florida State University and National High Magnetic Field Laboratory)

  Vladimir Dobrosavljevic
    (Florida State University and National High Magnetic Field Laboratory)

  Jaksa Vucicevic
    (Institute of Physics Belgrade, Serbia)

  Darko Tanaskovic
    (Institute of Physics Belgrade, Serbia)

  Eduardo Miranda
    (Campinas State University, Brazil)

We employ Dynamical Mean Field Theory (DMFT) with multidimensional optimization (Conjugate Gradient and Broyden method) to investigate the transport properties of the unstable solution in the Mott metal-insulator coexisting regime. Physically, this solution is expected to describe the properties of the domain wall separating the metallic and the Mott-insulating regions in a spatially inhomogeneous case. We show that the multidimensional optimization can efficiently converge not only to the local minima of the free energy, describing the two coexisting phases, but also to the saddle-point describing the unstable solution. This unstable solution represents a new phase of matter: its low temperature transport properties differ qualitatively from both the metal and the insulator, displaying incoherent metallic behavior down to lowest temperatures.

To cite this abstract, use the following reference: http://meetings.aps.org/link/BAPS.2015.MAR.Q21.11

Emergence of resonant waves in cigar-shaped Bose-Einstein condensates

Author(s):
Alexandru Nicolin, *Horia Hulubei National Institute for Physics and Nuclear Engineering*

Presenter:
Alexandru Nicolin, *Horia Hulubei National Institute for Physics and Nuclear Engineering*

Contribution type: Oral presentation

Abstract

Motivated by the continuous interest shown to the nonlinear dynamics of quantum gases we present in this talk the emergence of resonant waves in cigar-shaped Bose-Einstein condensates using which has been reported in Ref. [1].
We introduce the analytic treatment of the dynamics of a trapped, quasi-one-dimensional Bose-Einstein condensate subject to resonant and nonresonant periodic modulation of the transverse confinement. The dynamics of the condensate is described variationally through a set of coupled ordinary differential equations, and the period of the excited waves is determined analytically using a Mathieu-type analysis. For a modulation frequency equal to that of the radial confinement we show that the predicted period of the resonant wave is in agreement with the existing experimental results. Finally, we present a detailed comparison between the resonant waves and the Faraday waves that emerge outside of resonance.
[1] A.I. Nicolin, Phys. Rev. E 84, 056202 (2011).

Iterative Perturbative Method for a Study of Disordered Strongly Correlated Systems

Author(s):
Jaksa Vucicevic *Scientfic Computing Laboratory, Institute of Physics Belgrade, University of Belgrade*
Milos Radonjic, *Scientfic Computing Laboratory, Institute of Physics Belgrade, University of Belgrade*
Tanaskovic Darko, *Scientfic Computing Laboratory, Institute of Physics Belgrade, University of Belgrade*

Presenter:
Jaksa Vucicevic *Scientfic Computing Laboratory, Institute of Physics Belgrade, University of Belgrade*

Contribution type: Oral presentation

Abstract

Twenty years after the introduction of the Dynamical Mean Field Theory as a means of solving the Hubbard model, the focus has moved towards computationally very intensive

multi-site and multi-orbital calculations, which are aimed at including spatial correlations, disorder and detailed atomic structure to the otherwise fairly simple model. However, limited computational resources create a need for faster and more optimized codes and even approximative solutions. We present here a highly optimized parallel implementation of the approximative second order perturbative approach especially suitable for a study of strongly disordered correlated systems. On this example, we give an overview of numerical challenges that arise in dealing with large systems of non-linear equations, ill-behaved discretized functions and self-consistent calculations in general. In the end, we discuss results of performance tests, outline possible improvements and make a comparison to the exact, but computationally very demanding Quantum Monte Carlo method.

Electronic Structure and Lattice Dynamics Calculations of FeSb2 and CoSb2

Author(s):
Milos M. Radonjic, *Scientific Computing Laboratory, Institute of Physics Belgrade, University of Belgrade*
Nenad Lazarevic, *Center for Solid State Physics and New Materials, Institute of Physics Belgrade, University of Belgrade*
Darko Tanaskovic, *Scientific Computing Laboratory, Institute of Physics Belgrade, University of Belgrade*
Zoran Popovic, *Center for Solid State Physics and New Materials, Institute of Physics Belgrade, University of Belgrade*

Presenter:
Milos M. Radonjic, *Scientific Computing Laboratory, Institute of Physics Belgrade, University of Belgrade*

Contribution type: Oral presentation

Abstract

First principles calculations of the electronic structure and lattice
dynamics of FeSb2 and CoSb2 are performed using the Quantum Espresso package. Calculated vibrational modes and frequencies are used for proper assignation of the normal modes in the corresponding Raman scattering experiments.

Прилог

Позитивна цитираност научних радова кандидата

Web of Science ™ | InCites ™ | Journal Citation Reports ® | Essential Science Indicators ℠ | EndNote ™ | Sign In ▾ | Help | English ▾ |

WEB OF SCIENCE™

THOMSON REUTERS™

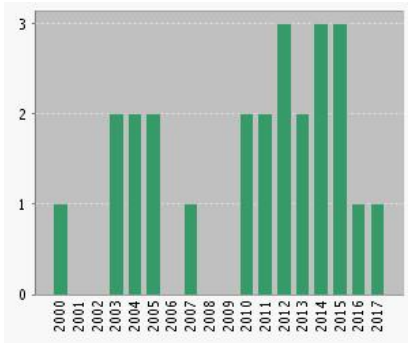Search | Return to Search Results   My Tools ▾ | Search History | Marked List   25

Citation Report: 25
(from Web of Science Core Collection)
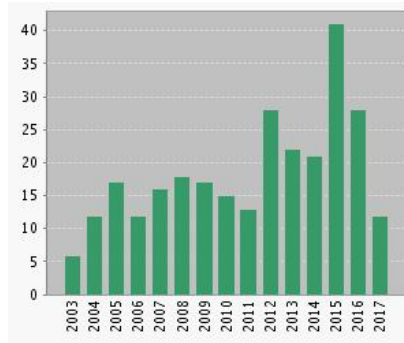
You searched for: **From Marked List: ...More**

This report reflects citations to source items indexed within Web of Science Core Collection. Perform a Cited Reference Search to include citations to items not indexed within Web of Science Core Collection.

Published Items in Each Year

The latest 20 years are displayed.

Citations in Each Year

The latest 20 years are displayed.

Results found: **25**
Sum of the Times Cited [?] : **278**
Sum of Times Cited without self-citations [?] : **255**
Citing Articles [?] : **236**
Citing Articles without self-citations [?] : **225**
Average Citations per Item [?] : **11.12**
h-index [?] : **10**

Sort by: **Times Cited -- highest to lowest**   Page 1 of 3

	2013 ◀	2014	2015	2016	2017 ▶	Total	Average Citations per Year
Use the checkboxes to remove individual items from this Citation Report or restrict to items published between 1996 and 2017 [Go]	22	21	41	28	12	278	18.53
1. Disorder screening in strongly correlated systems By: Tanaskovic, D; Dobrosavljevic, V; Abrahams, E; et al. PHYSICAL REVIEW LETTERS Volume: 91 Issue: 6 Article Number: 066603 Published: AUG 8 2003	2	1	3	1	1	42	2.80
2. Mechanism of hopping transport in disordered Mott insulators By: Nakatsuji, S; Dobrosavljevic, V; Tanaskovic, D; et al. PHYSICAL REVIEW LETTERS Volume: 93 Issue: 14 Article Number: 146401 Published: OCT 1 2004	4	2	0	0	2	41	2.93
3. Glassy behavior of electrons near metal-insulator transitions By: Dobrosavljevic, V; Tanaskovic, D; Pastor, AA PHYSICAL REVIEW LETTERS Volume: 90 Issue: 1 Article Number: 016402 Published: JAN 10 2003	0	1	5	2	0	41	2.73
4. Quantum Critical Transport near the Mott Transition By: Terletska, H.; Vucicevic, J.; Tanaskovic, D.; et al. PHYSICAL REVIEW LETTERS Volume: 107 Issue: 1 Article Number: 026401 Published: JUL 5 2011	4	3	5	5	2	24	3.43
5. Extended Hubbard model: Charge ordering and Wigner-Mott	2	4	2	2	1	15	1.88

transition

By: Amaricci, A.; Camjayi, A.; Haule, K.; et al.
PHYSICAL REVIEW B   Volume: 82   Issue: 15   Article Number: 155102
 Published: OCT 1 2010

6. **Green functions for nearest- and next-nearest-neighbor hopping on the Bethe lattice**

By: Kollar, M; Eckstein, M; Byczuk, K; et al.
ANNALEN DER PHYSIK   Volume: 14   Issue: 9-10   Pages: 642-657
 Published: SEP-OCT 2005

| 3 | 0 | 0 | 0 | 0 | 14 | 1.08 |

7. **Effective model of the electronic Griffiths phase**

By: Tanaskovic, D; Miranda, E; Dobrosavljevic, V
PHYSICAL REVIEW B   Volume: 70   Issue: 20   Article Number: 205108
 Published: NOV 2004

| 1 | 1 | 1 | 1 | 0 | 14 | 1.00 |

8. **Spin-liquid behavior in electronic Griffiths phases**

By: Tanaskovic, D; Dobrosavljevic, V; Miranda, E
PHYSICAL REVIEW LETTERS   Volume: 95   Issue: 16   Article Number: 167204   Published: OCT 14 2005

| 0 | 0 | 1 | 0 | 0 | 13 | 1.00 |

9. **Bad-Metal Behavior Reveals Mott Quantum Criticality in Doped Hubbard Models**

By: Vucicevic, J.; Tanaskovic, D.; Rozenberg, M. J.; et al.
PHYSICAL REVIEW LETTERS   Volume: 114   Issue: 24   Article Number: 246402   Published: JUN 18 2015

| 0 | 0 | 2 | 7 | 2 | 11 | 3.67 |

10. **Phase diagram, energy scales, and nonlocal correlations in the Anderson lattice model**

By: Tanaskovic, D.; Haule, K.; Kotliar, G.; et al.
PHYSICAL REVIEW B   Volume: 84   Issue: 11   Article Number: 115105
 Published: SEP 9 2011

| 1 | 1 | 3 | 0 | 2 | 10 | 1.43 |

Select Page   Save to Text File

Sort by: **Times Cited -- highest to lowest**   Page 1   of 3

25 records matched your query of the 37,044,483 in the data limits you selected.

Web of Science™ | InCites™ | Journal Citation Reports ® | Essential Science Indicators ᴿᴹ | EndNote™ | | Sign In ▾ | Help | English ▾ |

WEB OF SCIENCE™

THOMSON REUTERS®

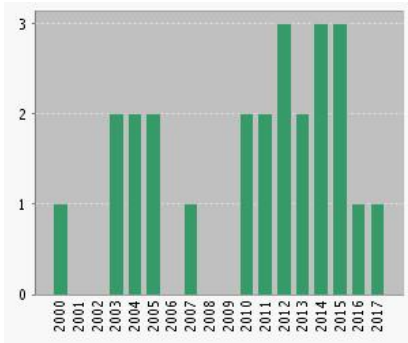| Search | Return to Search Results | | My Tools ▾ | Search History | Marked List | 25 |

Citation Report: 25

(from Web of Science Core Collection)

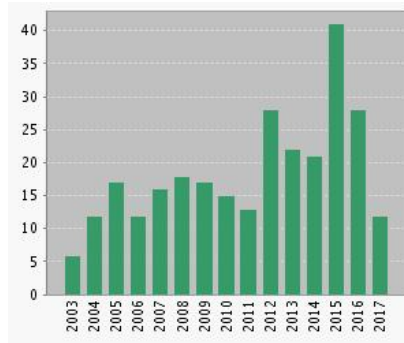You searched for: **From Marked List:** **...More**

This report reflects citations to source items indexed within Web of Science Core Collection. Perform a Cited Reference Search to include citations to items not indexed within Web of Science Core Collection.

Published Items in Each Year

The latest 20 years are displayed.

Citations in Each Year

The latest 20 years are displayed.

Results found: **25**
Sum of the Times Cited [?] : **278**
Sum of Times Cited without self-citations [?] : **255**
Citing Articles [?] : **236**
Citing Articles without self-citations [?] : **225**
Average Citations per Item [?] : **11.12**
h-index [?] : **10**

Sort by: **Times Cited -- highest to lowest**   Page 2 of 3

	2013 ◄	2014	2015	2016	2017 ▶	Total	Average Citations per Year
Use the checkboxes to remove individual items from this Citation Report or restrict to items published between **1996** and **2017** Go	22	21	41	28	12	278	18.53
11. **Lattice dynamics of KNi2Se2** By: Lazarevic, N.; Radonjic, M.; Scepanovic, M.; et al. PHYSICAL REVIEW B Volume: 87 Issue: 14 Article Number: 144305 Published: APR 22 2013	0	1	6	2	0	9	1.80
12. **RKKY interactions in the regime of strong localization** By: Sobota, J. A.; Tanaskovic, D.; Dobrosavljevic, V. PHYSICAL REVIEW B Volume: 76 Issue: 24 Article Number: 245106 Published: DEC 2007	1	1	2	1	0	9	0.82
13. **Wigner-Mott scaling of transport near the two-dimensional metal-insulator transition** By: Radonjic, M. M.; Tanaskovic, D.; Dobrosavljevic, V.; et al. PHYSICAL REVIEW B Volume: 85 Issue: 8 Article Number: 085133 Published: FEB 29 2012	2	1	2	2	1	8	1.33
14. **Finite-temperature crossover and the quantum Widom line near the Mott transition** By: Vucicevic, J.; Terletska, H.; Tanaskovic, D.; et al. PHYSICAL REVIEW B Volume: 88 Issue: 7 Article Number: 075143 Published: AUG 28 2013	0	0	4	2	1	7	1.40

15. **Lattice dynamics of FeSb2** By: Lazarevic, N.; Radonjic, M. M.; Tanaskovic, D.; et al. JOURNAL OF PHYSICS-CONDENSED MATTER Volume: 24 Issue: 25 Article Number: 255402 Published: JUN 27 2012	1	3	1	0	0	6	1.00
16. **Influence of disorder on incoherent transport near the Mott transition** By: Radonjic, Milos M.; Tanaskovic, D.; Dobrosavljevic, V.; et al. PHYSICAL REVIEW B Volume: 81 Issue: 7 Article Number: 075118 Published: FEB 2010	1	0	1	0	0	6	0.75
17. **Phonon and magnetic dimer excitations in Fe-based S = 2 spin-ladder compound BaFe2Se2O** By: Popovic, Z. V.; Scepanovic, M.; Lazarevic, N.; et al. PHYSICAL REVIEW B Volume: 89 Issue: 1 Article Number: 014301 Published: JAN 3 2014	0	1	2	0	0	3	0.75
18. **Signatures of the spin-phonon coupling in Fe1+yTe1-xSex alloys** By: Popovic, Z. V.; Lazarevic, N.; Bogdanovic, S.; et al. SOLID STATE COMMUNICATIONS Volume: 193 Pages: 51-55 Published: SEP 2014	0	0	0	2	0	2	0.50
19. **Anderson localization effects near the Mott metal-insulator transition** By: Braganca, Helena; Aguiar, M. C. O.; Vucicevic, J.; et al. PHYSICAL REVIEW B Volume: 92 Issue: 12 Article Number: 125143 Published: SEP 24 2015	0	0	0	1	0	1	0.33
20. **Intermolecular and low-frequency intramolecular Raman scattering study of racemic ibuprofen** By: Lazarevic, J. J.; Uskokovic-Markovic, S.; Jelikic-Stankov, M.; et al. SPECTROCHIMICA ACTA PART A-MOLECULAR AND BIOMOLECULAR SPECTROSCOPY Volume: 126 Pages: 301-305 Published: MAY 21 2014	0	0	1	0	0	1	0.25

Select Page   Save to Text File

Sort by: **Times Cited -- highest to lowest**   Page 2   of 3

25 records matched your query of the 37,044,483 in the data limits you selected.

| Web of Science ™ | InCites ™ | Journal Citation Reports ® | Essential Science Indicators ᔆᴹ | EndNote ™ | | Sign In ▾ | Help | English ▾ |

WEB OF SCIENCE™

THOMSON REUTERS®

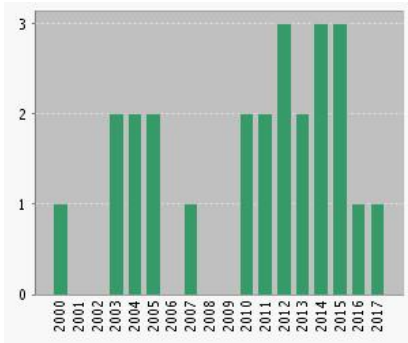| Search | Return to Search Results | | My Tools ▾ | Search History | Marked List　25 |

Citation Report: 25
(from Web of Science Core Collection)
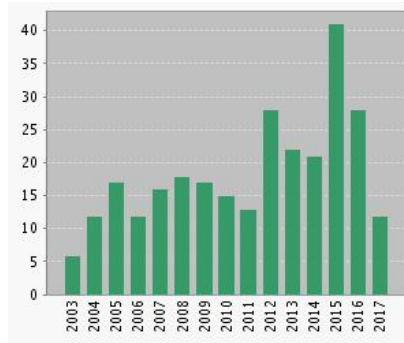
You searched for:　**From Marked List:　...More**

This report reflects citations to source items indexed within Web of Science Core Collection. Perform a Cited Reference Search to include citations to items not indexed within Web of Science Core Collection.

Published Items in Each Year

The latest 20 years are displayed.

Citations in Each Year

The latest 20 years are displayed.

Results found:	**25**
Sum of the Times Cited [?] :	**278**
Sum of Times Cited without self-citations [?] :	**255**
Citing Articles [?] :	**236**
Citing Articles without self-citations [?] :	**225**
Average Citations per Item [?] :	**11.12**
h-index [?] :	**10**

Sort by:　**Times Cited -- highest to lowest**

Page **3** of 3

Use the checkboxes to remove individual items from this Citation Report or restrict to items published between **1996** and **2017** [Go]

	2013 ◀	2014	2015	2016	2017 ▶	Total	Average Citations per Year
	22	21	41	28	12	278	18.53
21. **Phonon properties of CoSb2 single crystals** By: Lazarevic, N.; Radonjic, M. M.; Hu, Rongwei; et al. JOURNAL OF PHYSICS-CONDENSED MATTER　Volume: 24　Issue: 13　Article Number: 135402　Published: APR 4 2012	0	1	0	0	0	1	0.17
22. **Magnetic impurities in spin-split superconductors** By: Oei, W. -V. van Gerven; Tanaskovic, D.; Zitko, R. PHYSICAL REVIEW B　Volume: 95　Issue: 8　Article Number: 085115　Published: FEB 13 2017	0	0	0	0	0	0	0.00
23. **Raman spectroscopy of KxCo2-ySe2 single crystals near the ferromagnet-paramagnet transition** By: Opacic, M.; Lazarevic, N.; Radonjic, M. M.; et al. JOURNAL OF PHYSICS-CONDENSED MATTER　Volume: 28　Issue: 48　Article Number: 485401　Published: DEC 7 2016	0	0	0	0	0	0	0.00
24. **Lattice dynamics of BaFe2X3(X = S, Se) compounds** By: Popovic, Z. V.; Scepanovic, M.; Lazarevic, N.; et al. PHYSICAL REVIEW B　Volume: 91　Issue: 6　Article Number: 064303　Published: FEB 27 2015	0	0	0	0	0	0	0.00

25. **Spin paramagnetism in d-wave superconductors**

By: Tanaskovic, D; Radovic, Z; Dobrosavljevic-Grujic, L

PHYSICAL REVIEW B   Volume: 62   Issue: 1   Pages: 138-141   Published: JUL 1 2000

| | 0 | 0 | 0 | 0 | 0 | 0 | 0.00 |

Select Page   Save to Text File

Sort by: **Times Cited -- highest to lowest**   Page 3   of 3

25 records matched your query of the 37,044,483 in the data limits you selected.

Република Србија
МИНИСТАРСТВО ПРОСВЕТЕ,
НАУКЕ И ТЕХНОЛОШКОГ РАЗВОЈА
Комисија за стицање научних звања

Број:06-00-75/930
31.10.2012. године
Б е о г р а д

На основу члана 22. става 2. члана 70. став 6. Закона о научноистраживачкој делатности ("Службени гласник Републике Србије", број 110/05 и 50/06 – исправка и 18/10), члана 2. става 1. и 2. тачке 1 – 4.(прилози) и члана 38. Правилника о поступку и начину вредновања и квантитативном исказивању научноистраживачких резултата истраживача ("Службени гласник Републике Србије", број 38/08) и захтева који је поднео

Инсииииуи за физику у Београду

Комисија за стицање научних звања на седници одржаној 31.10.2012. године, донела је

ОДЛУКУ
О СТИЦАЊУ НАУЧНОГ ЗВАЊА

Др Дарко Танасковић
стиче научно звање
Виши научни сарадник

у области природно-математичких наука - физика

О Б Р А З Л О Ж Е Њ Е

Инсииииуи за физику у Београду

утврдио је предлог број 659/1 од 05.06.2012. године на седници научног већа Института и поднео захтев Комисији за стицање научних звања број 721/1 од 15.06.2012. године за доношење одлуке о испуњености услова за стицање научног звања **Виши научни сарадник**.

Комисија за стицање научних звања је по предходно прибављеном позитивном мишљењу Матичног научног одбора за физику на седници одржаној 31.10.2012. године разматрала захтев и утврдила да именовани испуњава услове из члана 70. став 6. Закона о научноистраживачкој делатности ("Службени гласник Републике Србије", број 110/05 и 50/06 – исправка и 18/10), члана 2. става 1. и 2. тачке 1 – 4.(прилози) и члана 38. Правилника о поступку и начину вредновања и квантитативном исказивању научноистраживачких резултата истраживача ("Службени гласник Републике Србије", број 38/08) за стицање научног звања **Виши научни сарадник,** па је одлучила као у изреци ове одлуке.

Доношењем ове одлуке именовани стиче сва права која му на основу ње по закону припадају.

Одлуку доставити подносиоцу захтева, именованом и архиви Министарства просвете, науке и технолошког развоја у Београду.
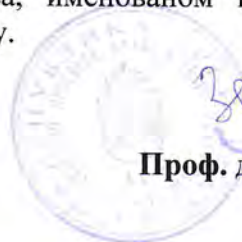
ПРЕДСЕДНИК КОМИСИЈЕ   МИНИСТАР
др Станислава Стошић-Грујичић,   Проф. др Жарко Обрадовић
научни саветник

Прилог

Научни ниво и значај резултата, утицај научних радова

Quantum criticality of Mott transition in organic materials

Tetsuya Furukawa[1]*, Kazuya Miyagawa[1], Hiromi Taniguchi[2], Reizo Kato[3] and Kazushi Kanoda[1]*

A many-body quantum system on the verge of instability between two competing ground states may exhibit quantum-critical phenomena[1,2], as has been intensively studied for magnetic systems. The Mott metal–insulator transition[3], a phenomenon that is central to many investigations of strongly correlated electrons, is also supposed to be quantum critical, although this has so far not been demonstrated experimentally. Here, we report experimental evidence for the quantum-critical nature of the Mott instability, obtained by investigating the electron transport of three organic systems with different ground states under continuously controlled pressure. The resistivity obeys the material-independent quantum-critical scaling relation bifurcating into a Fermi liquid or Mott insulator, irrespective of the ground states. Electrons on the verge of becoming delocalized behave like a strange quantum-critical fluid before becoming a Fermi liquid.

Mutually interacting electrons with sufficiently strong Coulomb repulsion U fall into the Mott insulating state when the carrier density corresponds to an electron per site (a half-filled band)[3]. As the bandwidth W is increased by pressure or chemical substitution, the electrons gain kinetic energy and become itinerant at a critical value of W/U. The Mott transition, a marked phase transition between a metal and an insulator, is a collective manifestation of imbalance in the particle–wave duality of electrons. As one of the main issues in the quantum physics of condensed matter, the quantum-critical nature of the Mott transition awaits clarification. In contrast to intensive theoretical studies[4–6], however, this issue has not yet been addressed experimentally because most Mott transitions in real systems have critical points at finite temperatures[7–11]; thus, they are not genuine quantum phase transitions.

In general, quantum criticality is observed at the temperature T sufficiently lower than the competing energy scales underlying the phase transition[1,2], which are the bandwidth W and on-site Coulomb energy U in the case of the Mott transition. Thus, even if the system's critical point, T_c, is finite, unlike the genuine quantum phase transition, in the case that T_c is orders of magnitude lower than W and U, there is a vast temperature region of $T_c < T \ll U, W$, where the system can experience quantum criticality (Fig. 1a). Indeed, using dynamical mean field theory (DMFT), which can properly describe the Mott transition[12], the authors of refs 4,13 have suggested the scaling of transport for quantum criticality in an intermediate temperature range well above T_c.

To explore the possible Mott quantum criticality from the experimental side, we performed pressure studies of the electron transport for three different quasi-two-dimensional organic Mott insulators with anisotropic triangular lattices, κ-(ET)$_2$Cu$_2$(CN)$_3$, κ-(ET)$_2$Cu[N(CN)$_2$]Cl and EtMe$_3$Sb[Pd(dmit)$_2$]$_2$ (hereafter abbreviated to κ-Cu$_2$(CN)$_3$, κ-Cl and EtMe$_3$Sb-dmit, respectively), where

ET and dmit represent bis(ethylenedithio)tetrathiafulvalene and 1,3-dithiole-2-thione-4,5-dithiolate, respectively (Fig. 1b,c). In the Mott insulating phases, κ-Cu$_2$(CN)$_3$ and EtMe$_3$Sb-dmit host quantum spin liquids (QSLs), whereas κ-Cl is an antiferromagnet[14–18] (AFM). In the metallic phases, κ-Cu$_2$(CN)$_3$ and κ-Cl are superconducting (SC) at low temperatures, whereas EtMe$_3$Sb-dmit remains a paramagnetic metal[9–11,19–21] (PM). Then, the three systems have different types of Mott transition in their ground states, for example, QSL–SC, AFM–SC and QSL–PM transitions (Fig. 1d–f). Clear first-order Mott transitions are observed in κ-Cu$_2$(CN)$_3$ and κ-Cl up to T_c values of 20 K (ref. 22) and 38 K (ref. 11), respectively, whereas there is no clear first-order nature in the Mott transition in EtMe$_3$Sb-dmit[21]; its critical temperature, if any, is well below 30 K. The critical temperatures of the three compounds are two or three orders of magnitude lower than the values of W, U, which are several thousand Kelvin or more[19] (Fig. 1a); the orders-of-magnitude difference between T_c and U, W preserves the possibility of quantum criticality in the intermediate temperature region ($T_c < T \ll U, W$). We measured resistivity curves $\rho(P, T)$ under continuously controlled He-gas pressure P at various fixed temperatures to cover the metal–insulator crossover region and tested the quantum-critical scaling of the $\rho(P, T)$ data. Figure 1d–f present coloured contour plots of the normalized $\rho(P, T)$ (explained later in detail), which is shown to follow the quantum-critical scaling almost perfectly in the fan-shaped region where the colour changes, as described in the following section.

First, we define metal–insulator crossover pressures at a given temperature, $P_c(T)$, as inflection points in the experimental log $\rho(P, T)$ versus P curve (Supplementary Information). The $P_c(T)$ determined at different temperatures forms a bow-shaped crossover line, which corresponds to the Widom line of the Mott transition[4,13]. The Widom line divides the insulating ($\delta P \equiv P - P_c(T) < 0$) and metallic sides ($\delta P > 0$), as observed in Fig. 1d–f. Figure 2 shows the normalized resistivity $\tilde{\rho}(\delta P, T) \equiv \rho(\delta P, T)/\rho_c(T)$ of κ-Cu$_2$(CN)$_3$ as a function of δP, where $\rho_c(T) \equiv \rho(\delta P = 0, T)$ is the crossover resistivity along the Widom line. It is observed that $\tilde{\rho}(\delta P, T)$ crosses continuously from the insulating state ($\delta P < 0$) to the metallic state ($\delta P > 0$). As a result of the normalization, all curves cross at a single point for which $\delta P = 0$ and $\tilde{\rho} = 1$, and the slope at the inflection point is steeper at lower temperatures. It is noted that the volume change of the sample, which can be large particularly near the Mott transition, has no practical influence on the $\rho(P, T)$ values, as explained in the Supplementary Information.

For a quantum phase transition[1,2], as a system approaches a quantum-critical point while remaining at zero temperature, not only the spatial correlation length ξ but also the correlation time τ diverges as $\xi \propto |g - g_c|^{-\nu}$ and $\tau \propto \xi^z \propto |g - g_c|^{-z\nu}$, where g is the

[1]Department of Applied Physics, University of Tokyo, 7-3-1 Hongo, Bunkyo-ku, Tokyo 113-8656, Japan. [2]Department of Physics, Saitama University, 255 Shimo-Okubo, Sakura-ku, Saitama-shi, Saitama 338-8570, Japan. [3]RIKEN, 2-1 Hirosawa, Wako-shi, Saitama 351-0198, Japan. *e-mail: furukawa@ap.t-u-tokyo.ac.jp; kanoda@ap.t-u-tokyo.ac.jp

the temperature range in which the scaling is valid is approximately $2T_c < T < 0.12t$, where t is the nearest-neighbour transfer integral in the Hubbard model. Both the lower and upper limits nearly coincide with the present results. Furthermore, the bow-shaped crossover line and the fan-shaped quantum-critical region are common to both the present and the DMFT works. As DMFT can treat only fluctuations independent of wavenumber k, the present agreement may indicate that the fluctuations of Mott quantum criticality, where electrons are neither particle-like nor wave-like objects, can be of the k-independent local nature.

In general, quantum-critical behaviour springs from a quantum phase transition associated with symmetry breaking. However, the Mott quantum criticality in question is associated with the charge delocalization transition without symmetry breaking and has been actually demonstrated here to occur irrespectively of the presence/absence of symmetry breaking in spin degrees freedom. Thus, the present quantum criticality is beyond the conventional symmetry-breaking framework. Unconventional quantum criticality has also been discussed for heavy-electron systems in light of the Kondo breakdown, where the reconstruction of Fermi surfaces or an orbital-selective Mott transition due to itinerant-localized competition of f electrons supposedly causes unconventional quantum criticality[28,29]. Moreover, theoretical investigations of the holographic duality of current interest have proposed that strange metals in heavy electrons and cuprates are in yet-unspecified quantum-critical regimes[30,31]. It is likely that correlated quantum systems of organics, heavy electrons and cuprates carry a new class of quantum criticality that originates from the itinerant-localized competition rather than symmetry breaking.

Methods

Single crystals of κ-(ET)$_2$Cu$_2$(CN)$_3$ and κ-(ET)$_2$Cu[N(CN)$_2$]Cl were grown by conventional electrochemical oxidation. Single crystals of EtMe$_3$Sb[Pd(dmit)$_2$]$_2$ were obtained by air oxidation of (EtMe$_3$Sb)$_2$[Pd(dmit)$_2$] in acetone containing acetic acid[32]. The typical sample sizes are $\sim$0.3 mm $\times$ 0.3 mm $\times$ 0.006 mm for κ-(ET)$_2$Cu$_2$(CN)$_3$, $\sim$ 1.0 mm $\times$ 0.5 mm $\times$ 0.2 mm for κ-(ET)$_2$Cu[N(CN)$_2$]Cl, and $\sim$0.8 mm $\times$ 0.9 mm $\times$ 0.05 mm for EtMe$_3$Sb[Pd(dmit)$_2$]$_2$. The in-plane electrical resistivity was measured using the standard d.c. four-probe method under an isothermal pressure sweep (descending processes), using helium gas as the pressure medium. To examine the sample dependence, measurements were performed for two samples of the same compound simultaneously in the same run. The reproducibility of the scaling behaviour was basically ensured for each compound. Gold wires of 25 μm in diameter were glued on the crystal faces with carbon paste as electrodes. Throughout the experiments, we confirmed that the resistivity was independent of the applied current.

References

1. Sachdev, S. *Quantum Phase Transitions* (Cambridge Univ. Press, 2011).
2. Sondhi, S. L., Girvin, S. M., Carini, J. P. & Shahar, D. Continuous quantum phase transitions. *Rev. Mod. Phys.* **69,** 315–333 (1997).
3. Mott, N. F. *Metal–Insulator Transitions* (Taylor & Francis, 1990).
4. Terletska, H., Vučičević, J., Tanasković, D. & Dobrosavljević, V. Quantum critical transport near the Mott transition. *Phys. Rev. Lett.* **107,** 026401 (2011).
5. Senthil, T. Theory of a continuous Mott transition in two dimensions. *Phys. Rev. B* **78,** 045109 (2008).
6. Misawa, T. & Imada, M. Quantum criticality around metal–insulator transitions of strongly correlated electron systems. *Phys. Rev. B* **75,** 115121 (2007).
7. McWhan, D., Menth, A., Remeika, J., Brinkman, W. & Rice, T. Metal–insulator transitions in pure and doped V$_2$O$_3$. *Phys. Rev. B* **7,** 1920–1931 (1973).
8. Yao, X., Honig, J., Hogan, T., Kannewurf, C. & Spałek, J. Electrical properties of NiS$_{2-x}$Se$_x$ single crystals: From Mott insulator to paramagnetic metal. *Phys. Rev. B* **54,** 17469–17475 (1996).
9. Lefebvre, S. *et al.* Mott transition, antiferromagnetism, and unconventional superconductivity in layered organic superconductors. *Phys. Rev. Lett.* **85,** 5420–5423 (2000).
10. Limelette, P. *et al.* Mott transition and transport crossovers in the organic compound κ-(BEDT-TTF)$_2$Cu[N(CN)$_2$]Cl. *Phys. Rev. Lett.* **91,** 016401 (2003).
11. Kagawa, F., Miyagawa, K. & Kanoda, K. Unconventional critical behaviour in a quasi-two-dimensional organic conductor. *Nature* **436,** 534–537 (2005).
12. Georges, A., Kotliar, G., Krauth, W. & Rozenberg, M. J. Dynamical mean-field theory of strongly correlated fermion systems and the limit of infinite dimensions. *Rev. Mod. Phys.* **68,** 13–125 (1996).
13. Vučičević, J., Terletska, H., Tanasković, D. & Dobrosavljević, V. Finite-temperature crossover and the quantum Widom line near the Mott transition. *Phys. Rev. B* **88,** 075143 (2013).
14. Shimizu, Y., Miyagawa, K., Kanoda, K., Maesato, M. & Saito, G. Spin liquid state in an organic Mott insulator with a triangular lattice. *Phys. Rev. Lett.* **91,** 107001 (2003).
15. Itou, T., Oyamada, A., Maegawa, S., Tamura, M. & Kato, R. Quantum spin liquid in the spin-1/2 triangular antiferromagnet EtMe$_3$Sb[Pd(dmit)$_2$]$_2$. *Phys. Rev. B* **77,** 104413 (2008).
16. Kanoda, K. & Kato, R. Mott physics in organic conductors with triangular lattices. *Annu. Rev. Condens. Matter Phys.* **2,** 167–188 (2011).
17. Kato, R. Development of π-electron systems based on [M(dmit)$_2$] (M = Ni and Pd; dmit: 1,3-dithiole-2-thione-4,5-dithiolate) anion radicals. *Bull. Chem. Soc. Jpn* **87,** 355–374 (2014).
18. Powell, B. J. & McKenzie, R. H. Quantum frustration in organic Mott insulators: From spin liquids to unconventional superconductors. *Rep. Prog. Phys.* **74,** 056501 (2011).
19. Komatsu, T., Matsukawa, N., Inoue, T. & Saito, G. Realization of superconductivity at ambient pressure by band-filling control in κ-(BEDT-TTF)$_2$Cu$_2$(CN)$_3$. *J. Phys. Soc. Jpn* **65,** 1340–1354 (1996).
20. Kurosaki, Y., Shimizu, Y., Miyagawa, K., Kanoda, K. & Saito, G. Mott transition from a spin liquid to a Fermi liquid in the spin-frustrated organic conductor κ-(ET)$_2$Cu$_2$(CN)$_3$. *Phys. Rev. Lett.* **95,** 177001 (2005).
21. Kato, R., Tajima, A., Nakao, A., Tajima, N., Tamura, M. in *Multifunctional Conducting Molecular Materials* (eds Saito, G. *et al.*) 32–38 (Royal Society of Chemistry, 2007).
22. Kobashi, K. *Transport Properties Near the Mott Transition in the Quasi-Two-Dimensional Organic Conductor κ-(ET)$_2$X* Thesis, Univ. Tokyo (2007).
23. Simonian, D., Kravchenko, S. V. & Sarachik, M. P. Reflection symmetry at a $B = 0$ metal–insulator transition in two dimensions. *Phys. Rev. B* **55,** R13421–R13423 (1997).
24. Amaricci, A. *et al.* Extended Hubbard model: Charge ordering and Wigner–Mott transition. *Phys. Rev. B* **82,** 155102 (2010).
25. Witczak-Krempa, W., Ghaemi, P., Senthil, T. & Kim, Y. B. Universal transport near a quantum critical Mott transition in two dimensions. *Phys. Rev. B* **86,** 245102 (2012).
26. Kravchenko, S. *et al.* Scaling of an anomalous metal–insulator transition in a two-dimensional system in silicon at $B = 0$. *Phys. Rev. B* **51,** 7038–7045 (1995).
27. Kosterlitz, J. M. The critical properties of the two-dimensional xy model. *J. Phys. C* **7,** 1046–1060 (1974).
28. Si, Q., Rabello, S., Ingersent, K. & Smith, J. L. Locally critical quantum phase transitions in strongly correlated metals. *Nature* **413,** 804–808 (2001).
29. Senthil, T., Sachdev, S. & Vojta, M. Quantum phase transitions out of the heavy Fermi liquid. *Physica B* **359–361,** 9–16 (2005).
30. Sachdev, S. Holographic metals and the fractionalized Fermi liquid. *Phys. Rev. Lett.* **105,** 151602 (2010).
31. Davison, R. A., Schalm, K. & Zaanen, J. Holographic duality and the resistivity of strange metals. *Phys. Rev. B* **89,** 245116 (2014).
32. Kato, R. & Hengbo, C. Cation dependence of crystal structure and band parameters in a series of molecular conductors, β'-(Cation)[Pd(dmit)$_2$]$_2$ (dmit = 1,3-dithiole-2-thione-4,5-dithiolate). *Crystals* **2,** 861–874 (2012).

Author contributions

T.F. and K.K. designed the experiments. T.F. performed the experiments and analysed the data. T.F. and K.K. interpreted the data. K.M., H.T. and R.K. grew the single crystals for the study. T.F. wrote the manuscript with the assistance of K.M. and K.K. K.K. headed this project.

Additional information

Supplementary information is available in the online version of the paper. Reprints and permissions information is available online at www.nature.com/reprints. Correspondence and requests for materials should be addressed to T.F. or K.K.

Competing financial interests

The authors declare no competing financial interests.

Critical Behavior in Doping-Driven Metal–Insulator Transition on Single-Crystalline Organic Mott-FET

Yoshiaki Sato,[*,†] Yoshitaka Kawasugi,[*,†] Masayuki Suda,[†,‡] Hiroshi M. Yamamoto,[*,†,‡] and Reizo Kato[†]

[†]RIKEN, Hirosawa, Wako, Saitama 351-0198, Japan

[‡]Research Center for Integrative Molecular System (CIMoS), Institute for Molecular Science, 38 Nishigo-naka, Myodaiji, Okazaki 444-8585, Japan

Ⓢ *Supporting Information*

ABSTRACT: We present the carrier transport properties in the vicinity of a doping-driven Mott transition observed at a field-effect transistor (FET) channel using a single crystal of the typical two-dimensional organic Mott insulator κ-(BEDT-TTF)$_2$CuN(CN)$_2$Cl (κ-Cl). The FET shows a continuous metal–insulator transition (MIT) as electrostatic doping proceeds. The phase transition appears to involve two-step crossovers, one in Hall measurement and the other in conductivity measurement. The crossover in conductivity occurs around the conductance quantum e^2/h, and hence is not associated with "bad metal" behavior, which is in stark contrast to the MIT in half-filled organic Mott insulators or that in doped inorganic Mott insulators. Through in-depth scaling analysis of the conductivity, it is found that the above carrier transport properties in the vicinity of the MIT can be described by a high-temperature Mott quantum critical crossover, which is theoretically argued to be a ubiquitous feature of various types of Mott transitions.

KEYWORDS: Mott transition, field-effect transistor, SAM patterning, metal–insulator transition, Hall effect, quantum critical scaling
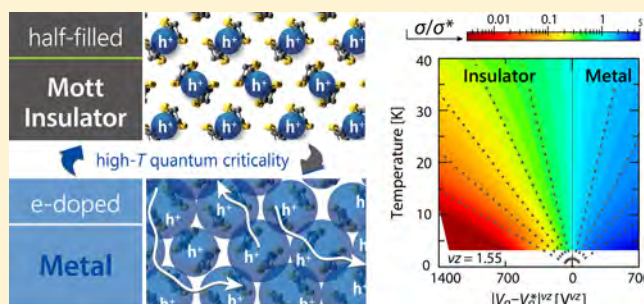
S trongly correlated electrons confined in two-dimensional materials exhibit a rich variety of anomalous phases, such as high-T_c superconductivity, Mott insulators, and quantum spin liquids. Enormous effort has been devoted to understanding the mechanisms of the phase transitions between them,[1,2] which are driven by the complex interplay between many-body interactions and charge–spin fluctuations. Mott insulators are particularly remarkable in viewpoints of nanoscience as well as fundamental physics since they are not only mother materials for a diverse range of strongly correlated systems but also serve as a molecular or atomic limit for coherently coupled arrays of single electron transistors (SETs).[3,4] In Mott insulating state, strong Coulomb repulsion between electrons in half-filled band leads to carrier localization, which can be viewed as a situation that the collective Coulomb blockade confines an electron to the individual "subnano-sized SET". The electronic/magnetic properties of Mott insulators are governed by quantum mechanics, and indeed various types of unconventional phase transitions occur due to imbalance in the particle–wave duality of electrons which is triggered by charge doping,[5] a magnetic/electric field,[6,7] pressure,[8,9] or introduction of disorders.[10,11] An important issue is the possibility of quantum phase transitions in Mott insulators,[12,13] where quantum fluctuations play an essential role in the transitions with the emergence of quantum critical points at 0 K.[14–18] This would hold true for a coherently coupled array of SETs, although it has not yet been recognized.

Even at finite temperatures, quantum fluctuations with an energy scale overwhelming the temperature k_BT give rise to a critical crossover feature observed as a power-law singularity in physical quantities in the vicinity of the quantum critical point.[13,19] It has been argued that the unconventional non-Fermi liquid behavior commonly observed near the Mott transition should pertain to such quantum criticality, although there is no general consensus on its origin.

To properly investigate the doping-driven Mott transition, it is required to dope carriers in a clean manner without introducing impurities because the modification of the local electronic environment by such disorders should destroy the intrinsic many-body states. Electrostatic doping techniques using the electric double-layer transistor (EDLT) or field-effect transistor (FET) configurations are promising for such investigation. Combined with recent advances in fabrication technology for crystalline nanosheets[1] and interfaces,[20–22] these techniques not only enable fine control of the charge density as an independent tunable parameter but also extend the possibility of novel device applications that utilize abrupt changes in physical properties triggered by a phase transition.

Supporting Information for

"Critical Behavior in Doping-Driven Metal–Insulator Transition on Single-Crystalline Organic Mott-FET"

Yoshiaki Sato,[1, *] Yoshitaka Kawasugi,[1, †] Masayuki Suda,[1, 2] Hiroshi M. Yamamoto,[1, 2, ‡] and Reizo Kato[1]

[1]*RIKEN, 2-1 Hirosawa, Wako, Saitama 351-0198, Japan*

[2]*Research Center of Integrative Molecular Systems (CIMoS),*

Institute for Molecular Science, 38 Nishigo-Naka, Myodaiji, Okazaki 444-8585, Japan
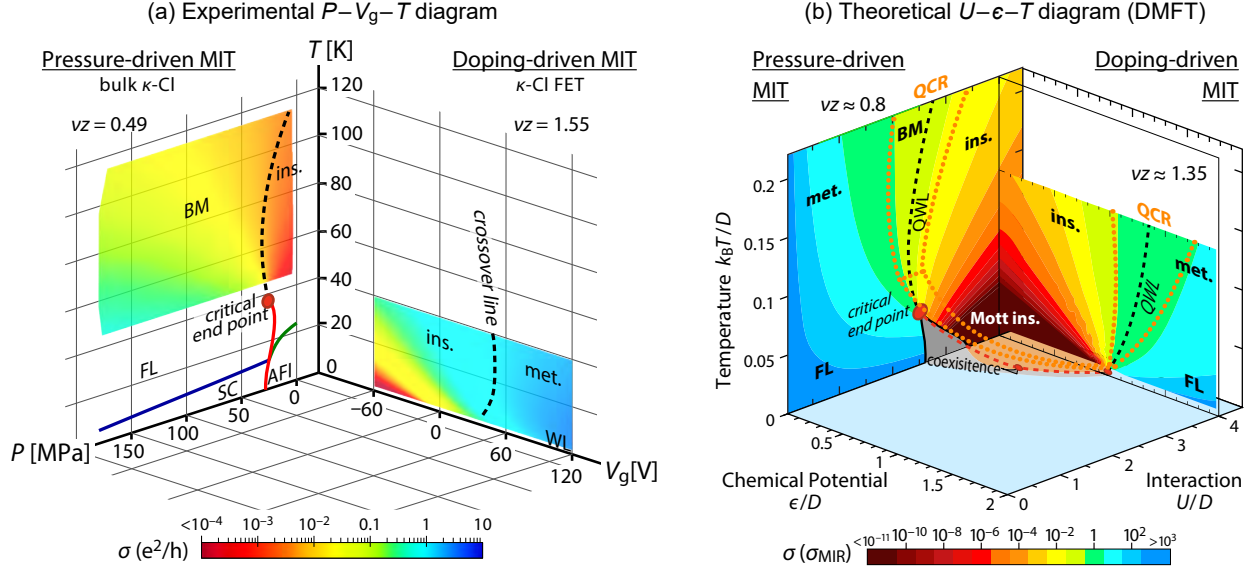
CONTENTS

Figure S6. **Phase diagrams for doping-driven and pressure-driven metal–insulator transitions around a Mott insulator.** (a) Experimentally determined pressure–gate-voltage–temperature($P − V_g − T$) phase diagram for κ-Cl with contour maps of conductivity in units of e^2/h. The phase diagram for a pressure-driven MIT at half-filling (left half of the panel) is determined from measurement for a bulk κ-Cl single crystal (adapted from ref. 21). (b) Interaction–chemical-potential–temperature ($U − \epsilon − T$) phase diagram based on DMFT solutions of the maximally frustrated Hubbard model, which is adapted from refs. 22 and 23. U and D represent on-site Coulomb repulsion energy in the Hubbard Hamiltonian and the half bandwidth, respectively, and ϵ is the chemical potential measured from the half-filled level.

driven and doping-driven Mott transitions. However, the nature of the QCR is significantly different between the two types of Mott transitions; the QCR for the doping-driven transition extends to low T ($vz \approx 1.35$, ref. 22) and the critical conductivity is $\sim \sigma_{MIR}$, whereas that for the pressure-driven transition at half-filling is observed above a high critical-end-point temperature ($vz \approx 0.8$, ref. 23) and the critical conductivity is suppressed to below $\sim 0.1\sigma_{MIR}$ (BM behavior). The experimental phase diagram is consistent with the theoretical one, although the weak localization (WL) is observed on the actual κ-Cl FET instead of FL behavior possibly due to disorders at the FET interface. (AFI: antiferromagnetic Mott insulator phase, SC: superconducting phase.)

G. SCALING ANALYSIS FOR QUANTUM CRITICALITY

As described in the main text, the quantum phase transition (QPT) is a phase transition between competing ground states, which can be tuned by a non-thermal parameter of the quantum systems. In contrast to classical phase transitions driven by the thermal fluctuation, the QPT is driven by the quantum fluctuation stemming from Heisenberg's uncertainty principle (or, more specifically,

[15] F. Kagawa, K. Miyagawa, and K. Kanoda, Nat. Phys. **5**, 880 (2009).

[16] K. Kanoda, J. Phys. Soc. Jpn. **75**, 051007 (2006).

[17] S. Lefebvre, P. Wzietek, S. Brown, C. Bourbonnais, D. Jérome, C. Mézière, M. Fourmigué, and P. Batail, Phys. Rev. Lett. **85**, 5420 (2000).

[18] Y. Kawasugi, H. Yamamoto, N. Tajima, T. Fukunaga, K. Tsukagoshi, and R. Kato, Phys. Rev. Lett. **103**, 116801 (2009).

[19] H. M. Yamamoto, M. Nakano, M. Suda, Y. Iwasa, M. Kawasaki, and R. Kato, Nat. Commun. **4**, 2379 (2013).

[20] M. Suda, Y. Kawasugi, T. Minari, K. Tsukagoshi, R. Kato, and H. M. Yamamoto, Adv. Mater. **26**, 3490 (2014).

[21] T. Furukawa, K. Miyagawa, H. Taniguchi, R. Kato, and K. Kanoda, Nat. Phys. **11**, 221 (2015).

[22] J. Vučičević, D. Tanasković, M. J. Rozenberg, and V. Dobrosavljević, Phys. Rev. Lett. **114**, 246402 (2015).

[23] J. Vučičević, H. Terletska, D. Tanasković, and V. Dobrosavljević, Phys. Rev. B **88**, 075143 (2013).

[24] O. Gunnarsson, M. Calandra, and J. E. Han, Rev. Mod. Phys. **75**, 1085 (2003).

[25] N. E. Hussey, K. Takenaka, and H. Takagi, Phil. Mag. **84**, 2847 (2004).

[26] G. Sordi, P. Sémon, K. Haule, and A. M. S. Tremblay, Phys. Rev. Lett. **108**, 216401 (2012).

[27] V. Dobrosavljević, in Conductor-insulator quantum phase transition, edited by V. Dobrosavljević, N. Trivedi, and J. M. Valles, Jr. (Oxford University Press, 2012) Chap. 1.

[28] V. F. Gantmakher and V. T. Dolgopolov, Physics-Uspekhi **53**, 57 (2010).

[29] D. A. Knyazev, O. E. Omel'yanovskii, V. M. Pudalov, and I. S. Burmistrov, Phys. Rev. Lett. **100**, 046405 (2008).

[30] N. R. Pradhan, A. McCreary, D. Rhodes, Z. Lu, S. Feng, E. Manousakis, D. Smirnov, R. Namburu, M. Dubey, A. R. Hight Walker, H. Terrones, M. Terrones, V. Dobrosavljević, and L. Balicas, Nano Lett. **15**, 8377 (2015).

[31] P. Limelette, A. Georges, D. Jérome, P. Wzietek, P. Metcalf, and J. M. Honig, Science **302**, 89 (2003).

[32] F. Kagawa, K. Miyagawa, and K. Kanoda, Nature **436**, 534 (2005).

[33] M. Abdel-Jawad, R. Kato, I. Watanabe, N. Tajima, and Y. Ishii, Phys. Rev. Lett. **114**, 106401 (2015).

[34] A. Pelissetto and E. Vicari, Phys. Rep. **368**, 549 (2002).

[35] G. G. Simeoni, T. Bryk, F. A. Gorelli, M. Krisch, G. Ruocco, M. Santoro, and T. Scopigno, Nat. Phys. **6**, 503 (2010).

Поглавље *Wigner–Mott Quantum Criticality: From 2D-MIT to 3*He *and Mott Organics,* аутора Проф. Владимира Добросављевића и др Дарка Танасковића у монографији *Strongly Correlated Electrons in Two Dimensions,* коју је уредио Проф. Сергеј Кравченко, базирано је пре свега на следећим радовима:

1. M. M. Radonjić, **D. Tanasković**, V. Dobrosavljević, G. Kotliar, and K. Haule, *Wigner-Mott Scaling of Transport Near the Two-dimensional Metal-insulator Transition*, Phys. Rev. B 85, 085133 (2012).
2. Terletska, J. Vučičević, **D. Tanasković**, and V. Dobrosavljević, *Quantum Critical Transport Near the Mott Transition*, Phys. Rev. Lett. **107**, 026401 (2011).
3. J. Vučičević, H. Terletska, **D. Tanasković,** and V. Dobrosavljević, *Finite-temperature Crossover and the Quantum Widom Line Near the Mott Transition*, Phys. Rev. B **88**, 075143(2013).

Тематика из монографије је такође обрађивана и у радовима:

4. J. Vučičević, **D. Tanasković**, M. J. Rozenberg and V. Dobrosavljević, *Bad-Metal Behavior Reveals Mott Quantum Criticality in Doped Hubbard Models*, Phys. Rev. Lett. **114,** 246402 (2015).
5. **D. Tanasković**, K. Haule, G. Kotliar, and V. Dobrosavljević, *Phase diagram, energy scales and nonlocal correlations in the Anderson lattice mode*l, Phys. Rev. B **84**, 115105 (2011), IF=3.774.
6. A. Amaricci, A. Camjayi, K. Haule, G. Kotliar, **D. Tanasković**, and V. Dobrosavljević, *Extended Hubbard model: Charge Ordering and Wigner-Mott transition*, Phys. Rev. B **82**, 155102 (2010).
7. M. M. Radonjić, **D. Tanasković**, V. Dobrosavljević and K. Haule, *Influence of disorder on incoherent transport near the Mott transition*, Phys. Rev. B **81,** 075118 (2010)

О значају тематике обрађене у монографији, за коју су В. Добросављевић и Д. Танасковић написали уводно поглавље, најбоље говори податак да је откриће Сергеја Кравченка из 1995. године о постојању металне фазе и метал-изолатор прелаза у јако интерагујућем дводимензионалном електронском гасу уврштено од стране Америчког друштва физичара међу 50 најважнијих открића у мезоскопској физици у двадесетом веку (видети копију последње стране књиге).

The properties of strongly correlated electrons confined in two dimensions are a forefront area of modern condensed matter physics. In the past two or three decades, strongly correlated electron systems have garnered a great deal of scientific interest due to their unique and often unpredictable behavior. Two of many examples are the metallic state and the metal–insulator transition discovered in 2D semiconductors: phenomena that cannot occur in noninteracting systems. Tremendous efforts have been made, in both theory and experiment, to create an adequate understanding of the situation; however, a consensus has still not been reached.

Strongly Correlated Electrons in Two Dimensions compiles and details cutting-edge research in experimental and theoretical physics of strongly correlated electron systems by leading scientists in the field. The book covers recent theoretical work exploring the quantum criticality of Mott and Wigner–Mott transitions, experiments on the metal–insulator transition and related phenomena in clean and dilute systems, the effect of spin and isospin degrees of freedom on low-temperature transport in two dimensions, electron transport near the 2D Mott transition, experimentally observed temperature and magnetic field dependencies of resistivity in silicon-based systems with different levels of disorder, and microscopic theory of the interacting electrons in two dimensions. Edited by Sergey Kravchenko, a prominent experimentalist, this book will appeal to advanced graduate-level students and researchers specializing in condensed matter physics, nanophysics, and low-temperature physics, especially those involved in the science of strong correlations, 2D semiconductors, and conductor–insulator transitions.

Sergey Kravchenko is professor of physics at Northeastern University, Boston, USA. He graduated from Moscow Institute of Physics and Technology, Russia, in 1982 and obtained his PhD from the Institute of Solid State Physics, Chernogolovka, Russia, in 1988. His research focuses on the low-temperature (millikelvin) properties of low-dimensional disordered systems by means of transport, capacitance, magnetization, and thermopower measurements. His primary interest is to understand the nature of the metallic state and the metal–insulator transition in strongly interacting 2D electron systems, discovered by him and his collaborators, and to determine its phase diagram. This discovery was listed among the 50 main discoveries in mesoscopic physics of the past century on the American Physical Society timeline in 1999 ("A Century of Mesoscopic Physics: 1899–1999").

Subject	**Fwd: JPCM highlights of 2016**
From	Nenad Lazarevic <nenadl@ipb.ac.rs>
To	Zoran Popovic <popozor@ipb.ac.rs>, Marko Opacic <mopacic@ipb.ac.rs>, Darko Tanaskovic <tanasko@ipb.ac.rs>, Milos Radonjic <milos.radonjic@ipb.ac.rs>, Cedomir Petrovic <petrovic@bnl.gov>, Maja Scepanovic <maja@ipb.ac.rs>
Date	2017-02-13 12:16

-------- Original Message --------
Subject: JPCM highlights of 2016
Date: 2017-02-08 15:19
From: Lucy Smith <Lucy.Smith@iop.org>
To: nenadl@ipb.ac.rs

 Dear Dr Lazarevic

I'm pleased to inform you that your 2016 Journal of Physics: Condensed
Matter (JPCM) article entitled "Raman spectroscopy of KxCo2-ySe2
single crystals near the ferromagnet—paramagnet transition" has been
selected as one of the journal Highlights of 2016. The papers in this
collection were chosen based on a number of criteria, including
presentation of outstanding research, popularity with our online
readership and high praise from referees.

You can view the full collection here:
http://iopscience.iop.org/journal/0953-8984/page/Highlights-of-2016 [1]

I would like to take this opportunity to thank you for publishing your
work with us and we hope to work with you again soon.

Best regards,
Lucy

DR LUCY SMITH
Executive Editor, Journal of Physics: Condensed Matter

IOP Publishing
Temple Circus, Temple Way, Bristol,
BS1 6HG, UK

Direct line +44 (0)117 930 1287

ioppublishing.org

JPCM Highlights of 2016 [1]

Links:
------
[1] http://iopscience.iop.org/journal/0953-8984/page/Highlights-of-2016

--
Institute of Physics Belgrade
Pregrevica 118, 11080 Belgrade, Serbia
http://www.ipb.ac.rs/

WEB OF SCIENCE™

THOMSON REUTERS

Search   My Tools ▾ | Search History | Marked List

Citing Articles: 24
(from Web of Science Core Collection)

For: Quantum Critical Transport near the Mott Transition **...More**

Times Cited Counts

25 in All Databases

24 in Web of Science Core Collection

1 in BIOSIS Citation Index

0 in Chinese Science Citation Database

0 data sets in Data Citation Index

0 publication in Data Citation Index

1 in Russian Science Citation Index

0 in SciELO Citation Index

View Additional Times Cited Counts

Refine Results

Search within results for...   🔍

Web of Science Categories   ▼

- ☐ PHYSICS CONDENSED MATTER (13)
- ☐ PHYSICS MULTIDISCIPLINARY (9)
- ☐ CHEMISTRY MULTIDISCIPLINARY (2)
- ☐ OPTICS (1)
- ☐ NANOSCIENCE NANOTECHNOLOGY (1)

more options / values...

Refine

Document Types   ▼

- ☐ ARTICLE (24)

Refine

Research Areas   ◀

Authors   ◀

Group Authors   ◀

Editors   ◀

Sort by: **Times Cited -- highest to lowest**   Page [1]   of 3

☐ Select Page   🗗 ✉   **Save to EndNote online**   **Add to Marked List**

≡ **Analyze Results**
Create Citation Report

☐ 1.   **Mott physics and first-order transition between two metals in the normal-state phase diagram of the two-dimensional Hubbard model**
By: Sordi, G.; Haule, K.; Tremblay, A. -M. S.
PHYSICAL REVIEW B   Volume: 84   Issue: 7   Article Number: 075161   Published: AUG 17 2011
View Abstract

Times Cited: 36
(from Web of Science Core Collection)

Usage Count

☐ 2.   **Kondo Metal and Ferrimagnetic Insulator on the Triangular Kagome Lattice**
By: Chen, Yao-Hua; Tao, Hong-Shuai; Yao, Dao-Xin; et al.
PHYSICAL REVIEW LETTERS   Volume: 108   Issue: 24   Article Number: 246402   Published: JUN 13 2012
View Abstract

Times Cited: 27
(from Web of Science Core Collection)

Usage Count

☐ 3.   **Divergent Precursors of the Mott-Hubbard Transition at the Two-Particle Level**
By: Schaefer, T.; Rohringer, G.; Gunnarsson, O.; et al.
PHYSICAL REVIEW LETTERS   Volume: 110   Issue: 24   Article Number: UNSP 246405   Published: JUN 13 2013
View Abstract

Times Cited: 26
(from Web of Science Core Collection)

Usage Count

☐ 4.   **Efficient real-frequency solver for dynamical mean-field theory**
By: Lu, Y.; Hoeppner, M.; Gunnarsson, O.; et al.
PHYSICAL REVIEW B   Volume: 90   Issue: 8   Article Number: 085102   Published: AUG 5 2014
View Abstract

Times Cited: 24
(from Web of Science Core Collection)

Usage Count

☐ 5.   **Importance of subleading corrections for the Mott critical point**
By: Semon, Patrick; Tremblay, A. -M. S.
PHYSICAL REVIEW B   Volume: 85   Issue: 20   Article Number: 201101   Published: MAY 1 2012
View Abstract

Times Cited: 19
(from Web of Science Core Collection)

Usage Count

☐ 6.   **c-axis resistivity, pseudogap, superconductivity, and Widom line in doped Mott insulators**
By: Sordi, G.; Semon, P.; Haule, K.; et al.
PHYSICAL REVIEW B   Volume: 87   Issue: 4   Article Number: 041101   Published: JAN 7 2013
View Abstract

Times Cited: 17
(from Web of Science Core Collection)

Usage Count

Source Titles ◀

Book Series Titles ◀

Conference Titles ◀

Publication Years ◀

Organizations-Enhanced ◀

Funding Agencies ◀

Languages ◀

Countries/Territories ◀

ESI Top Papers ◀

Open Access ◀

For advanced refine options, use

Analyze Results

7. **Quantum criticality of Mott transition in organic materials**

By: Furukawa, Tetsuya; Miyagawa, Kazuya; Taniguchi, Hiromi; et al.

NATURE PHYSICS   Volume: 11   Issue: 3   Pages: 221-224   Published: MAR 2015

View Abstract

Times Cited: 14
(from Web of Science Core Collection)

Usage Count

8. **Bad-Metal Behavior Reveals Mott Quantum Criticality in Doped Hubbard Models**

By: Vucicevic, J.; Tanaskovic, D.; Rozenberg, M. J.; et al.

PHYSICAL REVIEW LETTERS   Volume: 114   Issue: 24   Article Number: 246402   Published: JUN 18 2015

View Abstract

Times Cited: 11
(from Web of Science Core Collection)

Usage Count

9. **Wigner-Mott scaling of transport near the two-dimensional metal-insulator transition**

By: Radonjic, M. M.; Tanaskovic, D.; Dobrosavljevic, V.; et al.

PHYSICAL REVIEW B   Volume: 85   Issue: 8   Article Number: 085133   Published: FEB 29 2012

View Abstract

Times Cited: 8
(from Web of Science Core Collection)

Usage Count

10. **Finite-temperature crossover and the quantum Widom line near the Mott transition**

By: Vucicevic, J.; Terletska, H.; Tanaskovic, D.; et al.

PHYSICAL REVIEW B   Volume: 88   Issue: 7   Article Number: 075143   Published: AUG 28 2013

View Abstract

Times Cited: 7
(from Web of Science Core Collection)

Usage Count

Select Page   **Save to EndNote online**   **Add to Marked List**

Sort by: **Times Cited -- highest to lowest**   Page **1** of 3

Show: **10 per page**

24 records matched your query of the 37,150,529 in the data limits you selected.

Search   My Tools ▾ | Search History | Marked List

Citing Articles: 24
(from Web of Science Core Collection)

Sort by: **Times Cited -- highest to lowest**   Page 2 of 3

For: Quantum Critical Transport near the Mott Transition **...More**

Times Cited Counts

25 in All Databases

24 in Web of Science Core Collection

1 in BIOSIS Citation Index

0 in Chinese Science Citation Database

0 data sets in Data Citation Index

0 publication in Data Citation Index

1 in Russian Science Citation Index

0 in SciELO Citation Index

View Additional Times Cited Counts

Refine Results

Search within results for...   🔍

Web of Science Categories ▼

☐ PHYSICS CONDENSED MATTER (13)

☐ PHYSICS MULTIDISCIPLINARY (9)

☐ CHEMISTRY MULTIDISCIPLINARY (2)

☐ OPTICS (1)

☐ NANOSCIENCE NANOTECHNOLOGY (1)

more options / values...

Refine

Document Types ▼

☐ ARTICLE (24)

Refine

Research Areas ◀

Authors ◀

Group Authors ◀

Editors ◀

☐ Select Page   📑 ✉   **Save to EndNote online**   **Add to Marked List**

≡ **Analyze Results**
Create Citation Report

☐ 11. **Absence of a quantum limit to charge diffusion in bad metals**
By: Pakhira, Nandan; McKenzie, Ross H.
PHYSICAL REVIEW B   Volume: 91   Issue: 7   Article Number: 075124   Published: FEB 23 2015
View Abstract

Times Cited: 3
(from Web of Science Core Collection)

Usage Count

☐ 12. **Polarization field in a single-valley strongly-interacting 2D electron system**
By: Dolgopolov, V. T.; Shashkin, A. A.
JETP LETTERS   Volume: 95   Issue: 11   Pages: 570-574   Published: AUG 2012
View Abstract

Times Cited: 3
(from Web of Science Core Collection)

Usage Count

☐ 13. **Anderson localization effects near the Mott metal-insulator transition**
By: Braganca, Helena; Aguiar, M. C. O.; Vucicevic, J.; et al.
PHYSICAL REVIEW B   Volume: 92   Issue: 12   Article Number: 125143   Published: SEP 24 2015
View Abstract

Times Cited: 1
(from Web of Science Core Collection)

Usage Count

☐ 14. **Mott transition and antiferromagnetism of cold fermions in the decorated honeycomb lattice**
By: Lin, Heng-Fu; Chen, Yao-Hua; Liu, Hai-Di; et al.
PHYSICAL REVIEW A   Volume: 90   Issue: 5   Article Number: 053627   Published: NOV 24 2014
View Abstract

Times Cited: 1
(from Web of Science Core Collection)

Usage Count

☐ 15. **Stoner Instability Revisited: Emergence of Local Quantum Criticality?**
By: Kim, Ki-Seok
JOURNAL OF THE PHYSICAL SOCIETY OF JAPAN   Volume: 83   Issue: 4   Article Number: 044709   Published: APR 2014
Full Text from Publisher   **View Abstract**

Times Cited: 1
(from Web of Science Core Collection)

Usage Count

☐ 16. **Magnetic fluctuations near the Mott transition towards a spin liquid state**
By: Florens, Serge; Mohan, Priyanka; Janani, C.; et al.
EPL   Volume: 103   Issue: 1   Article Number: 17002   Published: JUL 2013
View Abstract

Times Cited: 1
(from Web of Science Core Collection)

Usage Count

☐ 17. **Fine Tuning the Performance of Multiorbital Radical Conductors by Substituent Effects**

Times Cited: 0
(from Web of Science Core Collection)

Source Titles ◀

Book Series Titles ◀

Conference Titles ◀

Publication Years ◀

Organizations-Enhanced ◀

Funding Agencies ◀

Languages ◀

Countries/Territories ◀

ESI Top Papers ◀

Open Access ◀

For advanced refine options, use

Analyze Results

By: Mailman, Aaron; Wong, Joanne W. L.; Winter, Stephen M.; et al.
JOURNAL OF THE AMERICAN CHEMICAL SOCIETY   Volume: 139   Issue: 4   Pages: 1625-1635   Published: FEB 1 2017

View Abstract

18.   **Critical Behavior in Doping-Driven Metal-Insulator Transition on Single-Crystalline Organic Mott-FET**
By: Sato, Yoshiaki; Kawasugi, Yoshitaka; Suda, Masayuki; et al.
NANO LETTERS   Volume: 17   Issue: 2   Pages: 708-714   Published: FEB 2017

View Abstract

Times Cited: 0
(from Web of Science Core Collection)

Usage Count

19.   **Fate of Spinons at the Mott Point**
By: Lee, Tsung-Han; Florens, Serge; Dobrosavljevic, Vladimir
PHYSICAL REVIEW LETTERS   Volume: 117   Issue: 13   Article Number: 136601   Published: SEP 20 2016

View Abstract

Times Cited: 0
(from Web of Science Core Collection)

Usage Count

20.   **Quantum critical transport at a continuous metal-insulator transition**
By: Haldar, P.; Laad, M. S.; Hassan, S. R.
PHYSICAL REVIEW B   Volume: 94   Issue: 8   Article Number: 081115   Published: AUG 30 2016

View Abstract

Times Cited: 0
(from Web of Science Core Collection)

Usage Count

Select Page   **Save to EndNote online**   **Add to Marked List**

Sort by: **Times Cited -- highest to lowest**

Show: **10 per page**

Page 2 of 3

24 records matched your query of the 37,150,529 in the data limits you selected.

Search   My Tools ▾ | Search History | Marked List

Citing Articles: 24
(from Web of Science Core Collection)

For: Quantum Critical Transport near the Mott Transition **...More**

Times Cited Counts

25 in All Databases

24 in Web of Science Core Collection

1 in BIOSIS Citation Index

0 in Chinese Science Citation Database

0 data sets in Data Citation Index

0 publication in Data Citation Index

1 in Russian Science Citation Index

0 in SciELO Citation Index

View Additional Times Cited Counts

Refine Results

Search within results for...   🔍

Web of Science Categories ▼

☐ PHYSICS CONDENSED MATTER (13)

☐ PHYSICS MULTIDISCIPLINARY (9)

☐ CHEMISTRY MULTIDISCIPLINARY (2)

☐ OPTICS (1)

☐ NANOSCIENCE NANOTECHNOLOGY (1)

more options / values...

Refine

Document Types ▼

☐ ARTICLE (24)

Refine

Research Areas ◀

Authors ◀

Group Authors ◀

Editors ◀

Sort by: **Times Cited -- highest to lowest**   Page **3** of 3

☐ Select Page   🗗 ✉   **Save to EndNote online**   **Add to Marked List**

≡ **Analyze Results**

Create Citation Report

☐ 21. **Pseudogap and superconductivity in two-dimensional doped charge-transfer insulators**

By: Fratino, L.; Semon, P.; Sordi, G.; et al.
PHYSICAL REVIEW B   Volume: 93   Issue: 24   Article Number: 245147   Published: JUN 24 2016

View Abstract

Times Cited: 0
(from Web of Science Core Collection)

Usage Count

☐ 22. **Quantum critical Mott transitions in a bilayer Kondo insulator-metal model system**

By: Sen, Sudeshna; Vidhyadhiraja, N. S.
PHYSICAL REVIEW B   Volume: 93   Issue: 15   Article Number: 155136   Published: APR 19 2016

View Abstract

Times Cited: 0
(from Web of Science Core Collection)

Usage Count

☐ 23. **Mott Quantum Criticality in the Anisotropic 2D Hubbard Model**

By: Lenz, Benjamin; Manmana, Salvatore R.; Pruschke, Thomas; et al.
PHYSICAL REVIEW LETTERS   Volume: 116   Issue: 8   Article Number: 086403   Published: FEB 26 2016

View Abstract

Times Cited: 0
(from Web of Science Core Collection)

Usage Count

☐ 24. **Shear viscosity of strongly interacting fermionic quantum fluids**

By: Pakhira, Nandan; McKenzie, Ross H.
PHYSICAL REVIEW B   Volume: 92   Issue: 12   Article Number: 125103   Published: SEP 1 2015

View Abstract

Times Cited: 0
(from Web of Science Core Collection)

Usage Count

☐ Select Page   🗗 ✉   **Save to EndNote online**   **Add to Marked List**

Sort by: **Times Cited -- highest to lowest**   Page **3** of 3

Show: **10 per page**

24 records matched your query of the 37,150,529 in the data limits you selected.

Source Titles	◀
Book Series Titles	◀
Conference Titles	◀
Publication Years	◀
Organizations-Enhanced	◀
Funding Agencies	◀
Languages	◀
Countries/Territories	◀
ESI Top Papers	◀
Open Access	◀

For advanced refine options, use

Analyze Results

Прилог

Ангажованост у развоју услова за научни рад, образовању и формирању научних кадрова

UNIVERSITY OF BELGRADE
FACULTY OF PHYSICS

Miloš M. Radonjić

INFLUENCE OF DISORDER ON CHARGE TRANSPORT IN STRONGLY CORRELATED MATERIALS NEAR THE METAL-INSULATOR TRANSITION

Doctoral Dissertation

Belgrade, 2014.

УНИВЕРЗИТЕТ У БЕОГРАДУ

ФИЗИЧКИ ФАКУЛТЕТ

Милош М. Радоњић

УТИЦАЈ НЕУРЕЂЕНОСТИ НА ЕЛЕКТРОНСКИ ТРАНСПОРТ У ЈАКО КОРЕЛИСАНИМ МАТЕРИЈАЛИМА БЛИЗУ МЕТАЛ-ИЗОЛАТОР ПРЕЛАЗА

Докторска дисертација

Београд, 2014.

Thesis advisor, Committee member:
Dr. Darko Tanasković
Associate Research Professor
Institute of Physics Belgrade
University of Belgrade

Committee member:
Prof. Dr. Zoran Radović
Professor
Faculty of Physics
University of Belgrade

Committee member:
Prof. Dr. Đorđe Spasojević
Associate Professor
Faculty of Physics
University of Belgrade

Committee member:
Dr. Antun Balaž
Associate Research Professor
Institute of Physics Belgrade
University of Belgrade

Захвалница

На пруженој љубави, разумевању и подршци, као и на свему што се не би могло ни побројати, захваљујем се својој породици, оцу Миливоју, мајци Љиљани, брату Милану и сестри Миљани.

Хвала ментору др Дарку Танасковићу на одличној сарадњи, вођењу и великодушној помоћи у току истраживачког рада и израде докторске тезе. Хвала др Владимиру Добросављевићу на изврсној сарадњи, подршци и гостопримству које ми је указао. На пријатном и конструктивном заједничком раду захваљујем се колеги Јакши Вучичевићу. Посебно се захваљујем др Зорану Поповићу и др Ненаду Лазаревићу на успешној и веома плодотворној сарадњи.

Др Александру Белићу хвала на указаном поверењу и прилици да будем део Лабораторије за примену рачунара у науци, као и свим колегама на пријатној и радној атмосфери.

Хвала и свим пријатељима који су непосредно или посредно допринели овом постигнућу.

UNIVERSITY OF BELGRADE

FACULTY OF PHYSICS

Jakša Vučičević

SIGNATURES OF HIDDEN QUANTUM CRITICALITY IN THE HIGH-TEMPERATURE CHARGE TRANSPORT NEAR THE MOTT TRANSITION

Doctoral dissertation

Belgrade, 2015.

Јакша Вучичевић

ПОКАЗАТЕЉИ СКРИВЕНЕ КВАНТНЕ КРИТИЧНОСТИ У ВИСОКО-ТЕМПЕРАТУРНОМ ТРАНСПОРТУ НАЕЛЕКТРИСАЊА У БЛИЗИНИ МОТОВОГ ПРЕЛАЗА

Докторска дисертација

Београд, 2015.

Thesis advisor, Committee member:
Dr. Darko Tanasković
Associate Research Professor
Institute of Physics Belgrade
University of Belgrade

Committee member:
Dr. Zoran Radović
Professor
Faculty of Physics
University of Belgrade

Committee member:
Dr. Đorđe Spasojević
Associate Professor
Faculty of Physics
University of Belgrade

Committee member:
Dr. Mihajlo Vanević
Assistant Professor
Faculty of Physics
University of Belgrade

Committee member:
Dr. Nenad Vukmirović
Associate Research Professor
Institute of Physics Belgrade
University of Belgrade

Acknowledgemets

Subject Scheduling my PhD topic defense
From Willem-Victor van Gerven <wvm.vangervenoei@gmail.com>
To <rvoja@ipb.ac.rs>
Cc Darko Tanaskovic <tanasko@ipb.ac.rs>
Date 2017-03-27 14:28

- form.pdf (~886 KB)
- biography.docx (~12 KB)
- Student index.pdf (~631 KB)
- 170324_thesis-topic_v6.pdf (~1003 KB)

Dear Prof. Radovanović,

I hope you don't that I write to you in English. I am doing my PhD research with Dr. Darko Tanaskovic at SCL. Recently I have finished the mandatory topic defense paper.

I would like to take the opportunity to send it to you, together with additional materials, and start a dialogue on when to schedule the seminar. In this regards I should mention to you that Darko, my mentor, will be away abroad from 10th till the 23rd of April.

I will attach to this email all materials in electronic form, and I'd be happy to hear from you what exactly should be presented in hard-copy, if anything, and where to deliver it.

I look forward to your response and thank you for your attention.

Sincerely,

Willem-Victor van Gerven

Докторске студије ФИЗИКЕ

Ужа научна област: КВАНТНА, МАТЕМАТИЧКА И НАНОФИЗИКА			
1.	ФИЗДФКН1	Виши курс класичне механике	Милан Дамњановић
2.	ФИЗДФКН2	Виши курс квантне мехнаике	Милан Дамњановић, Таско Грозданов, Зоран Поповић
3.	ФИЗДФКН3	Виши курс математичке физике	Татјана Вуковић
4.	ФИЗДФКН4	Квантна информација и заснивање квантне механике	Часлав Брукнер
5.	ФИЗДФКН5	Геометријски методи физике	Раде Живаљевић
6.	ФИЗДФКН6	Симетрија нискодимензионалних система	Иванка Милошевић
7.	ФИЗДФКН7	Нелинеарни динамички системи	Никола Бурић
8.	ФИЗДФКН8	Физика наноструктура	Иванка Милошевић, Татјана Вуковић, Ласло Форо
9.	ФИЗДФКН9	Квантна механика комплексних система	Таско Грозданов, Иванка Милошевић, Никола Бурић
10.	ФИЗДФКН10	Квантна статистичка теорија светлости	Мирјана Поповић-Божић

Ужа научна област: КВАНТНА ПОЉА, ЧЕСТИЦЕ И ГРАВИТАЦИЈА			
1.	ФИЗДФПЕ1	Квантна теорија поља	Воја Радовановић
2.	ФИЗДФПЕ2	Теорија гравитације 1	Марија Димитријевић
3.	ФИЗДФПЕ3	Теорија гравитације 2	Бранислав Цветковић
4.	ФИЗДФПЕ4	Квантна теорија градијентних поља	Бранислав Саздовић
5.	ФИЗДФПЕ5	Квантовање поља у закривљеном простору	Маја Бурић
6.	ФИЗДФПЕ6	Симетрије елементарних честица	Ђорђе Шијачки
7.	ФИЗДФПЕ7	Стандардни модел	Ђорђе Шијачки, Марија Димитријевић
8.	ФИЗДФПЕ8	Суперсиметрије	Воја Радовановић
9.	ФИЗДФПЕ9	Теорија струна	Бранислав Саздовић
10.	ФИЗДФПЕ10	Некумутативна геометрија и примене у физици	Маја Бурић, Марија Димитријевић
11.	ФИЗДФПЕ11	Космологија	Немања Калопер

Ужа научна област: ФИЗИКА ВИСОКИХ ЕНЕРГИЈА И НУКЛЕАРНА ФИЗИКА			
1.	ФИЗДФНФ1	Физика акцелератора	Петар Аџић
2.	ФИЗДФНФ2	Детектори у физици високих енергија	Петар Аџић
3.	ФИЗДФНФ3	Нуклеарна спектроскопија и радијациона физика	Јован Пузовић
4.	ФИЗДФНФ4	Виши курс нуклеарне физике 2	Јован Пузовић
5.	ФИЗДФНФ5	Виши курс физике елементарних честица 2	Петар Аџић, Јован Милошевић
6.	ФИЗДФНФ6	Феноменологија у физици честица	Љиљана Симић
7.	ФИЗДФНФ7	Анализа података у физици високих енергија	Љиљана Симић
8.	ФИЗДФПЕ7	Стандардни модел	Ђорђе Шијачки, Марија Димитријевић

Ужа научна област: ФИЗИКА АТОМА И МОЛЕКУЛА			
1.	ФИЗДФАМ1	Структура атома и молекула	Наташа Недељковић, Таско Грозданов
2.	ФИЗДФАМ2	Физика атомских судврних процеса	Драгољуб Белић
3.	ФИЗДФАМ3	Теорија расејања	Таско Грозданов
4.	ФИЗДФАМ4	Интеракције електрона са атомским системима	Горан Попарић
5.	ФИЗДФАМ5	Интеракције са површинама	Наташа Недељковић
6.	ФИЗДФАМ6	Експерименталне методе физике електрон-атомских судара	Братислав Маринковић, Александар Милосављевић, Горан Попарић
7.	ФИЗДФАМ7	Специјална поглавља физике атома и молекула	Ненад Симоновић
8.	ФИЗДФАМ8	Фото-електронска и масена спектроскопија биомолекула	Александра Милосављевић, Братислав Маринковић

Ужа научна област: ФОТОНИКА И ЛАСЕРИ

1.	ФИЗДФФЛ1	Виши курс оптике	Милорад Кураица
2.	ФИЗДФФЛ2	Ласери и ласерска спектроскопија	Никола Коњевић, Милорад Кураица
3.	ФИЗДФФЛ3	Квантна и атомска оптика	Бранислав Јеленковић
4.	ФИЗДФФЛ4	Класична и квантна интерференција и кохеренција	Мирјана Поповић-Божић
5.	ФИЗДФФЛ5	Увод у нелинеарну фотонику	Љупчо Хаџиевски, Александра Малуцков
6.	ФИЗДФФЛ6	Холографија и интерферометрија	Дејан Пантелић
7.	ФИЗДФФЛ7	Оптичка метрологија велике моћи разлагања	Дејан Пантелић
8.	ФИЗДФФЛ8	Макро и нано фотонске структуре у биофизици и оптичким комуникацијама	Бранислав Јеленковић
9.	ФИЗДФФЛ9	Фотонички сензори	Јована Петровић

Ужа научна област: ФИЗИКА ЈОНИЗОВАНОГ ГАСА И ПЛАЗМЕ			
1.	ФИЗДФЈП1	Извори јонизованог гаса	Стеван Ђениже, Владимир Милосављевић, Драгана Марић
2.	ФИЗДФЈП2	Извори плазме и магнетохидродинамика	Никола Коњевић, Најдан Алексић, Братислав Обрадовић
3.	ФИЗДФЈП3	Дијагностика плазме	Стеван Ђениже, Невена Пуач, Срђан Буквић
4.	ФИЗДФЈП4	Физика електричних гасних пражњења	Срђан Буквић, Драгана Марић
5.	ФИЗДФЈП5	Сударни и транспортни процеси у јонизованим гасовима	Зоран Петровић, Саша Дујко
6.	ФИЗДФЈП6	Одабрана поглавља физике јонизованих гасова	Гордана Маловић, Стеван Ђениже
7.	ФИЗДФЈП7	Интеракција плазме и ласера са површинама	Јагош Пурић, Срђан Буквић, Иван Дојчиновић
8.	ФИЗДФЈП8	Интеракција плазме и ласера са површинама	Јагош Пурић, Срђан Буквић, Иван Дојчиновић
9.	ФИЗДФЈП9	Физичке основе савремених примена плазме	Милорад Кураица, Зоран Петровић
10.	ФИЗДФЈП10	Физика фузионе плазме	Јагош Пурић, Душан Јовановић
11.	ФИЗДФЈП11	Кинетичка теорија јонизованих гасова и плазме	Ђорђе Спасојевић

Ужа научна област: ФИЗИКА КОНДЕНЗОВАНЕ МАТЕРИЈЕ И СТАТИСТИЧКА ФИЗИКА			
1.	ФИЗДФКМ1	Спектроскопске технике у физици кондензоване материје	Зоран Поповић
2.	ФИЗДФКМ2	Квантна теорија поља у физици нискодимензионалних система	Милица Миловановић, Едиб Добарџић
3.	ФИЗДФКМ3	Методе квантне теорије поља у физици кондензоване материје	Зоран Радовић
4.	ФИЗДФКМ4	Неравнотежна статистичка физика	Милан Кнежевић
5.	ФИЗДФКМ5	Физика неуређених система	Милан Кнежевић, Сунчица Елезовић-Хаџић
6.	ФИЗДФКМ6	Физика диелектрика и фероелектрика	Јаблан Дојчиловић
7.	ФИЗДФКМ7	Физика магнетизма	Ђорђе Спасојевић
8.	ФИЗДФКМ8	Физика танких слојева	Наташа Бибић
9.	ФИЗДФКМ9	Физика полимерних система	Јаблан Дојчиловић, Владимир Ђоковић
10.	ФИЗДФКМ10	Физика суперпроводности	Зоран Радовић
11.	ФИЗДФКМ11	Физика фазних прелаза	Милан Кнежевић
12.	ФИЗДФКМ12	Физика раста кристала	Мићо Митровић
13.	ФИЗДФКМ13	Квантне течности	Антун Балаж
14.	ФИЗДФКМ14	Теорија функционала густине	Ненад Вукмировић
15.	ФИЗДФКМ15	Електронски транспорт у јако корелисаним системима	Дарко Танасковић
16.	ФИЗДФКМ16	Компјутерско моделовање структурних и електронских особина материјала	Жељко Шљиванчанин
17.	ФИЗДФКМ17	Скенирајућа атомска микроскопија чврстих тела	Радош Гајић

Ужа научна област: ПРИМЕЊЕНА ФИЗИКА			
1.	ФИЗДФПФ1	Изабрана поглавља из медицинске физике	Мирослав Драмићанин
2.	ФИЗДФПФ2	Изабрана поглавља из метрологије	Љубиша Зековић, Стеван Стојадиновић
3.	ФИЗДФПФ3	Изабрана поглавља примењене физике	Иван Белча, Стеван Стојадиновић
4.	ФИЗДФПФ4	Луминесцентне појаве у танким филмовима	Љубиша Зековић, Стеван Стојадиновић
5.	ФИЗДФПФ5	Мерење ниских светлосних интензитета	Бећко Касалица

6.	ФИЗДФПФ6	Методе карактеризације наноматеријала	Мирослав Драмићанин
7.	ФИЗДФПФ7	Пројектовање оптичких система	Иван Белча, Бећко Касалица
8.	ФИЗДФПФ8	Пирометарски системи и безконтактне методе мерења температуре	Љубиша Зековић, Иван Белча
9.	ФИЗДФПФ9	Експерименталне методе биофизике	Милош Вићић
10.	ФИЗДФПФ10	Примена плазме у биологији и медицини	Невена Пуач, Зоран Петровић

Ужа научна област: НАСТАВА ФИЗИКЕ			
1.	ФИЗДФДФ1	Изабрана поглавља дидактике физике	Мићо Митровић
2.	ФИЗДФДФ2	Рад са талентованим ученицима	Мићо Митровић
3.	ФИЗДФДФ3	Методологија педагошких истраживања у физици	Андријана Жекић, Јаблан Дојчиловић
4.	ФИЗДФДФ4	Истраживање учења и наставе физике	Јосип Слишко
5.	ФИЗДФДФ5	Методе интерактивне наставе и учења физике	Мирјана Поповић-Божић, Братислав Обрадовић

РАЧУНАРСКИ ПРЕДМЕТИ ЗА ВИШЕ НАУЧНИХ ОБЛАСТИ			
1.	ФИЗДФВО1	Нумеричке методе у физици	Јован Пузовић, Зоран С. Поповић
2.	ФИЗДФВО2	Монте Карло симулације у физици	Горан Попарић, Антун Балаж
3.	ФИЗДФВО3	Методи нумеричке симулације у физици јонизованог гаса и плазме	Марија Радмиловић-Рађеновић, Најдан Алексић, Милован Шуваков
4.	ФИЗДФВО4	Нумеричке методе и симулације у квантној оптици	Душан Арсеновић

Координатори смерова:

1. Квантна, математичка и нанофизика: М. Дамњановић, М. Поповић Божић
2. Квантна поља, честице и гравитација: Б. Саздовић, В. Радовановић
3. Физика атома и молекула: Т. Грозданов, Н. Недељковић
4. Квантна оптика и ласери: М. Кураица, Љ.Хаџиевски
5. Физика јонизованог гаса и плазме: С. Буквић,З.Петровић
6. Физика кондензоване материје и статистичка физика: Н. Бибић, З. Радовић, М. Кнежевић
7. Примењена физика: М. Драмићанин, И. Белча
8. Настава физике: Ј. Дојчиловић

Прилог

Руковођење пројектима, потпројектима и пројектним задацима

ПОТВРДА О РУКОВОЂЕЊУ ПОТПРОЈЕКТОМ

Овим потврђујем да виши научни сарадник **др Дарко Танасковић** за кога се покреће избор у звање научни саветник, у оквиру Лабораторије за примену рачунара у науци Националног центра изузетних вредности за изучавање комплексних система Института за физику у Београду, односно у оквиру пројекта ОН171017 „Моделирање и нумеричке симулације сложених вишечестичних система" руководи потпројектом: „Испитивање јако корелисаних квантних система". На поменутом потпројекту су ангажовани следећи истраживачи: др Дарко Танасковић, др Милица Миловановић, др Јакша Вучичевић, др Милош Радоњић, Милан Јоцић, Вилем-Виктор ван Гервен Ои и Ана Вранић.

Београд, 19. април 2017. године

др Антун Балаж

научни саветник

Руководилац пројекта ОН171017

Руководилац Центра за изучавање комплексних система Института за физику у Београду

Република Србија
МИНИСТАРСТВО ПРОСВЕТЕ,
НАУКЕ И ТЕХНОЛОШКОГ РАЗВОЈА
Број: 451-03-38/2016-09/20
Датум: 11.07.2016.
Немањина 22-26, Београд

Институт за физику
Др Дарко Танасковић

Прегревица 118
11080 Земун

Поштовани господине Танасковић,

Обавештавамо Вас да је на осмом заседању српско-словеначке Мешовите комисије између Републике Србије и Републике Словеније, која је одржана у Београду, 28. и 29. јануара 2016. године, Ваш пројекат „Јаке електорнске корелације и суперпроводност" одобрен за финансирање у оквиру програма научно-технолошке сарадње између две земље. Информација о свим одобреним пројектима је постављена на интернет презентацији Министарства www.mpn.gov.rs одмах након одржаног заседања Мешовитог комитета у Београду.

Реализација осмог циклуса билатералних пројеката траје од 1. фебруара. 2016. до 31. децембра 2017. године и подразумева размену истраживача као што је одобрено на заседању Мешовите комисије.

Министарство просвете, науке и технолошког развоја Републике Србије ће суфинансирати путне трошкове истраживача из Србије (без трошкова боравка) као и трошкове боравка истраживача из Словеније (без путних трошкова) у укупном износу до 1000 евра (у динарској противвредности) по једној години реализације пројекта. У оквиру вашег пројекта планирана је и дужа посета у Словенији која укључују младог српског истраживача. Словеначка страна ће поред трошкова смештаја и исхране обезбедити додатна средства на име трошкова превоза у износу до 1500 евра по једној години реализације пројекта.

На основу благовремено достављене профактуре за путовање, односно најаве посете словеначких истраживача, потписане од руководиоца пројекта и директора/декана института/факултета, могућа је уплата средстава унапред, у складу са буџетским могућностима и обавезама Министарства. Руководиоци пројеката су дужни да поднесу стручни и финансијски извештај институцијама надлежним за спровођење програма сарадње у својој земљи, по завршетку прве и друге истраживачке године.

Истовремено бих желео да Вам честитам на одобреном пројекту и пожелим успешну реализацију планираних активности.

С поштовањем,

МИНИСТАР
Др Срђан Вербић

IPB webmail

Subject	**Program Pavle Savic**
From	Nada Milosevic <nada.milosevic@nauka.gov.rs>
To	<darko.tanaskovic@ipb.ac.rs>
Date	2012-03-01 15:45

- Peto zasedanje.pdf (~958 KB)
- Usvojeni projekti PAI 2012-2013.xls (~37 KB)

Poštovani gospodine Tanasković,

Obaveštavamo Vas da je na zasedanju Mešovitog komiteta između Republike Srbije i Republike Francuske, koji je održan 29. februara 2012. godine Vaš projekat „Kvantni kritični transport u blizini Motovog metal-izolator prelaza" (broj projekta 680-00-132/2012-09/04) stavljen na listu odobrenih projekata u okviru Programa integrisanih aktivnosti "Pavle Savić".

U prilogu vam dostavljam potpisan izveštaj sa Petog zasedanja Meštovitog komiteta, kao i Tabelu odobrenih projekata sa opredeljenim sredstvima za realizaciju projekta.

Zahteve za refundaciju troškova putovanja, odnosno najave posete francuskih istraživača, potpisane od rukovodioca projekta i direktora instituta, dostavite na obrasce koje možete pronaći na sajtu Ministarstva http://www.mpn.gov.rs/sajt/page.php?page=284

Zahteve dostavite na adresu:

Ministarstvo prosvete i nauke

Nada Milošević

Nemanjina 22-26

 11000 Beograd

Želim vam uspešnu saradnju i čestitam vam.

S poštovanjem,

Nada Milošević

Kontatk telefon 011/3616 529

PUBLIC DIPLOMACY DIVISION
COLLABORATIVE PROGRAMMES SECTION
DIVISION DIPLOMATIE PUBLIQUE
SECTION PROGRAMMES EN COOPÉRATION

NATO
OTAN

7 March 2008
PDD(CP)-(CBP.EAP.RIG 983235)

Name of Grantee: Dr. Darko Tanaskovic
Address: Institute of Physics
                       Pregrevica 118, 11080 Belgrade-Zemun, Serbia

Upon consideration by the Advisory Panel on Chemistry / Biology / Physics, the Assistant Secretary General for Public Diplomacy has awarded a Reintegration Grant to you as Return Fellow to fund your research activity on "Electronic Structure Calculations of Complex Materials" which will take place at the Institute of Physics, Belgrade-Zemun, Serbia, under the supervision of Dr Dragan Popovic.

Consequently, the sum of EUR 14,000.00 (FOURTEEN THOUSAND EUROS) is granted to you under reference EAP.RIG.983235. This sum includes a special award of EUR 3,000, granted to you for travel and attendance at scientific meetings/conferences. The Conditions of Award overleaf, which form an integral part of this award letter, should be noted carefully.

Payment of the grants will be made in three instalments, as outlined in the Conditions of Award overleaf. Your attention is drawn to the specific documents required in order to release these instalments.

Unless an extension of time is authorised by NATO, the duration of this grant cannot exceed three years from the date of acceptance, and a final scientific and financial report for grant closure is, therefore, due at the end of this period.

By separate letter, a grant for EUR 11,000 is also being awarded to the Host Institution Director, Dr Dragan Popovic. All reports, including the interim reports, should be signed by both you and the Host Institution Director.

Please note that the grant reference number should be referred to in any correspondence on the current grant.

On behalf of the Assistant Secretary General
for Public Diplomacy

Dr. F. Pedrazzini
Programme Director

cc: Dr Dragan Popovic

These grants are accepted under the conditions stated in this letter of award and the conditions overleaf.

_____   28. 3. 2008.
Signature of Return Fellow   Date

_____   28. 3. 2008
Signature of Director of Host Institution Date

Прилог

Активност у научним и научно-стручним друштвима

IP8 webmail

Mail   Address Book   Settings   Logout

Filter: All ▼   🔍▾ aps   ⚙

Folders	Subject				Fro
Inbox	To_referee TANASKOVIC BB1…	prb@aps.org	2017-03-15 14:11	2 KB	
Drafts	Referee communication BB13357	prb@aps.org	2017-03-15 14:09	2 KB	
Sent	Reminder: APS Referee Survey	member@surveymonkey.com	2017-03-07 19:29	8 KB	
Junk (955)	Review_request TANASKOVIC…	prb@aps.org	2017-03-01 19:39	6 KB	
Trash	APS Referee Survey	member@surveymonkey.com	2017-03-01 15:50	8 KB	
April2009	To_referee TANASKOVIC XY1…	prb@aps.org	2017-01-20 20:44	2 KB	
Drafts	Thank you for your report on X…	prl@aps.org	2017-01-12 19:15	4 KB	
Inbox10					

Select: Threads: Show preview pane: ☑   Messages 1 to 32 of 32

Inbox2010
Inbox2011
Inbox2012
Inbox2013
Inbox2014-2015
Inbox2015
Oktobar2009
Sent
Sent_2009-2011
Sent_2012-2013
SentApril2009
Trash

Subject	**APS Referee Survey**
From	member@surveymonkey.com 👤
Sender	survey-noreply@smo.surveymonkey.com 👤
To	tanasko@ipb.ac.rs 👤
Reply-To	no-reply@aps.org 👤
Date	2017-03-01 15:50

APS Referee Survey

APS is conducting a brief online survey about our review process so that we can make it more efficient and more compatible with our referees' needs and expectations. The survey should take approximately 10 minutes to complete. As a valued referee for *Physical Review,* your input is greatly appreciated. The survey will close on March 14th.

Pierre Meystre
Editor in Chief
American Physical Society

Begin Survey

Please do not forward this email as its survey link is unique to you.
Unsubscribe from this list

IP8 webmail

Dear Dr Tanaskovic,

This Paper has been submitted to Journal of Physics: Condensed Matter for consideration and you have been suggested as a possible expert who could referee the article. We would be very grateful if you could help us.

The abstract appears at the end of this letter, along with the names of the author(s). Please let us know as soon as possible if you will be able to accept our invitation to referee. You may follow the appropriate link at the bottom of the page or e-mail us with your reply. Once you accept our invitation to referee this manuscript, you will be notified via e-mail about how to access it through our online referee system. You will then have access to the manuscript and referee instructions in your Referee Centre.

We require your comments and recommendation by 27 Dec 2016. However, if you need more time, please contact the journal at jpcm@iop.org giving a provisional date you hope to report by. If you are unable to report on this occasion we would be grateful if you could provide the names and e-mail addresses of possible alternative referees when prompted.

Thank you for considering this manuscript. We look forward to hearing from you soon.

Yours sincerely

Jade Holt

On behalf of the IOP peer-review team:
Editor - Jade Holt
Associate Editors - Graham Stinton, Thomas Sharp and Andy Massey
Editorial Assistants - Kirsty Abbott and David Marquiss
jpcm@iop.org

Executive Editor - Lucy Smith

IOP Publishing
Temple Circus, Temple Way, Bristol
BS1 6HG, UK

www.iopscience.org/jpcm

IP8 webmail

Subject	**DECI-13 scientific reviews**
From	Chris Johnson <chrisj@epcc.ed.ac.uk>
To	Chris Johnson <chrisj@epcc.ed.ac.uk>
Date	2015-11-06 11:53

- DECI-scientific-review-letter-DECI-13.pdf (~317 KB)

Dear all,

I would like to ask if you would kindly perform some DECI-13 scientific reviews, having
reviewed similar proposals for DECI-12 earlier last year. These are reviews for requests
for year-long access to Tier-1 computing resources across Europe. The procedure and
reviewing process is the same as for DECI-12 and DECI-11. There are 32 proposals and
each should get 2 reviews meaning 64 reviews in total are needed so with a panel of 24 I
estimate is that there would be between 2-3 reviews each and I will expand the panel as
required.

Please can you let me know as soon as possible if you are available or not for
performing reviews? I can assign the reviews as soon as you reply and the deadline for
reviewing is Friday 27th November (three weeks today). Some more information is in the
attached pdf. Please ignore the slightly earlier deadline of the 23rd November in the
document.

Many thanks for your support so far,

Cheers,

Chris

--
The University of Edinburgh is a charitable body, registered in
Scotland, with registration number SC005336.

Записник

са **Изборне скупштине Друштва физичара Србије**

одржане 30. октобра 2008. године у Београду

Председник ДФС Проф. др Мирослав Весковић отворио је седницу у 13:15 часова и предложио следећи

Д Н Е В Н И   Р Е Д:

1. Избор радних тела Скупштине:
    радног председништва, верификационе комисије,
    изборне комисије и записничара.
2. Извештај верификационе комисије.
3. Извештај о раду ДФС у периоду од 1. новембра 2006. године
    до 1. новембра 2008. године (М. Весковић и И. Савић).
4. Извештај о финансијском пословању ДФС у периоду
    од 01.11.2006. до 01.11.2008. године (И.Савић).
5. Избор чланова председништва ДФС:
    председника, заменика председника, потпредседника за
    финансије, секретара и председнике Оделења ДФС.
6. Дискусија по поднетим извештајима и предлози (сугестије)
    за будући рад ДФС.
7. Избор чланова Суда части ДФС.
8. Избор чланова Надзорног одбора ДФС.
9. Измене и допуне Статута ДФС (Д.Танасковић).
10. Питања, предлози и обавештења.

Пошто је једногласно усвојен дневни ред, прешло са на прву тачку дневног реда.

1. ***Избор радних тела Скупштине.*** Изабрано је
   (а) Радно председништво (Илија Савић, Драгана Милићевић, Мирослав Весковић).
   (б) Верификациона комисија (Соња Јовићевић и Славиша Станковић).
   (в) Изборна комисија (Милијана Тодоровић и Југослав Богдановић).
   (д) Записничар (Дарко Танасковић).

2. Пошто је Радно председништво преузело вођење Скупштине, прешло се на другу тачку дневног реда: ***Извештај верификационе комисије.***

Известилац верификационе комисије Славиша Станковић саопштио је да Скупштини у својству делегата присуствује
   (а) 6 чланова Председништва (Мирослав Весковић, Александар Белић, Илија Савић, Дарко Танасковић, Маја Бурић и Горан Попарић).
   (б) 7 представника Одељења за научна истраживања и високо образовање који су делегирани од стране матичних институција – колективних чланова ДФС (Соња Јовићевић, Владимир Цвјетковић, Горан Ђорђевић, Мићо Митровић, Божидар Цекић, Душанка Обадовић и Горан Ристић).
   (в) 14 представника Одељења за основно и средње образовање, који су изабрани по принципу један представник по једном округу (Саша Стојановић – Јабланички округ, Мирјана Комар - Јужно-Бачки округ, Анђелија Спасић – Јужно-Банатски округ, Предраг Стојаковић – Колубарски округ, Вера Прокић – Косовско-Митровачки округ, Мирко Нагл – Мачвански округ, Татјана Мишић – Нишавски округ, Нина Јовановић – Пиротски округ, Драгана Милићевић – Расински округ, Милијана Тодоровић – Рашки округ, Мирко Киселички – Северно-Бачки округ, Југослав Богдановић – Средње-Банатски округ, Катарина Ђорђевић – Шумадијски округ, Љиљана Сфорцан – град Београд).

Пошто Скупштини присуствује 27 делегата што је више од половине укупног броја делегата скупштине (45/2), закључено је да Скупштина може пуноправно да одлучује.

3.   Председник ДФС Проф. Мирослав Весковић је саопштио да се **рад ДФС у периоду од новембра 2006. године до новембра 2008. године** одвијао на реализацији:

  (а) Традиционалних активности.
  (б) Активности везаних за популаризацију физике.
  (в) Међународних активности.
  (г) Побољшању рада поједиих одељења, одсека и подружница
  (д) Сакупљању података за електронску базу о физичарима у земљи и дијаспори.

Сваку од ових активности, Председник Весковић је у представио у кратким цртама, након чега је Потпредседник ДФС Проф. Илија Савић, уз помоћ Power Point презентације, изнео детаљније податке.

(а) *Традиционалне активности.*

  (а1) Такмичења из физике:
       На такмичењима из физике у шк. 2006/2007 и 2007/2008 учествовало је више стотина ученика. Одржане су две Српске физичке олимпијаде, прва 2007. и друга 2008. Ученици средњих школа из Србије учествовали су на 38 th и 39th IPhO. Ученици основне школе учествовали су на: 3rd и 4th IJSO. На Веб сајту: http://www.dfs.org.yu/takmicenja/ дати су детаљно сви подаци о такмичењима из физике.

  (а2) Семинари о настави физике:
  -Регионални семинари.
  -Акредитовани прогарами за усавршавање наставника физике.
  -Републички семинар о настави физике.

  (а3) Издавање часописа "Млади физичар":
       У оквиру традиционалних облика популаризације физике у извештајном периоду изашла су 2 броја (104 и 105) знатно иновираног часописа "Млади физичар" са просечним тиражом од 1000 примерака. Број сталних претплатника је за сада релативно мали са трендом пораста .

  (а4) Наставни планови и програми:

Извршене су корекције програма физике у сва три разреда основне школе, ради растерећења, другачијег структуирања и осавремењивања.

(а5) Опремање школских кабинета из физике:
Постоје планови, који чекају реализацију.

(б) *Активности везаних за популаризацију физике.*

(б1) Друга посета студената и ученика "CERN-u".
(б2) Организовано је такмичење "Откривање талената за физику".
(б3) Преводе се и припремају постер биографије познатих физичара.

(в) *Међународне активности.*

Представници ДФС су узели учешће у различитим активностима везаним за Balkan Physical Union и European Physical Society. Подружница ДФС из Ниша је носилац рада SEENET – MTP мреже sa математичку и теоријску физику. Представници ДФС су учествовали у раду III IUPAP конференције о женама у физици.

(г) *Побољшању рада појединих одељења, одсека и подружница.*

У оквиру ДФС постоје два одељења, три одсека у оквиру једног од одељења и око 10 подружница у појединим окрузима. По мишљењу И. Савића, Одељење за основно и средње образовање заслужује похвалу за свој рад у претходном периоду, док Одељење за Научна истраживања и високо образовање још увек има само спорадичне активности.

 (д) *Сакупљању података за електронску базу о физичарима у земљи и дијаспори.*

У току је припрема базе података с именима физичара који предају у основним школама, гимназијама и средњим стручним школама. Физичара запослених на факултетима и институтима у Србији, као и база података о физичарима српског порекла који раде у иностранству.

4. ***Извештај о финансијском пословању*** ДФС у периоду од 01.11.2006. до 01.11.2008. године је поднео потпредседник ДФС Проф. И.Савић.

Извори прихода садрже:
(а) Средства из буџета републике Србије:

(a1) Додељен од Министарства просвете.

(a2) Додељена од Министарства науке.

(б) Приход од продаје публикација ДФС.

(в) Чланарина колективних чланова.

(г) Донације и спонзорства.

Структура расхода:

(а) Путни трошкови и котизације за олимпијаде: IPhO и IJSO.

(б) Путни трошкови за такмичења из физике и семинаре.

(в) Ауторски хонорари за ауторе и "прегледаче" задатака на такмичењима из физике.

(г) Ауторски хонорари за ауторе чланака у публикацијама ДФС.

(д) Материјални трошкови.

Укупни приходи за 2006. години износе 6.992.885,00 дин., а расходи 6.904.703,00 дин. Укупни приходи за 2007. години износе 7.635.699,00 дин., а расходи 7.635.499,00 дин. Приходи у периоду од 01.01. до 18.10.2008. године износе 3.712.687,00 дин, а расходи 2.968.323,00 дин. Стање на рачуну дана 18.10.2008. године износи 744.365,00 дин.

5. Избор чланова Председништва ДФС.

И. Савић је поднео и образложио следећу листу кандидата:

а) За председника ДФС

Александар Белић - Институт за физику.

б) За заменика председника ДФС

Стеван Јокић - Институт за нуклеарне науке „ВИНЧА".

в) За потпредседника ДФС

Илија Савић - Друштво физичара Србије.

г) За секретара ДФС

Дарко Танасковић – Институт за физику

д) За председника Одељења ДФС за основно и средње образовање

Душанка Обадовић – Департман за физику ПМФ Нови Сад.

ђ) За председника Одељења ДФС за научна истраживања и високо образовање

Горан Ђорђевић - Одсек за физику ПМФ Ниш.

На предлог М. Весковића Скупштина је донела одлуку да се гласање обави јавно, подизањем руку. При томе се гласало појединачно за сваког од наведених кандидата и резултати гласања су:

а) За Александра Белића је гласало 26 делегата и 1 је био уздржан.

б) За Стевана Јокића је гласало 26 делегата и 1 је био уздржан.

в) За Илију Савића је гласало 26 делегата и 1 је био уздржан.

г) За Дарка Танасковића је гласало 25 делегата и 2 су била уздржана.

д) За Душанку Обадовић је гласало 26 делегата и 1 је био уздржан

ђ) За Горана Ђорђевића је гласало 25 делегата, 1 је био против и 1 уздржан.

Пошто се према члану 42, одлуке на Скупштини доносе већином присутних делегата, М. Весковић је констатовао да су за мандатни период 2008-2010. године изабрани:

Александар Белић за председника ДФС,

Стеван Јокић за заменика председника ДФС,

Илија Савић за потпредседника ДФС,

Дарко Танасковић за секретара ДФС,

Душанка Обадовић за председника Одељења ДФС за основно и средње образовање,

Горан Ђорђевић за председника Одељења ДФС за научна истраживања и високо образовање.

6. Шеста тачка дневног реда - *Предлози за будући рад ДФС*, је донела више запажених излагања.

(а) А. Белић је још једном истакао на важност превазилажења проблема везаних за финансирање активности које подржава Министарство просвете. Најновији пример је проблем у исплати средстава за рад Истрживачке станице "Петница" која је Министарство просвете раније већ одобродило.

А. Белић је затим још једном указао да је поред колективног чланства у ДФС, за кредибилитет Друштва веома важно и успостављање механизма за плаћање индивидуалне чланарине. Још једном је истакнуто да борба за права наставника у основним и средњим школама мора да буде један од главних приоритета у раду ДФС.

(б) Г. Ђорђевић је у свом излагању упознао делегате Скупштине са радом Подружнице у Нишу и навео низ активности које је Подружница организовала у претходном периоду. Међу запаженим активностима је рад Школе физике за ученике основних и средњих школа која ради већ четири године и окупља око 150 ученика. Затим, са успехом се организује Зимски камп физике у Соко Бањи. Школа физике за ученике средњих школа постоји већ шест година и сваке године окупи двадесетак ученика. У оквиру ове школе, повремено се одржавају и популарна предавања које се издвајају добром посећеношћу. Подружница у Нишу такође организује и Зимски

семинар за наставнике, а носилац је и веома успешне међународне сарадње у оквиру SEENET-MTP мреже за математичку и теоријску физику.

(в) М. Нагл је поздравио активности Подружнице у Нишу, али је истакао на велике проблеме са којима се срећу наставници у градовима у којима не постоје универзитетски центри и у којима је још теже заинтересовати ученике за физику. М. Нагл је указао да је због тога веома важно што боље искористити публицитет који физичари добијају поводом почетка рада експеримента у CERN-у.

Указано је такође на опасност истискивања физике из програма гимназија и указано је да немамо информације докле се стигло у плановима за реформу образовања у гимназијама.

(г) М. Весковић је обавестио о активностима ДФС везаним за усвајање Стандарда за физику у основним сколама .

(д) С. Јокић је најавио скуп посвећен образовању у Француској, који ће крајем новембра да буде одржан у згради Академије наука у Београду.

(ђ) М. Митровић је указао на неравномерно регионално интересовање ученика за такмичења из физике. Делегати су затим обавештени да су Министарству за просвету прослеђени захтеви за организовање три нове смотре из физике: такмичења ученика медицинских школа, такмичење "Еко физика" и "Откривање талената". Што се финансирања постојећих такмичења тиче, највећи проблеми се јављају у финансирању путовања на олимпијаде.

(е) М. Весковић је указао на значај налажења финансирања из различитих извора у чему до сада није било пуно успеха и углавном се ослањало на Министарства просвете и науке.

(ж) М. Ђурић је обавестила делегате о активностима за популаризацију физике које је у претходном периоду организовао Физички факултет у Београду и припремама за Фестивал науке у децембру. Наредних месеци је планиран једнодневни скуп ученика на Физичком факултету у чији ће програм интерактивно бити укључени сарадници из CERN-a. М. Ђурић је истакла недовољно добро информисање наставника и ученика везано за активности које популаризују физику.

(з) Д. Милићевић је истакла e-mail листе као најкориснији начин обавештавања, а М. Весковић значај обавештавања путем ДФС веб сајта. А. Белић је најавио да ће у наредном периоду бити посвећена већа пажња прављењу што функционалнијег веб сајта. А. Белић је такође указао на важност коришћења образовних ресурса CERN-a и важност медијске промоције коју експерименти у CERN-у омогућавају.

(и) М. Весковић је говорио поводом питања делегата о примени Болоњске декларације и последицама на средњошколско образовање. Један од главних недостатака је у томе што на нивоу Министарства још увек није донесен правилник који регулише које су квалификације неопходне за послове попут рада у основним и средњим школама, према којем би се онда управљали и факултети.

(ј) Д. Милићевић је још једном истакла значај иницијативе наставника у развијању веза са високошколским установама и развијања интересовања за физику код ученика. М. Поповић Божић је указала на важност укључивања у европске токове и истакла два квалитетна часописа који нису у довољној мери популарни, "EPS news" и "Science in School". М. Поповић Божић је такође известила делегате о IUPAP конференцији о заступљености жена у физици.

(к) В. Цвјетковић је указао да се заинтересованост за физику постиже путем извођења експеримената што је веома запостављено у нашим школама. Такође је у нашем образовању веома слабо истакнута повезаност физике са постојећим и новим технологијама. М. Митровић је такође, указао на слабу едукацију на нашим факултетима о коришћењу наставних средстава, што се одражава на рад у школама. Д. Обадовић је указала на позитивне ефекте извођења једноставних експеримената у основним школама.

7.   Једногласно су изабрани **чланови Суда части (**Милутин Вучковић, Милијана Тодоровић и Божидар Цекић).

8.   Једногласно су изабрани **чланови Надзорног одбора** (Предраг Стојаковић за председника, Нина Јовановић и Горан Ристић за чланове).

9. *Измене и допуне статута ДФС*
Једногласно су прихваћене следеће измене Статута:

(а) Брисање члана 21. који је гласио:
Друштво је члан Друштва физичара Србије и Црне Горе.

(б) Допуна члана 8:
У оквиру одељења за научна истраживања и високо образовање, поред комисије за међународну сарадњу, формира се посебна комисија:
Комисија за учешће жена у физици.

(в) Допуна члана 9:
У оквиру одељења за основно и средње образовање, формирају се две нове комисије:
Комисија за откривање талената за физику,
Комисија за физику околине.

Г. Ђорђевић је у дискусији је изнео предлог да се прецизније дефинише рад Скупштине одељења за основно и средње образовање. А. Белић је предложио да се о овом и, као и евентуалним другим предлозима, поведе расправа најпре у оквиру Председништва.

10. Обзиром да је предвиђено време за рад Изборне скупштине истекло, делегати су се сложили да сви они који имају преостала *питања, предлоге и обавештења* њих доставе Председништву ДФС путем e-mail-a, или их директно саопште члановима Председништва.

Београд 30.10.2008.

Записник саставио   Председник ДФС др Александар Белић
др Дарко Танасковић
Секретар ДФС

SFKM 2007
XVII Symposium on Condensed Matter Physics

Serbia - Vršac
16.9. - 20.9. 2007.

General Information   Useful Information   Invited Speakers   Register   Submitted Abstracts   Contact

..General Information:

Focused sessions

1. Nanostructures and Low-dimensional Systems
2. Superconductivity, Magnetism and Strongly Correlated Systems
3. Soft Matter
4. Semiconductors
5. Optics and Spectroscopy
6. Experimental Methods, Instruments, and Applied Condensed Matter Physics

Co-chairmen:

Z. V. Popovic, IF Belgrade
M. Damnjanovic, FF Belgrade
Z. Radovic, FF Belgrade

Scientific committee:

I. Bozovic, BNL USA
L. Forro, EPFL Switzerland
M. Kulic, M. Planck Germany
B. Tadic, J. Stefan Slovenia
V. Srdanov, Uni. di Milano Italy
B. Babic-Stojic, INN Vinca
N. Bibic, INN Vinca
R. Gajic, IF Belgrade
D. Kapor, PMF Novi Sad
M. Knezevic, FF Belgrade
M. J. Konstatinovic, IF Belgrade
V. Milanovic, ETF Belgrade
I. Milosevic, FF Belgrade
S. Milosevic, FF Belgrade
M. Milovanovic, IF Belgrade
N. Romcevic, IF Belgrade
F. Vukajlovic, INN Vinca
Lj. Zekovic, FF Belgrade

Organizing committee:

R. Zikic, IF Belgrade (chairman)
M. Savic, FF Belgrade (secretary)
D. Tanaskovic, IF Belgrade
E. Dobardzic, FF Belgrade
I. Savic, Serbian Physical Society

..NEW:

Agenda
Proceeding

Deadlines: July 15, 2007.
Abstract submission: on-line.
Paper submission: on-line, 4p max.
Proceedings will be distributed to participants at the beginning of the Conference.

..Organizers:

Društvo fizičara Srbije

Institute of Physics
Belgrade - Serbia

Fizički fakultet
Univerziteta u Beogradu

Institut za nuklearne nauke "Vinča"

..Sponsors:

Република Србија

Ministarstvo nauke

The Conference will be Held in Hotel "Srbija" - Vrsac

Komisija

Od školske 2015/2016. godine predsednik Državne komisije za takmičenja učenika srednjih škola iz fizike je docent dr Božidar Nikolić sa Fizičkog fakulteta u Beogradu.

Komisija za takmičenja srednjih škola u školskoj 2015/2016. godini ima sledeći sastav:

Predsednik komisije:
Božidar Nikolić boza@ff.bg.ac.rs

Sekretar komisije:
Svetislav Mijatović svemij@gmail.com

1. razred:
Autor: Petar Mali
Autor: Zoran Popović
Autor: Svetislav Mijatović
Recenzent: Božidar Nikolić

2.razred:
Autor: Nora Trklja
Autor: Petar Bokan
Recenzent: Nikola Petrović

3.razred:
Autor: Vladan Pavlović
Autor: Vladimir Veljić
Autor: Marko Kuzmanović
Recenzent: Dimitrije Stepanenko

4.razred:
Autor: Nenad Vukmirović
Autor: Veljko Janković
Autor: Nikola Jovančević
Recenzent: Antun Balaž

Autori eksperimentalnog zadatka za Srpsku fizičku olimpijadu:
Marko Opačić
Nenad Lazarević
Novica Paunović

_____

Predsednik DFS je 24. januara 2014. godine imenovao prof. dr Miću Mitrovića za vršioca dužnosti predsednika komisije za srednju školu.

Upravni odbor DFS je 1. februara 2014. godine postavio prof. dr Miću Mitrovića za predsednika komisije za srednju školu za 2014. godinu.

_____

Komisija za takmičenja srednjih škola je u školskoj 2012/2013. godini imala sledeći sastav:

Predsednik komisije:
dr Aleksandar Krmpot aleksandar.krmpot@dfs.rs

Sekretar komisije:
dr Milovan Šuvakov milovan.suvakov@dfs.rs

1. razred:
Autor: dr Zoran Mijić zoran.mijic@dfs.rs
Autor: Zoran Popović zoran.popovic@dfs.rs
Recenzent: dr Nevena Puač nevena.puac@dfs.rs

2.razred:
Autor: dr Sanja Tošić sanja.tosic@dfs.rs
Autor: dr Bojan Nikolić bojan.nikolic@dfs.rs
Recenzent: dr Dragan Markušev dragan.markusev@dfs.rs

3.razred:
Autor: dr Milan Radonjić milan.radonjic@dfs.rs
Autor: Vladimir Veljić vladimir.veljic@dfs.rs
Recenzent: dr Antun Balaž antun.balaz@dfs.rs

4.razred:
Autor: dr Nenad Vukmirović nenad.vukmirovic@dfs.rs
Autor: Veljko Janković veljko.jankovic@dfs.rs
Recenzent: dr Darko Tanasković darko.tanaskovic@dfs.rs

Autori eksperimentalnog zadatka za Srpsku fizičku olimpijadu:
dr Nenad Lazarević
mr Novica Paunović

_____

Komisija za takmičenja srednjih škola je u školskoj 2011/2012. godini imala sledeći sastav:

Predsednik komisije:

dr Aleksandar Krmpot aleksandar.krmpot@dfs.rs

Sekretar komisije:

dr Milovan Šuvakov milovan.suvakov@dfs.rs

1. razred:

Autor: dr Zoran Mijić zoran.mijic@dfs.rs

Autor: Zoran Popović zoran.popovic@dfs.rs

Recenzent: dr Nevena Puač nevena.puac@dfs.rs

2.razred:

Autor: dr Sanja Tošić sanja.tosic@dfs.rs

Autor: dr Bojan Nikolić bojan.nikolic@dfs.rs

Recenzent: dr Dragan Markušev dragan.markusev@dfs.rs

3.razred:

Autor: Milan Radonjić milan.radonjic@dfs.rs

Autor: Milan Žeželj milan.zezelj@dfs.rs

Recenzent: dr Antun Balaž antun.balaz@dfs.rs

4.razred:

Autor: dr Nenad Vukmirović nenad.vukmirovic@dfs.rs

Autor: dr Mihailo Rabasović mihailo.rabasovic@dfs.rs

Recenzent: dr Darko Tanasković darko.tanaskovic@dfs.rs

Прилог

Уводна предавања на конференцијама и друга предавања

Subject **Re: Title and abstract**
  From Darko Tanaskovic <tanasko@ipb.ac.rs>
    To Rok Žitko <rok.zitko@ijs.si>
  Date 2016-06-12 00:24

Here it is. See you on Monday.

Best regards,
Darko

"Phonon spectra of K_xFe_{2-y-z}Co_zSe_2 single crystals"

Iron based superconductor K_xFe_{2-y}Se_2 has recently drawn a lot of attention due to
the coexistence of superconducting and antiferromagnetic insulating phase with ordered
iron vacancies. The superconductivity gets quickly suppressed by cobalt doping. In this
talk, we will present the Raman spectra of Co-doped KFe2Se2 single crystals which show
phase separation for smaller Co doping and homogeneous phase when Fe is completely
substituted by Co. In this case the material is ferromagnetic for T<74 K. We will
discuss various physical mechanisms which influence the changes in the phonon
frequencies and linewidths near the FM-PM phase transition in K_xCo{2-y}Se_2.

On 2016-06-11 10:15, Rok Žitko wrote:
> Dear Darko,
>
> Please send my the title and abstract for your seminar (which is
> scheduled on Tuesday at 3pm).
>
> Looking forward to see you on Monday!
>
> Kind regards,
> Rok

Subject	**Re: Seminari iz superprovodnosti/topoloskih faza**
From	Darko Tanaskovic <tanasko@ipb.ac.rs>
To	Marija Dimitrijevic Ciric <dmarija@ipb.ac.rs>
Date	2016-04-20 09:58

Zdravo Marija,

evo naslova i apstrakta:

Неконвенционални суперпроводници

BCS теорија веома успешно објашњава суперпроводност која настаје спаривањем електрона у кондензат Куперових парова услед интеракције са кристалном решетком.Купрати и суперпроводници на бази гвожђа одступају од овакве парадигме, а суперпроводност у њима настаје као последица одбојне Кулонове интеракције између електрона, без значајне помоћи вибрација решетке.Ови материјали су слаби проводници са јаком тенденцијом ка магнетном уређењу. На предавању ће бити приказана основна својства купрата и суперпроводника на бази гвожђа, као и теоријски модели који описују њихова главна својства.

Pozdrav,
Darko

On 2016-04-18 12:10, Marija Dimitrijevic Ciric wrote:

> Zdravo Darko,
>
> nema problema za danas. Naslov i apstrakt mozes do srede da mi
> posaljes, nije hitno jos uvek.
>
> Vidimo se, pozdrav!
>
> Marija
>
> ---
> Marija Dimitrijevic Ciric
>
> University of Belgrade
> Faculty of Physics
> Studentski trg 12-16
> 11000 Belgrade
> Serbia
>
> On 18 Apr 2016 12:12, Darko Tanaskovic wrote:
>> Zdravo Marija,
>>
>> ipak necu stici danas da vam se pridruzim. Vidimo se narednog ponedeljka.
>>
>> Da li treba da posaljem naslov i apstrakt?
>>
>> Pozdrav,
>> Darko

> On 2016-03-24 13:39, Marija Dimitrijevic Ciric wrote:
>> Zdravo svima vama koji ste pristali da date doprinos seminarima za
>> studente :) Evo preeliminarnog rasporeda za ovaj nas "mini-kurs". Sva
>> predavanja su u amfiteatru 661 ili eventualno u "plavoj sali" 665. I
>> svaki predavac ima na raspolaganju dva skolska casa, tablu, krede,
>> projektor i racunar :)
>>
>> 28. mart u 13 casova: Zlatko Papic: Jako-korelisane topoloske faze
>> materije (neki pregled oblasti i nesto o (frakcionom) kvantnom Holovom
>> efektu). Ovo predavanje je trebalo da bude kasnije, ali je Zlatko samo
>> kratko u Beogradu, pa da iskoristimo...
>>
>> 6. april (videcemo za vreme): Srdjan Stavric: uvod u fiziku kond.
>> materije (osn. pojmovi, tipa krist. resetka, k-prostor, Blohova
>> teorema, fononi,...)
>>
>> 13. april (videcemo za vreme): Zorica Popovic: uvod u superprovodnost.
>>
>> 18. april u 15 casova: Mihajlo Vanevic: nastavak superprovodnosti i primena.
>>
>> 25. april u 15 casova: Darko Tanskovic: superprovodnosti u jako
>> korelisanim materijalima: kupratima, gvozdje pniktidima i sl.
>>
>> 4. maj: Dimitrije Stepanenko (videcemo za vreme): topoloski
>> izolatori, mada to nije bas njegova oblast, ali rece da ce spremiti :)
>>
>> 9. maj u 15 casova: Milica Milivanovic: topoloski superprovodnici.
>>
>> Postoji mogucnost da mozda i Vladimir Juricic "svrati" u Beograd u
>> periodu april-maj, pa smo i njega zamilile da isprica nesto. Jos uvek
>> se dogovaramo... Seminari su namenjeni studentima 3. godine B smera,
>> ali bi bilo jako lepo i korisno da (bar neke od njih) i studenti 4.
>> godine odslusaju. U tom smislu bih zamolila Mihajla da predavanje iz
>> Cvrstog stanja u ponedeljak 28. marta pocne ne u 14, vec malo kasnije,
>> da bi studenti 4. godine culi Zlatkov seminar. Mislim da bi im bilo
>> korisno...
>>
>> Hvala na pomoci, cujemo se i vidimo se ovih dana. Pozdrav svima,
>>
>> Marija

--
Institute of Physics Belgrade
Pregrevica 118, 11080 Belgrade, Serbia
http://www.ipb.ac.rs/

Subject	**Re: visit to Augsburg**
From	Darko Tanaskovic <tanasko@ipb.ac.rs>
To	Liviu Chioncel <liviu.chioncel@physik.uni-augsburg.de>
Cc	Milos Radonjic <radonjmi@physik.uni-augsburg.de>
Date	2015-10-07 13:40

Dear Liviu,

here is the abstract.

Best regards,
Darko

"""
Bad-metal behavior featuring linear temperature dependence of the resistivity extending
to well above the Mott-Ioffe-Regel (MIR) limit is often viewed as one of the key
unresolved signatures of strong correlation. Here we associate the bad-metal behavior
with the Mott quantum criticality by examining a fully frustrated Hubbard model where
all long-range magnetic orders are suppressed, and the Mott problem can be rigorously
solved through dynamical mean-field theory. We show that for the doped Mott insulator
regime, the coexistence dome and the associated first-order Mott metal-insulator
transition are confined to extremely low temperatures, while clear signatures of Mott
quantum criticality emerge across much of the phase diagram. Remarkable scaling behavior
is identified for the entire family of resistivity curves, with a quantum critical
region covering the entire bad-metal regime, providing not only insight, but also
quantitative understanding around the MIR limit, in agreement with the available
experiments.
"""

On 2015-10-05 16:37, Darko Tanaskovic wrote:
> Dear Liviu,
>
> thank you very much for your kind invitation. The title of the talk will be
>
> "Mott quantum criticality and bad metal behavior"
>
> I will send you the abstract in the next day or two.
>
> Best regards,
> Darko
>
> On 2015-10-05 11:48, Liviu Chioncel wrote:
>> Dear Darko,
>> We figured out the dates. We would like to invite you to give a
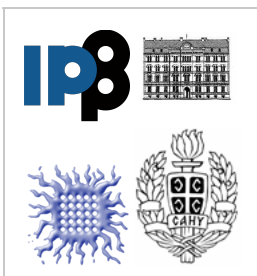>> seminar in Augsburg on the date of 02.12.2015.
>> this is a Wednesday and we have our regular Wednesday theory group
>> meetings. please send me the title and the abstract of the talk. I'll
>> be happy to support your travel and local expenses to/back and in
>> Augsburg.

> best regards,
> Liviu.

--
Institute of Physics Belgrade
Pregrevica 118, 11080 Belgrade, Serbia
http://www.ipb.ac.rs/

Invited Speakers

- Marco Aprili, Université Paris-Sud 11
- Fakher F. Assaad, University of Würzburg
- Dora Balazs, Budapest University of Technology and Economics
- Stefano Baroni, Scuola Internazionale Superiore di Studi Avanzati (SISSA)
- Wolfgang Belzig, University of Konstanz
- Nataša Bibić, Vinča Institute of Nuclear Sciences
- Alexandre Bouzdine, Université de Bordeaux 1
- Emil Božin, Brookhaven National Laboratory
- Ivan Božović, Brookhaven National Laboratory
- Christoph Bruder, University of Basel
- Harald Brune, Ecole Polytechnique Fédérale de Lausanne
- Hrvoje Buljan, University of Zagreb
- Emmanuele Cappelluti, Sapienza Università di Roma
- Milan Damnjanović, Faculty of Physics Belgrade
- Edib Dobardžić, Faculty of Physics Belgrade
- Gyula Eres, Oak Ridge National Laboratory
- Leonardo Golubović, West Virginia University
- Mirjana Grujić-Brojčin, Institute of Physics Belgrade
- Bjørk Hammer, Aarhus University
- Igor Herbut, Simon Fraser University
- Zoran Ikonić, University of Leeds
- Zoran Ivić, Vinča Institute of Nuclear Sciences
- Vladimir Juričić, University of Utrecht
- Jane Kondev, Brandeis University
- Zorica Konstantinović, Institute of Physics Belgrade
- Igor M. Kulić, Institut Charles Sadron
- Nenad Lazarević, Institute of Physics Belgrade
- Marjana Ležaić, Forschungszentrum Jülich
- Stergios Logothetidis, Aristotle University of Thessaloniki
- Aleksandar Matković, Institute of Physics Belgrade
- Ivanka Milošević, Faculty of Physics Belgrade
- Milorad Milošević, University of Antwerp
- Milica Milovanović, Institute of Physics Belgrade
- Zoran Mišković, University of Waterloo
- Marija Mitrović Dankulov, Institute of Physics Belgrade
- Stevan Nađ-Perge, California Institute of Technology
- Branislav Nikolić, University of Delaware
- Predrag Nikolić, George Mason University
- Čedomir Petrović, Brookhaven National Laboratory
- Dragana Popović, Florida State University
- Velimir Radmilović, Faculty of Technology and Metallurgy Belgrade
- Zoran Radović, Faculty of Physics Belgrade
- Milan Rajković, Vinča Institute of Nuclear Sciences
- Miljko Satarić, Faculty of Technical Sciences Novi Sad
- Rastko Sknepnek, University of Dundee
- Đorđe Spasojević, Faculty of Physics Belgrade
- Dimitrije Stepanenko, Institute of Physics Belgrade
- Željko Šljivančanin, Vinča Institute of Nuclear Sciences
- Nenad Švrakić, Institute of Physics Belgrade
- Bosiljka Tadić, Jožef Štefan Institute
- Milan Tadić, School of Electrical Engineering Belgrade
- Darko Tanasković, Institute of Physics Belgrade
- Christian Teichert, Montan University
- Mihajlo Vanević, Faculty of Physics Belgrade
- Ivana Vasić, Institute of Physics Belgrade
- Vladan Vuletić, Massachusetts Institute of Technology
- Ilija Zeljković, Boston College

Subject	**Re: visit to jozef stefan**
From	Darko Tanaskovic <tanasko@ipb.ac.rs>
To	Rok Žitko <rok.zitko@ijs.si>
Date	2014-06-02 10:38

Dear Rok,

I am fine, thank you. We will arrive to Ljubljana on June 8 as planned. We will not need a formal invitation letter.

Here is the abstract for my talk.

Cheers,
Darko

"Bad metal behavior reveals quantum criticality in the doped Hubbard model"

Scaling of physical quantities at finite temperature can reveal the existence of an otherwise experimentally inaccessible zero-temperature phase transition, or quantum critical point (QCP). However, it is not clear whether this generic QCP-dominated high-temperature behavior survives when the QCP is accompanied by a finite-temperature first order transition, or even completely masked by the emergence of an additional ordered phase in its vicinity. Here we show, using the dynamical mean field theory on the frustrated Hubbard model, that such phenomenology is possible in the case of the Mott metal-insulator transition. We find that the quantum critical scaling of resistivity is always present at temperatures sufficiently above the critical temperature Tc of the first order transition. Furthermore, in the limit of strong on-site interaction, Tc is significantly reduced and the scaling becomes valid even at very low temperature, revealing an almost fully blown quantum critical region. At high temperature, the quantum critical region extends to high doping and perfectly matches the region of the typical bad metal behavior with a linear growth of resistivity with temperature, which we interpret as a signature of connection between these two ubiquitous phenomena.

References:

1) J. Vucicevic, D. Tanaskovic, M.J. Rozenberg and V. Dobrosavljevic,
"Bad metal behavior reveals quantum criticality in the doped Hubbard model",
preprint

2) J. Vucicevic, H. Terletska, D. Tanaskovic and V. Dobrosavljevic,
"Finite-temperature Crossover and the Quantum Widom Line Near the Mott Transition",
Phys. Rev. B 88 (2013) 075143

3) H. Terletska, J. Vucicevic, D. Tanaskovic and V. Dobrosavljevic,
"Quantum Critical Transport Near the Mott Transition",
Phys. Rev. Lett. 107 (2011) 026401

On 02 Jun 2014 09:09, Rok Žitko wrote:
Dear Darko,

How are things in Belgrade? Everything OK with you and your close ones?

Are your plans for the visit to Ljubljana unchanged? If so, please
send me an abstract.

Kind regards,
Rok

On 15 May 2014, at 12:08, Darko Tanaskovic <tanasko@ipb.ac.rs> wrote:

Dear Rok,

thank you very much for so kind invitation. Everything suits perfectly.

I will send you a title and an abstract in the following days. I will also let you
know later if I need an invitation letter.

Regards,
Darko

On 15 May 2014 11:11, Rok Žitko wrote:
Dear Darko,

Ok, I arranged for a two-room suite at our guest house between June 8
and June 12. I hope this is fine with you. Let me know if there will
be any changes. We will cover your accommodation and local expenses,
as well as travel expenses (milage). In this latter case, our
regulation cap the maximum milage to 500 km which corresponds to
roughly 180 EUR.

Do you need a formal invitation?

I'll contact you again a few days before your visit to provide the
details about the location, parking, etc. At some point, please send
me a title and an abstract for the seminar.

Regards,
Rok

Dear Rok,

arrival on Sunday and sharing a suite in a guest house would be fine. Also,
staying until Wednesday or Thursday is both fine.

> Thank you very much for your help.
>
> Cheers,
> Darko
>
>
> On 14 May 2014 11:11, Rok Žitko wrote:
>> Dear Darko,
>>
>>> Nice, I am looking forward to the visit!
>>>
>>> I plan to come by car together with my PhD student Willem who is working on
>>> the SC problem in the PAM. I was thinking to spend 2 or 3 days in Ljubljana.
>>> The week that starts on June 9 would be very convenient.
>>
>> Ok. Let's try to fix the dates and find a suitable accommodation.
>> What about arrival on Sunday 8 and departure on Wednesday or Thursday?
>> We have a guest house right next to the Institute campus with some
>> multiroom suites. Would it be OK if you shared such a suite with your
>> student?
>> Alternatively, we can get you separate rooms in some hotel downtown.
>>
>> Regards,
>> Rok

--
Institute of Physics Belgrade
Pregrevica 118, 11080 Belgrade, Serbia
http://www.ipb.ac.rs/

Subject	**Invitation to speak at the workshop ""Wigner meets Mott: charge ordering and related phenomena in Mott system", Dec. 16-17 Grenoble**
From	Vladimir Dobrosavljevic <vlad@magnet.fsu.edu>
Sender	<vladica666@gmail.com>
To	Darko, Tanaskovic <tanasko@ipb.ac.rs>
Cc	Simone Fratini <simone.fratini@grenoble.cnrs.fr>, arnaud ralko <arnaud.ralko@grenoble.cnrs.fr>
Date	2013-10-10 01:02

Dear Darko,

we are pleased to invite you to speak and present your exciting new research results, at the upcoming mini-workshop entitled:

"**Wigner meets Mott: charge ordering and related phenomena in Mott system**",

which we are organizing for Dec. 16-17, 2013, at the Institut Neel - CNRS in Grenoble, France.

This mini-workshop will bring a friendly group of experts working on strong correlation phenomena near Mott transitions, in order to exchange ideas and stimulate collaborations in this exciting field. The workshop will include a comparable number of experimentalists and theorists, including the following invited speakers:

Adriano Amaricci (Sissa)
Vlad Dobrosavljevic (Florida)
Martin Dressel (Stuttgart)
Simone Fratini (Grenoble)
Henri Godfrin (Grenoble)
Markus Holzmann/Bernard Bernu (Grenoble)
Marc-Henri Julien (Grenoble)
Simon Kimber (Grenoble)
Florence Levy/Hervé Cercellier (Grenoble)
Emilio Lorenzo (Grenoble)
Luca de Medici (Paris)
Jaime Merino (Madrid)
Pierre Monceau (Grenoble)
Dragana Popovic (Florida)
Arnaud Ralko (Grenoble)
Marcelo Rozenberg (Paris)

Giovanni Sordi (London)
Darko Tanaskovic (Belgrade)

Please let us know if you would be able to attend this workshop. We were hoping
that you would be able to speak about your exciting new results about quantum
critical transport near Mott transitions.

We hope to see you in Grenoble soon,

Vlad Dobrosavljevic
Simone Fratini
Arnaud Ralko

--
Vladimir Dobrosavljevic
Professor of Physics
Director, CMS - Theory, NHMFL
Florida State University
http://badmetals.magnet.fsu.edu/index.html

DANI FIZIKE KONDENZOVANOG STANJA MATERIJE

Beograd, 10-12 Septembar 2013

Početak   Program   Lokacija   Kontakt

Opšte informacije

Cilj simpozijuma je da okupi istraživače aktivne u fizici kondenzovane materije i pruži uvid u aktuelne oblasti istraživanja sa pregledom najnovijih rezultata. Očekuje se da simpozijum bude od koristi istraživačima koji rade u različitim oblastima fizike kondenzovane materije i informativan za studente završnih godina Fizičkog fakulteta, master studente i doktorante.

Simpozijum će se održati u Beogradu **od 10 do 12 septembra** 2013 godine u prostorijama **Srpske akademije nauka i umetnosti**, ulica Kneza Mihaila 35. Predavanja na simpozijumu su po pozivu. Rok za slanje apstrakata je 15 jul 2013 godine.

Simpozijum se sastoji od predavanja u trajanju od **40 minuta + 10 minuta diskusija**. Predavanja treba da sadrže kratak uvod pristupačan širem auditorijumu i izbor aktuelnih rezultata.

Spisak predavača

[prikaži/sakrij apstrakte]

Antun Balaž, Institut za fiziku
Proučavanje dipolnih Bose-Einstein kondenzata u anizotropnim slabim potencijalima sa neuređenošću

Nataša Bibić, Institut Vinča
Modifikacija tankih slojeva metala i keramika primenom jonskih snopova

Ivan Božović, Brookhaven National Laboratory, USA
Novi rezultati u fizici visoko-temperaturnih superprovodnika

Ivanka Milošević, Fizički fakultet
Termalne osobine helikalnih ugljeničnih nanotuba

Milica Milovanović, Institut za fiziku
Geometrijski opis frakcionih Chernovih izolatora

Zoran Mišković, University of Waterloo, Canada
Interakcija grafena sa naelektrisanim česticama

Zoran Popović, Institut Vinča
Dinamički Jahn-Tellerov efekat u grafenu sa šupljinskim defektom

Velimir Radmilović, Tehnološko-metalurški fakultet
Šta znamo o klizanju bez trenja na atomskom nivou?

Zoran Radović, Fizički fakultet
Biharmonijska zavisnost Josephsonove struje od faze u superprovodnim spojevima sa nehomogenim feromagnetom

Đorđe Spasojević, Fizički fakultet
Analiza spening lavina u dvodimenzionalnom neravnotežnom Izingovom modelu na temperaturi T=0

Dimitrije Stepanenko, Institut za fiziku
Kvantni računari bazirani na kvantnim tačkama i spin-orbit interakciji

Željko Šljivančanin, Institut Vinča
Modelovanje atomske strukture djelimično oksidisanog grafena

Nenad Švrakić, Institut za fiziku

Pokrivanje i pakovanje u ravni: egzaktni i numerički rezultati za mešavine superdiskova

Darko Tanasković, Institut za fiziku
Kvantni kritični transport u blizini Mottovog metal-izolator prelaza

Mihajlo Vanević, Fizički fakultet
Kvantno proklizavanje faze u mezoskopskim superprovodnim žicama

Nenad Vukmirović, Institut za fiziku
Priroda nosilaca naelektrisanja u organskim kristalima

Last change: 7 Sep 2013

Subject	**Re: Seminar za studente III godine: predlog**
From	Darko Tanaskovic <tanasko@ipb.ac.rs>
To	Marija Dimitrijevic <dmarija@ipb.ac.rs>
Cc	Nenad Vukmirovic <nenad.vukmirovic@ipb.ac.rs>
Date	2013-04-18 22:18

Zdravo Marija,

nedelja mi je bila jako haoticna pa ti tek sada saljem naslov i apstrakt.

„Електронски транспорт у јако корелисаним материјалима близу метал-изолатор прелаза”

У материјале са јаким електронским корелацијама спадају купрати и суперпроводници на бази гвожђа, Мотови изолатори попут различитих оксида прелазних метала и органских корелисаних система, затим једињења на бази атома са делимично попуњеним f орбиталама и други. Њихова заједничка особина је веома богат фазни дијаграм где се различите супрепроводне, магнетне, металне и изолаторске фазе стабилизују уз помоћ мале промене температуре, спољашњег притиска, магнетног или електричног поља, или допирањем. Теоријско проучавање представља изазов јер су електрони негде на пола пута између слободних и потпуно локализованих. На предавању ће бити приказане основне особине ових материјала, као и динамичка теорија средњег поља као теоријски метод за њихово проучавање.

Vidimo se u ponedeljak!
Pozdrav,
Darko

On 16 Apr 2013 15:03, Nenad Vukmirovic wrote:
> Zdravo Marija,
>
> U nastavku poruke ti saljem naslov i apstrakt za moje predavanje 22.
> aprila. U principu ce to biti isto predavanje kao pre dve godine, samo
> cu mozda poneki slajd osveziti novim podacima ili rezultatima. Nadam
> se da ce se studenti pojaviti.
>
> Pozdrav,
> Nenad.
>
> Органски материјали - симулације електронских особина и примене
>
> Органски полупроводни материјали на бази конјугованих полимера или
> малих молекула имају велике могућности примене за електронске и
> оптоелектронске направе као што су соларне ћелије, диоде које емитују
> светлост и транзистори. Главни разлог томе је могућност њихове лаке и
> јефтине производње. Да би се разумели процеси у овим направама,
> неопходно је познавати просторну и енергетску расподелу електронских
> стања у материјалу, као и покретљивост електрона кроз материјал. На
> овом предавању ће бити дат преглед тренутне фазе развоја органских
> материјала и направа на бази њих, као и приказ метода којим се
> електронске особине ових материјала могу предвидети и симулирати.

SFKM 2007
XVII Symposium on Condensed Matter Physics

Serbia - Vršac
16.9. - 20.9. 2007.

General Information   Useful Information   Invited Speakers   Register   Submitted Abstracts   Contact

..**Invited Speakers:**

Marco	Aprili	CNRS, Universite Paris-Sud Orsay (France)
Assa	Auerbach	Technion (Israel)
Alfonso	Baldereschi	EPFL (Switzerland)
Ivan	Bozovic	Brookhaven National Laboratory (USA)
Milos	Bozovic	Faculty of Physics (Belgrade)
Natasa	Bibic	Instutute "Vinca" Belgrade
Katica	Biljakovic	Institute of Physics Zagreb (Croatia)
Alexandre	Buzdin	Universite Bordeaux 1 (France)
Nicolae	Cotfas	University of Bucharest (Romania)
Ana	Damjanovic	JHU & NIH (USA)
Jure	Demsar	Universitaet Konstanz (Germany)
Edib	Dobardzic	Faculty of Physics Belgrade
Vladimir	Dobrosavljevic	Florida State University (USA)
Ljiljana	Dobrosavljevic-Grujic	Institute of Physics Belgrade
Marija	Drndic	University of Pennsylvania (USA)
Diana	Dulic	LEM-SPEC, CEA Saclay (France)
Gyula	Eres	Oak Ridge National Laboratory (USA)
Laszlo	Forro	EPFL (Switzerland)
Leonardo	Golubovic	West Virginia University (USA)
Mark	Goerbig	Universite Paris-Sud Orsay (France)
Igor	Herbut	Simon Fraser University Burnaby (Canada)
Andrzej	Karwowski	West Virginia University (USA)
Milan	Knezevic	Faculty of Physics (Belgrade)
Nikola	Konjevic	Faculty of Physics (Belgrade)
Milan J	Konstantinovic	SCKCEN (Belgium)
Zorica	Konstantinovic	University of Barselona (Spain)
Jane	Kondev	Brandeis University (USA)
Miodrag	Kulic	Max Planck Institute Dresden (Germany)
Igor	Kulic	Harvard University (USA)
Stergios	Logothetidis	Aristotle University Thessaloniki (Greece)
Marko	Loncar	Harvard University (USA)
Janina	Maultzsch	Columbia University (USA)
Vincent	Meunier	Oak Ridge National Laboratory (USA)
Ivanka	Milosevic	Faculty of Physics Belgrade
Sava	Milosevic	Faculty of Physics Belgrade
Milica	Milovanovic	Institute of Physics Belgrade
Pierre	Monceau	Institut Nйel Grenoble CNRS (France)
Branislav	Nikolic	Universiy of Delaware (USA)
Zorka	Papadopolos	University of Tübingen (Germany)
Davor	Pavuna	EPFL (Switzerland)
Cedomir	Petrovic	Brookhaven National Laboratory NY (USA)
Danny	Porath	Hebrew University (Israel)
Dragana	Popovic	Florida State University (USA)
Helene	Raffy	CNRS, Universite Paris-Sud Orsay (France)
Stephanie	Reich	MIT (USA)
Valery	Ryazanov	ISSP Chernogolovka (Russia)
Maja	Scepanovic	Institute of Physics Belgrade
Steven H.	Simon	Alcatel-Lucent (USA)
Mario	Skrinjar	PMF Novi Sad
Zeljko	Sljivancanin	IRMA EPFL (Switzerland)
Djordje	Srajer	Argonne National Laboratory (USA)
Vojislav	Srdanov	Università degli Studi di Milano (Italy)

..**Deadlines:**

July 15, 2007-   Abstract submission & registration
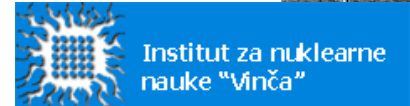July 15, 2007 -   Paper submission

Abstract submission: on-line.
Paper submission: on-line, 4p max.
Proceedings will be distributed to participants at the beginning of the Conference.

..**Organizers:**

Društvo fizičara Srbije

Institute of Physics
Belgrade - Serbia

Fizički fakultet
Univerziteta u Beogradu

Institut za nuklearne nauke "Vinča"

..**Sponsors:**

Република Србија
Ministarstvo nauke

Christoph	**Strunk**	**University of Regensburg (Germany)**
Bosiljka	**Tadic**	**"Jozef Stefan" Institute Ljubljana (Slovenia)**
Darko	**Tanaskovic**	**Institute of Physics Belgrade**
Christian	**Thomsen**	**Technischen Universitat Berlin (Germany)**
Christian	**Teichert**	**University of Leoben (Austria)**
Reshef	**Tenne**	**Weizmann Institute of Science (Israel)**
Zlatko	**Tesanovic**	**Johns Hopkins University (USA)**
Nened	**Vukmirovic**	**The University of Leeds (UK)**
Filip	**Vukajlovic**	**Instutute "Vinca" Belgrade**
Jan	**Zaanen**	**Universiteit Leiden (Netherlands)**
Ljubisa	**Zekovic**	**Faculty of Physics Belgrade**

* not confirmed yet